

LBATTS

LI-ION BATTERY TECHNOLOGY
FOR TRACTION AND
STATIC APPLICATIONS

The authors

The LBATTS project was mainly possible thanks to funds granted by the "Agentschap voor Innoveren en Ondernemen" also known as Vlaio. The main academic institutions of Flanders, VUB, KUL and U-Gent were taking part in it.

Authors from VUB:

Tom Turcksin
Lysander de Sutter
prof. Peter Van den Bossche
prof. Noshin Omar

Authors from U-Gent:

Ilya T'Jollyn
Jasper Nonneman
prof. Michel De Paepe

Authors from KUL:

Auguste Colle
prof. Jan Cappelle

Contents

I	State of the art	10
1	Introduction	11
1.1	Context of EES	11
1.2	EES Categorisation	13
1.2.1	Electrochemical EES	15
1.2.2	Electrical EES	16
1.2.3	Magnetic EES	17
1.2.4	EES with conversion in or through mechanical energy	17
1.3	Selection	20
1.4	Comparing battery cell technology	22
1.4.1	Batteries for grid applications	23
1.4.2	Batteries for Electric Transportation	26
2	Applications of batteries in particular Lithium-ion	32
2.1	Static applications	32
2.2	Mobile applications	40
2.2.1	Start-stop vehicles	42
2.2.2	Micro-hybrid, advanced micro-hybrid and mild-hybrid vehicles	42
2.2.3	Full hybrid electric vehicles HEV's	42
2.2.4	Plug-in hybrid electric vehicles PHEV's	42
2.2.5	Battery electric vehicle BEV's	43

2.3	Seconde-life applications	43
2.3.1	Refurbishing costs	44
2.3.2	Power electronics costs	46
2.3.3	Operation and maintenance costs	48
2.3.4	System cost	49
2.4	Market of energy storage based on Li-ion till 2020	50
2.4.1	Market size and evolution	51
2.4.2	Profitability	55
2.4.3	Conclusion	56
2.5	Cost evolutions	56
2.5.1	Cost of Lithium-ion	58
2.6	Battery °	59
3	Lithium-ion chemistries	62
3.1	Current lithium-ion technologies	62
3.1.1	Lithium-ion	62
3.1.2	Lithium polymer	66
3.1.3	Current state of Li-ion components	68
3.1.4	Cost evolution	73
3.1.5	Suppliers	73
3.2	Lithium-ion technologies till 2020	74
3.2.1	Lithium-ion-silicon batteries	74
3.2.2	Lithium-Sulphur batteries	78
3.2.3	Solid-state batteries	80
3.2.4	High-voltage batteries	82
3.2.5	Hybrid technologies and LICs	84
4	Thermal management	87
4.1	Introduction	87

4.1.1	Thermal battery behaviour	87
4.1.2	Present thermal management solutions	89
4.1.3	Novel thermal management solutions	92
4.1.4	Cost assessment	97
4.1.5	Suppliers	97
5	Battery management systems	102
5.1	Introduction of battery management systems	102
5.1.1	Present solutions	103
5.1.2	Characteristics	110
5.1.3	Future solutions	117
5.1.4	Cost assessment	117
5.1.5	Suppliers	120
5.2	Combination of battery + EDLCs/lithium-ion super capacitors	121
6	Testing and Standardization	123
6.1	Importance and hurdles of standards	123
6.2	Active organizations	123
6.3	Existing standards	124
 II Analysis of the applications and relevant problems in the industry		 127
1	Input of the user comittee	128
1.1	Introduction	128
1.1.1	What makes application and why would we choose it	129
1.2	Needs experienced by the Industry	130
1.3	List of applications proposed by the user comittee	130
1.3.1	Light electric vehicles - Altreonic	130

1.3.2	Start-stop systems for buses - Bluways	131
1.3.3	Terminal truck - Cloruyt and Mol	131
1.3.4	Light electric vehicle - Electric Drive	132
1.3.5	SmartRoof	135
1.3.6	I-generator and PV-installation - KUL	137
1.4	Selection of the most interesting casses for LBATTS	137
2	Techno economical analysis of the reconversion from lead-acid to Li-ion.	139
2.1	Set-up for battery benchmarking in hybrid domestic solar systems	139
2.1.1	Introduction	139
2.1.2	Solar panel	140
2.1.3	Battery	143
2.1.4	Load	144
2.2	Set-up for battery benchmarking in a hybrid genset	145
2.2.1	Introduction	145
2.2.2	Battery	146
2.2.3	Load	147
3	Load cycles	152
3.1	Introduction	152
3.2	Environment	153
3.2.1	Outdoor-applications	153
3.2.2	Indoor-applications	153
3.3	User profiles from international standard	157
3.3.1	Static Applications, profiles from standard	157
3.3.2	Mobile applications, profiles from standard	159
3.4	Static applications	160
3.4.1	I-generator	160
3.5	Mobile applications	162

3.5.1	Heavy duty Vehicles	162
3.5.2	Light electric Vehicle	164
3.6	Normalisation of the user profile	168
III	Electrical characterisation and modeling	171
1	Introduction	172
2	Battery specifications	175
2.1	Toshiba 20Ah LTO	175
2.2	Winston 100Ah LFP	175
3	Characterization methodology	177
3.1	Characterization tests	178
4	Battery Model	180
4.1	Electrical battery model	180
4.1.1	Equivalent circuit model	180
4.1.2	Electrical characterization	182
4.1.3	SoC estimation	189
4.2	Thermal battery model	194
4.2.1	Thermal characterization and thermal model calibration	195
5	Simulations and discussion	197
5.1	Dynamic Discharge Pulse Test	197
5.2	Simulation results	198
IV	Thermal characterisation and modeling	211
1	Introduction	212

2	Battery thermal management with heat buffering	213
2.1	Phase Change Materials (PCMs)	214
2.1.1	Organic PCMs	214
2.1.2	Salt hydrates	214
2.1.3	Eutectic mixtures	214
2.2	Enhanced PCM with structures	215
2.2.1	Metal foam	215
2.2.2	Expanded graphite	217
2.2.3	Carbon fibre	218
2.3	Overview PCMs	219
3	Thermal simulations	226
3.1	Simulation setup	226
3.1.1	Battery and load characteristics	226
3.1.2	PCM characteristics	231
3.1.3	Convective thermal resistance	233
3.2	Model governing equations	234
3.2.1	Overview	234
3.2.2	Equations	235
3.2.3	Assumptions and limitations of the model	237
3.3	Reference case: no heat buffering	237
3.3.1	Comparison of load cycles	237
3.3.2	Comparison of batteries	240
3.3.3	Comparison of natural and forced convective cooling	240
3.3.4	Comparison of current rates	240
3.4	Sensitivity study: thermal management with heat buffering	243
3.4.1	PCM layer discretization	243
3.4.2	Parameter sensitivity study	244

3.4.3	Thermal conductivity enhancement	254
4	Selection of battery thermal management system	260
4.1	Determine cell type and configuration	260
4.2	Determine battery properties	261
4.3	Determine cooling method	262
4.4	Determine buffering method	263
4.4.1	Estimate temperature variation	263
4.4.2	Determine melting temperature	264
4.4.3	Determine PCM mass and layer thickness	265
5	Conclusion	268
V	Construction of setups	271
1	Introduction	272
2	Construction battery modules	273
2.1	Winston module	273
2.2	Toshiba module	274
3	Construction of dedicated Thermal setup's	277
3.1	Thermal setup	277
3.2	Thermal conductivity measurement	281
VI	Testing of setups	283
1	Introduction	284
2	Testing of dedicated thermal setups	285
2.1	Thermal conductivity measurements	285

2.1.1	Inlet power calculation	286
2.1.2	Natural convection resistance	288
2.1.3	Solving process	288
2.1.4	Results	290
2.2	Thermal setup	290
2.3	PCM properties	292
3	Testing of battery modules	294
3.1	Winston module	294
3.2	Toshiba module	294
3.2.1	Usage tests	295
3.2.2	Thermal imaging	299
4	Conclusions	300
4.1	Lessons learned	300
4.2	General conclusions	300

Part I

State of the art

Chapter 1

Introduction

1.1 Context of EES

Energy Storage Systems or ESSs consist of all types of energy storage systems including gasoline, heat storage and many others, see Figure 1.1. It does not specify the type of energy stored, for example it can be thermal energy, stored in molten salts or electrical in capacitors.

It is important to note that electric energy transfer is relatively easy to control, this led to many noble applications from electronics to powering cities. The high quality of this energy transfer process can be explained through the second Law of Thermodynamics. This law takes into account the effect of irreversible processes. Exergy is defined as the amount of useful work that a system can produce when going from a charged state to a neutral state. The ratio of exergy to energy in a substance can be considered a measure of energy quality. Forms of energy such as macroscopic kinetic energy, electrical energy, and chemical Gibbs free energy are 100% recoverable as work, and therefore have an exergy equal to their energy. However, forms of energy such as radiation and thermal energy can not be converted completely. [219].

EES stands for Electric Energy Storage systems. This subgroup in ESS focuses only on the alternatives that consider electric energy as stored type of energy. This means that they must be able to easily absorb or produce electric power on demand. The possibilities are numerous as we will see in the following sections.

Often, the EES transforms the energy into another form but when electricity is needed, the system should be able to provide it in an acceptable time period (depending on the application). Energy losses can occur during the charge and discharge process and/or during the storage period itself. The strength and causes of these losses depends on the EES.

Two contemporary problems make highly performing EES very desirable:

- Climate change, probably caused by massive fossil fuel usage, leads to strong incentives for harvesting of renewable energy often intermittent in nature. In addition to the electrical utilities with their static applications, the scope of mobile applications broadens with time as well. The pollution of cars is so intense that strong incentives exist to electrify them and reduce pollution. The time scale ranges from hours to days and sometimes even seasons.
- AC Distribution related problems are due to the extensive usage of power electronic converters and to inductive losses. An electric converter (buck, boost, inverter, rectifier and others) draws or provides a repetitive but non-sinusoidal current profile. These disturbances can become large and spread like pollution over the grid. Massive usage of converters may lead to many perturbations which can add up, creating high voltage peaks at unexpected locations. These peaks can damage the installations resulting in a less resilient grid. Active and passive filters based on EES (for example a coil and capacitor in series yields a notch filter) are used to work on these problems. Inductive loads charge the distribution lines with a sinusoidal current however this reactive current does not add to the total energy transfer (ie. energy is shuttled in an alternating way to and from the reactive load). The reactive energy can be provided by the generator but this can lead to failure and is very inefficient because the reactive power is transmitted over distribution lines. To compensate, capacitors (a typical EES) are installed nearby the inductive loads. In this case the reactive energy is shuttled back and forth between the capacitive and inductive components.

Though historically the roots of these problems are different, the physical roots of these problems are exactly the same, namely the supply and demand power must be equal at all times (be it active or reactive). The only way to get around this is by introducing additional storage and/or generation assets into the system.

Luckily a lot of solutions for these ever demanding problems exist and the technology is continuously being improved upon. The downside is that choosing an adequate EES technology becomes more complex and specific towards the application and environment.

In the context of continuous improvement Figure 1.1 depicts the maturity levels of some thermal and electrical energy storage technologies. The picture is very interesting, the curve corresponds to the time derivative of the S-curve (a curve that depicts the commercialization process of a technical revolution). Figure 1.1 is certainly not exhaustive, additionally it dates back to 2013. The figure also shows the lithium based storage will clearly continue evolving the coming years.

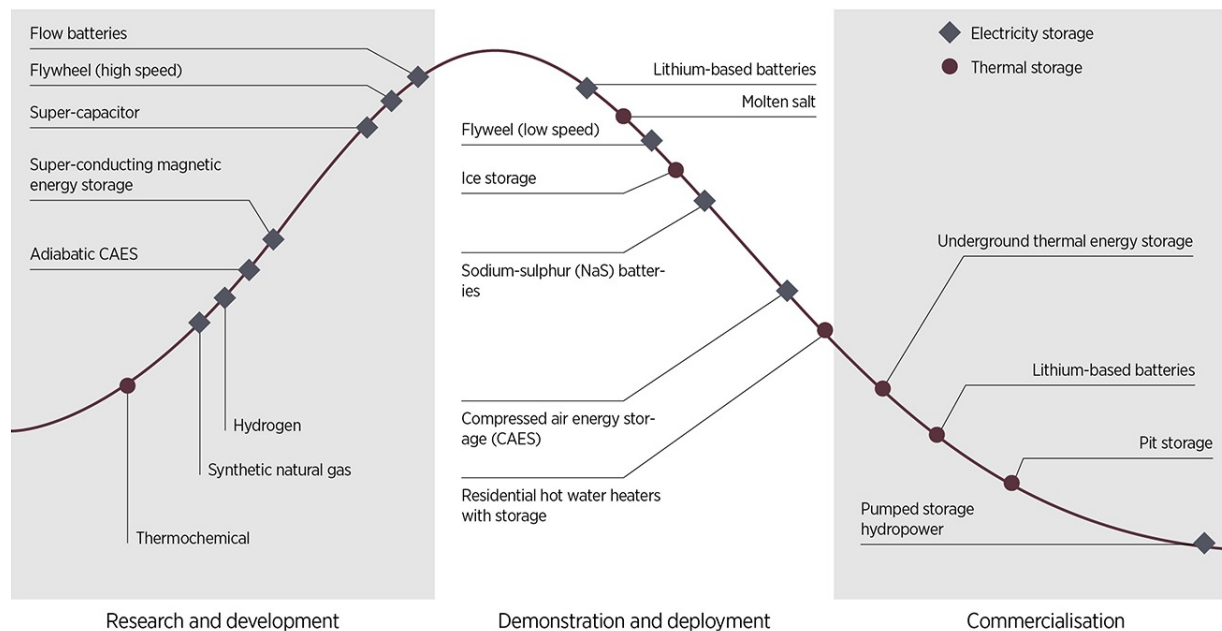


Figure 1.1: Maturity level of some thermal and electrical energy storage technologies, reference [11], 2013

1.2 EES Categorisation

To help understand the diverse approaches currently being deployed around the world, we can divide rechargeable EES in several categories and sub-categories as depicted in Figures 1.2 and 1.3.

Figure 1.2 divides EES into four categories. The first one, the electrochemical category, consists of a wide range of storage solutions. The electric, magnetic and mechanical categories are relatively speaking the simple EES, the knowledge of one state variable is usually enough to determine the energetic capacity left in the EES. This is different in the electrochemical category.

The electrochemical EES consists of a collection of rechargeable (also called secondary) and "non-rechargeable" (also called primary) battery technologies. For reasons of life cycle analysis (LCA), rechargeable technologies are the preferred alternative.

To get our head around this large set we can divide them further along the aggregation state of their main components, see Figure 1.3. The main components of modern cells are the two electrodes and the electrolyte. Depending on the technology, these components can operate in different phases. The last column in Figure 1.3, illustrates the layout of the components's phases in the following fashion: (*electrode/electrolyte/electrode*). Notice that a fluid can be in liquid or gaseous form, since it is defined as something that flows.

There are some limits in this classification. We may expect that several components take on

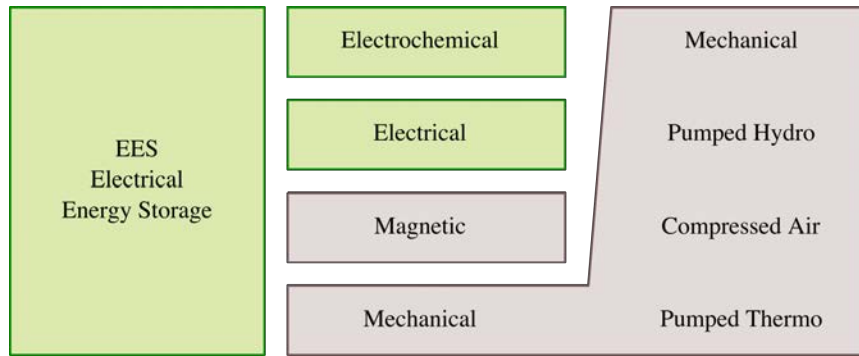


Figure 1.2: General classification of EES, (within LBATTS we will focus on the green classes)

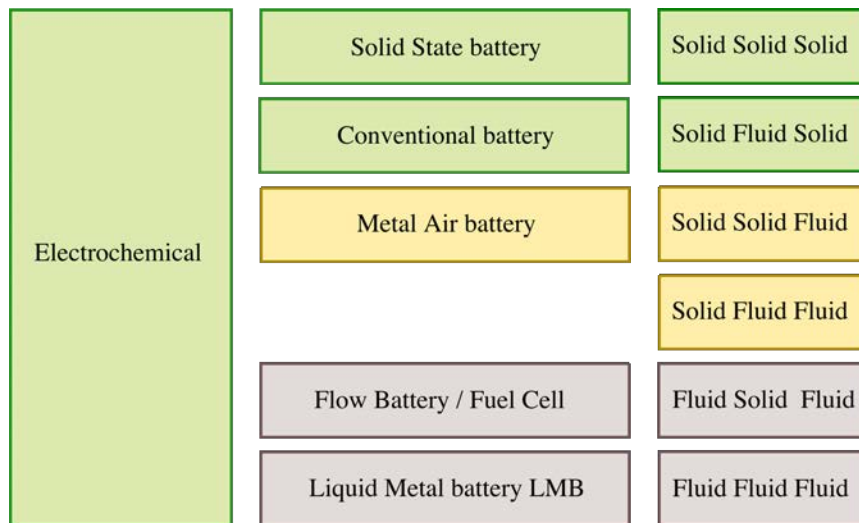


Figure 1.3: Classification of Electrochemical EES (within LBATTS we will focus on the green classes)

the form of non-Newtonian or highly viscous or infused substances obscuring the boundaries once again (ex. Lipo). The distinction between primary and secondary is not always clear as well. In theory, secondary means an infinite cycle life though in reality, this is never really the case. Much work in adjusting the cell chemistries such that primary cells evolve into rechargeable technologies is being realized around the world (ex. Metal-air technologies).

In regard to this classification we notice that the different configurations gives rise to some well established battery families, such as the conventional -, metal-air -, flow - and solid state batteries.

As time evolves new hybrid components come on the market, sometimes it is unclear into which category they belong. For example capacitors and batteries are differentiated clearly by the fact that a capacitor stores energy in the electric field and batteries store it in a

chemical form, however since the existence of LICs (Lithium Ion Capacitors) and Ultra Batteries, the boundaries in classification remain accurate but become more obscure.

1.2.1 Electrochemical EES

Principle of electro-chemical EES

Electrochemical energy storage allows for a direct transition from electrical to chemical energy and back. A specific characteristic of electrochemical EES is the presence of chemical reactions. Oxidation occurs at the anode and reduction takes place at the cathode. A salt bridge containing inert electrolytes is used to connect the two solutions so that anions and cations can flow to complete the circuit. If no salt bridge or separator was used, the redox reaction would carry on without producing any useful electrical work.

Determination of energetic content

The determination of the energetic content of a battery is less straightforward than is the case in other EES. Indeed a single state variable like open circuit voltage does by itself not provide sufficient information to determine the remaining energy.

Equation 1.1 can be applied to calculate the stored energy but it requires stepwise discharge of the EES (such that the open circuit voltage can be integrated over time).

As we saw previously the process of energy transfer (charging or discharging) brings its own type of energy losses. This loss may not be accounted for when determining the energy content (situation before discharge). For this reason, the energy losses are added explicitly in the term Z_i (internal impedance). The value of Z_i is function of internal temperature, internal pressure, state of charge and state of health. Standardization of procedures for determining the state of health are still in the making. In the mean time, a stepwise integration of the open-circuit voltage eliminates the term Z_i .

$$E = \int_{t_0}^{t_{end}} (V.I - Z_i \cdot I^2) \cdot dt = \int_{t_0}^{t_{end}} U.I \cdot dt \quad (1.1)$$

In equation 1.1, U is the open circuit voltage, also called the "internal" voltage, V represents the battery voltage (under operation) and Z_i represents the internal impedance.

Useful data

Table 1.1 provides some examples of noticeable and commercially available electrochemical cell technologies, ordered along the previously specified categories. The presented list is of course non-exhaustive. For informative purposes, Table 1.2 provides some characteristics of secondary electrochemical cells.

Note that this data is very subjective to the actual working conditions.

Lithium-ion batteries

In Chapter 3 we explore the contemporary and future (5-10 years) promising conventional and solid state Li-based battery options. Alongside the Li-ion SSBs, it is difficult not to mention Lithium ion capacitors or LICs, see section 3.2.5.

1.2.2 Electrical EES

Typical capacitors have low energy content compared to electrochemical capacitor. They are extensively used in electronics. We will not get into detail of this class. Electrochemical capacitors, sometimes referred to as EDLC (electric double-layer capacitor) yields much higher capacities. The double-layer refers to the physical separation of the electrodes by a separating layer. Because the charge is stored in the electric field, with no chemical reactions or phase changes taking place, the process is fast and highly reversible. As a consequence the cycle life is nearly endless. Because of the high surface area and the small thickness of the double layer, these devices have very high specific and volumetric capacitances. This enables them to combine a previously unattainable capacitance density with an essentially unlimited charge-discharge cycle life. The operational voltage of one cell is limited only by the breakdown potential of the electrolyte and is usually less than 3 V. Thus, cells are connected in series for higher voltage operation.

There are two types of electrochemical capacitors:

1. Symmetric designs, where both positive and negative electrodes are made of the same high-surface-area carbon. Symmetric EDLCs have specific energy values up to 6 Wh/kg and higher power performance than asymmetric capacitors.
2. Asymmetric designs with different materials for the two electrodes, one high-surface-area carbon and the other a higher capacity battery-like electrode. Specific energy values approach 20 Wh/kg.

Because of their high power, long cycle life, good reliability, and other characteristics, the market and applications for EDLC's have been steadily increasing. There are dozens of manufacturers and more entering the market because of market growth. Applications range from portable electronics and medical devices to heavy hybrid and other transportation uses. EDLC's are better suited than batteries for applications requiring high cycle life and charge or discharge times of 1 second or less. The largest barrier to market growth has been the lack of understanding the technology and the applications for which it is best suited. Aqueous electrolyte asymmetric EDLC's technology offers opportunities to achieve exceptionally low-cost bulk energy storage. [202]

Symmetric EDLC's have response times on the order of milliseconds and are well-suited for short duration high-power applications related to both grid regulation and frequency regulation. Asymmetric EDLC's are better suited for grid energy storage applications that have long duration, for instance, charge-at-night/use-during-the-day storage (i.e. bulk

energy storage). Some asymmetric EDLC products have been optimized for 5 hour charge with 5 hour discharge. Advantages of EDLC's in these applications include long cycle life, good efficiency, low life-cycle costs, and adequate energy density. [202]

1.2.3 Magnetic EES

The Magnetic category, contains highly performing coils also called SMES (Super Magnetic Energy Storage). A SMES system consist of a vacuum torus-like vessel, a super conductor and a refrigeration system. The highest cost comes from the superconductor materials and refrigeration.

It is said that SMES loses the least amount of electricity in the energy storage process compared to other methods of storing energy. The round-trip efficiency is greater than 95%. However this value does not take into account the necessary power to keep the system at cryogenic temperatures. [83] Two technologies (high and low temperature super conductor materials) are pursued. Figure 1.4 illustrates the typical time scale (1s-1min). The existing implementations are clearly utility level with energy capacities ranging from 1kWh up to 10kWh and power rating from 100kW up to 10MW.

Today SMES is not yet economical. Some say that 1GWh systems with a circumference of 160km are necessary to make this an economically viable option.

Notice that a capacitor with infinite capacity acts like an ideal voltage source whereas a coil with infinite self inductance acts as an ideal current source.

1.2.4 EES with conversion in or through mechanical energy

The EES in the brown category see Figure1.2, are the ones where the stored energy transitions the mechanical form at some stage. Most of these are only implemented at utility scale.

Flywheels

Flywheels are mechanical devices that store electricity in kinetic energy to deliver instantaneous electricity. The power is limited by the electric motor and electrical converters. They come in many sizes, some are designed for residential use, they are about the size of a refrigerator, other are for industrial use. Power electronics are designed to enable extraction of energy over a wide range of rotations per minute, others only provide a pulse of DC energy for instance to power a railgun, in this application the needed converters are not required.

Modern flywheels have rotors running up to approximately 50000 rpm. They consist of a vacuum chamber which houses the wheel, which is held in place with magnetic bearings or hard ceramic ball bearings. The wheel itself should be a lightweight high tensile strength

material. The wheel is in some cases made of an aluminum hub, around which several material layers with increasing tensile-strength/weight-ratio are added. Flywheels with magnetic bearings and high vacuum can maintain 97% mechanical efficiency, and 85% round trip efficiency, reference [168] are reported.

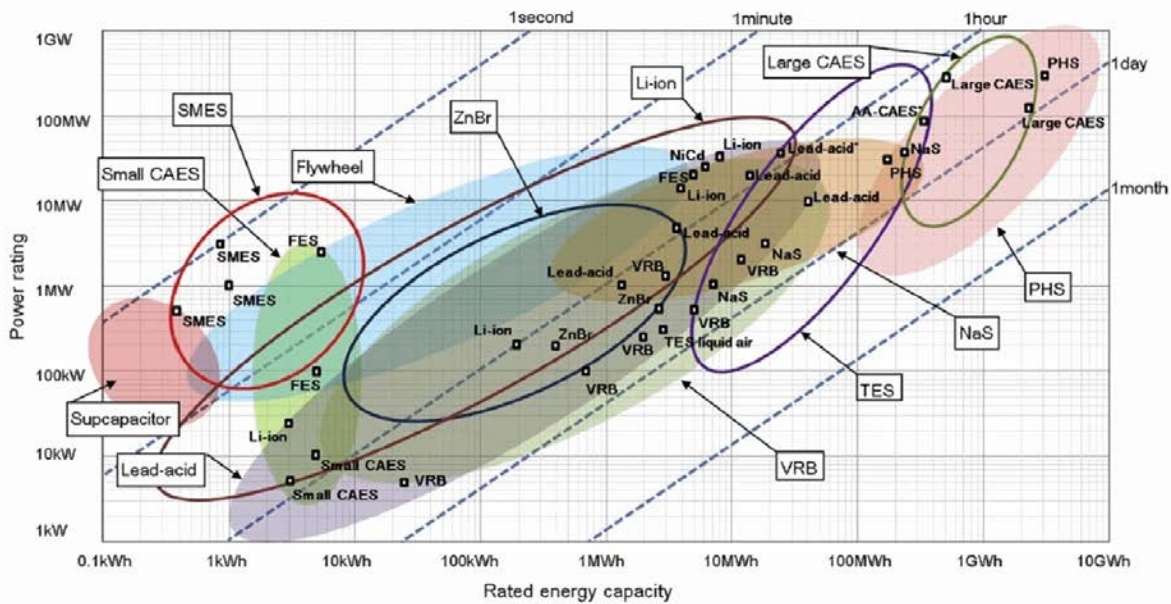


Figure 1.4: Comparison of power rating and rated energy capacity with discharge duration at power rating, from reference [122] 2015

Compressed air

Compressed Air Energy Storage or CAES utilizes compressed air to store potent energy. When doing so, we try to reduce the losses as much as possible. Important rules to keep in mind when working with gases are the following: when compressing an ideal gas, the gas heats up. Additionally, the required energy for compressing a gas is proportional to its begin temperature. During expansion the opposite is true. A gas cools down during expansion, and more mechanical energy on the turbine is created when the temperature before expansion is higher. The term adiabatic means with no heat exchange, the term isentropic implies adiabatic as well as reversible. In advanced CAES an isentropic process is the holy grail. To achieve the next best thing inter-cooling during compression and reheating during expansion is integrated. The thermal energy is stored in thermal buffers. Round trip efficiencies of 70% up to 80% are achievable according to reference [202].

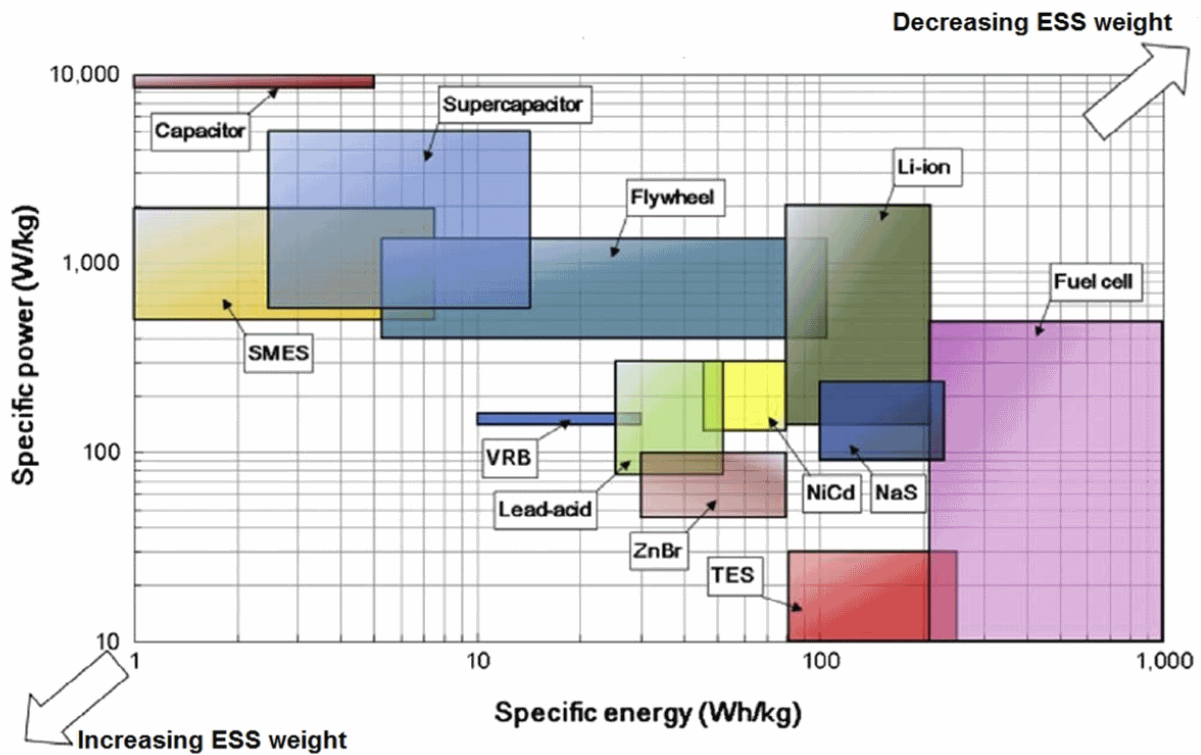


Figure 1.5: Mass specific energy and power density, from [122]

Pumped heat electrical storage PHES

In thermal energy storage electric energy drives a compressor which allows to transfer thermal energy form one buffer to another. Two distinct approaches can be differentiated depending on the use of a cold (Liquid air energy storage LAES) or hot thermal mass (Pumped heat electrical storage PHES). The second thermal mass is typically at environmental temperature.

The electric energy is transformed into the transfer of thermal energy, but also used to bring other thermal energy to a higher temperature. In an ideal situation the same electric energy can then be recovered from part of the high temperature thermal energy, while the other part is channeled again to low temperature thermal energy.

Pumped hydraulic storage PHS

Pumped Hydraulic Storage PHS uses large-scale water reservoirs situated at different heights. In many cases natural landscape provides these reservoirs at least partially, making it very economical. Another approach would be to use chambers in old mines, but

determination of the impact of fatigue on the cavern walls is difficult to estimate. It is clear that most landscapes are not always prone to this solution. According to [188], PHS accounts for more than 99% of the worldwide EES energy capacity. This is mainly due to the low price per installed kWh compared to other EES.

1.3 Selection

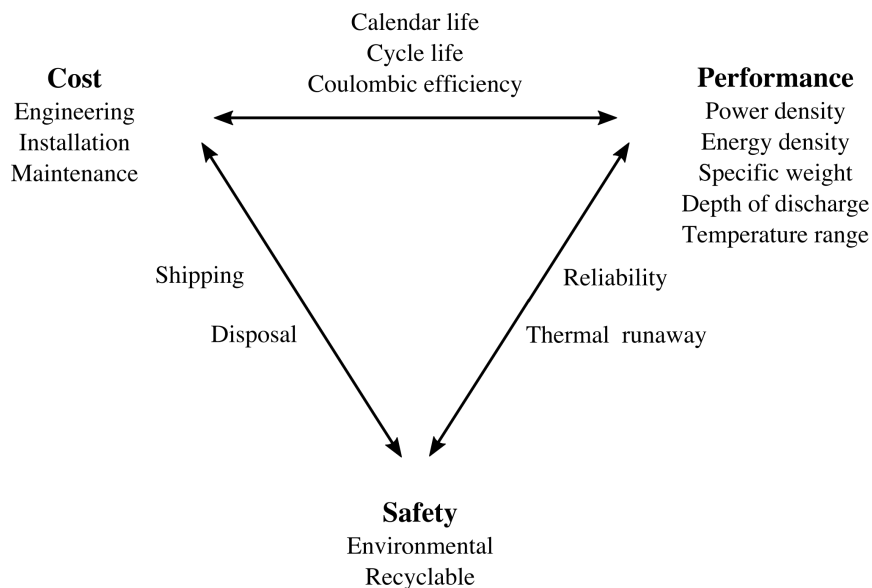


Figure 1.6: Battery design considerations, adapted from reference [67]

For a specific application the most fitted EES depends on several factors as depicted in Figure 1.6. The main characteristics to take into account are safety, cost, and performance. It is difficult to uncouple these factors because they are not orthogonal. Many charts can be found relating some of these key metrics but none of them shows the whole picture so precaution is important when using these.

Figure 1.4 illustrates the relationship between energy and power capacity of existing installations. Straight lines of fixed slope (depending on the units) correspond to a fixed discharge time.

Since Li-ion is still evolving, we may expect that the brown Li-ion bubble will continue expanding these coming years (Tesla is currently building their Giga factory). TES and VRB respectively stand for thermal energy storage and valve regulated lead-acid batteries. Their existence was briefly mentioned in the first chapter. In this comparison, one can get an impression of the actual size of these installations. We notice for instance that CAES and PHS are situated in the GWh scale. The graph also illustrates the broad scope in energy capacity of lithium-ion systems.

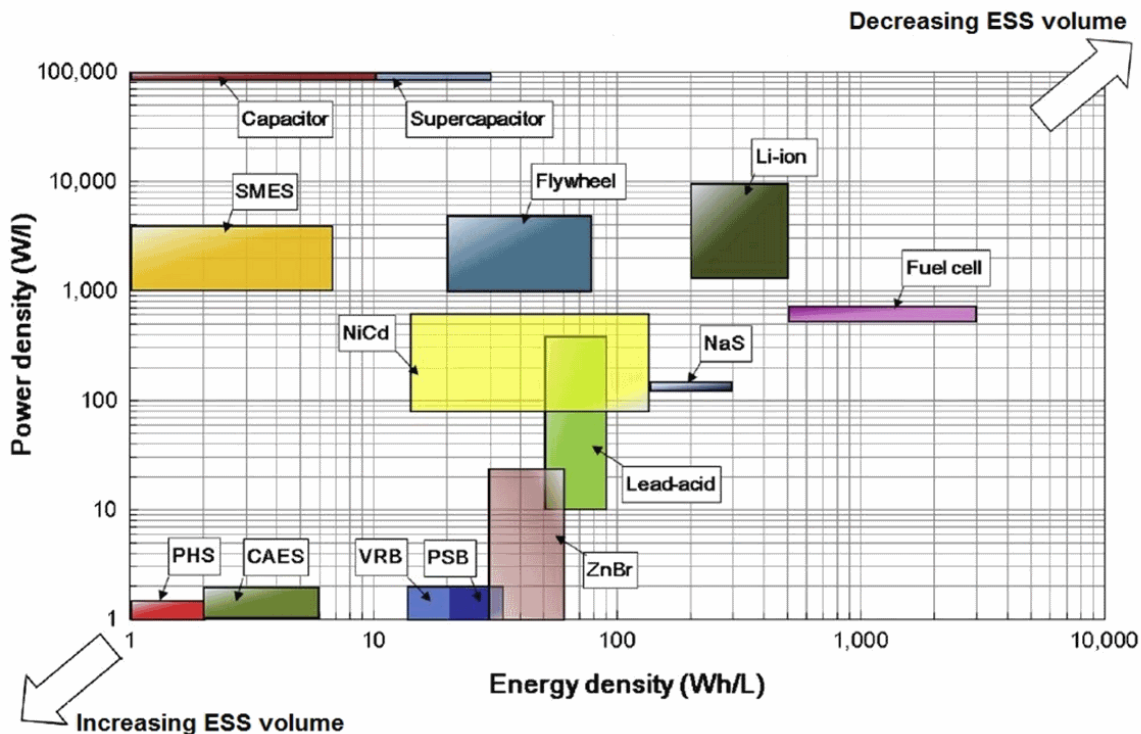


Figure 1.7: Volume specific energy and power density, from [122]

EES technologies can be classified by the nominal discharge time at rated power [122]:

- discharge time less than 1 hour: flywheel, supercapacitor and superconducting magnetic energy storage (SMES);
- discharge time up to around 10 hours: over ground small-scale compressed air energy storage (CAES), lead acid, Li-ion, nickelcadmium (NiCd), zinc-bromine (ZnBr) flow battery and polysulfide bromine (PSB) flow battery;
- discharge time longer than 10 hours: pumped hydroelectric storage (PHS), underground large-scale CAES, liquid air energy storage, vanadium redox flow battery (VRB), solar fuel, fuel cell and thermal energy storage (TES).

In essence discharge time is equal to the ratio of useful energetic capacity over nominal power. If weight, volume, cycle durability, costs and safety are not considered in the equation, EES with identical discharge time are "interchangeable".

Figures 1.5 and 1.7 respectively illustrate the mass specific and volume specific Ragone charts. These charts are very useful for applications where weight and/or mass are severely constrained (for instance mobile applications). From these figures one can easily deduce

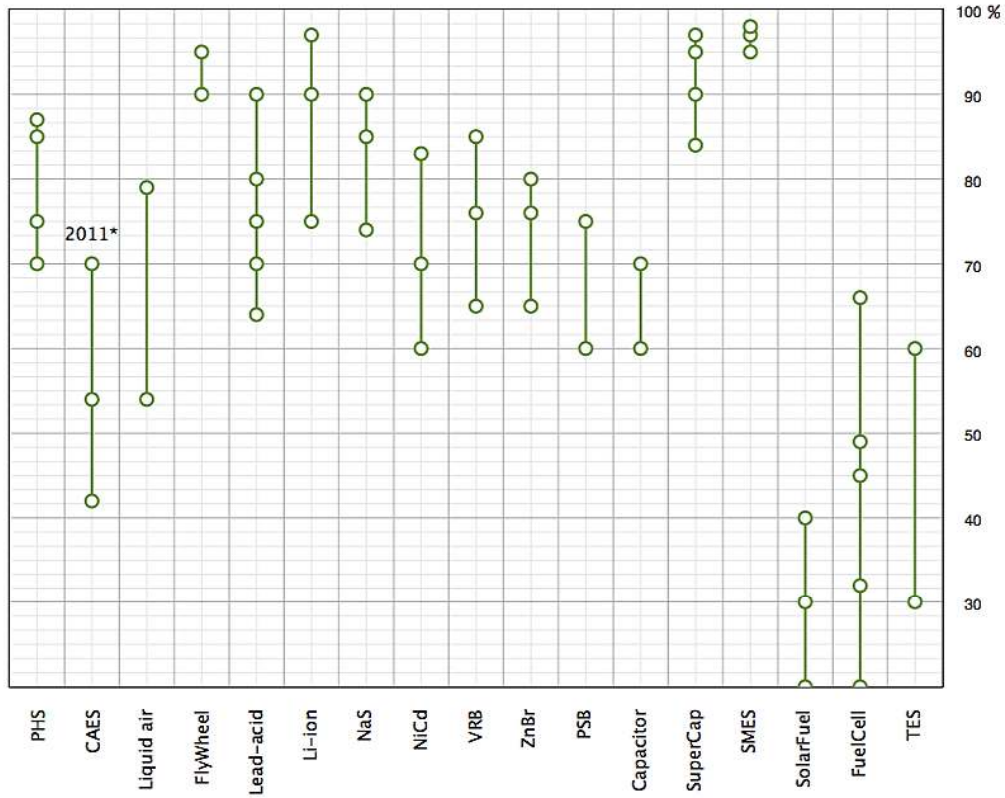


Figure 1.8: Cycle efficiencies of EES technologies, (*) building proces was initiated, little information on the considered discharge profiles is available, self-discharge loss is not taken into account. Reproduced from [232] (2014)

why lithium batteries are so attractive. Within the class of rechargeable electrochemical EES, it yields a good compromise between power and energy density.

Figure 1.8 illustrates the cycle efficiency of EES, reference [232] (2014). Within the category of electrochemical EES, Li-ion can achieve the highest efficiency (75% to 94%).

1.4 Comparing battery cell technology

There are hundreds of different batteries available in the market today, and the technical characteristics and performance differ per technology, per manufacturer, and per supplier [86]. Their discharge time ranges from one second to a day. Furthermore, there are variations within each technology depending on the voltage level, the desired depth-of-discharge, maintenance and load requirements [86]. Therefore, there is no single battery technology that serves a particular application, but rather a multitude of options depending

on the decision criteria. Furthermore, there are a number of projects where batteries are combined to achieve the required functionality (the so-called hybrid storage solutions). For example, a battery system connected to a wind turbine park in Braderup combines a 2 MWh li-ion battery with a 1 MWh vanadium redox flow battery [86].

1.4.1 Batteries for grid applications

Batteries for grid applications should be considered as stationary installations specifically developed to fulfill functionalities for grid applications, such as: supporting primary and secondary reserve power, ancillary services, grid systems to support transmission, support the grid quality and reliability and integration of renewables like wind or PV. Batteries have high potential because of their flexibility in size and characteristics but can only contribute efficiently if correctly designed and tailored. For stationary grid applications, improvement on cycle life time and calendar life time are decisive in the development of reliable and cost-effective products [209]. Some smart grid plans in Europe include using the EV (electrical vehicles) batteries for grid storage applications. The idea to use batteries on board vehicles as balancing component in the grid is a paradigm shift, (Grid to vehicle: G2V and vehicle to grid: V2G). Battery electrical vehicles are marketed with a typical driving range up to 150 km (except Tesla). In practice, this is usually considerably lower due to need for auxiliary power in the vehicles (defrosting, cabin heating, air conditioning etc.) as well as weather conditions and road friction [209]. The chances that batteries in vehicles can play the described balancing role in the electrical grid depend on the consumers demand for those vehicles and this will in turn be stimulated by improved battery technology (in the form of higher endurance (higher energy density in the battery) and shorter charging times (more rapid chemical reactions and faster transport within the battery). Further logistical obstacles must be overcome, including ways to avoid compromising the battery warranty emitted by the car manufacturers [209].

Lead-Acid A few large demonstration plants have been built starting from the second half of 80s: in Berlin (17 MW and up to 14 MWh), by BEWAG for grid frequency regulation and spinning reserve applications, in Chino (California), a plant of 10 MW and 40 MWh for load leveling, in San Juan, Puerto Rico a 20 MW / 18 MWh plant was built [3], there is even a demonstration operating in a village in the Amazon region of Peru [36] [47] [120]. Nevertheless, the primary disadvantages of lead-acid batteries are their poor energy density and short cycle life. Marginal gains to specific energy can be achieved by improving the active material and design of the electrodes, but will always be limited by the chemistry's relatively low theoretical boundaries. Cycle life potentially can be increased by adding carbon in various forms to either the anode or cathode [169], or by replacing the traditional lead acid anode with a carbon anode similar to that of an asymmetrical electrochemical capacitor [169]. Another approach to improve cycle life is the so-called lead acid flow battery, in which lead is dissolved in an aqueous methane sulfonic acid electrolyte.

This system differs from traditional flow batteries by using of just one electrolyte and the subsequent lack of troublesome electrolyte separators [169]. If long deep discharge cycle life is proven and costs can be kept low, these technologies may be promising for grid-based bulk electricity storage applications.

Lithium-ion Lithium-ion batteries consist of a range of different chemistries, each with unique cost and performance characteristics. These can generally be grouped into two categories of cathode materials to complement lithium: iron phosphate and mixed metal (cobalt and manganese oxide) (Albright and Al-Hallaj, 2012) [86]. Titanate is an anode material that can complement lithium with relatively low energy density and very high cycle life, however also most expensive. One of the greatest obstacles facing lithium-ion is safety. The energy density of the cells and combustibility of lithium, as well as the presence of oxygen, mean cells can overheat and catch fire [86]. This situation, known as thermal runaway can additionally cause neighboring cells overheat and in the worst case a cascading effect can take place. This leads to leaks, smoke, gas venting and/or the cell pack coming alight. A variety of external conditions may cause this, leading to internal cell distress. These include for instance external heating, over-charging, over-discharging, and high current charging (Albright and Al Hallaj, 2012) [86]. Design and thermal management integrating performance characteristics by limiting DoD, must therefore be considered.

High Temperature Sodium-Beta Sodium-beta batteries use molten (liquid) sodium for the anode, with sodium ions transporting the electric charge [169]. The two main types of sodium-beta batteries are distinguished by the type of cathode they use. The sodium-sulfur (Na-S) type employs a liquid sulfur cathode, while the sodium-nickel chloride (Na-NiCl₂) type employs a solid metal chloride cathode. Both types include a beta-alumina solid electrolyte material separating the cathode and anode [169]. There are several R&D efforts associated with sodium-beta batteries. One is to develop a stacked planar cell design that could cut cell costs in half [169]. This departure from the traditional tubular design has the ability to increase specific energy and power (the latter a limiting factor for the use of these batteries in many applications), improve packing efficiency, and improve modularity. It also presents the opportunity to address long term corrosion problems. However, planar designs face sealing and material selection challenges [169]. Other R&D efforts focus on low temperature sodium based chemistries using new cathodes and/or sodium ion conductors [169]. While cost is a major R&D focus, longevity and reliability still have room for some marginal improvement using improved cell configurations and designs.

Flow Batteries Flow battery R&D efforts include improving the performance of commercially available products and developing new chemistries. For vanadium redox cells, research seeks to decrease the vanadium required and increase energy density, for example, by up to 70 % [169]. New redox couples that increase efficiency, improve specific energy, or utilize more cost effective or less toxic materials are also the subjects of investigation. These

chemistries include iron-chromium, zinc chloride, hydrogen-halogen, hydrogen-bromine, lead, and others [169]. An earlier flow battery type (sodium-bromide/sodium-polysulfide) reached the initial stages of commercialization, but was discontinued. It is unclear if development of this chemistry is being pursued [169]. Another key requirement for large-scale deployment will be achieving demonstrated reliability and longevity. These requirements are complicated by the toxic and corrosive electrolytes, which pose significant materials challenges for the hydraulic subsystems and ion exchange membrane, particularly for chemistries other than vanadium in which electrolyte mixing is unacceptable [169].

Other Emerging Technologies Slight modifications to the ubiquitous alkaline battery (e.g., Duracell batteries) utilizing a powdered zinc anode, manganese dioxide cathode, and potassium hydroxide electrolyte, make the system rechargeable. These batteries are currently plagued by very short and highly DoD dependent cycle lives (on the order of 10 or fewer cycles at high DoD) with excessive capacity loss between cycles (approaching 50% between the first and second cycle in some cases) [169]. Due to this massive life cycle performance differential between this chemistry and others, rechargeable alkaline batteries have only a small and declining market share. However, modifications have been proposed to overcome cycling challenges, with one ARPA-E supported high-risk project [169]. Sodium ion batteries function in principle like lithium-ion batteries do-by shuttling positively charged ions between electrodes. Sodium ion batteries differ from the sodium beta batteries by the use of non-reactive electrode materials allowing the elimination of the ceramic separator and enabling room temperature operation [169]. The combination of highly available materials with aqueous electrolyte and low voltage cells has the potential to provide the low cost and high safety necessary for grid applications, with cost claims competitive with lead-acid, but with cycle life exceeding 5000 cycles and 100% DoD [169]. There are a number of other emerging chemistries in the early stages of research, including nitrogen-air¹³⁷ and a liquid metal battery [169].

Challenges There are a large number of diverse battery chemistries in various stages of development and commercialization. Several projects have demonstrated competitive or near competitive economics for power grid applications [169]. The rapid response of batteries makes them well suited for ancillary service applications such as frequency regulation, although they must demonstrate long calendar and cycle life, which is a challenge for many available battery technologies [169]. Batteries will compete with other newly commercialized technologies such as flywheels for short duration ancillary services. For longer-duration application, reduced capital cost is the primary requirement. A single battery technology has yet to emerge as a likely market leader for the many potential applications for grid storage. R&D will likely further improve battery technical performance and reduce costs for multiple technologies. Engineering and improved manufacturing techniques will also reduce costs and increase reliability for many of the battery types under development [169].

1.4.2 Batteries for Electric Transportation

This section discusses battery technologies with the greatest potential for use in electric transportation. Compared to more grid-oriented storage technologies, batteries for electric vehicles need to have higher energy density, storing more energy for a given weight or volume, and therefore can be lighter, offering longer drive ranges. Because some vehicle battery technologies may also be suited for grid applications, the distinction may not be a rigid one, but it highlights significant differences in specifications and development that ease the discussion [169]. In general, DOE R&D efforts on vehicle batteries are in two main programs: Batteries for Advanced Transportation Technologies, which is a fundamental research program focused on new materials, and Advanced Battery Research, which focuses on scale-up and commercialization of technologies [169]. Private sector R&D efforts in the United States are conducted by the United States Advanced Battery Consortium (USABC), led by the big three U.S. auto makers Chrysler, Ford, and General Motors in cooperation with the DOE. USABC has funded a number of advanced battery development and technology assessment contracts, in some cases with DOE cofunding [169].

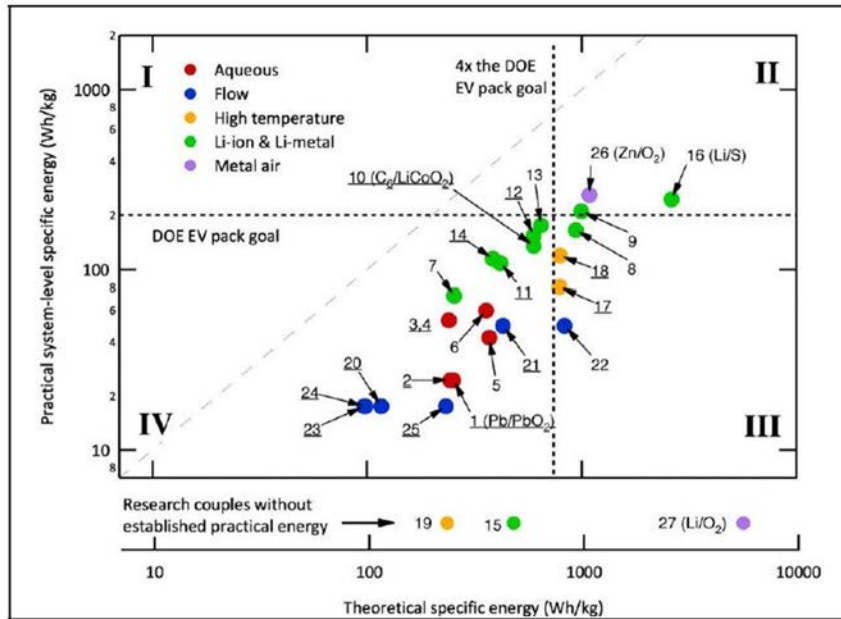
Nickel Further development of nickel-cadmium and nickel-hydrogen batteries is unlikely due to the use of toxic cadmium and high cost, respectively. R&D topics for NiMH batteries include improving cold temperature performance, reducing self-discharge rates, increasing power, and extending cycle life [169]. Cost is also an issue, but is difficult to address through R&D since economies of scale in production have already been achieved, and a large fraction of the cost of NiMH batteries is due to the cost of nickel. Nickel-zinc batteries offer improvements relative to NiMH, but they are currently limited by poor cycle life. Overcoming this obstacle requires a solution to the zinc dissolution and plating problems [169].

Lithium-Ion A significant number of research efforts in industry, national laboratories, and academia are presently devoted to improving cost, safety, energy density, cold temperature performance, and longevity of Li-ion batteries - a key focus of DOE vehicle technology R&D [169]. Especially for large format automotive cells, increasing the scale of manufacturing is often cited as a likely pathway to reduce cost. To this end, \$2.4 billion in ARRA funds were awarded in late 2009 to create a U.S. manufacturing base capable of supporting the annual production of 500,000 electric vehicles by 2015, resulting in a projected 70% decrease in battery cost [169]. A large portion of such scale-induced cost reductions is based on the commoditization of materials, reported to make up 60% of current cell costs [169]. The active materials alone (anode, cathode, and electrolyte) have been shown to make up approximately 20% of costs [169]. Thus, development of anodes and cathodes incorporating lower-cost materials (such as iron rather than cobalt) is another route actively being pursued. Safety is the foremost concern for many current and potential Li-ion bat-

tery markets, especially in light of well publicized laptop computer fires and fires following Chevrolet Volt crash tests involving Li-ion battery technology. Although such events are isolated, they merit concern, particularly in automotive applications. Electrode coatings currently under investigation can stabilize the electrode-electrolyte interface, benefiting not only safety but also cell longevity. Non-flammable electrolyte systems, still in development, hold similar promise [169]. Finally, system level approaches have introduced better thermal management and protective circuitry. Low-temperature response, long-term degradation, specific energy, and other aspects of battery performance also show room for improvement, although in many cases they are already superior to competing technologies. It should be noted that long-term improvements in cell degradation and specific energy, achievable with advanced cathodes and anodes, electrode coatings, and other technical enhancements, also have the potential to reduce the cost of Li-ion cells on a dollars per kWh basis. Noteworthy are efforts funded by ARPA-E, including three-dimensional electrodes developed by Applied Materials and all solid-state batteries developed by Planar Energy [169].

Lithium titanate has been offered as an alternative to graphite as an anode material. Lithium titanate anodes may provide high stability by operating at a much higher voltage versus lithium than carbon anodes do, by greatly reducing the chance of lithium plating, and by eliminating electrolyte reduction and the need for the SEI layer. This chemistry improves safety, longevity, and efficiency, but has a significantly lower cell voltage. Combined with a specific capacity (capacity per unit mass) about half that of graphite, a lithium titanate cells energy storage capability is reduced by as much as 50% compared to the conventional lithium-ion cells [169]. Similar concerns arise for other metal-oxide anodes currently under evaluation. Using a silicon anode also is under extensive study, as it offers an extremely high theoretical specific capacity. Volume change in the cell during charge/discharge is the major concern. Such extreme volume expansion can cause particle fracturing and loss of electronic conductivity, leading to high irreversible capacity loss and vastly reduced cycle life [169].

Lithium-Sulfur The promise of practical specific energy that is at least twice that of Li-ion is enticing to long-term PHEV goals. However, much work remains to be done to improve Li-ion specific energy while addressing capacity decline, self-discharge, and safety [169]. There are many ongoing efforts to address these challenges, such as new cathode structures reliant on different porous carbons [169], and possibly doped or fictionalized porous carbons to stabilize the polysulfide products. Surface coatings for increased sulfur utilization, stability, and conductivity, as well as new electrolytes formulated for increased conductivity and shuttle control, etc. are also under investigation [169]. The ARPA-E BEEST program awarded \$ 5 million last year to a consortium including Sion Power, LLC, BASF, Lawrence Berkeley National Laboratory, and Pacific Northwest National Laboratory to develop lithium-sulfur batteries with a 300 mile range between charges (about three times that of conventional lithium batteries).



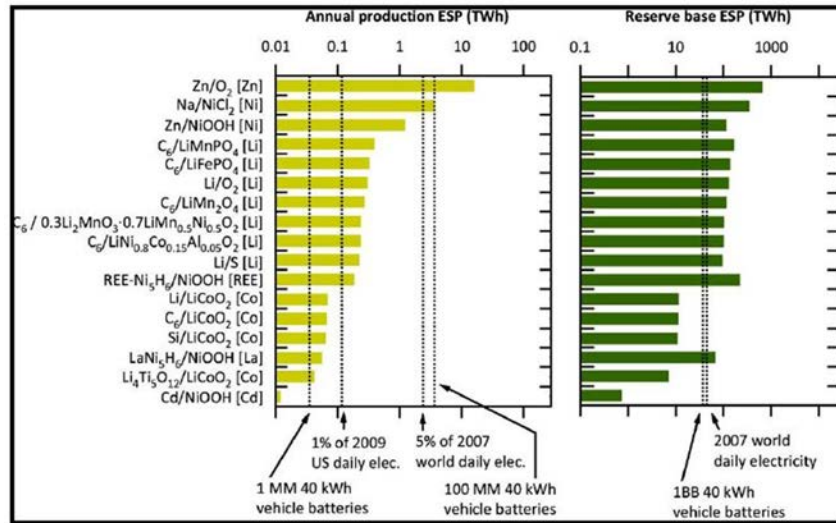
Source: C. Wadia, P. Albertus, and V. Srinivasan, 2011.

Key: 1= Lead-Acid, 2=Ni-Cd, 3-5=Nickel Metal Hydride, 7-16=Li-ion and Li-Metal, 17=Sodium Nickel Chloride, 18=Sodium Sulfur, 20=Vanadium Redox, 21=Zinc Bromine, 22-25=Other Flow Batteries, 26-27=Metal-air.

Notes: Specific energy is based on the weight of active materials alone. The DOE pack goal for an EV with a 40 kWh battery pack is shown, as well as the approximate theoretical energy required for a couple to have a chance of meeting the pack goal. Chemistries that have demonstrated very good reversibility (i.e., a long cycle life) are underlined.

Figure 1.9: Parctical versus theoretical energetic capacity [169]

Metal-Air With some minor differences among the different design variants, the core challenges for metal-air batteries lie with the obstruction of the active electrode surface, along with other challenges typical of metallic anodes, such as volume change and loss of uniformity during cycling [169]. Protecting and stabilizing the anode is of particular importance where lithium is used, as it not only represents a barrier to long-term performance, but also to safety. Most current R&D efforts focus on overcoming the energy loss between charge and discharge at the air cathode by employing suitable catalysts [169]. Additional challenges include evaporation of the electrolyte and contamination when using ambient air. The use of ionic and solid electrolytes has the potential to address evaporation, but typically degrades efficiency and increases cost. Alternatively, evaporation and air contamination can be approached at the system level by using closed or filtered air systems, but such systems bring added cost, complexity, and mass. Noteworthy funding for metal-air battery R&D includes a \$5 million grant under the ARPA-E program and support from the Oregon Department of Energys Small Scale Energy Loan Program (SELP), to ReVolt Technology, LLC in 2010, that published datasheets demonstrating a few hundred cycles of charge-and-discharge on their Zinc-air batteries [169].



Source: C. Wadia, P. Albertus, and V. Srinivasan, 2011.

Notes: The elements in brackets at the right side of the labels are the limiting elements in each couple. Production is raw material for all uses

Figure 1.10: Potential of energy storage with respect to the available material resources [169]

Challenges The primary deployment challenges of electric vehicle batteries are high initial cost and limited performance. Achieving large-scale deployment will require batteries with higher energy density and battery chemistries that use abundant materials. Figure 1 provides the specific energy of a range of battery types compared to the DOE target for electric vehicle battery packs (200 Wh/kg) [169]. Currently, only three chemical couples can practically meet that goal: one variant of lithium-ion, one variant of lithium-metal, and one variant of metal-air (the upper right quadrant in Figure 1). Another potential deployment challenge is the potential scarcity of raw materials. Figure 2 provides an estimate of the 2010 production and reserves of materials for the batteries discussed in this chapter. The material requirements are measured in TWh, with total annual production (for all uses) compared to the potential worldwide needs of 1 million and 100 million 40 kWh battery packs, and total estimate reserves compared to the need for 1 billion battery packs. This demonstrates that large-scale deployment of lithium-based batteries will require greatly increased production rates. Total material availability may also be a challenge for batteries using cobalt.

Type	Primary (non-rechargeable)	Secondary (rechargeable)
Solid State batteries or SSB		Thin film Li-cells Li-Polymer based Na-based SSB
Conventional Batteries	Zn-MnO ₂ (alkaline) Li-SO ₂ Li-SOCl ₂ Li-FeS ₂ (Li/(CF) _x)	Pb-acid Pb-PbO ₂ Nicad Ni-Cd Li-ion LCO Li-ion LMO Li-ion NMC Li-ion LFP Li-FePO ₄ Li-ion Li-S Li-ion Li-Si
Metal air batteries	Zn-air Mg-air Al-air Li-air Carbon-air	
Flow Batteries		Hydrogen fuel cell PEM Sodium Nickel chloride Sodium-sulfur (NaS) Iron-Chromium (ICB) Vanadium redox (VRB) Zinc-Bromine(ZNBR)
Liquid		Hot Mg-Sn LMB Hot Na-based

Table 1.1: Summery of electrochemical EES

Chemistry	Nominal Voltage [V]	Specific Energy [Wh/kg]	Energy Density [Wh/L]	Specific Power	Operating Temperature Range [°C]	Cycle Life
Pb-Acid	2,0	30	90	High	-40 to +60	250 - 500
Ni-Cd	1,2	35	100	Med./High	-40 to +45	300 - 700
Ni-MH	1,2	60 - 80	200 - 270	Med./High	-30 to +65	800 - 1200
Li-FePO ₄	3,3	70 - 140	220 - 290	Med./High	-40 to +55	1000 - 2000
LTO	2,2	70 - 90	90 - 110	Very High	-40 to +55	5000 - 30000
NMC	3,7	140 - 200				1000 - 2500
LCO	3,7	160				1000
Li-Sulphur*	2,15	550	320	High	-20 to +45	300 - 650
Li-Silicon*		>300				500 - 600
Hot Na*	1,7	200		Medium		4500

Table 1.2: Summary of commercially available secondary battery characteristics, (*) close to commercialisation, data from reference [200] and [212].

Chapter 2

Applications of batteries in particular Lithium-ion

2.1 Static applications

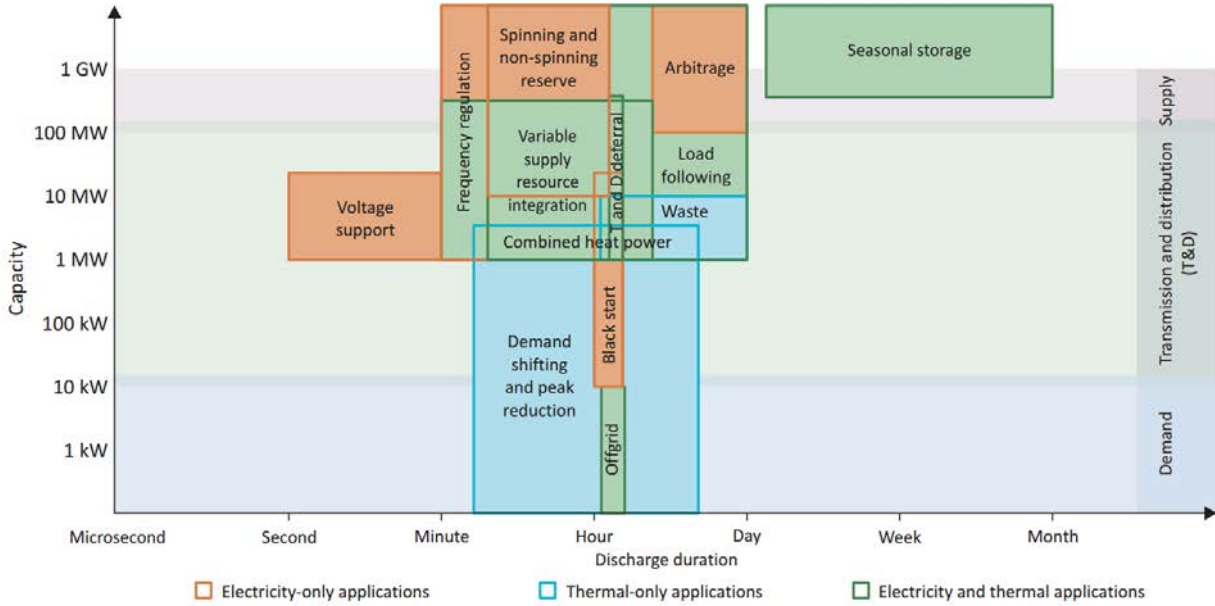


Figure 2.1: Power requirement versus discharge duration for some applications in today’s energy system, from reference [11]

Figure 2.1 illustrates the power requirements and cycle duration of typical static applications.

Li-ion batteries have been deployed in a wide range of energy-storage applications, ranging

from energy-type batteries of a few kilowatt-hours in residential systems with rooftop photovoltaic arrays to multi-megawatt containerized batteries for the provision of grid ancillary services.

The Li-ion battery is considered as a good candidate for applications where the response time, small dimension and/or weight of equipment are important (milliseconds response time, ~ 1500 to $10\,000$ W/L, ~ 75 to 200 Wh/kg, ~ 150 to 2000 W/kg). Li-ion batteries also have high cycle efficiencies, up to $\sim 97\%$. The main drawbacks are that the cycle DoD can affect the Li-ion battery's lifetime and the battery pack usually requires an on-board computer to manage its operation, which increases its overall cost. [122]

Several companies have experience in using Li-ion batteries in the utility-scale energy market. The U.S. based AES Energy Storage has been commercially operating a Li-ion BES system (8 MW/2 MWh in 2010, enlarged 16 MW in 2011) in New York for supplying frequency regulation. The AES also installed a 32 MW/8 MWh Li-ion BES system (Laurel Mountain) for supporting a 98 MW wind generation plant in 2011 [204]. Currently, the largest European Li-ion battery EES trial is happening in the UK. The project will deploy a 6 MW/10 MWh Li-ion battery at a primary substation to assess the cost effectiveness of EES as part of the UK's Carbon Plan [91]. The companies claimed that the storage could save more than \$9 million compared to traditional system upgrades; the project can be used to balance the intermittency of wind and other renewables [91]. Also, in December 2013 Toshiba announced a project to install a 40 MW/20 MWh Li-ion battery project in Tohoku, which will help integrate renewables into the grid [80].

The actual applications of Li-ion storage are difficult to pinpoint because many studies reach different conclusions. This can be caused by the continuous improvement with respect to cost, performance and safety in Li-ion technologies. The rated power of Li-ion systems ranges from several kW to 100 kW according to [70] (2009), from 1 to 100 MW according to [43] (2010).

The rated energy capacity ranges from 4 kWh to 10 MWh [122], larger installations will certainly become a reality in the near future. Tesla is pushing the boundaries building its first 1 GWh storage plant in the Californian desert. Personally I suspect that they will use old car batteries in these applications.

With respect to safety, older Li-ion batteries containing metallic lithium are the least safe (another factor is the structure of the cathode (for instance LFP vs LTO) as we will see in Chapter 3. The prismatic pouch cell utilizing polymer electrolytes are much safer than their predecessor. However the polymer electrolyte is in some cases still flammable. Some new generation solid state electrolytes are said to be completely non-flammable. In addition they can not leak making them safer than what we had up until now. This is of key importance when scaling battery technology because even though the possibility of a cell catching fire might be small, scaling means stacking and if one cell catches fire, it might possibly cause a chain reaction.

Static applications can be divided in many classes and subclasses. In all these applications

batteries are considered as an alternative [211]. On the GWh scale, Li-ion technology is still too expensive. Second use of BEV batteries can drastically reduce the cost. These batteries have less than 80% of their initial capacity. Nevertheless, when looking at the capacity in time, the capacity decreases due to parasitic reactions. Two evolutions can be identified. The first, calendar aging, leads to a logarithmic decrease (assuming a constant ambient temperature). The second evolution is function of the number of cycles (assuming a constant DoD). This yields a linear decrease in capacity however the slope of this decrease is not constant. At a certain moment, depending on many factors, the slope suddenly drops leading to an accelerated decrease in capacity. An effective cheap and fast solution in determining the state of health will certainly help in the second life applications as this will enable to better predict this steep and sudden drop [68].

Understanding the economics of energy storage is often challenging because the value streams associated to such investments are very case sensitive. For example, an EES might be designed for a particular cases (capacity and power), the same system could also provide a value stream through frequency regulation or could enable deferral of investment in upgraded power substations.

To conclude, today Li-ion is not always the best solution for storage but it is with no doubt the swiss army knife among electrochemical EES. In situations where **size, weight and reactivity** matter, it offers great advantages over other technologies, combining several value streams is also important when choosing adequate technology. As production builds up and costs comes down, Li-ion becomes increasingly appropriate in a broad range of applications. With respect to safety SSBs are the preferred option, Manganese, Li-FePO₄, and polymer electrolytes are currently the best commercially available options.

Compared to lead-acid batteries, Li-ion is much more investigated. For this reason Li-ion will probably evolve faster than competing technologies. A study made by AllCell [67] makes a good comparison between both technologies. They conclude that the difference in value over cost makes Li-ion even more desirable than lead acid and even more in hot climates despite the higher initial cost.

Tables 2.1, 2.2, 2.3, 2.4 and 2.5 present a qualitative answer to when batteries and more specifically Li-ion technology is desirable, competing technologies are indicated as well. In these tables we assume the broad scope of Li-ion technology, (ie. from high power LIC to high energy capacity).

It is noticeable that Li-ion technology can be used in many applications. In back-up power systems, the batteries are nearly always charged. This shortens the calendar life, additionally advantages such as high Coulombic efficiency (75% to 94%) are of no use in these applications. For this reason a cheaper battery seems more appropriate.

Application	Power [kW or MW] Used	Response time Promising	Discharge duration Li-ion potential	References
Peak shaving	1-500MW or 100kW- 100MW PHS, CAES, Batteries	minutes Flow batteries, Solar fuel, Fuel cell, TES	2-8h <10h Medium	[122] [41] [57] [195] [118] [158]
Load following	1- 500MW PHS, CAES, Batteries	minutes Flow batteries, Solar fuel, Fuel cell, TES	2-4h Medium	[122] [41] [57] [95] [98]
Light commercial load following	<200kW Batteries, SMES Flow batteries	milliseconds Fuel cells	min-h High	[122] [41] [57] [113] [75]
Residential load following	<5kW Batteries, SMES	milliseconds Flow batteries Flywheels and Super-capacitors	5min-5h High	[99] [85]
Load leveling	1MW-500MW PHS, CAES, Batteries	minutes Flow batteries, Fuel cell, TES	12h and more Medium	[122] [41] [95] [98]

Table 2.1: Specifications of static applications along with desirable EES, *part 1*

Application	Power [kW or MW] Used	Response time Promising	Discharge duration Li-ion potential	References
Area regulation	1-40MW Batteries Flywheels	seconds Super-capacitors	15-30min High	[119] [57]
Standing reserve	1-500MW 1-100MW Batteries	<10min CAES, Flow batteries PHS, Fuel cells	1- 2h 1-5h High	[122] [57] [55] [39] [24]
Spinning reserve	Up to MW level Batteries	a seconds CAES, Flywheel Flow batteries SMES, Fuel cells	30min-a few h High	[122] [57] [94] [53] [134]
Emergency back-up	< 1MW Batteries, Flywheels, Flow batteries	milliseconds CAES, Fuel cells	< 24h Low	[122] [48] [181] [104]
Tele- communication back-up	A few kW Batteries	milliseconds Fuel cells Super-capacitors Flywheels	min-a few h Low	[122] [41] [195] [181] [101]

Table 2.2: Specifications of static applications along with desirable EES, *part 2*

Application	Power [kW or MW]	Response time	Discharge duration	References
	Used	Promising	Li-ion potential	
UPS	Up to 5MW Super-capacitors, Batteries, Flywheels	seconds SMES, Flow batteries, CAES, Fuel cells	min-h Low	[122] [41] [247] [173] [105]
Voltage support	1-10MW Batteries, Flow batteries	milliseconds SMES, Flywheels, Super-capacitors	15min-1h High	[122] [57] [33] [135] [172]
Transmission support	10-100MW Batteries SMES	milliseconds Flow batteries, Flywheels Super-capacitors	2-5sec. High	[122] [57] [41] [82] [195] [184] [87]
Transmission congestion relief	1-100MW Batteries SMES	>1h Flow batteries, Flywheels Super-capacitors	3-6h High	[122] [119] [41] [57] [82] [195] [184] [87]
Transmission upgrade deferral	250kW-5MW Batteries SMES	>1h Flow batteries, Flywheels Super-capacitors	3-6h High	[122] [119] [41] [57] [82] [195] [184] [87]

Table 2.3: Specifications of static applications along with desirable EES, *part 3*

Application	Power [kW or MW] Used	Response time Promising	Discharge duration Li-ion potential	References
Substation on-site power	1,5-5kW Batteries	>1h Flow batteries, Flywheels Super-capacitors	8-16h Medium	[57]
Time-of-use, energy cost management	1kW-1MW PHS, CAES, TES, Flow-batteries, Batteries	minutes Fly wheels Fuel cells	4-6h hours-days High	[122] [57] [8] [46]
Demand charge management	50kW-10MW Batteries	< 15min Flow batteries	5-11h High	[57]
Electric service reliability	0,2kW-10MW Flywheels, Batteries, SMES, Super-capacitors	milliseconds Flow batteries	5min-1h High	[122] [57] [82] [9] [198]
Power quality	0,2kW-10MW Flywheels, capa- citors, Batteries Super-capacitors	milliseconds Super-capacitors SMESS	10sec.-1min msec.-sec. High	[122] [57] [82] [9] [198]

Table 2.4: Specifications of static applications along with desirable EES, *part 4*

Application	Power [kW or MW] Used	Response time Promising	Discharge duration Li-ion potential	References
Renewables time-shift	1 kW -500 MW Flywheels, Batteries Super-capacitors	1 s Flow batteries Fuel cells, SMES	3-5 h High	[122] [41] [57] [46] [178] [71] [235]
Renewables capacity farming	1 kW -500 MW Flywheels, Batteries Super-capacitors	1 s Flow batteries Fuel cells, SMES	2-4 h High	[122] [41] [57] [46] [178] [71] [235]
Wind/PV grid integration short duration	0,2 kW -500 MW Flywheels, Batteries Super-capacitors	1 s Flow batteries Fuel cells, SMES	10 s-15 min High	[122] [41] [57] [46] [178] [71] [235]
Wind/PV grid integration long duration	0,2 kW -500 MW Flywheels, Batteries Super-capacitors	1s Flow batteries Fuel cells, SMES	1-6 h High	[122] [41] [57] [46] [178] [71] [235]

Table 2.5: Specifications of static applications along with desirable EES, *part 5*

2.2 Mobile applications

Because of the high energetic density (mass-specific and volume-specific) and good power capabilities of Li-ion, Li-ion batteries can be found in a broad range of mobile applications. We can separate them in small and large scale applications.

Portable:

- cellphone;
- portable computer;
- medical application;
- vacuum cleaners;
- electric bikes;
- robotics small;
- drones;
- and others.

Traction:

- traction for heavy duty;
- traction of EV, PHEV;
- drones, (even manned: solar impulse);
- and others.

The most famous and demanding application using battery technology is without a doubt the electric vehicle. With respect to scope of LBATTS we choose to only address this last application in more detail.

The flexibility of Li-ion technology in EV applications, from small high-power batteries for power buffering in hybrids, to medium-power batteries providing both electric-only range and power buffering in plug-in hybrids, to high-energy batteries in electric-only vehicles, make them an attractive solution for EVs.

Figure 2.2 illustrates the different types of electric vehicles along with their electric characteristics. The first class (EV) are often denominated with BEV (Battery Electric Vehicle). We notice that voltage can reach up to 750 Vdc. Higher voltages are possible but the

		Vehicle category				
		Micro HEV	Mild HEV	HEV	Plug-in Hybrid	EV
Function	Start / Stop					
	Regen. Brake					
	Power assist					
	Electric Drive			+/- 100m	+/- 10km	Up to 200km
Electrical specifications	Operating Voltage	12V		750V		
	Energy level	0,3kWh		200kWh		

Figure 2.2: Classes of electrical vehicles, roadmap 2030 [176]

price of the switching IGBT's becomes so high that constructors prefer to avoid this. The Eurobat road-map 2030, see reference [176], predicts that BEV will have capacities up to 200 kWh. This is several times higher than the contemporary BEVs. Today's battery packs have capacities of 15 to 20 kWh for HEVs and up to 50 kWh for EV's [10]. For comparison Tesla's model S (2012) comes in three models, the lowest and highest capacity versions are listed below:

- 75 kWh 225 kW NEDC: 390 km EPA: 335 km
- 90 kWh 569 kW NEDC: 502 km EPA: 426 km

Additionally the Tesla model S is a high end car, when we look at the Nissan LEAF which is one of the more affordable BEV, the energetic capacity is much less. The Leaf has also two versions:

- 30 kWh EPA: 172 km
- 24 kWh EPA: 135 km

Standardized test procedures are necessary to compare different vehicles. The EPA Federal Test Procedure, commonly known as FTP-75 for the city driving cycle, consists of several tests defined by the US Environmental Protection Agency (EPA) which allow to measure exhaust gas emissions and fuel economy of passenger cars (excluding light trucks and heavy-duty vehicles). The NEDC-test is another standardized test procedure often used in Europe. The NEDC-test (New European Driving Cycle) is known to overestimate the actual range. In 2017/2018 the test-procedures will be harmonized under the WLTP (Worldwide Light Vehicle Test Procedure).

Aside from Li-ion technology, other technologies will still play an important role in this market the coming decade. Each type of vehicle has specific requirements towards the used EES.

2.2.1 Start-stop vehicles

Start-stop vehicles automatically shut down the IC-engine (Internal Combustion) when the vehicle is at a halt (and when the battery is charged enough). The installed 12 Vdc battery must provide higher deep cycle and cycle capabilities in order to deal with the frequent stops.

Appropriate technologies are: advanced lead-based, like the AGM (Absorbent Glass Matt) or enhanced flooded batteries (EFB). [176]

2.2.2 Micro-hybrid, advanced micro-hybrid and mild-hybrid vehicles

In this application the start-stop function is combined with regenerative braking. The kinetic energy is stored in a high-power, low-energetic capacity EES and is used to boost the next acceleration.

Appropriate technologies are: advanced lead-based (AGM or EFB) or lithium-ion batteries. [176]

2.2.3 Full hybrid electric vehicles HEV's

These vehicles have similar characteristics as the previous class but the battery has a higher capacity allowing for a small range full electric driving. The energetic capacity is around 1-2 kWh. The batteries are designed for high cycle life ($\sim 300\ 000$ shallow cycles)

Appropriate technologies are: Nickel-Metal-hydrate and Li-ion batteries. [176]

2.2.4 Plug-in hybrid electric vehicles PHEV's

PHEV's are equipped with high energetic capacities (10-15 kWh). The battery is the main energy source for short distances (50-100 km). Once depleted the battery takes on the function of HEV's. The internal combustion engine can run at optimal working conditions to recharge the battery. Batteries for PHEV's are optimized for shallow as well as deep cycle durability. The technology is mature and provides a good combination in range and efficiency.

Appropriate technologies are: Lithium-ion and Sodium-Nickel-Chloride for the heavy duty vehicles. [176]

2.2.5 Battery electric vehicle BEV's

BEV's are sometimes referred to as EV's. In these vehicles the battery is the only energy source. A high-energy capacity is required but lower cycle life can be tolerated (2000-3000). The use of hybrid systems (super-caps) for energy recuperation and strong acceleration allows for less high power requirements on the main battery. Today the capacities range from 24 kWh for the Nissan Leaf to around 90 kWh for the most high-end vehicles. With the advance in Li-ion technology one can expect that the capacity will double in the next 10 to 15 years.

Appropriate technologies are: Lithium-ion and Sodium-Nickel-Chloride for the heavy-duty vehicles. [176]

2.3 Second-life applications

Initial investigations into the further use of electric vehicle batteries in a secondary system were motivated by the need to decrease the capital cost of electric vehicles [130]. It was presumed that by making an EV price competitive with traditionally powered vehicles, a sustainable market for electric vehicles could be created. In 2008, studies reveal that the battery was responsible for approximately 2/3 of the vehicle price [214]; it was the natural starting point for driving cost reductions. In order to make EVs competitive, the cost of the battery would need to be reduced by approximately 50% [152]. This could be accomplished either through dramatic technology improvements, or by decoupling the battery from the vehicle and analysing different value opportunities such as battery second use.

The first study for battery second use was conducted by Argon National Laboratories (ANL) by Pinsky et al. for the United States Advanced Battery Consortium (USABC) in the late 1990s. The study was based on nickel metal hydride (NiMH) batteries as they were the most promising EV battery technology at the time. The goal of the study was to assess if used, de-rated, EV batteries could provide the same performance as lead-acid batteries in stationary applications. The study compared the performance of used NiMH cells and new lead-acid cells when cycled through application specific load profiles. In every case the used batteries performed at least as well if not better than the new lead-acid batteries [130].

After Pinsky et al. concluded that used EV batteries were competitive in terms of performance, Sandia National Laboratories (SNL) conducted a study to determine if used batteries could be priced competitively in the stationary market. The study, documented in a report by Cready et al. assumed a used EV battery could be sold at a price that

would make EVs price competitive with traditional vehicles; not based on a market price. In other words if battery prices need to be 150 \$/kWh to compete with traditionally powered vehicles, but the actual price of the battery is 300 \$/kWh then the battery would be sold for 150 \$/kWh after vehicle use. The price to refurbish the battery would be added to the 150 \$/kWh, to get the price a stationary storage system integrator would pay for the battery. The cost to the system integrator was then compared to high and low thresholds for system costs for eight stationary applications [42].

The majority of subsequent studies have either built upon or refined the work done by Cready et al. [146], [140] and [145]. Narula et al. used the reprocessing cost estimates from Cready et al., and integration cost estimates and system benefit data from Corey and Eyer [58], to determine the potential benefit/cost ratios for energy storage systems using used EV batteries [140]. Neubauer et al. used the same data to compare the potential market volume for suitable stationary applications and the volume of returned EV batteries [145]. This analysis was then later expanded on to determine the payback period of systems using secondary batteries [146]. In another related study Williams et al. used the same ground data from Corey and Eyer, and Cready et al. to analyze the sensitivity of initial EV battery lease payments to various second use cost assumptions [224]. On the other hand, Navigant Research expects that the global second-life battery business will grow from \$3 million to \$16 billion between 2014 and 2035 (see Figure 2.3) [21], [179]. For example, in 2015, CEO of FreeWire told that GTM has purchased repurposed Nissan batteries for 100 \$/kWh [177], [129]. Besides, Tesla expects that selling large Power pack batteries for grid use will reach up to 90% of its energy storage business [129].

The studies mentioned above found that there is a potential for second-life batteries in the future provided that the needed cost for refurbishing, operation, maintenance and power electronic circuits should be reduced to make the overall cost of the second-life systems more competitive.

2.3.1 Refurbishing costs

To refurbish the used batteries, this step includes collecting, testing, inspecting, disassembling, sorting, and reassembling the battery pack or modules as needed [130]. Costs associated with refurbishment depend on the facility, labor, variable material, and capital equipment costs. The size of the facility and most cost efficient processes will depend on the required production volume and reprocessing level [130]. Most of studies use, or extrapolate upon, the reprocessing costs calculated by Cready et al. These costs assume that vehicle battery modules are repurposed at a volume of about 318 modules per day. Each NiMH module has a capacity of 2.1 kWh and module voltage of 12 V. Each module is tested for 40 hours in order to establish its capacity and power rate capabilities, sorted according to state of health and then assembled into a standardized battery unit consisting of 21 modules connected in series. The final product or StatPack has a nominal 25 kWh capacity and a voltage of 235 V. Each StatPack includes all equipment required for the

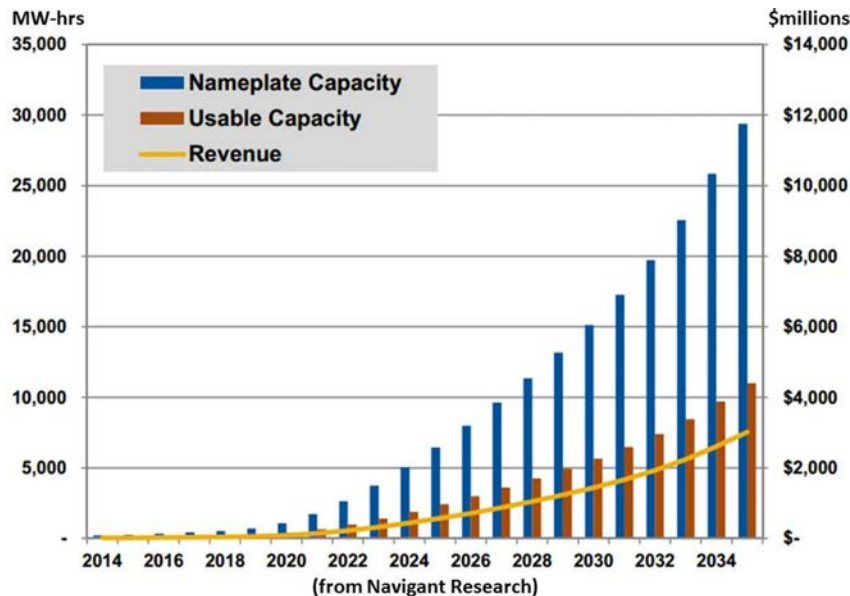


Figure 2.3: Capacity and revenue of second-life batteries, world markets: 2014-2035 [179]

thermal and electrical management of the cells including fans or coolant channels, module interconnects, sensors, and electronics. The cost breakdown of this system can be seen in Figure 2.4. The final product would then be sold to a system integrator.

Although this analysis was established with NiMH batteries, the same general procedures can be directly applied to lithium ion cells. The resulting refurbishment cost is 65 \$/kWh, which includes an internal 15% rate of return for and a facility lifetime of 10 years. Narula extrapolated upon these numbers to determine costs associated with a facility capable of refurbishing 142,300 full packs per year. In their study Narula et al. assumed that the same equipment and facility requirements as Cready et al. This is not correct since Cready assumed reprocessing on a module level with a volume of 2,880 packs per year. Therefore Narula established a much lower repurposing cost of 2.66 \$/kWh.

Neubauer et al. also extrapolated upon Creadys data, but assumed the same annual throughput on a per kWh basis. As part of their study, Neubauer et al. also included an analysis on the effects of module size and cell failure rate. In order to incorporate this into their study, they had to normalize the facility costs and equipment costs to be able to scale with their module properties. In other words, Cready specified test equipment to test 318 x 2.1 kWh modules per day at 1 C, which cost 1,049,400 \$in 2002. Updating that number to account for inflation in 2011 the equipment cost is approximately 2000 \$/kW. Through their analysis, Neubauer found that at a cell failure rate of $\leq 0.1\%$ there is a very little change in repurposing costs for modules greater than 8 kWh. Therefore a point value of 32 \$/kWh was taken for repurposing costs. If modules are less than 8 kWh, repurposing costs are higher (Figure 2.5).

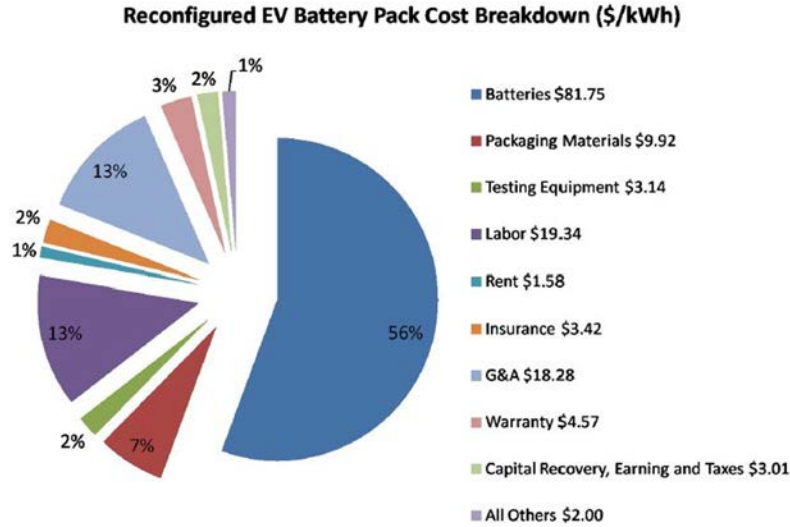


Figure 2.4: Repurposing Cost Breakdown from Cready et al. [42]

2.3.2 Power electronics costs

In addition to the cost of batteries, the system cost includes cost of the power electronics converter for grid connection [140]. The cost of the inverter includes all the wiring costs for the connections of battery packs and/or modules (for series/parallel connections for desired voltage and current levels) and the cost of the inverters control system (digital signal processor for inverter control). As the entire pack from a vehicle will be acquired, the wiring costs will be minimal for the internal connections [140]. In addition, the packs taken from the vehicle will include the voltage, current, and temperature sensors, which will be used in the secondary application, too. Therefore, the costs of the sensors can be deducted from the cost of a regular inverter including necessary sensors. Furthermore, the battery pack in the vehicle will be equipped with required thermal management systems (forced air cooling, heat sink, etc.) and the required pack enclosure. Therefore, the cost of the packing material and the cost of the thermal management unit have not been included in the cost of the power electronic converter [140].

Although all the cost components of the complete storage system are based on dollars per kilowatt-hour, the cost of the power electronics should be based on the power rating. Therefore, the cost of power electronics is given in dollars per kilowatt. Grid connected photovoltaic applications are similar to grid connected battery applications in terms of power electronic conversion systems because in both applications the direct current (DC) input is inverted to alternating current (AC) output at required voltage and frequency. The only difference is the operation of the control system, which does not have any impact on the cost of the power electronics. According to SolarBuzz, a solar market research and analysis company, the current inverter cost is 715 \$/kW as of May 2011 [140]. This cost is based on the average of all current retail prices from inverter manufacturers and weighted

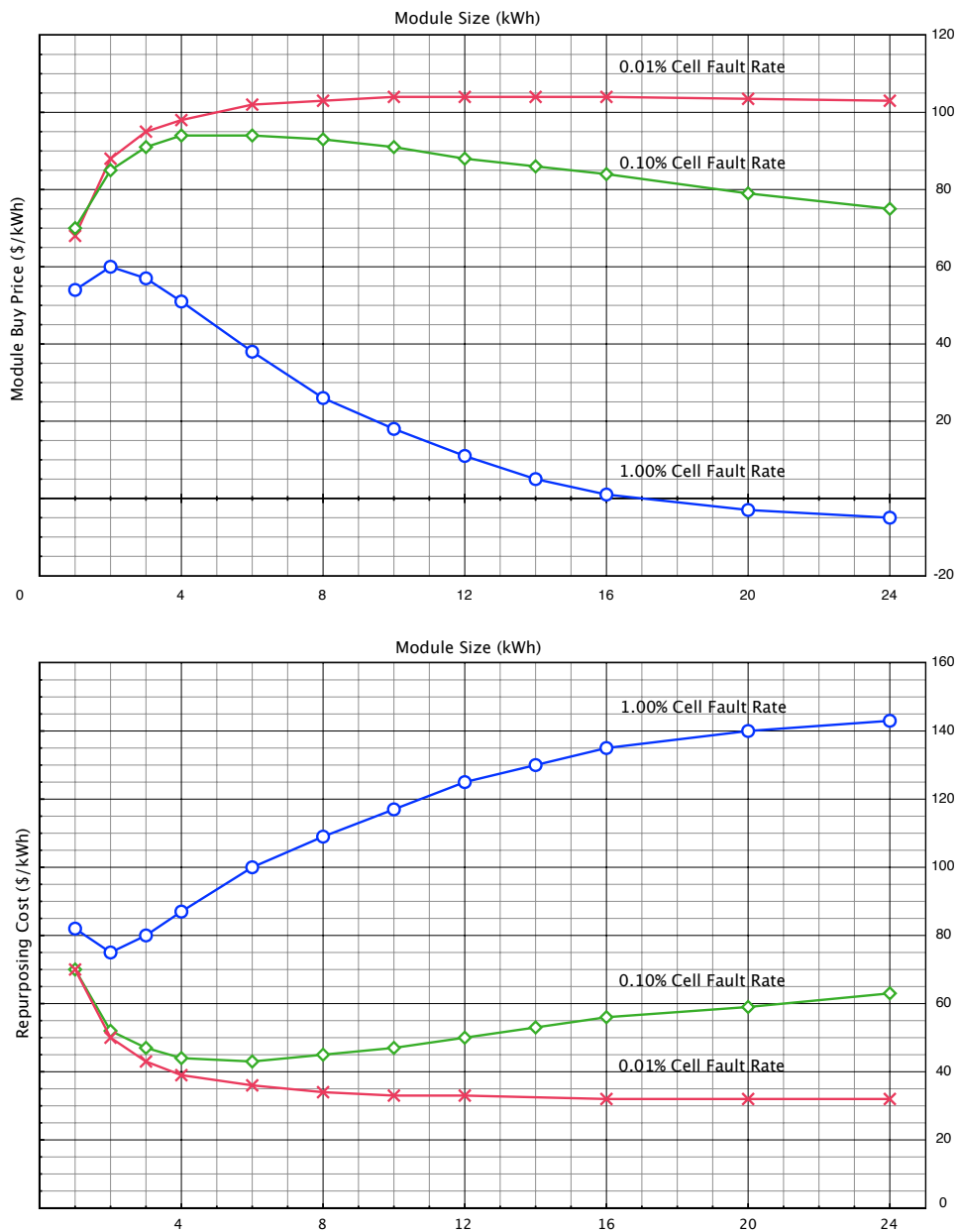


Figure 2.5: Repurposing cost and required module buy price as a function of module size and cell fault rate for a repurposed battery selling price of 132 \$/kWh, reproduced from Neubauer et al. [146]

according to the power level. In this average pricing method, all the global inverter prices, in U.S. dollars, are aggregated into a single index. The cost target of the DOE Office of Energy Efficiency and Renewable Energy Solar Energy Technology Program (SETP) is 100 \$/kW by 2020, including the inverter warranty and the control system functionality [140]. The DOE Vehicle Technologies Program cost target for power electronics is 12 \$/kW peak by 2015 and 8 \$/kW by 2020 [140]. The same targets were also identified in the DOE Electrical and Electronics Technical Team Roadmap [140]. Based on these DOE targets, high and low values for power electronics costs can be estimated at 100 \$/kW and 8 \$/kW, respectively. In a report prepared by Navigant Consulting Inc., experience curves models were developed to determine the relationship between cost of production and production volume, which indicates the level of experience in power electronic product development [140]. In the experience curve models, the cost of production declines by a constant percentage with each doubling of the total number of units produced. This cost reduction rate is called the learning rate and typically ranges from 0% to 35% depending on various technologies. Learning rate typically identifies the rate of cost reduction as the number of units produced increases. For the inverter development technology, the typical value of the learning rate is 10% [140]. Based on 10% and 20% experience learning rates, the relationship between the cumulative production and the production cost percentage is presented in Figure 2.6.

According to the analysis in Figure 2.6, the cost of the inverter is expected to decrease by about 50% if the units produced reaches 100 for a particular application. To have a realistic cost reduction percentage, a learning rate of 10% has been applied to the cost of power electronics targeted by DOE's SETP. Therefore, if 100 units were produced for a particular application, the cost of the power electronic converter would decrease to 50 \$/kW. Therefore, the final high value of power electronics cost is 50 \$/kW, whereas the low value of power electronics cost has been estimated at 8 \$/kW.

2.3.3 Operation and maintenance costs

Operation and maintenance costs or O&M costs include the periodic and unscheduled maintenance, repair, or replacement of failed or damaged battery packs and the maintenance of the power electronic converter.

The annual O&M cost is estimated based on a similar system; the O&M cost of an existing system is divided by the power rating to obtain the dollars per kilowatt per year value. The annual O&M cost does not include the recharging costs of the batteries as the recharging costs will be application dependent. The annual O&M cost used here considers the hardware related O&M costs rather than the application related operational costs. Eyer and Corey [58] and Klein [140] determined the typical O&M cost to be 10 \$/kW-year. However, Rittershausen and McDonagh [183] found \$10,000 annual O&M costs for a 2 MW Li-ion-battery-based energy storage application, which results in 5 \$/kW-year O&M cost. Therefore, for this study, the high and the low value of O&M costs are considered to be 10 \$/kW-year and 5 \$/kW-year, respectively. It should be noted that this also matches the

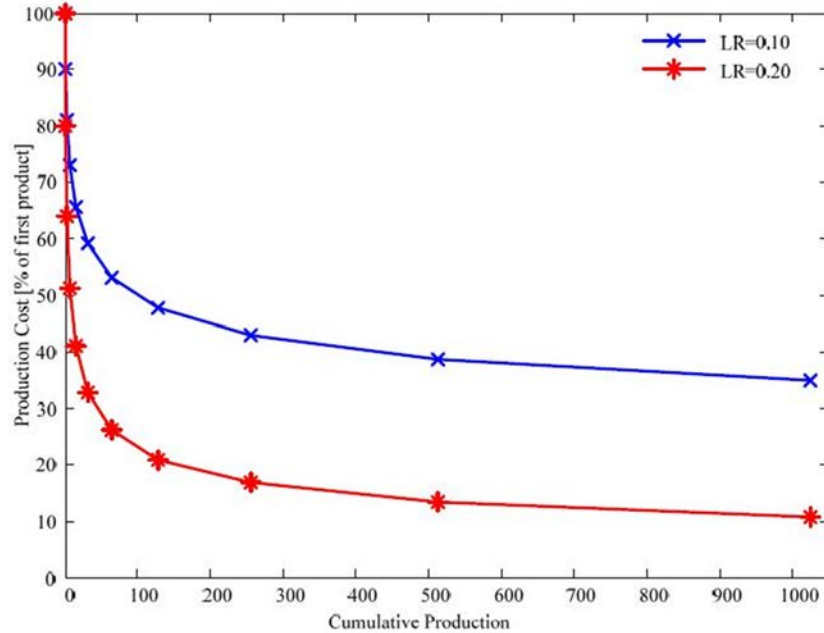


Figure 2.6: Relationship between cumulative production and production cost based on learning rates (LRs) of 10% and 20%, from [140]

assumptions of the EPRI report on electricity energy storage technology options [44]. In the EPRI report, it is stated that the O&M costs were difficult to obtain or unknown for most technologies; therefore, an assumption of roughly 0.5% to 2.0% of the capital costs were used to represent the annual fixed O&M costs in dollars per kilowatt-year. Considering a lifetime of 5 years for the secondary application of batteries, the fixed annual O&M costs can be referred to the capital cost by multiplying the annual O&M cost by the expected lifetime. Therefore, the capitalized O&M costs used for this study are 50 \$/kW (high value) and 25 \$/kW (low value) [140].

2.3.4 System cost

In [140], the total system cost has been calculated to include the price of batteries, transportation cost, power electronics cost, and O&M cost. It should be obvious that the price of batteries depends on the supply, demand, and the price of new batteries. Table 2.6 presents the summary of unitary system costs including the high and low value of the itemized costs for power system-connected energy storage systems employing used batteries.

These data can be used to calculate system costs for a given application. For example, the high and low values of the total cost for an energy storage system with 500kW peak power capability and 1 MWh storage capacity are summarized in Table 2.7 and Figure 2.7.

	Cost of used batteries	Balance of System cost	Refurbishment cost	Transport cost	Operation and maintenance cost
	\$/kWh	\$/kWh	\$/kWh	\$/kWh	\$/kWh
High Value cost	220	50	2.52	126.17	50
Low value cost	75	8	1.68	63.08	25

Table 2.6: Summeary of costs [140]

	Cost of used batteries	Balance of System cost	Refurbishment cost	Transport cost	Operation and maintenance cost
	\$	\$	\$	\$	\$
High Value cost	220000	25000	2520	12617	25000
Low value cost	75000	4000	1680	63080	12500

Table 2.7: Cost breakdown for an example system with 500 kW peak power and 1 MWh capacity [140]

2.4 Market of energy storage based on Li-ion till 2020

When analyzing a certain market, three key questions arise:

- Is the market big enough?
- What are the market trends?
- Is the market profitable enough?

It is important to note that many of the reference documents remain extremely vague with respect to the actual representations they provide, for instance revenue can mean turnover or gain, also few references clearly distinct between cell and module level. Additionally I want to mention that several serious discrepancies (sometimes with a factor 10) between diverse predictions were found, even when the data was provided by the same source. For this reason, the data in this section must be handled with extreme care. To my knowledge the market size expressed in money corresponds to turnover, and the module level is considered. The data is presented as found.

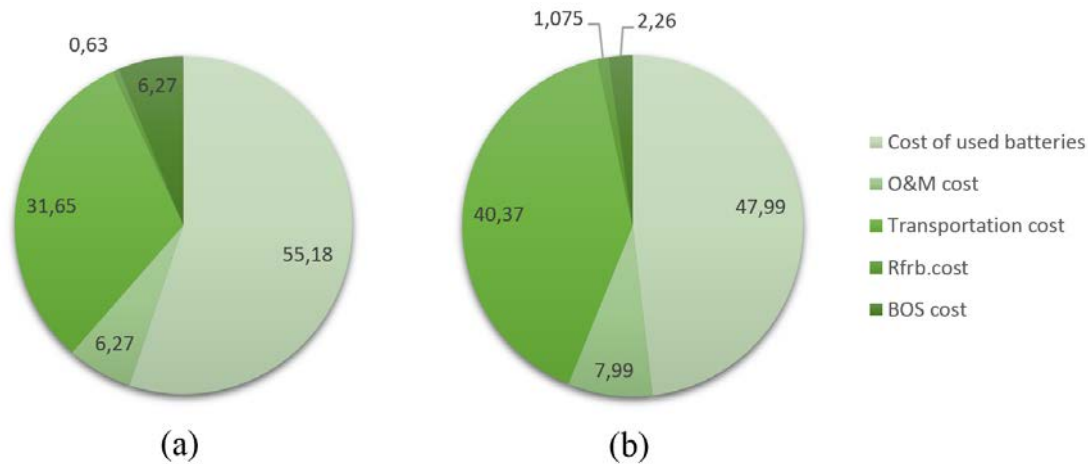


Figure 2.7: Cost share percentages of the energy storage system with 500 kW peak power capability and 1 MWh storage capacity: (a) high value total cost is \$398690, and (b) low value total cost is \$56260, reproduced from [140]

2.4.1 Market size and evolution

The global market for lithium-ion batteries is a fast growing market. The current evolution in production of large-format high-power and -capacity cells facilitates penetration into medium and eventually large-scale applications.

In this market, lithium-ion chemistry competes heavily with established energy storage technologies, such as lead acid. However, key performance characteristics have enabled lithium-ion to increase market penetration, [67], [72]. Today the typical applications are still oriented towards consumer electronics, but the EV market is in full expansion and grid-scale storage is taking off as well.

Reference [180] expected the global lithium-ion market to be worth around \$30 billion in 2015, they predict it will reach approximately \$60 billion by 2020. Reference [123] is a bit more conservative and predicts \$50 billion by 2020. The largest part of this market is in mobile applications, see Figure 2.8.

Static applications

Global electric generation has grown swiftly in order to fulfill the demands of consumers. For instance, from 1973 to 2013, the annual aggregate production of electricity increased from 6144 TWh to 23391 TWh. This represents an average annual grow rate of 3.4% [80].

In cannon with renewable integration we expected that the storage market for stationary and industrial applications will increase, considerably, until 2050. According to the International Energy Agency IEA [80], electricity will play a central role in the future energy system and its consumption is likely to double at global level in its **2 degree scenario (2DS)** by 2035. Within the 2030 EU policy framework, the targets of at least 27% of

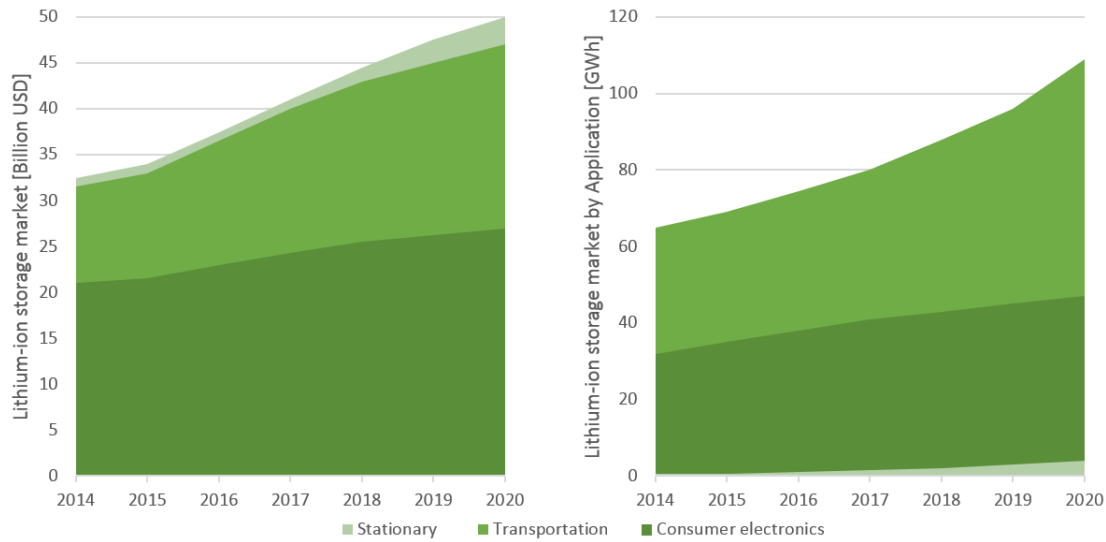


Figure 2.8: Evolution in market share of Li-ion technology [123]

energy savings by 2030 (through renewables) are targeted. This scenario foresees that the use of renewable energy sources (RES) grows rapidly and generates more than half (57%) of the global electricity, with solar and wind each providing around 15% in 2050. Overall, during 2014, 26.9 GW of new power generating capacity was installed in the EU [211]. Figure 2.9 illustrates the commissioned generation assets in the European Union in 2014.

Wind integration

A total of 128.8 GW wind power generation is now installed in the European Union (2014), a growth of 9.8% on the previous year and lower than the record growth registered in 2012 (+12% compared to 2011). Germany remains the EU country with the largest installed capacity, followed by Spain, the UK, France and Italy. Ten other EU countries have over 1 GW of installed capacity: Austria, Belgium, Denmark, Greece, Ireland, the Netherlands, Poland, Portugal, Romania and Sweden. Wind power was the energy technology with the highest installation rate in 2014: 11.8 GW, accounting for 43.7% of all new installations, see Figure 2.9.

Photovoltaic integration

In 2014, 8 GW of new PV installations were commissioned in the European Union. This accounts for 29,7% of all new installations, see Figure 2.9. In comparison, 11 GW of new PV capacity were connected to the grid in 2013, 17.7 GW in 2012 and 22.2 GW in 2011. Germany was the top European market with 3.3 GW followed by UK (1.5 GW), Italy (1.4 GW), Romania (1.1 GW) and Greece (1.04 GW). However, several European markets that performed well in the past went down in 2013. Indeed, as a consequence of political decisions to reduce PV incentives, new Belgian installations went from 600 MW to 215 MW and French installations went from 1,115 MW to 613 MW. Nevertheless, the European PV

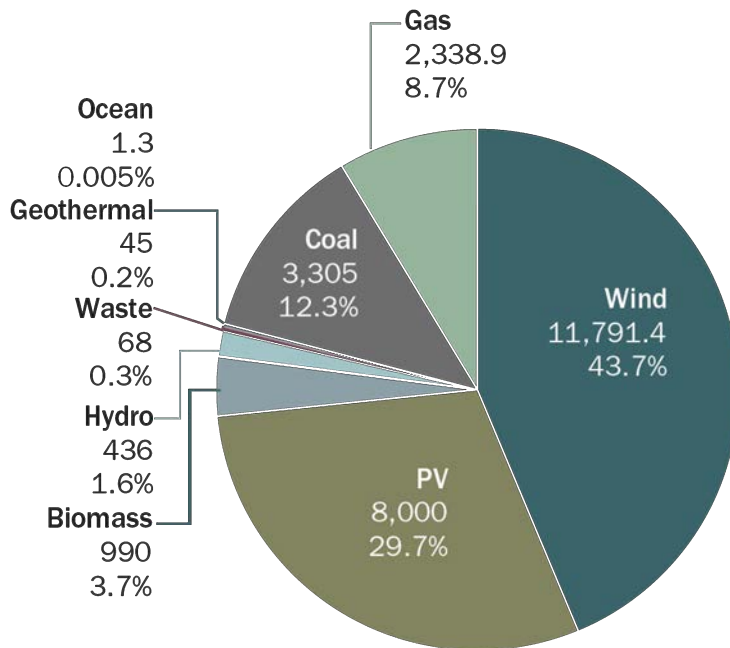


Figure 2.9: GigaWatts of new generating assets commissioned in 2014 in the European Union. From reference [166]

market remained stable with around 6 GW per year of new PV capacity, in the last two years. [211].

In general

The estimates for grid-scale market growth vary widely among industry analysts and will depend significantly on policy implementation and the availability of low-cost options. A report by Lux Research estimated that the grid-scale market would reach \$114 billion by 2017 with half of the installed capacity for the integration of renewable energy (primarily wind power) [211]. Piper Jaffrey estimates that the market for grid-scale storage is \$600 billion over 10-12 years, and Boston Consulting Group predicts that the market will reach \$400 billion by 2020 [211].

With the increasing implementation of renewable energy sources, and competitiveness of Li-ion storage, static applications of Li-ion are likely to become a reality. However, the bulk of the Li-ion market will not be in static applications, see Figure 2.8. Approximately 4 GWh (market value \$3 billion) of Li-ion technology will be installed annually for static applications in 2020 on a global scale.

Mobile applications

The market in electric vehicles expands at an amazing rate, this in return fuels the production of large format lithium cells. Tesla recently commissioned its giga-factory enabling a strong cost reduction with respect to their battery cells. Figure 2.10 illustrates the global

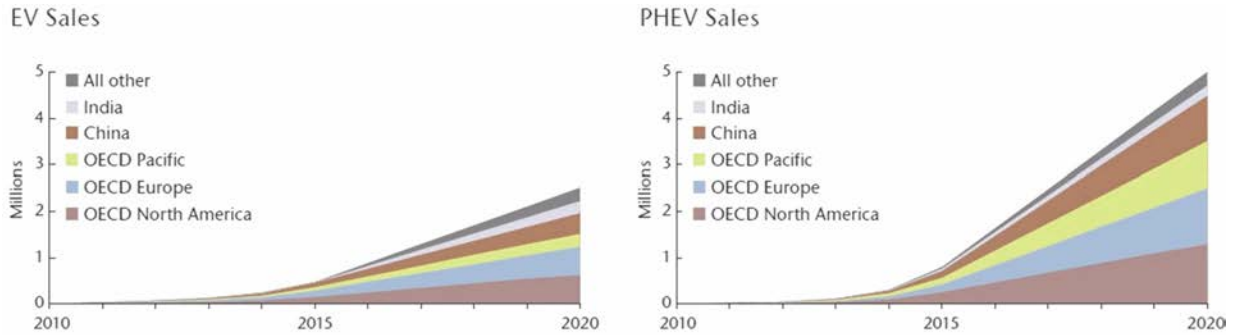


Figure 2.10: Global sales of PHEV and EV per region [81]

expected EV and PHEV sales these coming years. The global EV market will increase from fewer than 200,000 units sold in 2012 to almost 2.4 million in 2020, according to a report from Pike Research. We can also deduce that the European market will account for approximately one million PHEV's and one half a million EV's by 2020 a year.

The market share of lithium-ion batteries in mobile applications will see a strong growth these next 5 years, see Figure 2.8. Pike Research reported in 2013 that the global transportation Li-ion battery market will reach approximately \$22 billion by 2020. They also expect that a large portion (approximately \$7 billion) is destined for the European market, see Figure 2.11 and 2.8. In Europe, 50% of trips are less than 10 km and 80% of trips are less than 25 km [81].

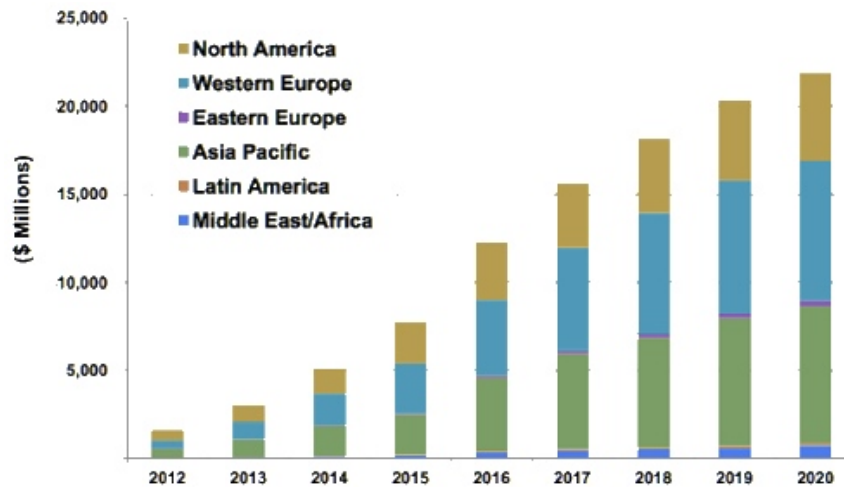


Figure 2.11: Global market of Li-ion batteries for tranportation by region, in million \$, [72]

2.4.2 Profitability

In the production of Lithium cells

The pressure to reduce the cost of electric vehicles is high, and the cost of the battery pack is the most important factor in determining the cost of EVs. Large research and development funds have been invested, but only small incremental improvements have been achieved so far. Pike Research forecasts that as the market develops, Li-ion battery manufacturers will be forced to consolidate. They say that this has already begun with several manufacturers filing for bankruptcy protection. It is obvious that good technology and high production is important for defending or conquering a good or better market position [38].

Static applications

Reference [38] has studied the profitability of some static applications in a study around the commercialization of energy storage in Europe. In this study, profitability is defined as the net present value (NPV) of project cash flows, excluding initial outlay divided by initial outlay. A profitability index greater than one denotes a positive NPV based on values of different storage technologies. This results in a representation for short term, economically viable applications which indicate the early markets. The study yields some interesting insights in the current and future (2030) profitable markets for static application.

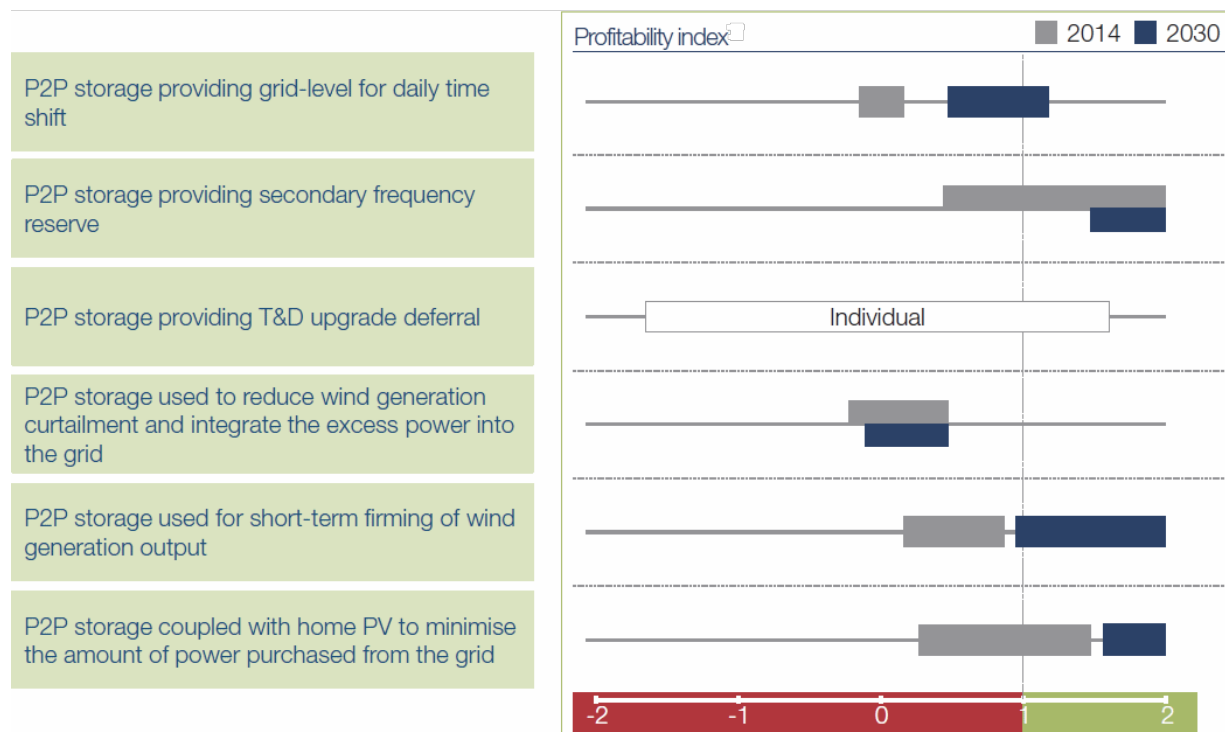


Figure 2.12: Profitability index, from [38]

From Figure 2.12, one can deduce that, frequency regulation and behind the meter PV integration offer the highest profitability. In both cases electrochemical EES and more specifically Li-ion based storage is an appropriate technology.

2.4.3 Conclusion

From this section we should remember:

- Li-ion will first penetrate the EV market. Near 2020, Li-ion will begin its proliferation in grid storage applications.
- Second life applications of Li-ion batteries will present great value in grid storage. However, better techniques with respect to the determination of the state of health are necessary.
- The grid storage market follows (with a time shift) the trends in renewables.
- The market of maintenance, especially offshore wind will expand in the coming decade.
- The grid storage market potential is big and will continue to expand until 2050.
- The market of Li-ion batteries is worth about \$30 billion in 2015 and will expand to approximatively \$50 billion by 2020.
- Frequency regulation and PV integration offer the highest profitability, followed closely by Wind power integration.
- The profitability in deferral of T&D upgrades can offer the highest profitability but a case by case approach is necessary.

2.5 Cost evolutions

An interesting resource emitted by the American investment bank Lazard [109] makes a comparison of several cases for storage applications. In this document they define several energy storage cases which they compare to one another in terms of levelized cost, see Table 2.8.

The assumptions made in this levelized cost analysis are:

1. the study describes only cost per energy capacity;

	Projected life [Years]	Power [MW]	Useful Capacity [MWh]	Cycles per day	days per year	Project [MWh]
Transmission system	20	100	800	1	300	4800 000
Peaker replacement	20	25	100	1	350	700 000
Frequency regulation	20	10	5	4,8	350	168 000
Distribution services	20	4	16	1	300	96 000
PV integration	20	2	4	1,25	350	35 000
Micro grid	20	2	2	2	350	28 000
Island grid	20	1	6	1	350	42 000
Industrial	10	1	4	1	350	14 000
Commercial	10	0,1	0,2	1	250	500
Residential	10	0,005	0,01	1	300	30

Table 2.8: Cases compared in Lazard’s study [109]

2. due to different DoD depending on the technology, some systems are oversized such that comparable useful energy capacity are compared;
3. the study only focuses on the cost inspired on industrial data provided by their partners in the energy industry;
4. the levelized cost generates an estimate of the installed cost over the indicated project life time;
5. the study assumes no subsidies making it applicable to the global EES market;
6. it does not look at the actual environmental conditions;

The outcome of this study is illustrated in Figures 2.14 and 2.15 for respectively in front of the meter and after the meter cases. The Zinc battery comes forward as one of the strong contenders. Zinc batteries cover a wide range of technologies including metal air derivatives. The potentially low cost of zinc is mainly due to its abundance. It should be noted that the technology has not yet been proven in wide spread commercial deployment. Li-ion batteries remain relatively high cost, however, their high efficiency, high energy and power capacity make them a serious contender especially in second life applications where batteries formerly used in mobile applications are reused in less demanding static applications.

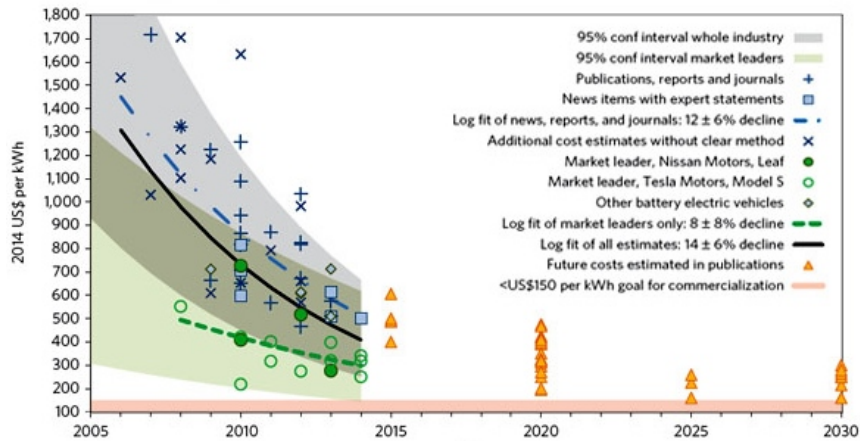


Figure 2.13: Cost evolution of Lithium-ion battery pack for BEV (system level) in US\$, from [150]

2.5.1 Cost of Lithium-ion

Rapidly Falling Costs of Battery Packs for Electric Vehicles a study in Nature Climate Change [150], evaluates the future prospects for battery packs for use in BEVs.

The study's authors, Bjorn Nykvist and Mans Nilsson of the Stockholm Environment Institute, analyzed more than 80 estimates from 2007 to 2014 to trace the costs of Li-ion battery packs for BEVs. The literature reveals that **costs are coming down, but with large variance/uncertainties on past, current and future costs** of the dominating Li-ion technology. Figure 2.13 illustrates the general tendency. The effect of learning on the price of Li-ion batteries (at system level) is clearly visible.

They show that industry-wide cost estimates declined by approximately 14% annually between 2007 and 2014, from above 1,000 \$/kWh to around 410 \$/kWh, and that the cost of battery packs used by market-leading BEV manufacturers are even lower, at 300 \$/kWh, and has declined by 8% annually.

Today, in the field of static applications, the cost of LFP batteries at cell level is around 200 Euro/kWh. Due to the presence of expensive materials such as nickel and cobalt, the price for NMC and NCA batteries is considerably higher. Around 400 - 500 Euro/kWh can be expected. LMO cells are priced at approximately 300 Euro/kWh. The LTO battery is still expensive, around 800 Euro/kWh can be expected. This is mainly due to the lack in mass production.

The general target by the automotive industry is a total cost of 150 Euro/kWh at cell level by 2020. Under the assumption of producing 100,000 25 kWh EV packs per year using 180 Wh NMC cells, the portion of cost at system level accountable by the cells is only around 45% of the total value (Cells: 45%, Electronics and pack: 24%, warranty 1% and gross profit 30%). Therefore one must remain careful when using previous values. [212]

2.6 Battery °

BYD	Intel IBM	Kokam
Saft Batteries	Priets Battery	Toshiba
TDK Corporation	Tianjin Lishen	Leclanche Emrol
Samsung SDI	Sony	Amperex
LG Chemical	Microvast	Electrovaya
Panasonic	Jhonson Controls	ATL
Hitachi Maxwell	BAK	Ambri
3M	Umicore	Bosch
ENVIA	BASF	Nexeon
Harbin Coslight	B&K	ShenZehn WISEWOD
Ningbo Veken Battery	Wanxiang EV	DLG
Herewin	OceanSun	AEEnergy
CHAM	Great Power	Sion Power
Oxis Energy	PolyPlus	NOHMs Technologies
Toyota	Pellion Technologies	Sakti3
Planar Energy	SEEO	Infinite Power Solutions
Front edge Technology	Excellatron	SI Microelectronics
Idemitsu Kosan	Cymbet	Yardney Technical Products
AER Energy Resources Inc.	Metallic Power inc.	Powerzinc Electric Inc.
Revolt Technology	NGK	GE
MES-ZEBRA	REDFlow	UniEnergy Technologies
Siemens	UTC	Starwood
Arkema	Solvay	JM Energy
Yunasko	Shin-Kobe	Nippon Chemi-Con
Taiyo Yuden	Vionyx Inc.	BMW

Table 2.9: An overview of electrochemical battery and cell manufactures

Many companies have recognized the enormous market potential and are active in the electrochemical EES market. South Korean companies were having the biggest market share thanks to the impressive cost competitiveness. In contrast, Japanese and Chinese firms have struggled to get their market share. A report by Pike Research in 2013 [72] states that China will take a leading position in the production of lithium-ion cells by 2015.

Table 2.9 presents an overview of current electrochemical battery manufactures.

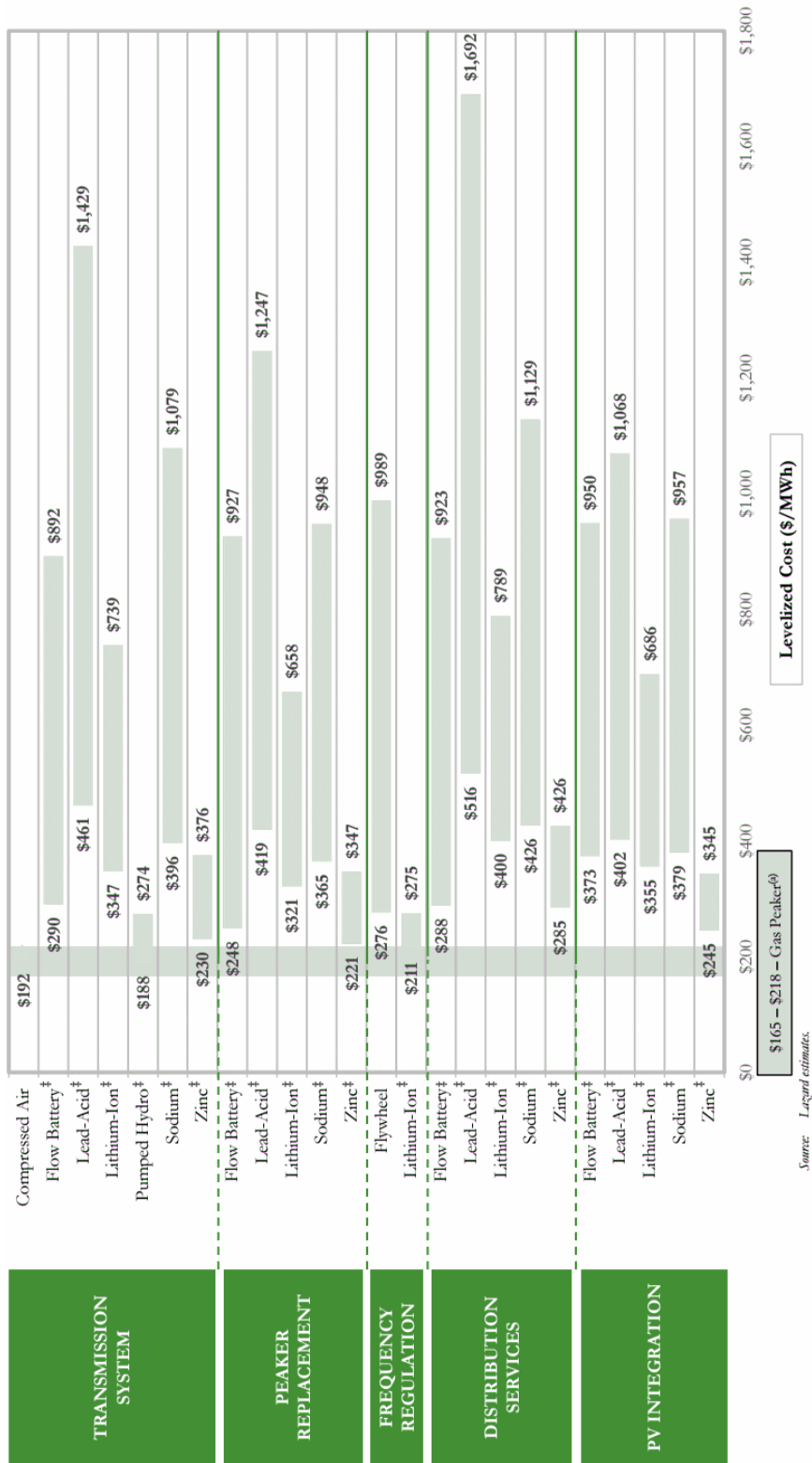


Figure 2.14: In front of the meter energy storage cases [109]

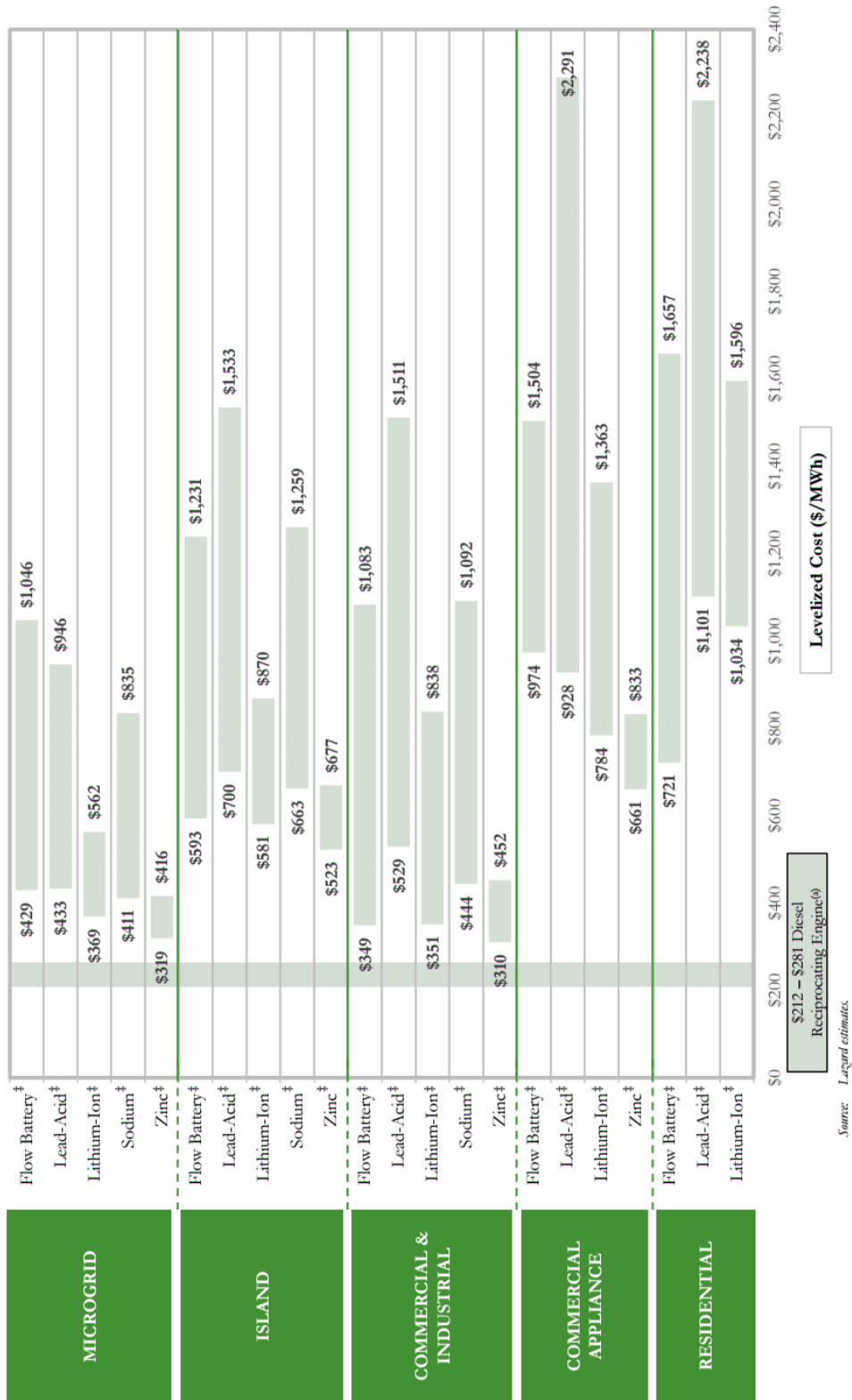


Figure 2.15: After the meter energy storage cases [109]

Chapter 3

Lithium-ion chemistries

As specified in the introduction, we will focus on rechargeable (secondary) electrochemical EES and more precisely lithium based batteries.

In previous chapters we already discussed some insights and characteristics applicable to Li-ion chemistries:

- In Chapter 1, we discussed how to determine the energy content of electrochemical EES, we discussed the principle of electro-chemical EES and presented useful data with respect to the performances and working conditions of several battery types.
- in Chapter 2, we presented some design considerations, revised some key characteristics and analyzed the applicability and market of lithium-ion EES.

In this chapter we delve into the world of Li-ion batteries and provide an overview of current and future technologies.

3.1 Current lithium-ion technologies

The term lithium-ion refers to **a wide array of different chemistries**, all of which are characterized by the transfer of lithium ions between the electrodes during charge and discharge reactions. Lithium is the lightest metal and therefore provides the largest energy density per unit weight.

3.1.1 Lithium-ion

Pioneering work with lithium batteries began in 1912 under G.N. Lewis but it was not until the early 1970s when the first non-rechargeable lithium batteries became commercially

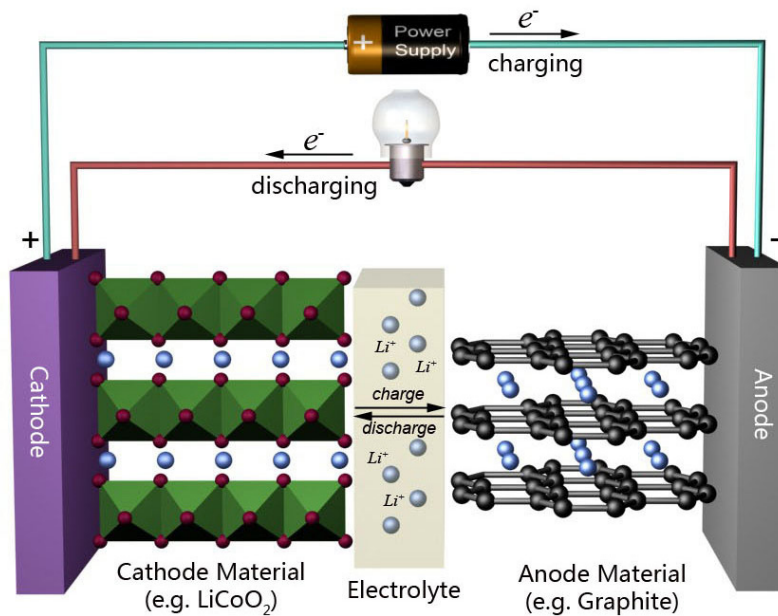


Figure 3.1: Principle of an LCO Li-ion battery, [116]

available. Early attempts to develop rechargeable lithium batteries failed due to safety problems (because of the inherent instability of lithium metal, especially during charging). Research shifted to a non-metallic lithium battery using lithium ions. Although slightly lower in energy density than lithium metal, lithium-ion is safe, provided certain precautions are met when charging and discharging. In 1991 Sony and Asahi Kasei released the first commercial lithium-ion battery.

Today's Li-ion cells do not contain metallic lithium. Lithium ions are inserted into the structure of other materials, such as lithiated metal oxides or phosphates in the positive electrode (cathode). The negative electrode (anode) is made of carbon, typically graphite, see Figure 3.1 or lithium titanate (LTO-cells). The chemical reactions at anode and cathode are illustrated in Figure 3.2.

Technologies with lithiated metal oxide for cathode (positive) and carbon as anode (negative) have high cell voltages (typically 3,6 V to 3,7 V) and corresponding high energy densities. These technologies have widely differing lifetime and safety characteristics. Cells with positive materials based on lithium iron phosphate are inherently safer than their metal oxide/carbon counterparts but the voltage is lower (around 3,2 V), as is the energy density. Designs with lithiated metal oxide as cathode and lithium titanate as anode have the lowest voltage (around 2,5 V) and energy density but have much better power capability and safety advantages.

The energy density of lithium-ion technologies is typically several times higher than with the standard nickel-cadmium. There is potential for higher energy densities. The load

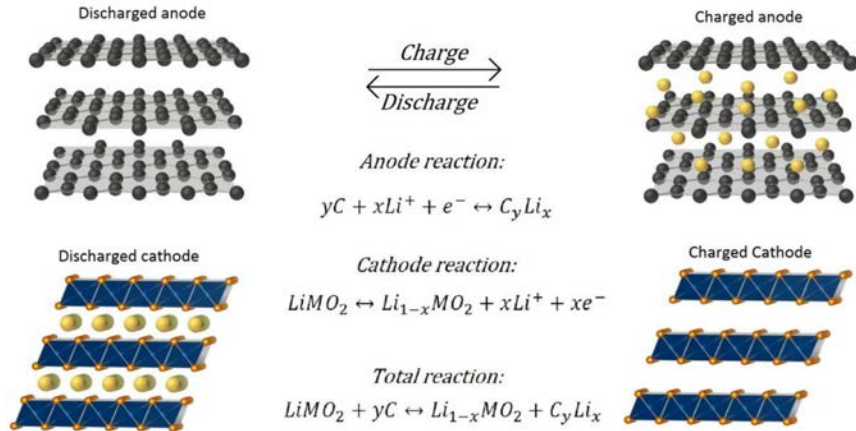


Figure 3.2: LCO cell charge and discharge reactions, from [18].

characteristics are reasonably good and behave similarly to nickel-cadmium in terms of discharge. The high cell voltage of 3,6 V allows for battery pack designs with only one cell. Most of today's mobile phones run on a single cell. A nickel-based pack would require three 1,2 V cells connected in series.

Lithium-ion is a low maintenance battery, an advantage that most other chemistries cannot claim. There is no memory and no scheduled cycling is required to prolong the battery's life. In addition, the self-discharge is less than half compared to nickel-cadmium. Lithium-ion cells cause little harm when disposed.

Despite its overall advantages, lithium ion has its drawbacks. It is fragile and requires a protection circuit to maintain safe operation. Cells are typically built into multi-cell modules in series/parallel arrays, and the modules are connected together to form a battery string at the required voltage. Each string is controlled by a battery management system (BMS). Because Li-ion batteries lack the capability of aqueous technologies and thus to dissipate overcharge energy, electronic subsystems are an important feature. Safety characteristics of Li-ion batteries are ultimately determined by the attributes of the overall system design, including mechanical characteristics, thermal characteristics, electronics and control algorithms. Built into each pack, the protection circuit limits the peak voltage of each cell during charge and prevents the cell voltage from dropping too low on discharge. In addition, the cell temperature is monitored to prevent temperature extremes. The maximum charge and discharge current on most packs is limited to 1 C or 2 C. With these precautions in place, the possibility of metallic lithium plating occurring due to overcharge is virtually eliminated [202].

Aging is a concern with most lithium-ion batteries and many manufacturers remain silent about this issue. Capacity deterioration is noticeable after several years, whether the battery is in use or not (depending on storage conditions of course). The battery frequently fails after several years. It should be noted that other chemistries also have age-related

degenerative effects. This is especially true for nickel-metal-hydride if exposed to high ambient temperatures. Lithium-ion packs are known to have served for 5 years in some applications.

Manufacturers are constantly improving lithium-ion. New and enhanced chemical combinations are introduced every six months or so. With such rapid progress, it is difficult to assess how well the revised battery will age.

Storage in a cool place slows the aging process of lithium-ion (and other chemistries). Manufacturers recommend storage temperatures of 15°C. In addition, the battery should be partially charged during storage. The manufacturer recommends a 40% charge.

Li-ion cells may be produced in cylindrical or prismatic (rectangular) format. The most economical lithium-ion battery in terms of cost-to-energy ratio is the cylindrical 18650 (size is 18 mm x 65,2 mm). This cell is used for mobile computing and other applications that do not demand ultra-thin geometry. If a slim pack is required, the prismatic lithium-ion cell is the best choice. These cells come at a higher cost in terms of stored energy.

Advantages:

- High energy density and potential for even higher capacities.
- Does not need prolonged priming when new. One regular charge is all that's needed.
- Relatively low self-discharge (less than half that of nickel-based batteries).
- Low maintenance, no periodic discharge is needed because there is no memory effect.
- Cells can provide very high current to applications such as power tools.

Limitations:

- Li-ion cells require a protection circuit to maintain voltage and current within safe working limits.
- Subject to calendar aging, even if not in use. Storage in a cool place at 40% charge reduces the effect.
- Restrictions for transportation of large quantities (restriction does not apply to personal carry-on batteries).
- Expensive to manufacture, about 40% higher in cost than nickel-cadmium batteries.
- Not fully mature, metals and chemicals are changing on a continuing basis.

3.1.2 Lithium polymer

The lithium-polymer battery differentiates itself from conventional battery systems in the type of electrolyte used. The original design, dating back to 1970, uses a dry solid polymer electrolyte. This electrolyte resembles a plastic-like film that does not conduct electrons but allows for ions exchange (electrically charged atoms or groups of atoms). The polymer electrolyte replaces the traditional porous separator, which is soaked with electrolyte.

The dry polymer design offers simplifications with respect to fabrication, ruggedness, safety and thin-profile geometry. With a cell thickness measuring as little as one millimeter, equipment designers are left to their own imagination in terms of form, shape and size.

Unfortunately, the dry lithium-polymer suffers from poor ion conductivity. The internal resistance is too high and cannot deliver the current bursts needed to power modern communication devices. Heating the cell to 60°C and higher increases the conductivity, a requirement that is unsuitable for portable applications.

To compromise, some liquid electrolyte had to be added. In commercial cells, the electrodes are bonded together by a porous polymer matrix (separator/membrane) prepared from the same traditional porous polyethylene or polypropylene material used for separators in the liquid electrolyte version. Liquid electrolyte is infused into this porous matrix where it becomes immobilized, resulting in a gel-like substance. **Thus the commercial lithium-ion polymer cells are very similar in chemistry and materials to their liquid electrolyte counterparts.**

The electrode stacks to be assembled into foil pouches that provide geometric flexibility and improved energy density (compared to cylindrical cells), see Figure 3.3. However, such advantages are less significant as the cells are scaled up to larger capacities. An application specific approach towards thermal management is advised. Figure 3.3 illustrates the current density on each electrode, heat generation due to the Joule effect is stronger in zones where the current density is high. Notice that the bottom of the cell is clearly less impacted, cells with electrode connectors on both sides will probably reduce this effect gaining considerably in cycle life and other performances, although the layout may be considered less practical for some applications.

Lithium-ion-polymer has not caught on as quickly as some analysts had expected. Its superiority compared to other systems and low manufacturing costs have not been fully realized but showed great progress in the last few years. Little improvements in capacity gains were achieved, in fact the capacity is slightly less than that of older lithium-ion battery.

Advantages:

- Very thin profile (batteries resembling the shape of a credit card are feasible).
- Flexible form factor, manufacturers are not bound by standard cell formats. With

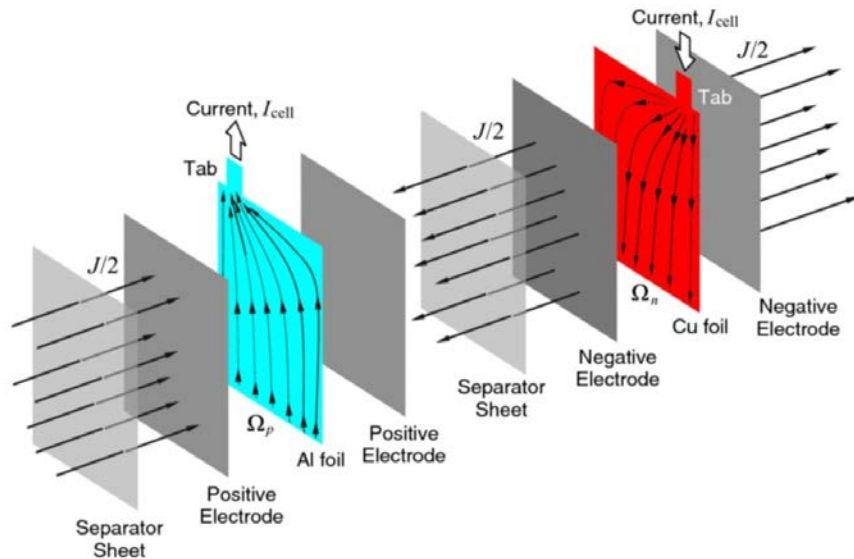


Figure 3.3: Lithium ion polymer cell in its typical pouch format [165]

high volume, any reasonable size can be produced economically.

- Lightweight - gelled electrolytes enable simplified packaging by eliminating the metal shell.
- Improved safety - more resistant to overcharge; no risk for electrolyte leakage.

Limitations:

- Lower energy density and decreased cycle count compared to (liquid electrolyte) lithium-ion.
- Expensive to manufacture.
- No standard sizes. Most cells are produced for high volume consumer markets.
- Higher cost-to-energy ratio than conventional lithium-ion
- Restrictions on lithium content for air travel

Traveling regulations

With respect to air travel regulations, we differentiate between two battery types: lithium metal and lithium-ion. Most lithium metal batteries are non-rechargeable and are used in film cameras. Lithium-ion packs are rechargeable and power laptops, cellular phones and camcorders utilize these. Both battery types, including spare packs, are allowed as carry-on but cannot exceed the following lithium content:

- 2 grams for lithium metal or lithium alloy batteries (primary)
- 8 grams for lithium-ion batteries (secondary)

Lithium-ion batteries exceeding 8 grams but no more than 25 grams may be carried in carry-on baggage if individually protected to prevent short circuits and are limited to two spare batteries per person.

How do we know the lithium content of a lithium-ion battery? From a theoretical perspective, there is no metallic lithium in a typical lithium-ion battery. There is, however, equivalent lithium content that must be considered. For a lithium-ion cell, this is calculated at 0.3 times the rated capacity (in ampere-hours).

Anyone shipping lithium-ion batteries in bulk is responsible to meet transportation regulations. This applies to domestic and international shipments by land, sea and air.

Lithium-ion cells whose equivalent lithium content exceeds 1,5 grams or 8 grams per battery pack must be shipped as "Class 9 miscellaneous hazardous material." Cell capacity and the number of cells in a pack determine the lithium content.

Exception is given to packs that contain less than 8 grams of lithium content. However, if a shipment contains more than 24 lithium cells or 12 lithium-ion battery packs, special markings and shipping documents will be required. Each package must be marked and cells and batteries must be separated with slots and packed in strong boxes.

To obtain shipping documents, all lithium-ion batteries must be tested in accordance with specifications detailed in UN 3090, regardless of lithium content (UN manual of Tests and Criteria, Part III, subsection 38.3). This precaution safeguards against the shipment of flawed batteries.

Note: There are also lithium metal polymer technologies, in which metallic lithium is implemented with a conductive polymer to make a solid-state battery SSB system. Such technologies have not yet been successfully deployed but will most likely be in the near future. More information on SSB's can be found in section 3.2.3.

3.1.3 Current state of Li-ion components

In general we can say that all components of Li-based batteries continue to evolve. But the goal of making better batteries can not be subdivided into partial problems. Even when the ultimate cathode is found, the compatibility with the electrolyte and other electrode is of key importance.

Table 3.1, compares the most relevant anode-cathode combinations.

Cathode - anode material	Nominal cell voltage [V]	Specific capacity pos/neg [mAh/g]
LiCoO ₂ - graphite	3.7	120-140/370
LiMn ₂ O ₄ - graphite	3.8	100/370
LiNiO ₂ - graphite	3.9	170/370
LiFePO ₄ - graphite	3.3	150-160/370
LiNiMnCoO ₂ - graphite	3.7	200/370
LiNiCoAlO ₂ - graphite	3.7	180/370
LiFePO ₄ - LiTiO ₂	2.2	150-160
LMn ₂ O ₄ - LiTiO ₂	2.2	100/160

Table 3.1: Comparison of most relevant cathode and anode materials, [212] [151]

Cathodes

The criteria to choose a specific cathode material are energy density, rate capability, cyclability, safety and cost [114]. Current cathodes can be divided according to their crystal structure, see Figure 3.4.

- Layered LiMO₂
- Spinel LiM₂O₄
- Olivines LiMPO₄

Where M is the transitional metal atom.

LiCoO₂ (also called LCO) as positive electrode material was demonstrated by John Goodenough [132]. The LiCoO₂/graphite system has been widely used in portable electronics and power tools. The drawbacks are the use of expensive and toxic cobalt and poor safety (due to the instability of Co⁴⁺ in overcharged state).

Li(Ni_xMn_xCo_(1-2x)O₂, generally known as NMC, can deliver a very high capacity (over 250mAh/g) when cycled between 2,5 and 4,6 V (vs. Li). The NMC was developed for the HEV and EV applications and is up to now one of the best cathode material. The properties can easily be altered by adding more of a certain compound. Adding more nickel, manganese, or cobalt results in respectively more capacity, safety or reversibility [215].

Spinel manganese oxide compounds were studied by M.M. Thackeray and Goodenough [210]. They have a specific capacity of 120mAh/g and a voltage between 3.5 V and 4.3 V (halfcell: versus lithium). LiMn₂O₄ showed good prospects due to lower cost (no cobalt), better safety and high specific power.

The olivine structure is intrinsically safer than the other structures. Among them LiFePO_4 or LFP is an excellent candidate. However the price of LFP is still relatively high (200 Euro/kWh), although no expensive materials are used.

In some cases different types of cathodes structures are mixed to create a hybrid form.

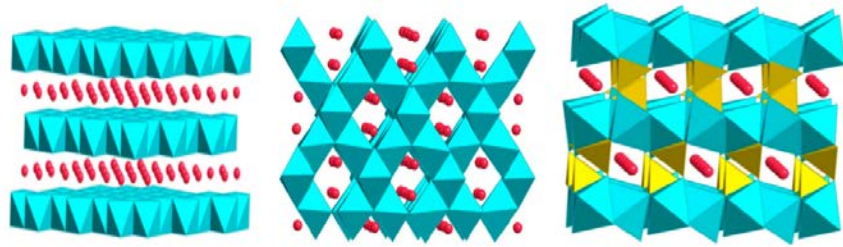


Figure 3.4: Cathode structures from left to right: layered, spinels and olivines [212].

Anodes

In most commercial lithium-ion cells graphite or other carbon-based materials are used as negative electrode [28]. The structures differ from each other in terms of morphology, structure, micro-structure and texture [54]. Graphite (stacked layers of graphene) is the best candidate thanks to the high specific capacity (372 mAh/kg [225]). Lithium insertion happens at a potential of less than 1 V (versus Li). However they show less performance at low temperatures (lithium plating can occur). Formation of the solid electrolyte interface layer (SEI) leads to an important capacity fade (very obvious during the first cycle). The SEI continues to grow with cycling and reduces the active surfaces while increasing the internal resistance leading to irreversible capacity loss [217], [52], [149], [27].

Endo et al. and Patterson [54], [133] have described the main properties of graphite and soft and hard carbon materials as negative electrode. Graphite consists of stacked graphene layers. The space between the planes is about 0,335 nm. During the intercalation process 10% volume expansion occurs. It should be noted that the practical specific capacity available is about 310 mAh/g. The discharge curve for LIB anode made of graphite is characterized by a flat and wide range. For hard carbon, the discharge profile is characterized by a steadily declining curve across most of the charge range. The motivation to find other anode materials is mainly motivated to lower the cost and increase the capacity.

Natural graphite being readily reactive with electrolytes renders it useless as anode material even though it is inexpensive. Thus, there is a need to coat them with a carbon layer to enhance its resistance towards the electrolyte. Hard carbons are one of the well-known, highly recommended anode materials used for HEV applications [141].

In the last years new anodic materials have been proposed based on spinel lithium titanate oxides (LiTiO_2). Lithium titanate oxide is a better insertion material with a specific capacity of 175mAh/g [237]. It is safer, low-cost, non-toxic and no SEI layer occurs on

the anode surface. The lithium insertion potential of this oxide is around 2 V versus Li. This value is located in the stability window of common organic electrolytes. Lithium titanate oxide based batteries have a spinel structure, of which the surface area is much bigger ($100 \text{ m}^2/\text{g}$ versus $3 \text{ m}^2/\text{g}$ for carbon based electrodes). Contrary to graphite-based electrodes, the volume expansion during intercalation of lithium is 0,2% [133]. The energy density of lithium titanate oxide based cell is in the range of 70 to 90 Wh/kg (depending of the used cathode material), which is much lower than the NMC and NCA batteries. This technology cannot be used in electric vehicles but they have high potential in applications where high peak current is needed.

Bruce et al. [28], have documented that the specific capacity of $\text{Li}_4\text{Ti}_5\text{O}_{12}$ can be improved by using nanotubes/nanowires composed of $\text{TiO}_2(\text{B})$. This technology still has the advantages of $\text{Li}_4\text{Ti}_5\text{O}_{12}$ but the specific capacity can be improved from 175 mAh/g up to 300 mAh/g. Additionally the reversible capacity of nano-wires is much higher.

Electrolyts

Current Li-ion batteries tend more towards the lithium polymer design. In this design, the electrolytes take over the function of the separator. Figure 3.5 illustrates the ionic conductivity of a wide range of electrolytes.

According to Janek and Taige [207] [88], the requirements of the electrolyte can be summarized as follows:

- Large electrochemical stability,
- High thermal stability,
- Wide operating voltage range,
- Low vapour pressure,
- High conductivity,
- High capacity,
- High cycling rates.

Xu et al. [233], concluded that LiPF_6 is the most common lithium salt in lithiumion batteries and it has a high conductivity compared to other electrolytes. However, during charging, the organic solvent forms a SEI layer with the graphite-based anode ($<1,2 \text{ V}$), which decreases the ionic conductivity. Moreover, lithiumions cannot be used with aqueous electrolyte because lithium ions react with it and form lithium hydroxide (LiOH).

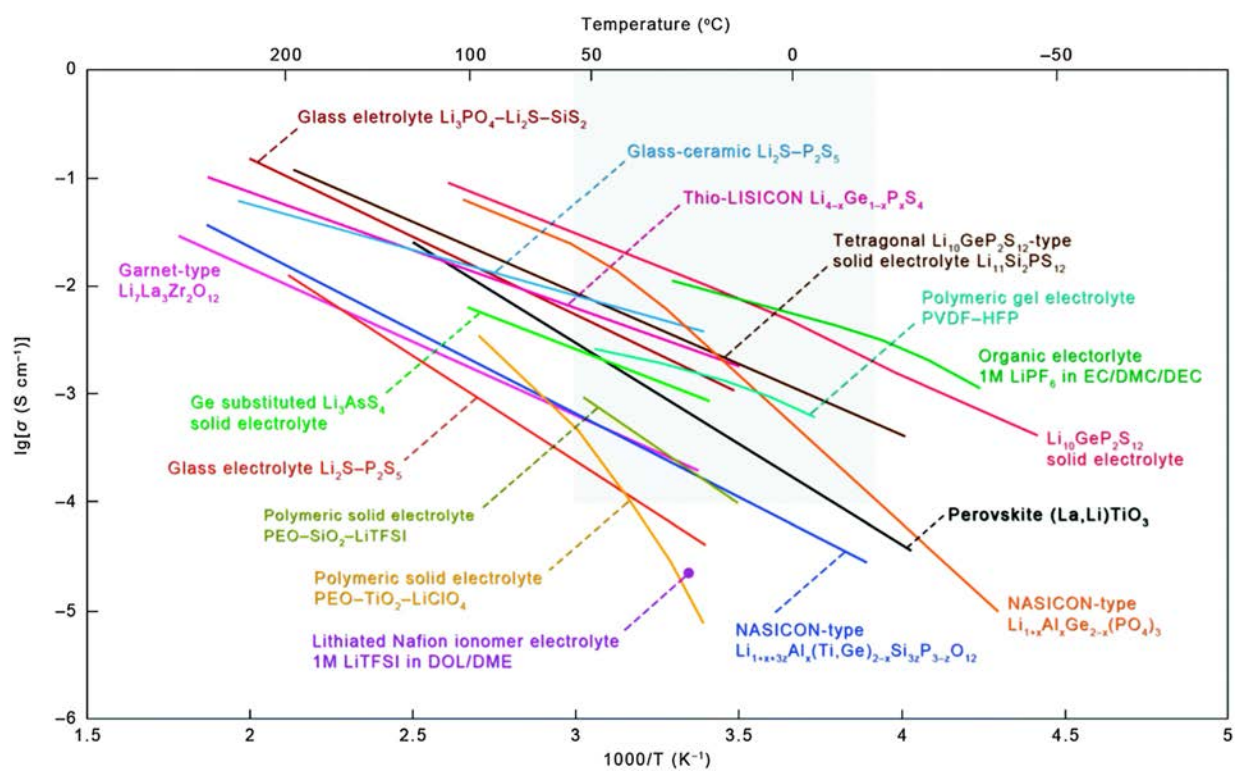


Figure 3.5: Conductivity of common solid state electrolytes as function of temperature, from reference [245]

3.1.4 Cost evolution

The cost of Li-ion battery at cell level depends on the considered technology following approximate values can serve as a guide. [212]

- LFP 200 Euro/kWh
- NMC 400 to 500 Euro/kWh
- NCA 400 to 500 Euro/kWh
- LMO 300 Euro/kWh
- LTO 800 Euro/kWh

To put this in perspective, the target for the automotive market (at system level) is 150 Euro/kWh by 2020.

3.1.5 Suppliers

From reference [187]

- Panasonic (Japan)
- NEC (Japan)
- GS Yuasa (Japan)
- Evonic Industries (Germany)
- Samsung SDI (Korea)
- Ener1 (US)
- Lishen (China)
- A123 (US)
- BYD (China)
- Sanyo (Japan)
- Toshiba (Japan)
- Hitachi Vehicle energy

- JSC Johnson Controls (US)
- Saft (US)
- Electrovaya (Canada)

3.2 Lithium-ion technologies till 2020

3.2.1 Lithium-ion-silicon batteries

Characteristics

Silicon is a good alternative for the graphite or carbon anode because of its extremely high capacity (approximately 8500 mAh/ml [108] and 3579 mAh/g), low cost and low working potential (0,05 V). For comparison, the theoretical capacity is approximately ten times higher than that for graphite (372 mAh/g). Cyclability is the key issue and prevented commercialization up to now.

The main hurdle of the Si anode is the high volume expansion (275%) which leads to pulverization of the active material. This in turn creates nanoparticles which do not participate in the useful reactions and increase the internal resistance [197] [93].

A SEI (Solid Electrolyte Interphase) layer is formed during the first lithiation of Si particles when the potential of the anode is below 1 V (vs. Li). This is due to the decomposition of the electrolyte, which is not stable at low potentials, on the surface of the Si particles. This SEI layer prevents further secondary side reactions and is electronically insulating and ionically conducting. Due to huge volume variations during lithiation/delithiation, the SEI layer cracks, exposing fresh Si surface to further decompose the electrolyte, which leads to endless consumption of Li and thus to capacity fade. The isolation and disconnection of some Si particles from the conductive network and thus from the current collector also leads to a drastic increase of the internal resistance [141] [69] [212].

Development is actively perused. The principle consists of encapsulating the silicon in a nanowire (NW) or nanospheres. This increases the lithiation delithiation process but the increased surface area allows for more SEI development. Additionally new binders are tested. It appears that the commonly used PVDF (PolyVinylidene Fluoride) reacts with the silicon rendering it useless for this battery [60]. An alternative approach consists of growing the nanowires directly on the current collectors. It is claimed that the small NW diameter allows a better adaptation of the large volume variations over lithiation/delithiation cycles. This involves particle sizes below 200 nm, where according to literature particles do not fracture [17].

Wu et al. proposed a new concept where the anode material consists of an active silicon

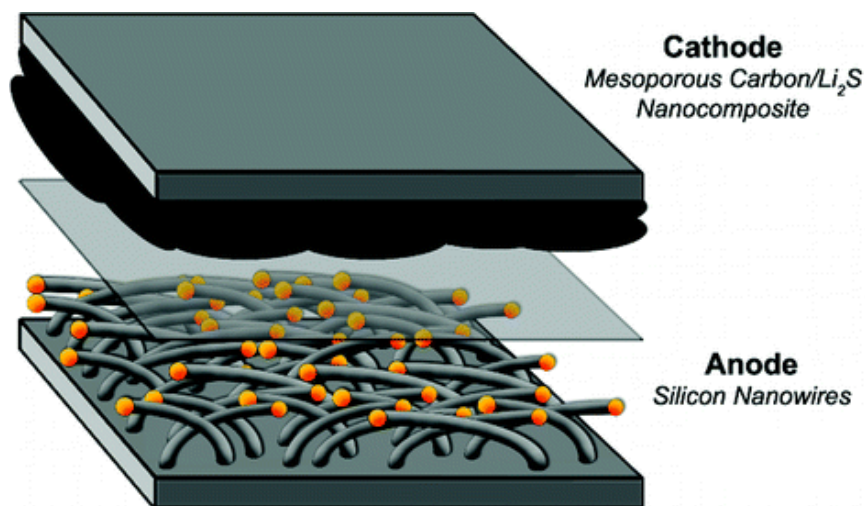


Figure 3.6: Cell with Si-nanowire anode, [182]

nanotube surrounded by an ion-permeable silicon oxide (SiO_x) shell, see Figure 3.6. This material can cycle over 6000 times in a half-cell, while retaining more than 85% of its initial capacity. Volume expansion is prevented by the oxide shell, and the expanding inner surface is not exposed to the electrolyte, resulting in a stable solid electrolyte inter-phase. Batteries containing these double-walled silicon nanotube (DWSiNT) anodes exhibit charge capacities approximately eight times larger than conventional carbon anodes and charging rates of up to 20 C. The main drawback of this anode material is mainly the relatively low anode capacity (600 mAh/g) induced due to constraining caused by SiO_x layer, but extraordinary cyclability is possible [226].

Liu et al. came up with a so-called yolk shell model where Si nanoparticles have been completely sealed inside conformal, thin, self-supporting carbon shells, with wisely designed void space in between the particles and the shell. This model is illustrated in Figure 3.7. This yolk-shell structured Si electrode allows reaching a high capacity (2800 mAh/g at C/10), long cycle life (1000 cycles with 74% capacity retention) and high Coulombic efficiency (99.84%). Nevertheless, it seems that these performances were obtained with very low electrode loadings, the concept still needs to be proven with acceptable loadings [115].

Numerous studies done on composite materials in which active particles are finely dispersed in an active or inactive solid matrix indicate that the matrices help buffering the expansion of the active materials. But these studies also reveal that dispersing Si in an inactive host matrix leads to a decrease of the reversible capacity and that dispersing Si in an active metal matrix does not always provide a satisfying capacity retention [197]. Liu et al. proved that conductive additives graphite flakes and/or nano-scale carbon black can give a good capacity but only for a few cycles [117]. It has also been observed that negative electrodes prepared by depositing 20% Si nanoparticles on the graphite surface showed high initial

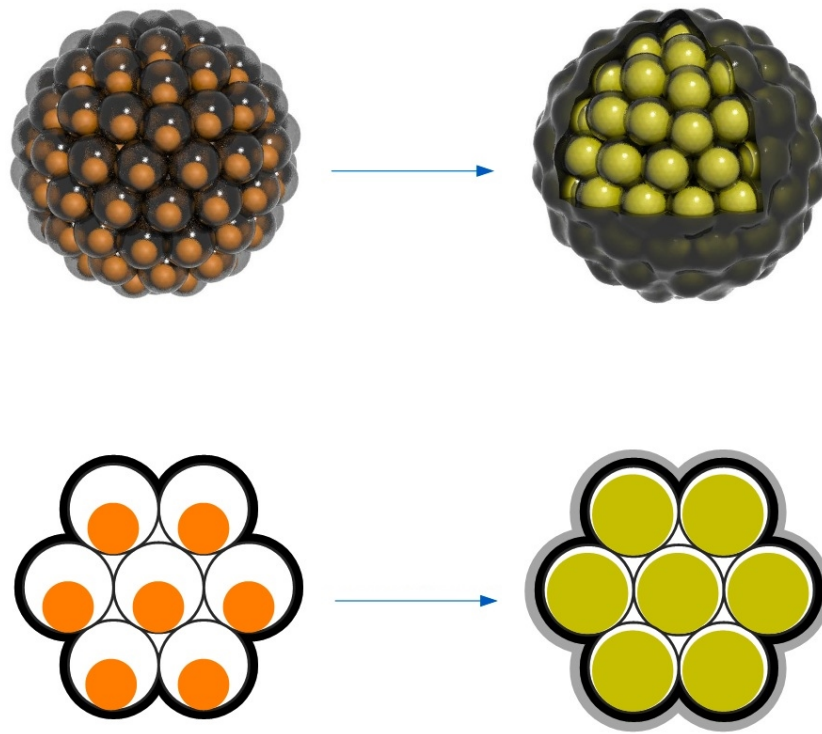


Figure 3.7: Yolk shell design for silicon anode, left before and right after cycling [50]

charge and discharge capacities of 1350 and 1000 mAh/g, and a capacity retention which could reach 900 mAh/g after 100 cycles [76].

As was discussed in these 4 paragraphs, many solutions have been proposed in the past years to try to increase the cyclability of Si-based anodes. Today, these solutions allow reaching stable capacity and decent cycle life, but only in half-cells (vs. Li). As soon as full cells are made using Si based anode, the low coulombic efficiency inevitably leads to fast capacity fade. This means that the material integrity problems have been solved, but that the SEI layer could not really be stabilized yet. One of the solutions that have been recently investigated is the prelithiation of Si, in order to create a stable SEI layer and to increase the coulombic efficiency.

Garcia et al. synthesized $\text{Li}_x\text{V}_2\text{O}_5$ by chemical prelithiation of V_2O_5 by using n-butyl lithium, which brought new variations in the material and a capacity improved by 15-20% compared to non-prelithiated V_2O_5 [66]. Similarly, the electrochemically prelithiated carbon nanotubes (CNT) by Landi et al. showed an improvement in the cyclability [107]. Li_3N was used by Pereira et al. [136] as well as Zhang et al. [242]: their respectively prelithiated metal fluoride sample and phosphide sample, prepared through high energy ball milling led to exceptional results. The phosphide sample for example showed an increase of coulombic efficiency in the first cycle from 62.8 to 72.8%. Zhamu et al. filed a patent in 2008 stating the techniques for producing prelithiated silicon and claimed that prelithiation of silicon followed by comminuting the particles leads to the production of sub-micron particles, which exhibit high specific capacity, long cycle life and high reversibility [17].

Yakovleva et al. from FMC, engineered a new type of lithium called SLMP (Stabilized Lithium Metal Powder), which is stable in air, thanks to a coating. They claimed that this SLMP could be used to prelithiate anodes, which could enhance battery performances at a lower cost, since the cathode material is no longer the main provider of lithium for the anode [128]. Forney et al. used this SLMP to prelithiate silicon-carbon nanotubes. They used SLMP during battery assembly and prelithiated the Si/C nanotubes to eliminate 20-40% irreversible capacity loss during the first cycle owing to SEI layer formation [61].

Cost and °

Since, this technology is under progress, there are not real price indications. The present prices are based on small lab cells. However, the goal is to achieve a cost below 150 Euro/kWh.

Key players in this field are:

- Umicore
- 3M
- Bosch

- ENVIA
- BASF
- Nexeon

3.2.2 Lithium-Sulphur batteries

Characteristics

Among the recent solutions of high power density rechargeable energy storage for automotive applications, lithium-sulphur system is very promising. According to the recent progress, lithium-sulphur can be seen as a most promising commercially viable product in near future [239] [125] [12] [34] [56] [35]. Theoretically a lithium-sulphur system can provide an energy density as high as 2600 Wh/kg (considering lithium anode and sulphur cathode). In a practical system, it can be as high as 600 Wh/kg [126] [29], which will improve as the research progresses. Moreover, sulphur abundance in the nature makes the system economically beneficial. Lithium-sulphur is based on conversion chemistry and a typical system consists of a Li anode and S cathode as can be seen in Figure 3.8. During discharge, at the anode Li metal is oxidized to Li^+ . At the cathode, solid sulphur (S_8) is stepwise reduced to lower oxidation state and form sulphide precipitates Li_2S_x (where x values are 8,6,4,2 and 1 at different discharge state).

Oxis energy is in production of lithium-sulphur pouch cells since 2013 with an expected specific energy of 165 Wh/kg and cycle life 1500 cycles. In addition, Saft Batteries developed the first prototypes of cylindrical lithium-sulphur cells with an energy density over 500 Wh/kg and lifetime over 500 cycles. Sion Power and BASF are working of Li-S as-well.

There are a number of technical challenges to be overcome to make lithium-sulphur batteries a commercial success. At the cathode, firstly, the low ionic and electric conductivity of sulphur and polysulphides make the electric efficiency of the system very low (< 70%).

Secondly, the polysulphides create a number of difficulties during operation. Polysulphides (mainly Li_2S_4 - Li_2S_8) dissolve in the conventional organic electrolytes, which can result in serious capacity fade [34], [56], [126], [126], [246], [127], [90].

Thirdly, the overwhelming volume change of the system, which can be as high as 79%, can be problematic [37], [144]. As a result the battery performance deteriorates and it rises the safety concerns. Besides, having a Li metal anode, technical challenges related to the Li anode are also a part of Li-S system by default. These include the strong SEI formation and dendrite formation.

In general, in order to overcome the shortcoming of low conductivity, sulphur composites are used, mostly sulphur-carbon. Composites are generally synthesized in two forms. One type of composite is in the form of coating on sulphur and the other type is sulphur loaded porous substrates. According to recent findings, 2D graphene [246] [220] [20], conductive

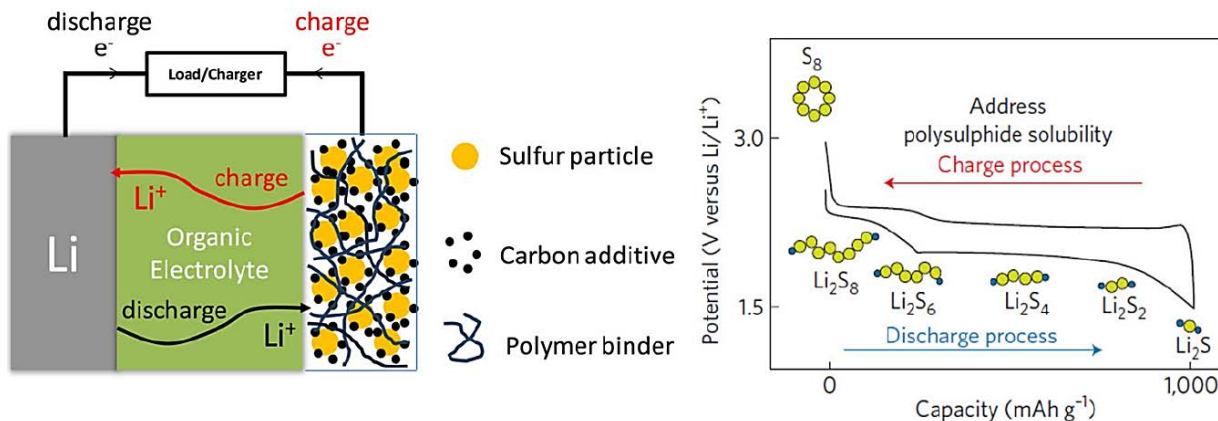


Figure 3.8: At the left a principle representation of a Li-S cell, at the right the discharge voltage curve of Li-S cell [126]

polymer such as polypyrrol [65], [64] and metal oxide (such as TiO₂, [222], [110]) coatings have not only showed improvement in terms of conductivity but also (due to their flexibility) the detrimental effect of volume change can be minimized.

A unique S-TiO₂ yolk-shell nano architected cathode allowed Li⁺ transport but restricted polysulphide dissolution. With this configuration an impressive cycle life of 1000 cycles was achieved [222].

Reducing the pore size has proven to be extremely beneficial in terms of performance and life cycle [239], [125], [34], [56], [126], [90]. It was shown that by creating very small sized pore and confining sulphur into these pores, sulphur allotropes can be controlled and thereby polysulphide shuttle can be diminished [231]. Another direction of the cathode development is using metal sulphide cathode such as Li₂S, FeS₂, MoS₂ etc., [126], [127], [90]. Manthiram et. al. introduced a carbon interlayer between the cathode and the separator, which can preferentially block polysulphide shuttle and thereby shows improved capacity and life cycle [203].

A novel nitrogen and sulphur co-sulphur doped and 3D structured mesoporous carbon based cathode has been reported. The reported cell showed high rate capability, as high as high as 4 C with capacity fade of only 0.085% per cycle for over 250 cycles [228]. Another recent report showed a cell with a specific capacity of approximately 750 mAh/g for over 500 cycles and capacity fade was limited to less than 25% [111].

This technology is extremely suitable for EV, PHEV etc. as a traction battery as well as in portable electronics. Lightweight and less expensive material makes it highly suitable for electronic equipment. This technology can also be implemented in stationary use, for example as energy storage.

Cost and suppliers

Lithium-sulphur technology is still under development and thus there are no real prices that can be indicated. However, a target < 150 Euro/kWh should not be an obstacle in the long term.

Key player in this field are:

- Saft Batteries
- BASF
- Sion Power
- Oxis Energy
- PolyPlus
- NOHMs Technologies

3.2.3 Solid-state batteries

As one can see in Figure 3.9, a solid-state version exists for nearly all typical electrode combinations lead-, nickel-, lithium-based batteries each have a SSB counterpart. Because of the high cost of the electrolyte, research mainly focuses on high-end and consequently lithium-based solutions [212].

Solid state batteries have picked up the interest of several big companies like Samsung and Toyota these past few years.

Many solid electrolytes structures have been tested: glass, (high temperature) ceramic, thermo-tropic-ionic-liquid-crystals, solid polymeric (SPEs), NASICON ($\text{LiM}_2(\text{PO}_4)_3$ with M usually Ti, Ge or Hf), garnet structure, vanadium based and organic structures. Li_3ClO (doped glass) seems to show promising conductivity of 25 mS/cm at 25°C. Due to its stable character and high ionic conductivity, LiPON (Lithium-phosphorus-oxy-nitride) is currently the most used thin film electrolyte.

Several approaches can be differentiated.

The bulk-solid state electrolyte approach consists of a solid electrolyte layer that can be around 100 μm . In the thin film approach the electrolytes layer thickness can be approximately 1000 thinner. The thin film approach is currently pursued in consumer electronics, where it will enable flexible batteries (for use in among others, wearables). Recently, the small company Priets Battery partnered up with Intel to produce the worlds first 3D meshed SSB. This technology increases the surface area several time to yield higher power than its competitors. It is expected that the technology will be commercialized around 2018.

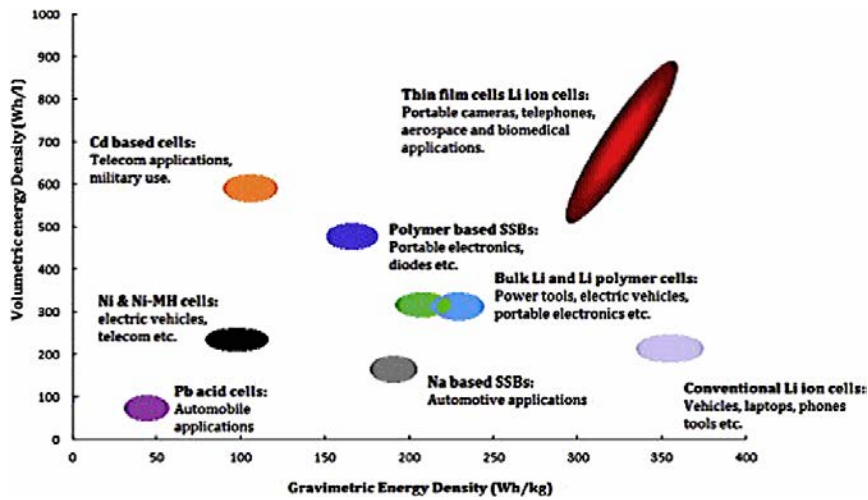


Figure 3.9: Ragone plot of SSBs along with expected applications, [212]

Figure 3.9 depicts a Ragone plot of SSB technologies. From this chart it is clear that the thin film SSB show exceptional properties. Due to its thin shape, a single cell can easily be cooled in regular ambient conditions. However, to scale this up, a high performance cooling system will be necessary.

Characteristics

The main characteristic of SSBs are:

- no leakage possible,
- dendrite formation is countered by the solid electrolyte,
- higher cell voltages are possible,
- self discharging can be avoided,
- poor conductivity (at room temperature) compared to liquid electrolytes
- high manufacturing cost (atomic layer deposition),
- low power portable electronic applications are already available, to take this up to BEV scale, 5 to 10 years if not longer will be necessary.
- hybridization with high power EES can be useful

Cost and °

Several key players are:

- Toyota
- Samsung
- Sakti3
- Planar Energy
- Seeo
- Infinite Power Solutions
- Front edge technology
- Hiatchi
- Planar Energy
- Priets Battery

3.2.4 High-voltage batteries

Characteristics

In order to enhance the energy density, the operating cell voltage can be increased from 3,7 V for LFP and 4,2 V for NMC and NCA to 5 V. The increase of the operating voltage will allow us to reach an energy density close to 300 Wh/kg compared to 200 Wh/kg for state-of-the-art Li-ion cells. In this regard, there is a need for high-voltage (~ 5 V) electrolyte instead of lithium hexafluorophosphate (LiPF_6).

During the last decades, numerous salts were proposed as candidates to replace LiPF_6 . Lithium hexafluoroarsenate (LiAsF_6) was proposed as it has a high ionic conductivity in the typical solvents, but it could not be used because of the toxicity of AsF_6 and its degradation products. Lithium perchlorate (LiClO_4) was a popular salt due to its acceptable solubility and high conductivity, but again, safety issues limited its commercial application, as this salt is highly reactive and can even explode under abusive oxidative conditions. Lithium tetrafluoroborate (LiBF_4) is less moisture sensitive than LiPF_6 , shows better cycling performance at elevated temperatures and has good performance at low temperature up to its freezing temperature at 20°C. Unfortunately, LiBF_4 is often criticized because of its low conductivity, its low solubility in commonly used carbonate-based solvents

and the formation of a highly resistive solid electrolyte interface (SEI). The high solubility, ionic conductivity and electrochemical stability of lithium bis(trifluoromethylsulfonyl)imide (LiTFSI) makes it an attractive candidate, but it corrodes aluminum.

Its mono-fluorinated homologue lithium bis(fluorosulfonyl)imide (LiFSI) is thermally stable, gives good performance at high temperature and is a good compromise to LiTFSI, because it has a higher ionic conductivity, has better electrochemical stability and it forms a passivation layer on the Al current collectors. This passivation was shown to be highly dependent on the purity of this salt. In order to get a high purity LiFSI at low cost, Arkema developed a new process: the HF chemistry. Thanks to this process, Arkema was able to get a high purity LiFSI called PEA (Power Electrolyte Arkema) with a very low content of chlorine impurities [212].

In addition to electrolyte development, there is a need to develop high-voltage cathode electrodes as well. In this context, the high-voltage spinel from Umicore is the only close-to-market technology. However, the specific capacity of this cathode is lower than with NMC. From the anode side, the most promising and close to the market solution is silicon alloy as discussed in section 2, which additionally has a high specific capacity.

There are several European projects (e.g. FIVEVB) ongoing with high technological readiness level (TRL): > 5. The estimated time to market is between 5 to 10 years. The maturity level of the individual materials is in the meantime high. Since, the energy density of this technology is higher than the commercial Li-ion batteries, the targeted applications are battery electric vehicles and plug-in hybrid electric vehicles. [212]

Cost and °

The high-voltage batteries are still under development and thus there are no real price indications. However, high-voltage cathode, high-voltage electrolyte and silicon alloy anode will allow to reduce the battery cell by 20-30% compared to existing Li-ion batteries. Thus, the target cost will be about 150 Euro/kWh.

Key players are:

- Umicore for the cathode
- 3M for the anode
- Arkema for the electrolyte
- BASF for the electrolyte
- Solvay for electrolyte

3.2.5 Hybrid technologies and LICs

Hybrid technologies cover a wide range of topics including:

- Using capacitor and batteries in a tandem working principle. This allows to combine the benefits of high power (from the capacitor) with the high energetic capacity of electrochemical EES. Typically the components are individual elements but real hybrids like the ultra battery can be found aswell. The cell consists of a capacitor and electrochemical cell internally. (Because this technology can effectively be considered as two separate technologies, we will not discuss this here).
- The term hybrid components is also used for LIC (Lithium Ion Capacitors). These are EDLC's (electric double layer capacitors) and consequently do not store energy in electrochemical form (like LIB's) but they store it in the electric field (over a separating membrane). This can effectively be considered as a separate cell technology which we discuss a bit further in this section.

General information with respect to capacitors was covered in Chapter 1. Further in this section we discuss Lithium Ion Capacitors.

Characteristics

In LIC's, the ions in the electrolyte come from the interface of the activated carbon (AC) electrode. This process is thus non-faradaic, as can be observed in Figure 3.10. This indicates that EDLC's can obtain a very high power density (10 kW/kg) and lifetime (over one million cycles), but as a drawback have only a limited energy density of around 5 Wh/kg [62], [199], [199], [30], [31], [190].

In order to increase their energy density, several concepts are currently under research: new materials, such as MXenes [138], pseudocapacitors that use redox-active materials like RuO₂ and MnO₂ [51], [206] and hybrid batteries. This concept results in a RESS that combines the high power capability of EDLCs with the high energy density of LIB's [153], [185], [154]. Therefore the hybrid capacitor technology has its own specific place on the Ragone plot in between the LIBs and EDLC's [185]. The hybrid capacitor technology is thus very interesting in applications that need a RESS with a high power capability combined with the need for a considerable amount of energy content, such as heavy transport applications like hybrid buses, trams, trains and metros but also in uninterruptible power supply (UPS) systems.

Several companies are already commercially offering specific types of hybrid batteries. JM Energy, as subsidiary of JSR Corporations, started commercialization of lithium-ion capacitors (LICs) in 2007.

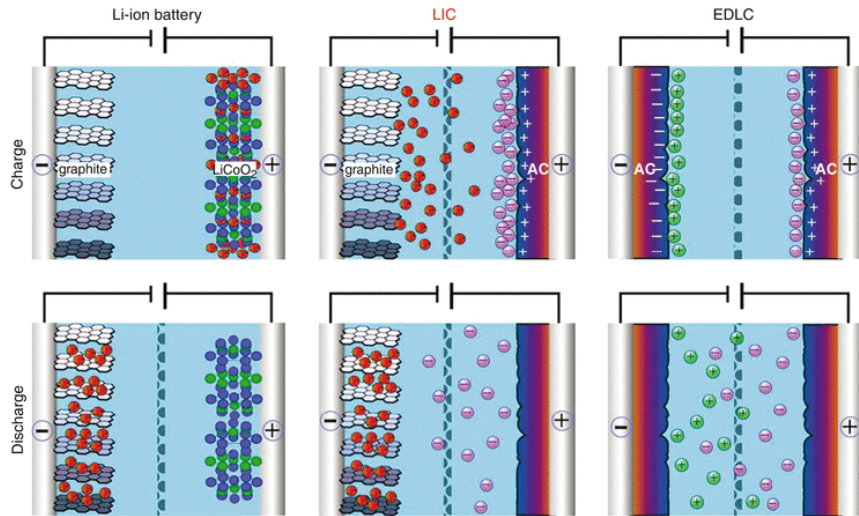


Figure 3.10: Hybrid capacitor principle, [139]

The concept of hybrid batteries was applied for the first time in the academia field by Amatucci, who presented in 2001 the combination of a lithium titanate $\text{Li}_4\text{Ti}_5\text{O}_{12}$ negative electrode with an AC positive electrode, obtaining a cell with an energy density of more than 20 Wh/kg, [15]. JM Energy uses a pre-lithiated (pre-doped with lithium ions) graphite negative electrode in combination with an AC positive electrode. The pre-lithiation of the graphite electrode allows decreasing its reference potential meaning that the cell voltage can be increased up to 3,8 V, compared to a maximum voltage of 2,7 V for typical EDLC's. LICs however also have a minimum voltage of 2,2 V, while EDLC's can be discharged up to 0 V.

The Ukrainian company Yunasko offers, aside from several EDLC cells, a hybrid capacitor with a capacitance of 5200 F. It is a pouch type with a very low mass of only 85g which results in a very high energy density of 30 Wh/kg according to Burke et al. [32] and 37 Wh/kg based on the data-sheet [234]. The high energy content of the Yunasko cell however has a drawback in terms of limited cycle life of around 10.000 cycles, while the JM Energy cells can obtain a cycle life over 1 million cycles.

Table 3.2 compares some key metrics of some discussed hybrid capacitors.

Cost and Suppliers

The cost of a lithium-ion capacitor is about 0.05 Euro/F compared to 0.01 Euro/F for electrical double layer capacitors. However, the first one is still not in mass production, thus the cost will decrease to approximatively the same cost as EDLCs

It should be noted that the cycle life of lithium-ion capacitor is in general higher than that of electrical double-layer capacitors (based on the 2300 F model of JM Energy: 2.000.000 cycles). Thus the cost in Euro/(kWh.cycle) for lithium-ion capacitor will be lower than

	JM	JM	Yunasko	EDLC
Capacity [F]	2300	3300	5200	3400
Operating Voltage [V]	2,2 3,8	2,2 3,8	1 - 2,8	0 2,85
Energy density [Wh/kg]	8	12	30	7,6
Power density [kW/kg]	10.6	9,3	4	18
R_i [m Ω]	0,7	0,8	1,5	0,22
Opp. Temp [°C]	-30 to 70	-30 to 70	-40 to 60	-40 to 65
Mass [g]	365	350	85	520
Appearance	Prismatic	Prismatic	Pouch	Cylindrical
Dimensions [mm]	150	150	75	138
	91,5	91,5	120	60,4
	15,5	15,5	11	60,7

Table 3.2: Comparison of the discussed hybrid capacitors

for EDLCs.

Key players are:

- JM Energy
- Yunasko,
- Shin-Kobe (affiliate of Hitachi)
- Nippon Chemi-Con
- Taiyo Yuden.

Chapter 4

Thermal management

4.1 Introduction

Thermal battery management is essential for good battery performance, operation and lifetime [161]. The thermal management system usually consists of battery cooling, but can also include heating or heat buffering. The main goal of the thermal management system is to allow the battery to operate in a desired temperature region. The first target is to avoid battery failure related to thermal causes. A second target can be to control the battery temperature in a more narrow temperature region, where the battery performance is maximal and the battery ageing is minimal.

4.1.1 Thermal battery behaviour

Many chemical and electrochemical reactions take place during charge and discharge of batteries. These reactions can be either exo- or endothermic. For Li-ion batteries, the chemical reaction is endothermic during charging and exothermic during discharge [157]. This refers to the chemical reaction taking up heat from the environment during charging and generating heat during discharging. Heat will also be generated by the internal resistance of the battery, during both charging and discharging. The combined effect of these two phenomena is that during discharging, the battery always generates heat and that during charging, the battery can be either releasing or taking up heat. Figure 4.1 shows such a charge/discharge cycle, where heat is released during both the charging and discharging periods. In this figure, Q_{irr} is the irreversible heat, which is equal to the thermal losses of the battery. Q_{rev} are the reversible heat flows, resulting from the heat generation and intake of the reversible chemical reactions. When regarding an entire charge and discharge cycle, the net effect will always be heat generation by the battery.

The heat generation, temperature distribution and heat capacity varies between different

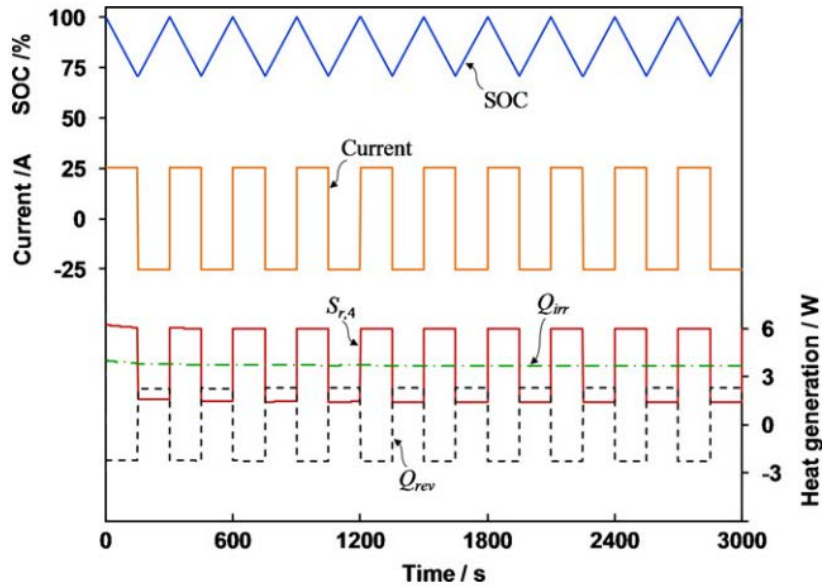


Figure 4.1: Charge and discharge cycle of a Li-ion battery [124]

types of battery modules. Knowledge of these characteristics is essential for adequate design of the thermal management system. Characteristics of several battery modules have been measured and reported by Pesaran & Keyser [162].

Safety and reliability of Li-ion battery packs is a key issue for several applications, such as EVs and HEVs [221]. The possible risks that need to be avoided are overheating, combustion and explosion. Overheating usually results from overloading the battery or from internal short circuits. In turn, overheating can lead to combustion or explosion, mostly as a result of a situation called thermal runaway. The chemical reactions inside the batteries generate heat, by which the battery temperature increases. Due to the increase in battery temperature, the chemical reactions create more heat, causing an unstable positive feedback situation during which the temperature rises dramatically and which ultimately results in the destruction of the battery. Figure 4.2 shows thermal images of the several stages on thermal runaway of a Li-ion battery.

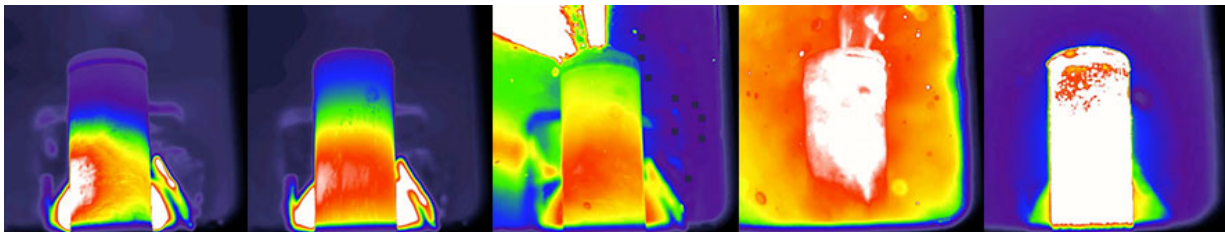


Figure 4.2: Thermal imaging of the stages of thermal runaway of a Li-ion battery [59]

One of the main problems related to thermal runaway in battery packs is that the over-

heating of one of the cells can cascade to overheating and thermal runaway of all the cells, which in turn can result in large fires and explosions. Thermal management systems should be designed to control the temperature of the battery cells, to avoid overheating and thermal runaway and, in worst case, to avoid propagation of thermal runaway of one cell to all cells.

Thermal runaway is the result of extreme temperatures that should absolutely be avoided during the battery life. However, avoiding these extreme temperatures is not the only use of a thermal management system. The performance of batteries will decrease if they are stored or operated at elevated temperatures. After 22 months of battery cycle load of a typical electric vehicle, Sarre et al. observed that when operated at 20°C the cell power and energy were quite stable, but at 40°C both reduced by 4% [194]. Wu & Chiang performed similar tests by storing Li-ion batteries for 60 days at either room temperatures or at 60°C [229]. At 0.2 C discharge, the capacity of the battery was decreased from 800mAh for a fresh battery to 680mAh for the battery stored at 60°C. At 3 C discharge, the results are even more drastic: the discharge capacity of the battery stored at room temperature is 650mAh, compared to 20mAh for the one stored at 60°C. The performance of batteries is also affected by the instantaneous operating temperature. Saito et al. measured the heat generated by discharging a Li-ion battery at temperatures from 10°C to 60°C [189]. The authors found that the heat generation was least around 27°C. Because of these effects, thermal battery management systems should be able to keep the temperature within a desired temperature range where the performance is maximal and the ageing is minimal.

Temperature distribution in batteries is also an important factor affecting performance and lifetime. On cell level, non uniform temperature distribution can locally cause very high temperatures, which can lead to faster ageing effects and thermal runaway. For example, the heat produced at the positive electrode can be three times more than that of the overall battery [79]. On system level, temperature uniformity is also very important. When temperatures are not equal between cells, these cells will be charged and discharged slightly differently during each cycle. Eventually this results in the battery pack being unbalanced, hereby reducing the battery pack peak performance [163].

4.1.2 Present thermal management solutions

Currently, many techniques have been applied and studied for thermal management systems such as passive and active air cooling, liquid cooling with water, glycol, oil, acetone and several refrigerants, heat pipe cooling and thermal buffering using phase change materials (PCM) [174]. An overview of these techniques and their characteristics will be provided in the next sections.

For most of these techniques, the distinction can be made between passive and active cooling or heating. In this context, passive cooling or heating suggests that only heat exchangers are used to exchange heat. Active cooling or heating requires a refrigeration

cycle or a heater or heat pump. The main difference between both techniques is that the passive system is always dependent on the ambient temperature for its performance, while this is not the case for the active system. The active system is however more complex and requires additional energy input.

Air thermal management

Air cooling of batteries is the most straight forward and simple technique available, also requiring the least space. There is no requirement for extra fluids, channels or containers and it directly uses the medium to which the heat will always be released eventually. When using natural convective cooling, there is no requirement for a fan. However, with natural convection the heat transfer is very low and there is no possibility to control the cooling. Because of these reasons, it should not be applied for high power applications.

Using forced convective cooling requires a fan to be implemented for the thermal management system. The heat transfer rate is an order of magnitude higher than for natural convective. Also control is possible by controlling the fan power and thus the air flow to the batteries.

Figure 4.3 illustrates some possibilities for the thermal management system for battery packs of EVs or HEVs. The first topology (A) uses solely ambient air to cool the batteries. The drawback of this system is that there is no conditioning of the ambient air. So the performance of the thermal management system is very dependent of the ambient air temperature, which can be problematic for both low and high ambient temperatures. The second topology (B) uses the conditioned air from the cabin for thermal management. This assures that the temperature of the air is always around 20°C, which is close to the optimal temperature needed for the batteries. It can be used for heating and cooling of the battery, without needing auxiliary heaters or heat exchangers. However, the mostly fixed temperature of the cabin air limits the heat transfer performance and the rate of heating and/or cooling. The third topology (C) implements auxiliary heaters and/or heat exchangers. This requires more components and extra energy use of the cooling system. However, the heat transfer will be increased compared to the previous two topologies by also regulating the air temperature.

Being the most simple thermal management system, air cooling is widely applied. However, the thermal performance is not always adequate. Sabbah et al. concluded that for plug-in hybrid electric vehicles, active forced air cooling is not able to keep cell temperatures below the safety limit for high discharge rates of 6.67 C [186]. Wu et al. found natural convective heat transfer to be ineffective for removing heat from the battery system and that forced convective cooling is not adequate to achieve a uniform temperature at the battery surface [230]. Nelson et al. concluded that sufficient cooling but also rapid heating of battery packs with air is not feasible [142].

When an air cooled battery pack releases heat, the air that is forced through the pack

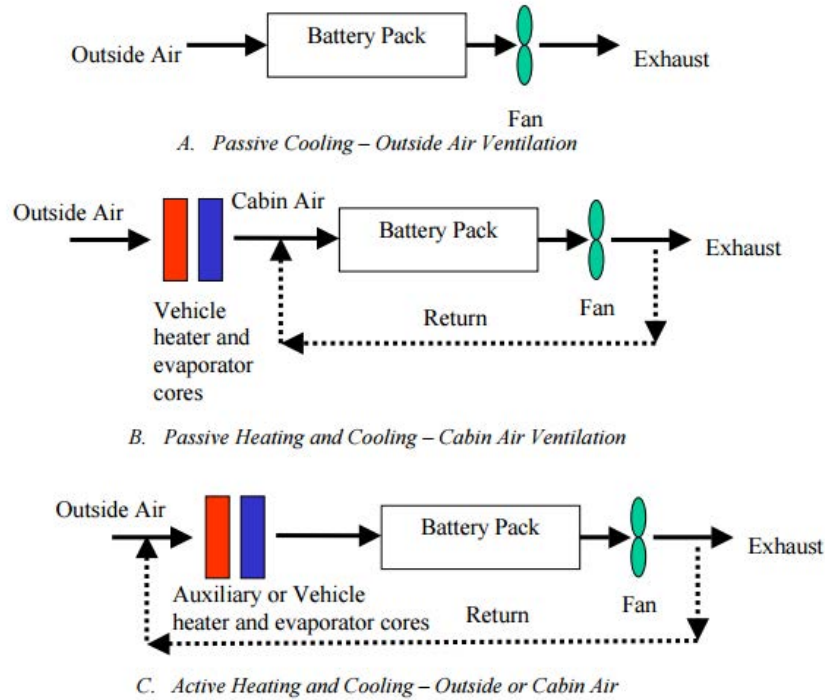


Figure 4.3: Air thermal management topologies for EVs and HEVs [161]

increases in temperature from the inlet to the outlet. This causes the cells at the air outlet of the battery pack to be at higher temperatures than those at the air inlet. As explained before, this causes a difference in charging of the cells and a reduction in peak performance of the battery pack. Mahamud & Park thermally modelled a battery pack with reciprocating air flow, where the in- and outlet of the air is alternated between the two outer ends, as shown in figure 4.4. This allowed for a better temperature uniformity with the maximum temperature difference of the cells reduced by 4°C or 72% [124].

Liquid thermal management

Using a liquid can increase the local heat transfer coefficient drastically when compared to forced air cooling or heating. This requires a separate cooling liquid system and a pump to circulate the liquid. The liquid heated by the batteries can in turn be cooled by different systems. A radiator that immediately removes the heat to the ambient air can be used. This system has the drawback that the performance is dependent on the ambient temperature. Another possibility is to implement a heat exchanger which extracts the heat from the cooling liquid. Also, a refrigeration system can be used to cool and/or heat the entire system. This increases the complexity by adding a separate circuit and will use more energy. However the cooling liquid temperature can be regulated, therefore the heat transfer rate can be higher.

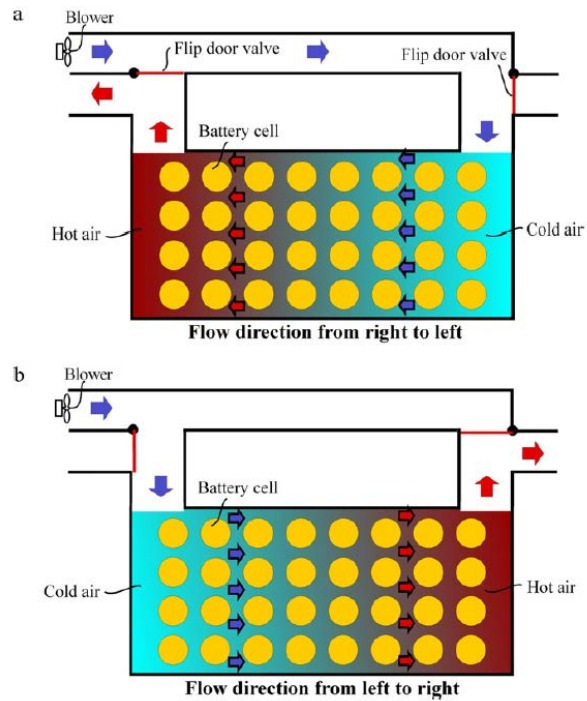


Figure 4.4: Schematic view of reciprocating air thermal management system [124]

Figure 4.12 shows the possible topologies for battery cooling using a liquid cooling fluid for EVs and HEVs. The first topology (D) uses a radiator to cool the liquid and vent the heat to the ambient air. The second topology (E) uses the engine coolant to remove the heat and cools the liquid in a liquid/liquid heat exchanger. The third topology (F) uses the air-conditioning unit (AC) to cool the liquid. This is the only topology where the liquid temperature can be truly controlled.

4.1.3 Novel thermal management solutions

The distinction is made between present and novel thermal management solutions, where the present techniques are already widely applied and the novel are still being researched. This distinction however is a bit arbitrary, because there is naturally an overlap between research and practical applications.

Two-phase evaporative thermal management

Two-phase evaporative thermal management consists of bringing the batteries in contact with a saturated liquid refrigerant. Upon the release of heat from the batteries to the refrigerant, the liquid refrigerant will start to evaporate. The refrigerant is usually brought

into contact with the batteries through tubing or cold plates. There are several advantages to two-phase evaporative thermal management. Firstly, the heat transfer coefficient related to evaporation is higher than the heat transfer coefficient of single phase liquid heat transfer. This results in a lower temperature of the batteries for the same heat release. Evaporation occurs at a constant temperature when the pressure is constant. This results in only a small temperature change of the refrigerant when evaporating, due to the pressure drop in the tubing. The related advantage is that the temperature distribution between the different cells will be more uniform. A third advantage is the possibility to directly use a refrigeration cycle to cool the batteries. Compared to active liquid cooling, this requires one less cooling circuit.

There are however several drawbacks. When cooling large battery packs, a large quantity of refrigerant is needed which can be expensive. Another factor influencing this cost are the environmental regulations. These regulations prohibit the use of several refrigerants with too high ozone depletion potential (ODP) and global warming potential (GWP). Over time these regulations become more strict, resulting in the banning of cheaper refrigerants. Another drawback is the difficulty of sealing of the cooling circuit. This is very important for good operation, but can be very complex and costly to manufacture.

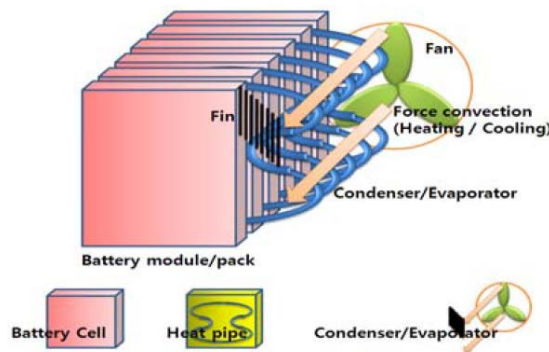


Figure 4.5: Loop thermosyphon thermal battery management system [89]

A loop thermosyphon is a kind of two-phase evaporative cooling system where fluid is transported naturally through density differences. At the batteries, the fluid evaporates and the vapour bubbles rise through the density difference with the liquid. On top of the system, heat is removed and the vapour condenses. Gravity returns the liquid back to the batteries. Jang & Rhi built and tested a loop thermosyphon battery thermal management system, which is shown in figure 4.5 [89]. The cell temperature was maintained below 50°C when every cell released 50W of heat.

Heat pipe thermal management

Strictly speaking, heat pipe thermal management is a kind of two-phase evaporative thermal management, similar to a thermosyphon. However, it is considered here as a different topic, because of its specific characteristics. A schematic representation of a heat pipe is shown in figure 4.6.

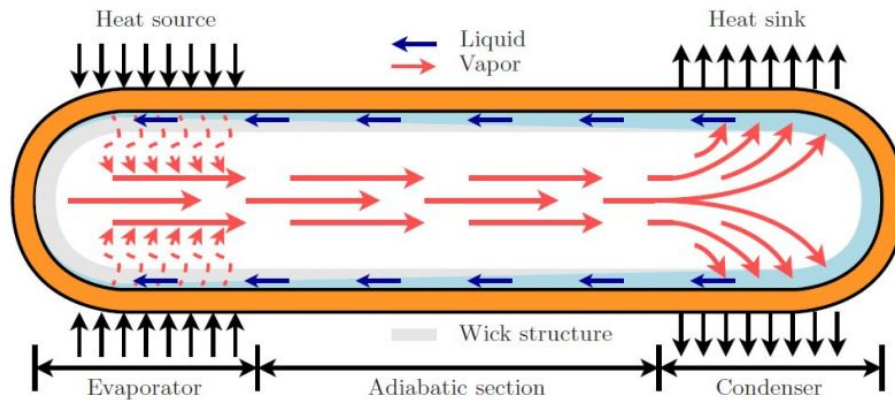


Figure 4.6: Heat pipe working principle

A heat pipe is a sealed container incorporating wick material at the inside. A fluid which is partly in gaseous and partly in liquid phase is trapped inside the container. When a temperature difference is introduced over the heat pipe, for example by heat generated by a battery, liquid will start to evaporate at the high temperature side (evaporator). The formed vapour moves to the low temperature side of the heat pipe, where it condenses by releasing heat (condenser). Through capillary forces, the liquid is moved back through the wick material to the high temperature side. This cycle repeats and so heat transfer is achieved with a low temperature difference.

Rao et al. experimentally investigated heat pipe implementation in a thermal management system [175]. Heat pipes were connected to heaters which simulate the batteries. The condenser side of the heat pipe was cooled with water. It was concluded that heat pipes are an effective method for power batteries thermal management.

Park et al. performed a design optimization for loop heat pipes (LHP) for the cooling of Li-ion batteries in military aircraft [159]. Loop heat pipes are heat pipes where the vapour and liquid transport do not occur in the same area, but in different connections between the evaporator and the condenser side. The authors concluded that the loop heat pipe performed according to the battery cooling needs and that a weight reduction with an optimized design was possible.

Pulsating heat pipes (PHP) were investigated by Swanepoel for implementation in thermal battery management systems [205]. Pulsating heat pipes have a different working principle from regular heat pipes. They consist of a series connection small diameter U-bended tubes

filled with a partially liquid and partially gaseous fluid. When heat is transferred to one side of the PHP, the plugs of vapour and liquid inside will start to oscillate and transfer heat to the other side. An example of a PHP constructed for the experiments of Swanepoel is shown in figure 4.7. A theoretical model was made and validated with experiments, which can be used to design PHPs for thermal battery management systems.

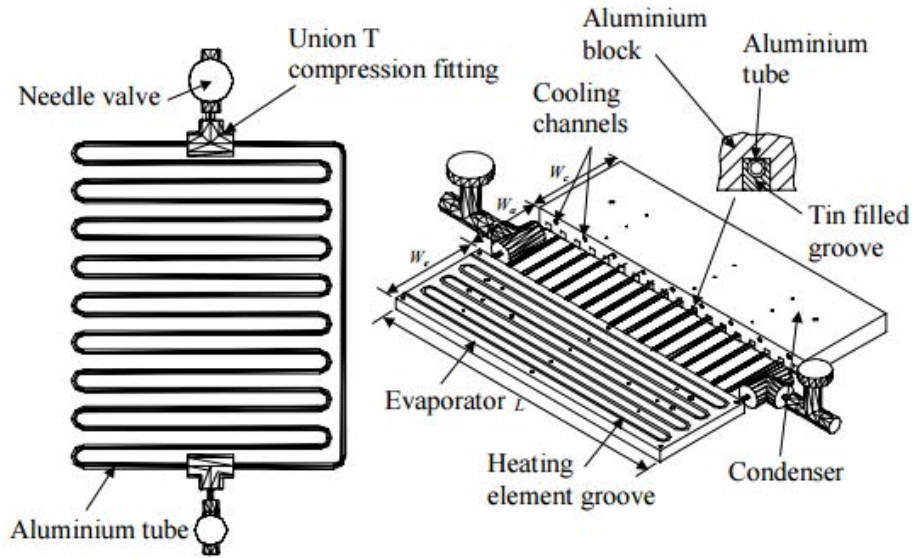


Figure 4.7: Pulsating heat pipe for thermal battery management [205]

Overall, it can be summarized that heat pipes can offer high heat transfer rates with low temperature differences. However, heat from the condenser side of the heat pipe still has to be removed to the environment. The conclusion is that heat pipes are very useful to transport heat from central spaces and/or local hot spots where it is difficult to cool, to the outside of the battery pack or to a larger surface area, where it is easier to remove the heat by other means of heat transfer.

PCM thermal management

Phase change material or PCM thermal battery management was first introduced by Al Hallaj & Selman [13] and is patented by Al Hallaj & Selman [14]. PCMs are substances which change phase from solid to liquid by taking up or releasing heat. When applied to a battery pack, the PCM can take up heat by melting. The temperature of the PCM stays constant during the melting process, by which the temperature increase of the batteries is mitigated. Essentially the temperature of the battery is buffered by the PCM, by which overheating but also too low temperatures can be avoided.

Sabbah et al. compared a passive cooling system with PCM to an active air cooled system [186]. The authors concluded that at high discharge rates and high ambient temperatures,

the air cooled system does not keep the temperature of the cells in the desired operating range, while the passive PCM system is able to meet the required temperature demands. Khateeb et al. designed and experimentally tested and compared four different methods of heat dissipation: natural convection cooling, aluminium foam heat transfer enhanced cooling, PCM enhanced and a combination of PCM and the aluminium foam [96]. For natural convective cooling, the temperature rise of the batteries was too high. Using the aluminium foam, temperature rise was reduced, but still too high for high discharge situations. The implementation of only PCM between the cells resulted in a large drop of the temperature rise, but heat dissipation to the environment was limited, which can cause complete melting of the PCM and overheating during long operation. The combination of the aluminium foam and PCM resulted in a small temperature drop compared to the PCM alone, but better heat dissipation.

Kizilel et al. modelled PCM thermal battery management system to evaluate the performance [97]. The modelled PCM thermal battery management system is illustrated in figure 4.8. The authors concluded that the system performs well for nominal and stressful loading conditions. A uniform temperature of the cells can be achieved. Thermal runaway can be limited to one cell, removing the possibility of propagation of thermal runaway to the other cells.

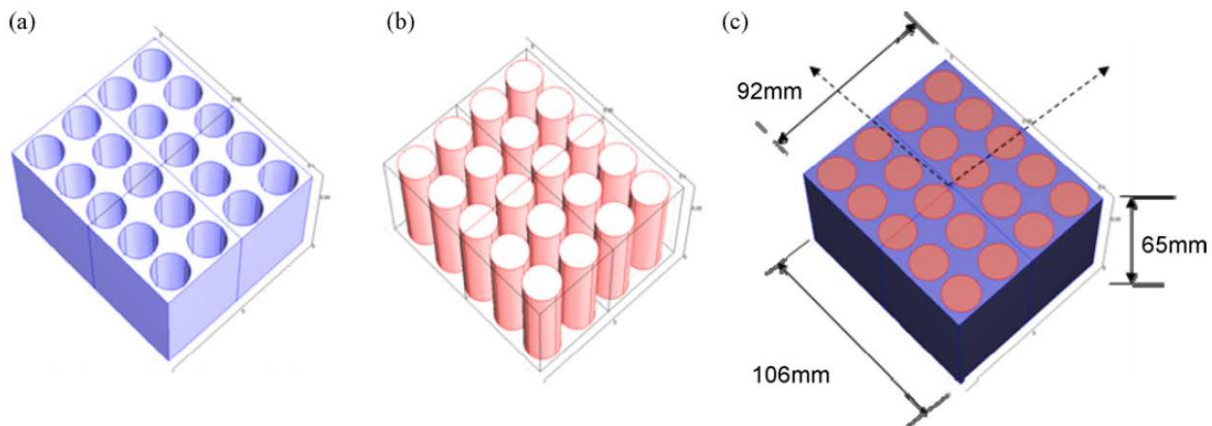


Figure 4.8: Schematic representation of module configuration: (a) PCM filled closed box; (b) Li-ion cells; (c) battery module [97]

The PCMs that are most applied are paraffins because of their large latent heat, availability at different melting temperatures, non-toxicity, non-corrosive nature, stability and low cost. Their low thermal conductivity is however the biggest drawback [174]. A lot of research has been done in order to increase the thermal conductivity. Possibilities are the insertion of a metal matrix in the PCMs or composite PCMs which are combination of PCM with a high thermal conductivity material. An overview of many of the results found in literature is given by Rao & Wang [174]. They conclude that more research has to be done on the thermo-mechanical behaviour of PCMs and the system behaviour.

4.1.4 Cost assessment

The cost of a battery thermal management system is highly dependent on the application: type of batteries, load cycles, weight/volume limitations, other limitations, etc. A detailed analysis of the cost of a thermal management system is therefore very hard to perform. We can however compare the different techniques with each other.

A trade-off analysis was made by Cosley & Garcia [40] and later adapted by Rao & Wang [174]. The overview of this analysis is shown in table 4.1. Two-phase evaporative cooling was not incorporated in this overview.

Table 4.1: Trade-off analysis of battery thermal management systems [174]

	Air forced	Liquid	Heat pipe	PCM
Ease of use	Easy	Difficult	Moderate	Easy
Integration	Easy	Difficult	Moderate	Easy
Efficiency	Low	High	High	High
Temperature drop	Small	Large	Large	Large
Temperature distribution	Uneven	Even	Moderate	Even
Maintenance	Easy	Difficult	Moderate	Easy
Lifetime	≥ 20 years	3-5 years	≥ 20 years	≥ 20 years
Initial cost	Low	High	High	Moderate
Annual cost	Low	High	Moderate	Low

Generally speaking, increased complexity results in increased cost. The most simple system is of course the natural convective air cooling system, which is no thermal management system. Passive air cooling with a fan is also relatively cheap. Passive liquid cooling is a bit more complex, but does not require very expensive components. Active air cooling and active liquid cooling require a refrigeration unit, which increases the cost. Liquid systems require more maintenance than air systems.

Two-phase evaporative cooling is very complex and requires complex design for sealing. Refrigerants can be very expensive, which makes it the most expensive system. Also regular maintenance is necessary. Common heat pipes are not very expensive, however for thermal battery management a dedicated and complex design is needed, which increases the cost. Maintenance for heat pipes is limited. A well designed PCM thermal management system is not too complex and can be quite inexpensive. For this system, maintenance should be very limited.

4.1.5 Suppliers

An overview of some of the most prominent thermal battery management system ° is given in the next sections.

Air International Thermal Systems

Air International Thermal Systems provides thermal solutions for vehicle applications. They provide advanced battery cooling systems for electric and hybrid electric vehicles using both air or liquid systems.¹

Dana

Dana Holding Corporation is a supplier of powertrain components for vehicles. Dana offers thermal managements solutions for batteries in the form of liquid cooled cold plates and battery interelement cooling plates.² An example of an interelement cooling plate is shown in figure 4.9.

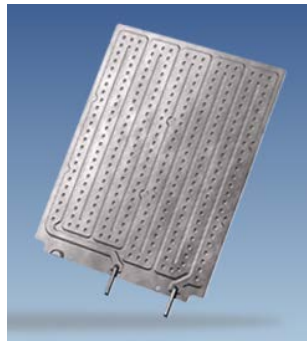


Figure 4.9: Interelement cooling plate by Dana

GCoreLab

GCoreLab is a clean tech thermal management company performing research and development of thermal management systems for the next generation of electric vehicles. They provide a thermal battery management system with high performance cooling and heating using an integrated liquid cooling solution.³ The heat sinks applied to the batteries use oblique fins introduced in mini/microchannels to enhance heat transfer and cooling capability. This patent pending technology is shown in figure 4.10.

Modine

Modine Manufacturing Company designs, manufactures and tests heat transfer products for a wide variety of applications and markets. For battery thermal management systems,

¹<http://www.ai-thermal.com/products/green-systems-electric-vehicle-hybrid->

²<http://www.dana.com/light-vehicle/products/electric-and-hybrid/thermal-solutions>

³<http://gcorelab.com/>

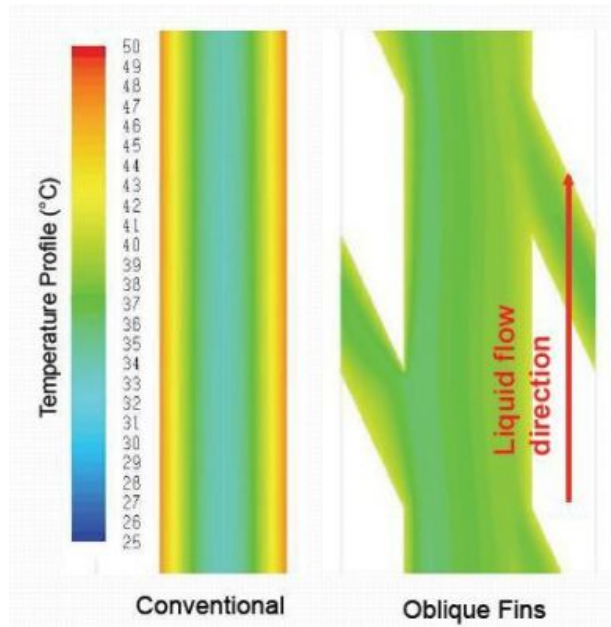


Figure 4.10: Temperature profile of a conventional channel and a channel with oblique fins by GCoreLab

Modine provides brazed heat exchangers and stamped cooling plates with turbulators for two-phase heat transfer systems.⁴

CapTherm Systems

CapTherm specializes in development and commercialization of next-generation high-power electronics cooling technologies. They focus on evaporative two-phase heat transfer. For thermal battery management, CapTherm provides a evaporative two-phase heat transfer system with natural circulation of the refrigerant.⁵

AllCell Technologies

AllCell technologies designs and manufactures lithium-ion battery packs.⁶ They have a patented thermal management technology based on PCMs [14]. The thermal battery management system consists of a graphite and wax enclosure for batteries. The graphite ensures good thermal conductivity while the wax is the PCM which renders a high heat capacity. The product is able to maintain the battery temperature within the desired operating range, render a uniform temperature over the battery pack and prevent thermal runaway

⁴<http://www.modine.com/web/en/battery-cooling-heating.htm>

⁵<http://captherm.com/electric-vehicle-cooling/>

⁶<https://www.allcelltech.com/>

of one cell to propagate to other cells. Systems for cylindrical and prismatic cells are shown in figure 4.11.

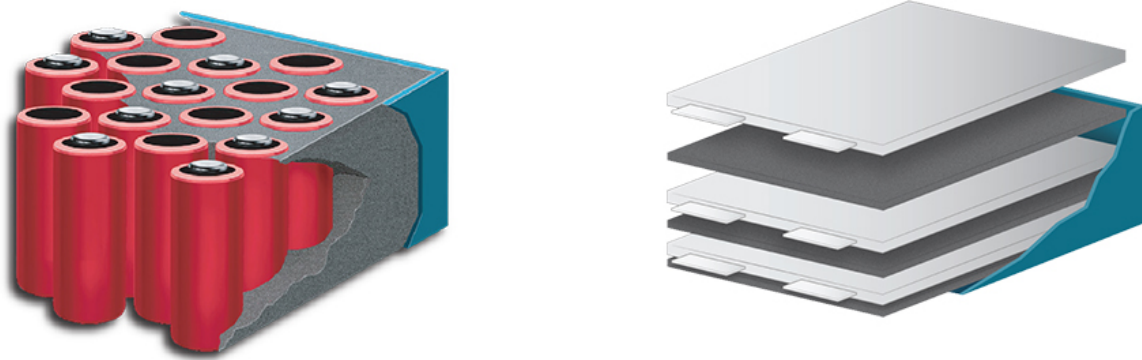
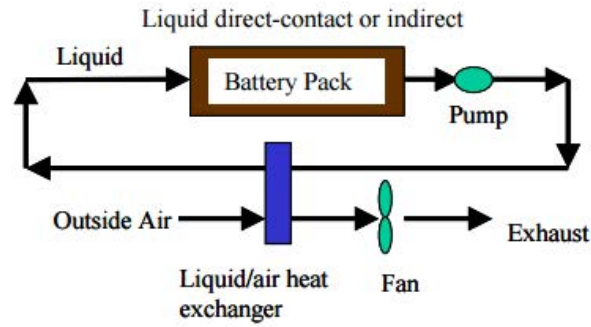
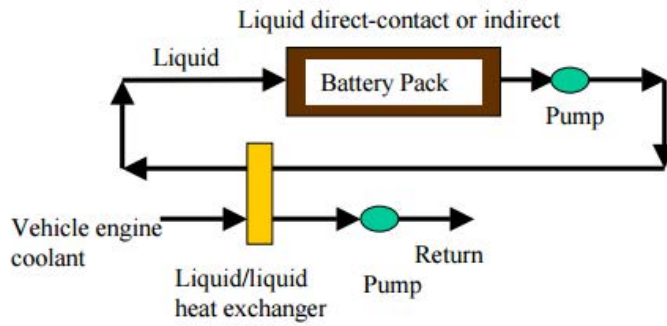


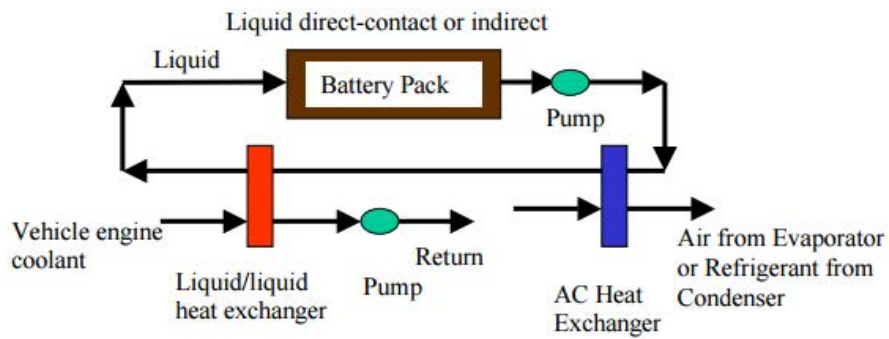
Figure 4.11: AllCell thermal management system for cylindrical (left) and prismatic (right) cells



D. Passive Cooling – Liquid Circulation



E. Active Moderate Cooling/Heating – Liquid Circulation



F. Active Cooling and Heating – Liquid Circulation

Figure 4.12: Liquid thermal management topologies for EVs and HEVS [161]

Chapter 5

Battery management systems

5.1 Introduction of battery management systems

The *Battery Management System* (BMS) is the central control unit of the battery pack. It consists of at least a master controller, which presents itself as a *Printed Circuit Board* (PCB). The existence of slave control PCBs depend on battery pack configuration and peripheral sensors. The tasks subscribed to a BMS may typically include:

- Monitoring the battery, this is in most cases measuring any variable of the set voltage, current and/or temperature (V, I, T), and more recently also the magnetic field H [213].
- Monitoring environmental parameters, i.e. coolant temperature, coolant flow, ambient temperature, etc.
- Protecting the battery, i.e. protecting the individual cells from overcharging, overvoltage, undervoltage, etc.
- Estimate the *State Of Charge* (SOC), also known as “Fuel Gauge”
- Estimate the *State Of Health* (SOH)
- Estimate the *Remaining Useful life* (RUL)
- Maximizing the performance of the battery pack
- Communicate with slaves and report the status of the battery pack to the user

Since there is no exact definition of a BMS, many people call many things a BMS. As such a *Protection Circuit Module* (PCM) is often called a BMS and vice versa. The distinction

between both is here defined as the lack of the PCM in being able to directly report to the user (visually or through a well defined communication protocol as CAN, I2C, SMBus, SPI, etc.) and the intrinsic ability of the PCM to interrupt the charge or discharge current by means of a switching device.

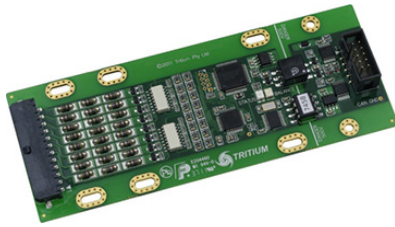


Figure 5.1: Example of a PCB

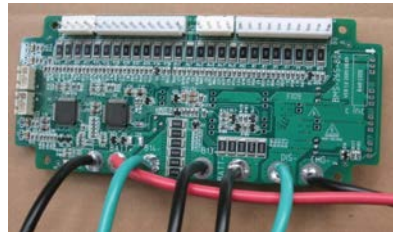


Figure 5.2: Example of a PCM

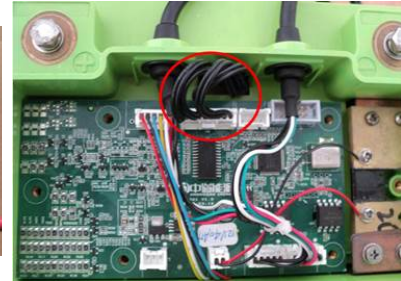


Figure 5.3: Example of a BMS

Figure 5.4: Example of a PCB, a PCM and a BMS

5.1.1 Present solutions

In this section the present solutions are discussed on how to keep the battery pack within its *Safe Operating Area* (SOA) by means of a BMS.

Protection against: cell imbalance

If overcharged, Li-Ion cells are prone to accelerated cell degradation and can catch fire or even explode. Hardware and software protection is in place to mitigate these immediate dangers. In a multicell battery pack, placing cells in series opens up the possibility of cell imbalance.

No two cells are identical. There are always slight differences in the state of charge (SOC), self-discharge rate, capacity, impedance, and temperature characteristics, even for cells that are the same model from the same manufacturer and even from the same batch of production. When building multicell packs, manufacturers usually sort cells with similar SOC's by voltage. However, variations in an individual cell's impedance, capacity, and self-discharge rate can still lead to a divergence in its voltage over time. Since most battery chargers detect full charge by checking whether the voltage of the entire string of cells has reached the voltage-regulation point, individual cell voltages can vary as long as they do not exceed the limits for overvoltage protection. However, weak cells, i.e. cells with lower capacity or higher internal impedance, tend to exhibit higher voltage than the rest of the series cells at full charge termination. These cells are weakened further by continuous

overcharge cycles. The higher voltage of weak cells at charge completion causes accelerated capacity degradation.

On the other hand, in discharge, the weak cells tend to have lower voltage than the other cells, due to either higher internal resistance or the faster rate of discharge that results from their smaller capacity. This means that if any of the weak cells hits the cell undervoltage-protection limit while the pack voltage is still sufficient to power the system, the full capacity of the battery will not be used [223].

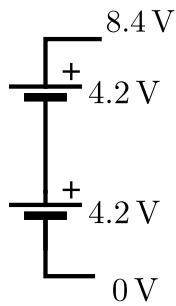


Figure 5.5: Balanced battery pack

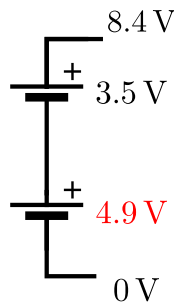


Figure 5.6: Unbalanced battery pack

Figure 5.7: Example of imbalance in a two cells series configuration

Solution: cell balancing

Passive cell balancing

The passive cell-balancing method, also known as “resistor bleeding balancing”, is simple and straightforward: discharge the cells that need balancing through a dissipative bypass route. This bypass can be either integrated or external to the IC. Such an approach is favorable in low-cost system applications. The fact that 100% of the excess energy from a higher energy cell is dissipated as heat makes the passive method less preferable to use during discharge because of the obvious impact on battery run time [223].

Balancing is not only a hardware concern, on the software side one can differentiate between charging algorithms based on the set of inputs the algorithm takes into account. There exist voltage based, voltage based with fuel gauging, SOC based, SOC and capacity based, . . . A suggestion for further reading is chapter 4 “Cell-Balancing Techniques: Theory and Implementation” in “Battery Power Management for Portable Devices” [236].

Active cell balancing

Active cell balancing overcomes the energy loss of the passive method by using capacitive or inductive charge storage and shuttling to deliver energy to where it is needed most. This is

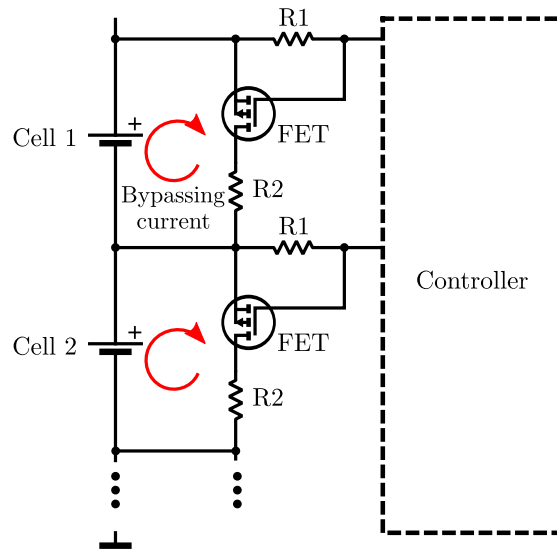


Figure 5.8: Working principle passive balancing

preferable for efficiency-conscious designs and for applications where delivering maximum run time is a priority.

One simple approach for redistributing the energy among cells is to connect a capacitor first to the higher voltage cell, then to the lower voltage cell, as shown in figure 5.9.

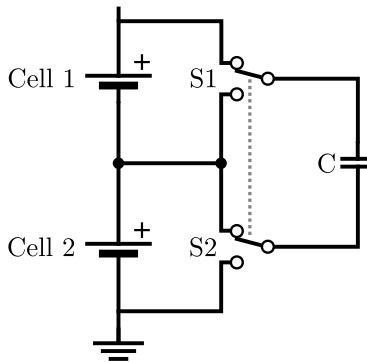


Figure 5.9: Simple capacitor based cell balancing (reproduced figure from [236])

As with passive balancing, active balancing is not only a hardware concern. The same differentiation as made with passive balancing algorithms can be made here.

Redistribution

Redistribution is a technique that shuffles energy in a battery in such way that all of its energy can be used. While discharging, additional energy is taken from the cells with the highest capacity, so that the cells with the lowest capacity are no longer the limiting factor

in the battery capacity. An effect of redistribution is that the SOC of the battery and the SOC of each cell are always equal.

A sketch of a simple example can be found in figure 5.12. Suppose that the capacity of cell 1 is 20% higher and the capacity of cell 2 is 20% lower than the nominal value. Without redistribution, the battery capacity is limited by cell 2 and the battery will be fully discharged in 48 minutes. With redistribution, extra energy is taken from the cell 1 to make up for the cell 2's low capacity. In this case they will both discharge for 60 minutes. The DC-DC converter powered by cell 1 converts its cell voltage to the full battery voltage, while the one across cell 2 remains off.

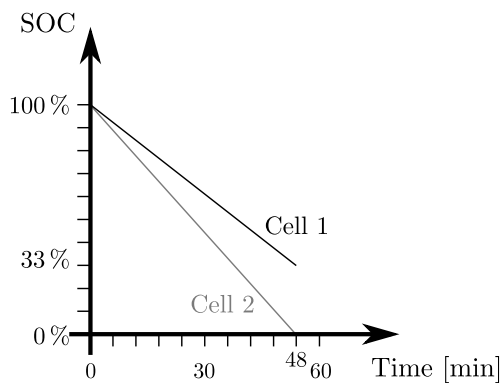
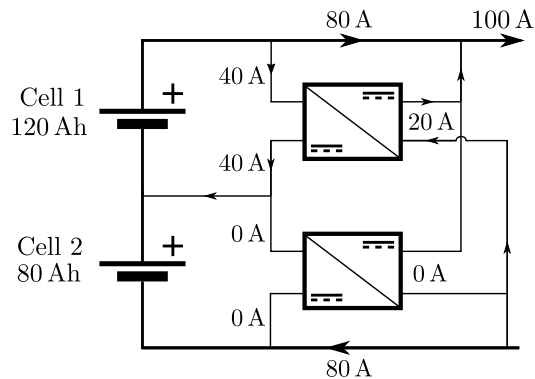
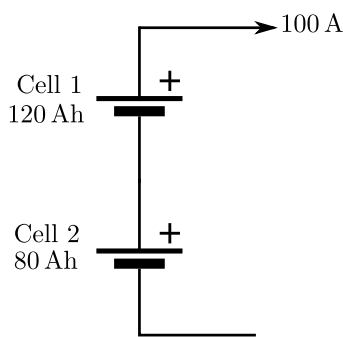


Figure 5.10: Without redistribution

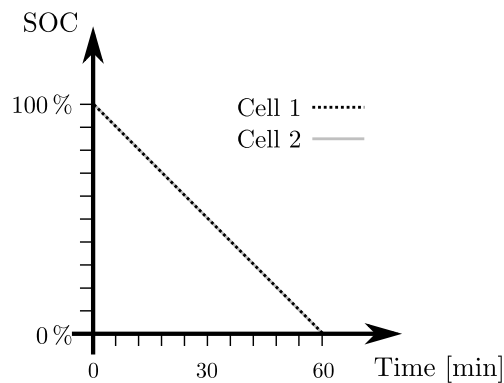


Figure 5.11: With redistribution

Figure 5.12: Simple example of redistribution in a 2 cell battery (reproduced figure from [16])

Protection against: overvoltage

When lithium ion cell voltage exceeds 4.2V by a few hundred millivolts, it can undergo thermal runaway, melting the battery pack and melting the device it is powering. If the maximal recommended charging voltage is exceeded even a little, it will cause very

accelerated degradation. Just increasing the charging voltage from 4.2 V to 4.25 V causes the degradation rate to increase by 30 %.

One can think that with cell balancing, the problem of overvoltage is excluded. While this limits overvoltages due to some of the underlying causes of cell imbalance, it does not limit it for all and in some cases even worsens the situation. For example, consider a LiFePo4 battery chemistry. Typical for this kind of battery is the flat curve when plotting *Open-Circuit Voltage* (OCV) in function of SOC, this is shown in figure 5.13. Due to this flat voltage profile, differences in SOC between the cells as large as 10 % are not noticeable in the cell voltage when it is in midrange of SOC but can nevertheless cause drastic voltage deviations close to the end of charge and discharge. As such, a simple voltage based passive balancing algorithm might detect the SOC difference too late and, if the charge current is bigger than the bleeding current (which is quasi always the case), will not be able to balance the cells at charge termination nor be able to balance the cells after multiple charge-discharge cycles.

Moreover, SOC estimation by means of measuring OCV inherently has the problem of distortion due to impedance differences in the different cells. The voltage drop across the cell terminals will be proportional to the current flowing through and has little to do with SOC. If most of the difference in SOC is caused by an impedance imbalance, bypassing more current through this cell will result in the opposite effect. It will increase the SOC difference from other cells to a larger value than it would be without the balancing. This is a problem for all voltage-controlled balancing methods (such as for capacitive/inductive energy redistribution) and not just to simple bypass balancing.

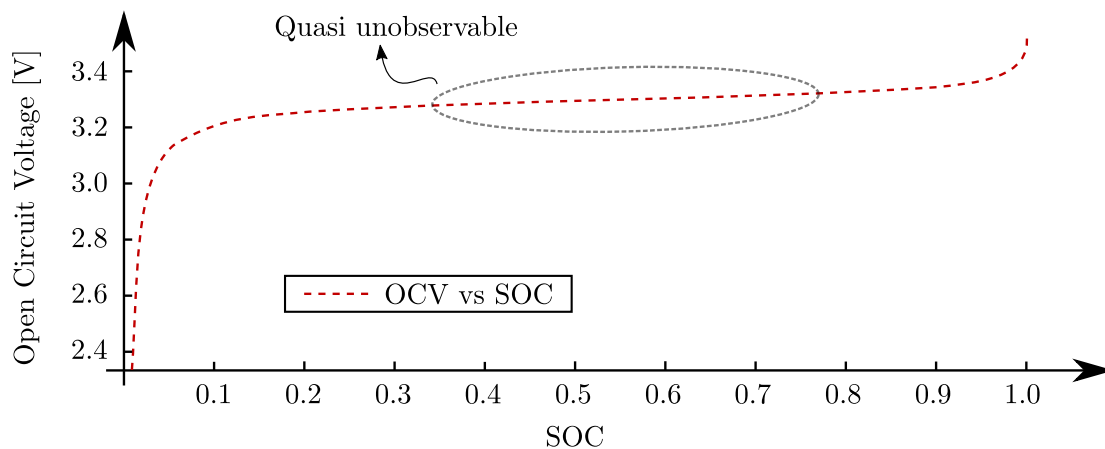


Figure 5.13: OCV in function of SOC for LiFePo4 battery (reproduced from [208])

Solution: charge current shut off

When an overvoltage is detected, the charge cycle should be interrupted by means of current cut-off. If a cooling mechanism is available, it should be turned on.

Protection against: undervoltage

If the Li-ion cell voltage goes below 2V, the actual dissolution of the Cu-current collector will occur. This is deadly to the cell if the process is allowed to continue to a significant extent (no current collector, no charge/discharge). For this reason any device using a Li-ion battery absolutely has to have a discharge termination based on voltage. Some naive attempts to introduce a consumer-replaceable Li-ion battery, for example as a drop-in replacement for coin cells, have so far faltered for the very reason that primary cells that are being replaced did not require any undervoltage shutdown (they just die, being primary) and might keep draining substantial current regardless of battery voltage even when no useful operation is taking place. If a Li-ion cell is placed into a device that was not designed for it, the cell will be overdischarged below 2V and die just like the primary cell that it replaces [236].

Solution: discharge current shut off

When an undervoltage is detected, the discharge cycle should be interrupted by means of current cut-off.

Protection against: low temperature

At low temperatures the chemical insertion of Li^+ into the graphite electrode (intercalation) becomes slow, whereby the excess of Li^+ ions may deposit as metallic Li. This process is called lithium plating and leads to degradation and failure of the cell.

It is caused by low-temperature charging with high current and at a high state of charge (SOC). However, poor capacity balance can also lead to metallic lithium deposition at higher temperatures. Besides capacity loss and impedance rise, lithium plating also presents a serious safety hazard. The metallic lithium can grow dendritically which may cause an internal short circuit of the cell [164].

Solution: turn on heater

To avoid lithium plating one should increase the temperature of the battery (within its Safe Operating Area).

Protection against: high temperature

High temperature leads to degeneration of the cell and builds up to thermal runaway, a situation where an increase in temperature changes the conditions in a way that causes a

further increase in temperature, often leading to a destructive result. One can distinct the following stages:

- Breakdown of the thin passivating *Solid-Electrolyte Interphase* (SEI) layer on the anode. The initial overheating may be caused by excessive currents, overcharging or high external ambient temperature. The breakdown of the SEI layer starts at the relatively low temperature of 80 °C and once this layer is breached the electrolyte reacts with the carbon anode just as it did during the formation process but at a higher, uncontrolled, temperature. This is an exothermic reaction which drives the temperature up still further.
- As the temperature builds up, heat from anode reaction causes the breakdown of the organic solvents used in the electrolyte releasing flammable hydrocarbon gases (ethane, methane and others) but no oxygen. This typically starts at 110 °C but with some electrolytes it can be as as low as 70 °C. The gas generation due to the breakdown of the electrolyte causes pressure to build up inside the cell. Although the temperature increases to beyond the flashpoint of the gases released by the electrolyte, the gases do not burn because there is no free oxygen in the cell to sustain a fire. The cells are normally fitted with a safety vent which allows the controlled release of the gases to relieve the internal pressure in the cell, avoiding the possibility of an uncontrolled rupture of the cell - otherwise known as an explosion or more euphemistically “rapid disassembly” of the cell. Once the hot gases are released to the atmosphere they are inflammable.
- At around 135 °C the polymer separator melts, allowing short circuit between the electrodes.
- Eventually heat from the electrolyte breakdown causes breakdown of the metal oxide cathode material releasing oxygen which enables burning of both the electrolyte and the gases inside the cell. The breakdown of the cathode is also highly exothermic sending the temperature and pressure even higher. The cathode breakdown starts at around 160 °C for Lithium Cobalt Oxide cells but at higher temperatures for other cathode chemistries, see figure 5.14.

Solution: current cut-off and turn on cooling

To avoid overtemperature one should cut off the current by means of a switching device (as such, one prevents further heating due to $R \cdot I^2$) and turn on any available cooling mechanism (ventilation, coolant circulation, etc.).

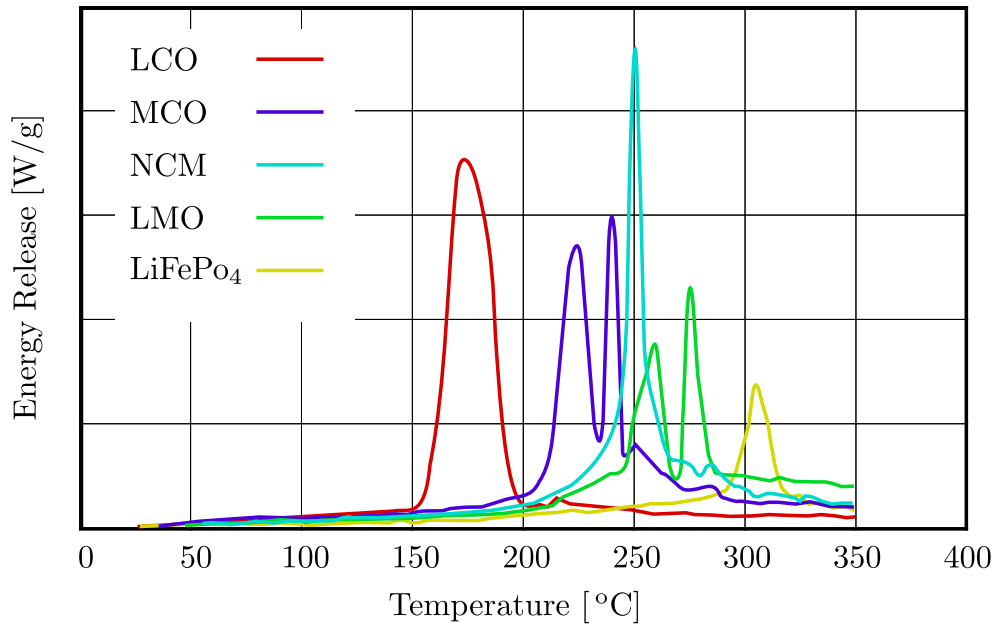


Figure 5.14: Breakdown of the cathode depends on used chemistry (reproduced from: http://www.mpoweruk.com/lithium_failures.htm)

5.1.2 Characteristics

The content of this section is roughly based on chapter 2 “*BMS Options*” of the book “*Battery Management Systems for Large Lithium-Ion Battery Packs*” [16].

The wide range of BMS technologies can be broken down by categorizing them based on functionality, technology and topology.

Functionality

BMSs can be found in a wide range of functionality, from products that do little or nothing to manage cells to complex systems that monitor and protect batteries in every conceivable way. In increasing order of complexity one can differentiate between:

1. Constant current/constant voltage (CCCV) chargers
2. Regulators
3. Meters
4. Monitors
5. Balancers

6. Protectors

CCCV chargers

CCCV chargers are standard, regulated power supplies, which are used to charge batteries. They can only operate in two distinct charge stages, constant current and constant voltage (see figure 5.17), hence the name. A CCCV charger is not sufficient as a BMS because:

- By itself, it does not prevent overcharging of individual cells.
- It does not prevent overdischarging of cells.
- It does not balance the pack

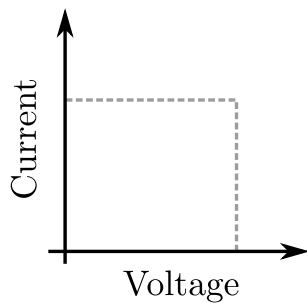


Figure 5.15: CCCV charger characteristics

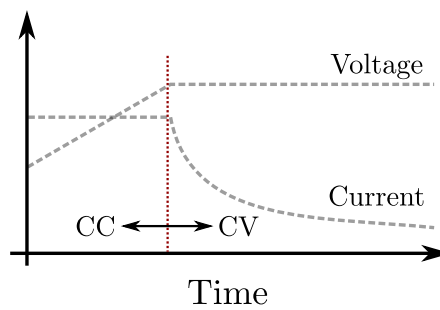


Figure 5.16: Typical charge curve

Figure 5.17: CCCV characteristics

Regulators

Regulators are, in its simplest form, voltage clamps that conduct little or no current up to the fully charged voltage of the cell at which point it turns on, drawing current in trying to maintain that voltage. They operate on cell level. Use of regulators alone is not sufficient as a BMS because:

- If the regulator's nominal current is lower than the charge current, it can't prevent overcharging of individual cells.
- It does not prevent overdischarging of cells.

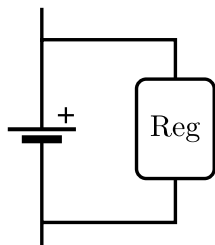


Figure 5.18: A regulator across a cell

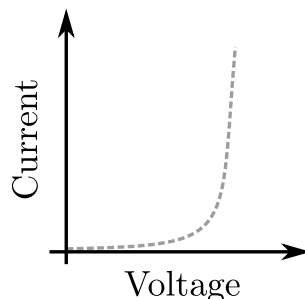


Figure 5.19: Regulator operating characteristic

Figure 5.20: Regulator characteristics

Meters

Meters simply monitor parameters but do not actively control charging or discharging. A meter is not sufficient as a BMS because:

- It does not prevent overcharging of individual cells.
- It does not prevent overdischarging of cells.
- It does not balance the pack.

Monitors

Monitors are like meters in the sense that they measure each cell voltage, but they do close the control loop. Should anything be amiss, they can take corrective action without human interference. Monitors are commonly used for testing batteries and are not sufficient as BMS because:

- It can not interrupt charge or discharge current, it can only request it.
- It does not balance the pack

Balancers

A balancer is like a monitor, but is is also able to maximize the pack’s performance by balancing the cells. It, more often than not, supports communication to report pack data to the rest of the system. It is sufficient as a BMS as long as it is wired in a way that allows it to control the charging source and the discharging load.

Protectors

A protector is like a balancer, except that it includes a switch to turn off the pack current. A protector is usually an integral part of a battery, physically located inside the same enclosure, leaving only two power terminals coming out of its enclosure. It is sufficient as BMS as long as the integrated switch is able to handle high-power loads.

Summary

	Measure	Compute	Report	Balance	Protect	
					Charge	Discharge
CCCV chargers						
Regulators				✓		✓*
Meters	✓	(✓)	✓			
Monitors	✓	(✓)	✓		✓*	✓*
Balancers	✓	(✓)	(✓)	✓	✓*	✓*
Protectors	(✓)	(✓)	(✓)	✓	✓	✓

Table 5.1: Comparison of the features of the various BMS functionalities. (✓) = Some may provide this feature. ✓* = Requires additional measures.

Technology

There are basically two classes of technologies used to implement a BMS: analog and digital. The distinction between analog and digital is related to how the cell voltage is processed. While all systems require some form of analog front end, BMSs that process the cell voltage with analog circuitry (an analog comparator, op-amp, differential circuit, etc.) is considered to be analog. BMSs that process the cell voltage digitally are considered to be digital.

Analog

Analog BMSs are cheaper but this comes at a cost. Consider an analog regulator as shown in figure 5.21. The regulator may use a power supply supervisor IC, powered by the cell's voltage, and driving a balancing shunt when the cell's voltage exceeds the IC's threshold voltage. Inside the IC there are two components: a voltage reference and an analog comparator, whose output changes state when the cell voltage exceeds the reference's voltage. However, in a battery pack, information on which cell is too low, how long it has been too low, temperature of the cell, etc. is not available. As such, one possibly bad cell

dragging down the performance of the whole pack, cannot be recognized by the battery pack as is.

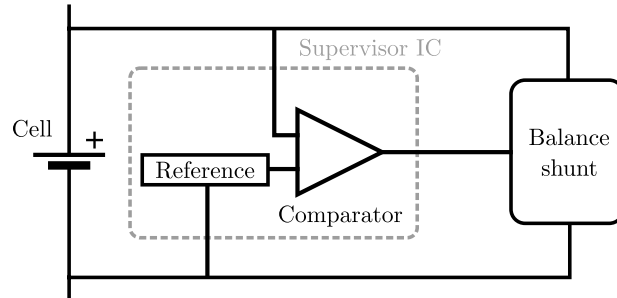


Figure 5.21: Example of an analog regulator

Digital

A digital BMS is more complex and comes at a higher cost but provides full information on each cell's voltage and possibly more (temperature, SOH, SOC, etc.). It is able to report this data which is necessary to perform an analysis of the pack. An example of a digital BMS is shown in figure 5.22. This device includes an analog multiplexer, able to sample the voltage at one of the taps between adjacent cells, and send it to an analog-to-digital converter. From there on, the BMS performs its functions digitally, such as subtracting the reading from two adjacent taps to calculate the voltage of the cell between those two taps.

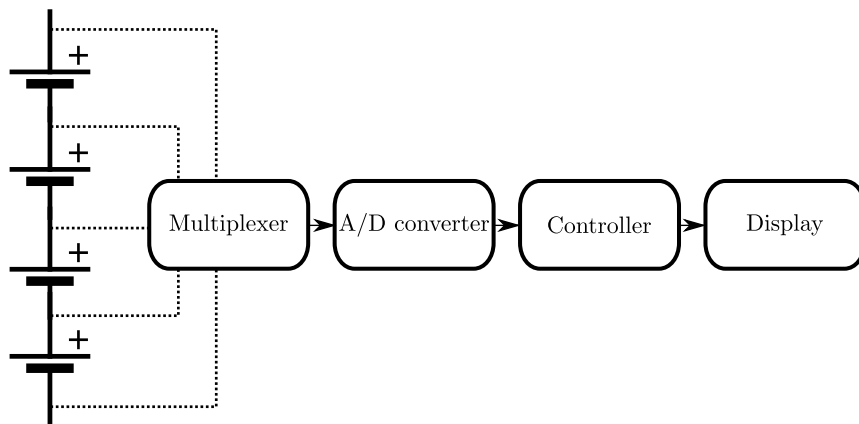


Figure 5.22: Example of a digital BMS, a meter

Topology

BMSs can be categorized based on how they are installed: separately and directly on each cell, altogether in a single device, or in some intermediate form. The topology affects cost,

reliability, ease of installation, ease of maintenance and measurement accuracy. There exist centralized, master-slave, modular and distributed BMS topologies.

Centralized

A centralized BMS, see figure 5.23, is entirely located in a single assembly from which a bundle of wires ($N + 1$ wires for N cells in series if only voltage is measured) goes to the cells. The advantages of this topology are:

- Compact
- Least expensive topology
- Easy to replace

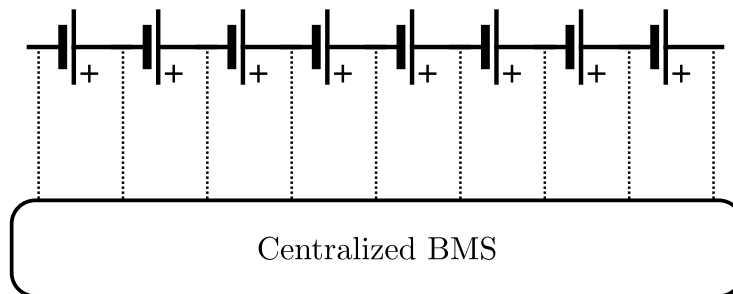


Figure 5.23: Centralized topology

Modular

A modular BMS is similar to a centralized one, except that the BMS is divided into multiple, identical modules, each with its bundle of wires going to one of the batteries in the pack (see figure 5.24). Typically, one of the modules is designated as a master and communicates with the rest of the system. The other modules act as simple remote measuring devices. The advantages are:

- The wires are easier to manage, each module can be placed close to the battery it handles.
- Expansion to larger packs is straightforward, more BMS modules are added.

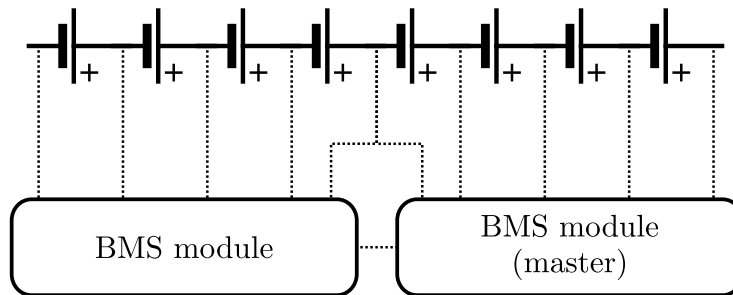


Figure 5.24: Modular topology

Master-slave

As with modular topology the master-slave topology uses multiple identical modules (the slaves), each measuring a number of cells (see figure 5.25). The master is different from the modules and does not measure voltages, it handles computation and communication. This topology has the same advantages as the modular topology and is cheaper, since the slave modules are optimized for one job (and are not expandable to masters).

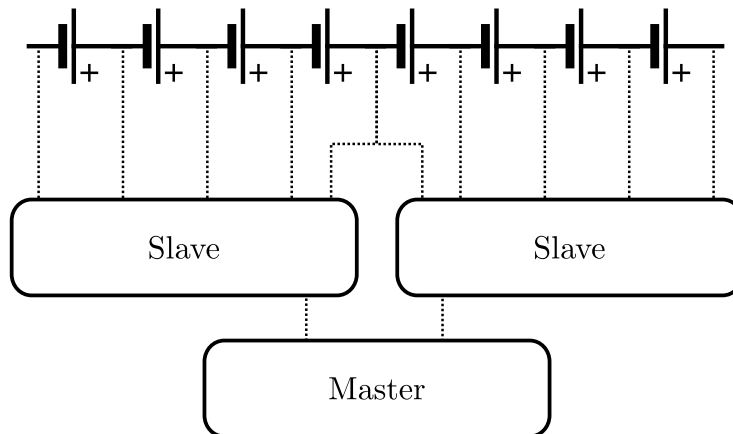


Figure 5.25: Master-slave topology

Distributed

A distributed BMS, see figure 5.26, is significantly different from the other topologies. In a distributed BMS, the electronics are contained on cell boards that are placed directly on the cells being measured. Instead of many wires between cells and electronics, a distributed BMS uses just a communication link between the cell boards. There is one BMS controller that handles computation and communication. Since more PCBs and components are needed, this is a more expensive topology, the advantages are:

- More reliability, direct mount on cell electrodes

- Replacement cost is less
- High measurement precision
- Ease of expansion

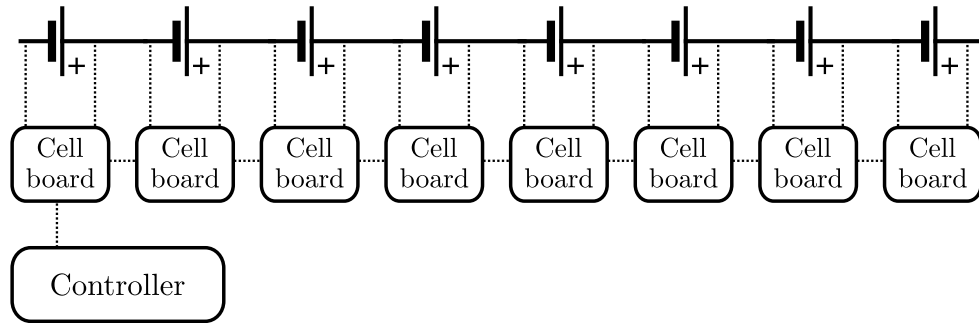


Figure 5.26: Distributed topology

5.1.3 Future solutions

On module or pack level the BMS takes about 10 % (larger packs) to 40 % (smaller packs) of the production cost depending on the amount of installed cells in series [84],[143],[191]. Future advances in mining and manufacturing technologies may reduce the cost of the BMS but will not have a big impact on module or pack level. However, since batteries are complex electrochemical devices with a distinct nonlinear behavior depending on various internal and external conditions, their monitoring is a challenging task. Advances can be made by cost-effective implementation of computationally intensive algorithms which give a better estimation of SOC, impedance, SOH, capacity, available power and remaining useful life (RUL). With better estimation comes better control and performance of the battery pack. Furthermore, the ever increasing accuracy of cost-effective sensors gives room for implementation of currently unfeasible algorithms.

An overview of today's cost-effective algorithms is given in figure 5.30 (figure based on information from review [218]).

5.1.4 Cost assessment

The cost of a BMS is closely related to the installed hardware, thus depends on topology, technology, functionality and number of cells. Figure 5.27 shows an overview of cost evolution of digital BMSs in function of number of cells installed. One can explain the curves where flat periods are alternated by periods of sudden increase (Genasun, Reap,

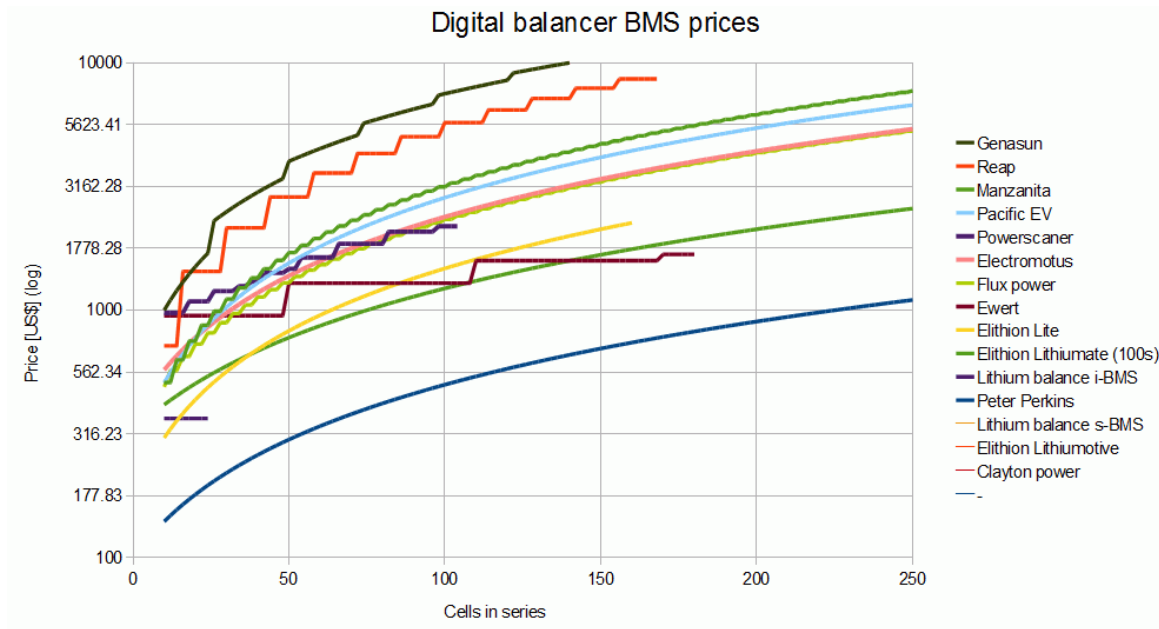


Figure 5.27: Cost evolution of different BMSs (from: http://liionbms.com/php/bms_options.php with permission)

Tritium, Powerscanner and Ewert) by a modular or master-slave topology. The curves with a more “smooth” increase of cost can be explained by a distributed topology.

By digitizing the plot and curve fitting the discretized data an estimation on cost per extra cell installed can be done, this is shown in figure 5.28. The expectation for distributed BMSs is a constant for the price per extra cell installed ($\frac{\text{euro}}{\text{cell}}$), however, this is not the case with the plots in figure 5.28. After contacting one of the manufacturers about this unexpected behavior of cost evolution:

... I have looked at the graphs that you have sent and something doesn't look right about the graphs. At least for our BMS, the cost of the system as the number of cells goes up should start at a fixed number and then the price should go up somewhat linearly. This is because that all systems need a BMS master, current sensor and a number of connectors. As the number of cells goes up, you will only be adding cell boards, cabling and communication connectors. There is a bit of wobble in the price increase, but it should approximate a line. If you are talking about the price per cell, then the curve should asymptotically approach a level. Keep in mind that the max number of cells that our BMS can handle is 256.

But, I think you are correct in that for the derivative, it should be a constant as the function of price vs number of cells should be close to linear ...

This throws up the question whether the data supplied is accurate or whether the accuracy

loss by curve fitting is the underlying cause. However, investigating this is not within the scope of this project.

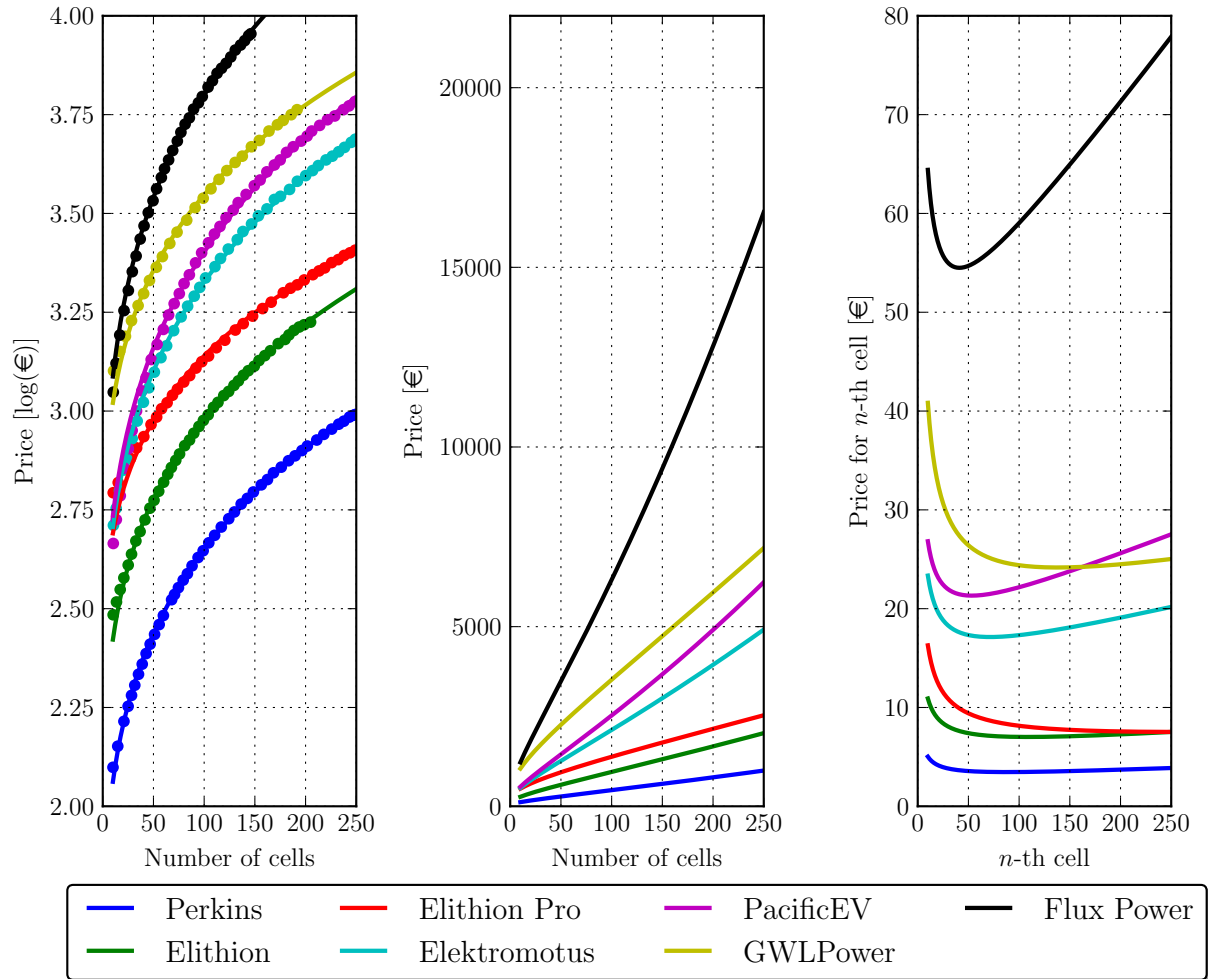


Figure 5.28: Cost in function of number of cells (left and middle) and cost per extra cell installed (right)

5.1.1.5 Suppliers

Supplier	Country	Website	E-mail
BESTGO Power Co., Ltd.	Hong Kong	www.bestgopower.com	info@bestgopower.com
Frunhofer	Germany	www.smart-power.fraunhofer.de	peter.spies@iis.fraunhofer.de
Texas Instruments	USA	http://www.ti.com/tool/TIDA-00239	
JTT Electronics LTD.	Canada	http://www.jttelectronics.com/	sales@jttelectronics.com
LION Smart GmbH	Germany	http://www.lionsmart.com	geor.walder@lionsmart.com
Lithium Balance	Denmark	www.lithiumbalance.com	Contact@lithiumbalance.com
EWERT Energy Systems	USA	http://www.ewertenergy.com/	info@ewertenergy.com
PUES EV	Japan	http://www.pues.co.jp/en/	
REC	Slovenia	www.rec-bms.com	info@rec-bms.com
AA Portable Power Corp	USA	http://www.batteryspace.com/	sales@batteryspace.com
GWL Power Ltd.	UK	http://www.ev-power.eu/	export@i4wif.eu
Tritium Pty Ltd	Australia	http://tritium.com.au/	enquiries@tritium.com.au
Ashwoods Energy	UK	http://www.ashwoodsenergy.org/index.php	info@vayongroup.com

Table 5.2: BMS Suppliers

5.2 Combination of battery + EDLCs/lithium-ion super capacitors

A super capacitor is an energy storage device which utilizes high surface area carbon to deliver much higher energy density than conventional (=ordinary) capacitors. Ordinary capacitors have higher power, super capacitors still have high power (relative to batteries) and have higher energy density than ordinary capacitors. Super capacitor technology provides:

- Secure power: Provides reliable interim power, even if the primary source fails or fluctuates.
- Energy storage: Stores energy from low power sources, enabling support for high power loads.
- Pulse power: Supplies peak power to the load while drawing average power from the source.

Super capacitors have a lifetime of ~ 2 million cycles and are excellent in delivering high power but the energy density is very low compared to batteries. Furthermore, as with lithium based batteries, when installing multiple super capacitors in series additional balancing circuits are needed. Combining the power of super capacitors with the energy of batteries provides superior performance, operating range and life. This is due to the nature of battery chemistry which degrades fast when drawing peak currents. The difference in behavior of a stand alone battery system and a combined super capacitor - battery system is shown in figure 5.29.

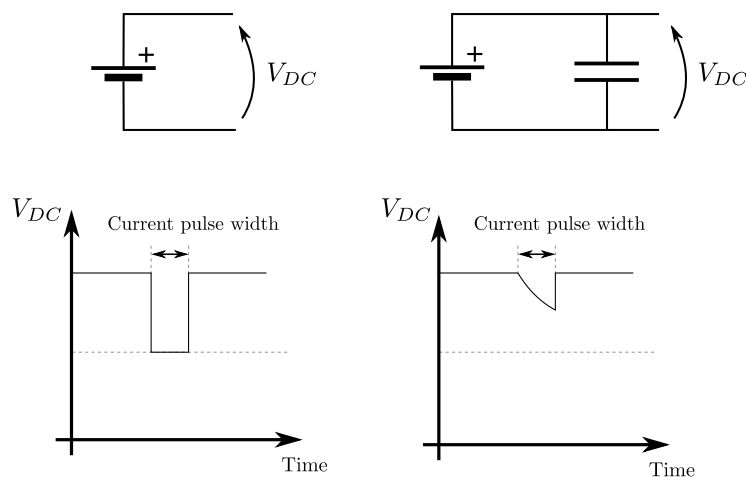


Figure 5.29: Performance difference of stand alone battery pack and combined system

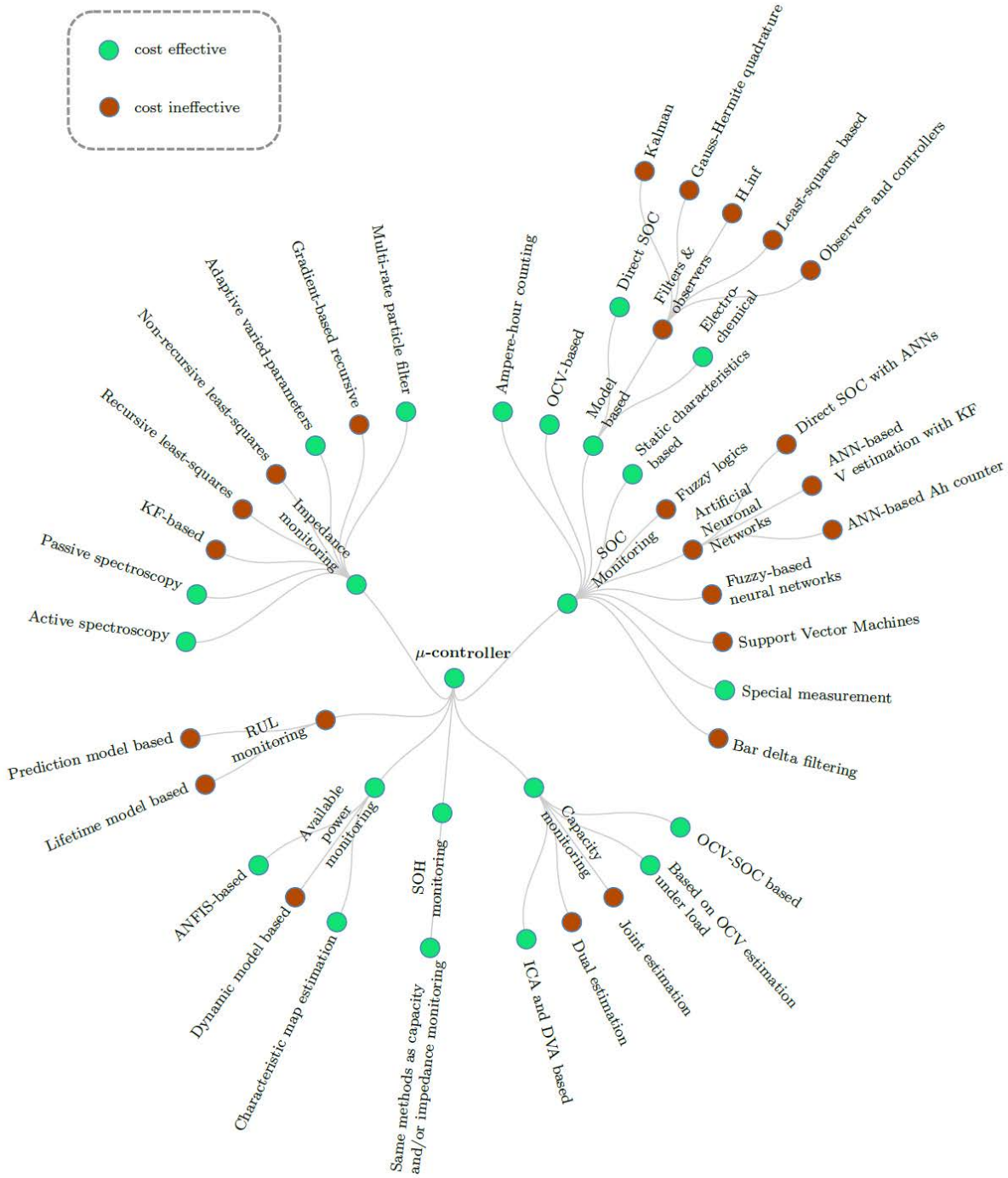


Figure 5.30: Future solutions on cost-effective algorithm implementation

Chapter 6

Testing and Standardization

6.1 Importance and hurdles of standards

Standards are important because they allow for interchangeability. When standards are well defined, work can be done in a cost-effective manner. Standards allow for better comparison between products. They describe many subjects covering testing procedures, shape and formats and many others.

6.2 Active organizations

Following organizations are active in the field of battery standards:

- IEC: International Electro-technical Commission
- ISO: International Organization for Standardization
- CENELEC: European Committee for electro-technical standardization
- SAE: International Society of Automotive & Aerospace Engineers
- JISC: Japanese Industrial Standards Committee
- BATSO: Battery Safety Organization
- USABC: U.S. Advanced Battery Consortium
- Others

6.3 Existing standards

Table 6.1 presents a non-exhaustive list of standards applicable to battery industry.

Year Reference	Category Organization	Title
2011 12405-1	Packs & Systems ISO	Electrically propelled road vehicles, Test specification for lithium-ion traction battery packs and systems, Part 1: High-power applications
2012 12405-2	Packs & Systems ISO	Electrically propelled road vehicles, Test specification for lithium-ion traction battery packs and systems, Part 2: High-energy applications
2015 18300-2	Packs & Systems ISO	Electrically propelled road vehicles, Specifications for lithium-ion battery systems combined with lead acid battery or capacitor
2010 62660-1	Battery IEC	Secondary lithium-ion cells for the propulsion of electric road vehicles - Part 1: Performance testing
2010 62660-2	Battery IEC	Secondary lithium-ion cells for the propulsion of electric road vehicles - Part 2: Reliability and abuse testing
2015 62660-3	Battery IEC	Secondary lithium-ion cells for the propulsion of electrical road vehicles - Part 3: Safety requirements <i>Draft</i>

Table 6.1: Standards applicable to battery technology

Appendix

List of acronyms

AGM	Absorbent Glass Matt. (adv. Pb-acid)
BES	Battery Electric Storage
BEV	Battery Electric Vehicle
BMS	Battery Management System
CAES	Compressed Air Energy Storage
CNT	Prelithiated carbon Nano Tubes
DoD	Depth of Discharge
DWsiNT	Double Walled Si Nano Tube
EDLC	Electric Double Layer Capacitor
EES	Electric Energy Storage
EFB	Enhanced Flooded Batteries (adv. Pb-acid)
EPA	Environmental Protection agency (US.)
EV	Electric Vehicle
FIVEVB	Five Volt Battery (European project)
HEV	Hybrid Electric Vehicle
IEA	International Energy Agency
LCA	Life Cycle Analysis
LCO	Lithium Cobalt Oxide
LFO	Lithium Iron-Phosphate
LIB	Lithium Ion Battery
LIC	Lithium-ion Capacitor
LiFSI	Lithium bis (Fluorosulfonyl)imide (electrolyte)
Lipo	Lithium Polymer
LiPON	Lithium phosphorus oxy nitride (Film Electrolyte)
LMO	Lithium Metal Oxide

LTO	Lithium Titanate
NCA	Lithium Nickel Cobalt Aluminum Oxide
NEDC	New European Driving Cycle (Eu.)
NMC	Nickel Manganese cobalt
NMH	Nickel Metal Hydrate
NPV	Net Present Value
PEA	Power Electrolyte Arkema
PEM	Proto Exchange Membrane
PHES	Pumped Hydro Storage
PHEV	Plug in Hybrid Electric Vehicle
PHS	Pumped Hydro Storage
PV	Photo Voltaic
PVDF	Ply Vinylidene Fluoride (common binder)
REES	Rechargeable Electrical Energy Storage
RES	Renewable Energy Sources
RGIE	AREI Algemeen Reglement Electrische Installaties
SEI	Solid Electrolyte Interface
SLMP	Stabilized Lithium Metal Powder
SMES	Superconducting Magnetic Energy storage
SSB	Solid State Battery
T&D	Transmission and Distribution
TES	Thermal energy storage
UPS	Uninterruptable Power Supply
VRB	Valve Regulated lead-acid Battery
WLTP	World Light Vehicle Test Procedure (Int.)
WP	Work Package

Part II

**Analysis of the applications and
relevant problems in the industry**

Chapter 1

Input of the user committee

1.1 Introduction

It is easy to believe that a certain application works best with a specific battery technology and to some extent this is certainly true however, due to the sensitivity of thermal influences on performance, it is equally important to consider the environmental conditions like the ambient temperature.

The combination, application, environment and applicable cooling allows to choose a fitting battery cell, i.e. the combination battery technology, format and scale.

When a battery system reaches a certain scale and specific power, a thermal management system gains in importance. For this reason, the design problem expands from a purely electric problem to a thermo-electric problem. In other words; two energy streams should always be channeled, the electrical power and the heat (be it when cooling or heating the battery system).

Huge discrepancies exist between the different families of EES with respect to their resilience towards ambient temperatures. Capacitors are usually better at handling extreme cold and hot weather than batteries. Fuel cells typically operate from the mid to very high range temperatures.

In practice however, the thermal operating envelope of most battery Li-ion cells is rather similar. For this reason a first approach consists of uncoupling the problem as follows:

$$\begin{aligned} & \textit{Application} \implies \textit{CellTechnology} \\ & \textit{Environement} \implies \textit{ThermalManagementSystem} \end{aligned}$$

This uncoupling allows to split up the analysis and make the problem easier to handle. One quickly realizes that both the electric and thermal user profile are of key importance.

The scope of WP2 lead us over the following topics:

- In the context of WP2, some emails were sent to the users committee members, to inquire the user needs and expressed the call for applications.
- A description of the most interesting applications proposed.
- Several case studies are set as goal.
- A techno-economical analysis was performed to analyze the PV and I-generator at KUL (funded with previous tetra programs) in terms of an upgrade to Li-ion technology.
- Users profile data is collected.

1.1.1 What makes application and why would we choose it

An application has characteristic thermal and electrical cycles, this was already mentioned in the introduction section. We are interested in subjecting our modules to representative load cycles. The load-curves differ greatly from one application to another. In addition it is important to highlight that differences in the power electronic drive train between for instance on-off controlled DC traction motor and a four quadrant working thyristor drive.

A simplification arises if we assume a scalable solution. This hypothesis becomes valid if an adequate thermal management system gets integrated preferably also in a modular way.

In this project, a good application is one with the following characteristics:

- The user profiles are easily available.
Several user profiles are interesting, for example:
 - the current profile,
 - the voltage profile,
 - the ambient temperature profile
 - cell surface temperature of a particular cell.
- The applications has to be existing. We will only integrate the battery module into an existing application.

- The applications should be easily available to work on.
- The applications should be of some scale and power to enable accurate testing of the thermal management system.

1.2 Needs experienced by the Industry

During our visits to the user committee members and through e-mail conversations, we inquired some of the needs that are experienced by the user committee members. At a general level all comes down to reducing the total cost, better safety and increasing performance.

The following needs were expressed:

- Networking and public relations
- Lower cost
- Battery technology overview
- Footprint reduction
- Wider temperature envelope
- Longer lifetime
- Simpler systems
- Scalable design
- Modular design
- Increased safety

1.3 List of applications proposed by the user committee

1.3.1 Light electric vehicles - Altreonic

Altreonic focuses on the market of light electric vehicles. The vehicles are conceptualized with modularity and scalability in mind. At this moment they use NMH for indoor and



Figure 1.1: Altreonic's LEV

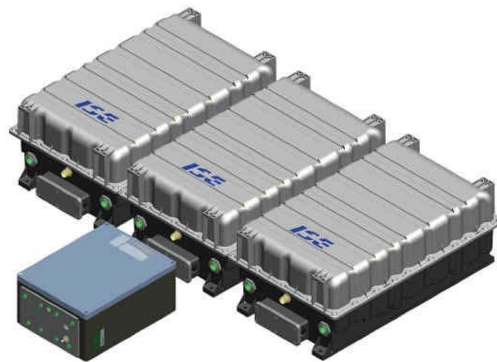


Figure 1.2: Bluways start-stop system

LFP for outdoor applications. The used battery modules have voltages ranging from 12 to 48Vdc and capacities from 500 to 2000Wh. Typical use considers charging during the night with a standard power outlet at 10A. Ambient temperature can go from -20°C to $+50^{\circ}\text{C}$. At this moment only a prototype exists therefore users profiles remain unavailable. The power train consists of four quadrant working converters which allow for start stop recuperation.

1.3.2 Start-stop systems for buses - Bluways

Bluways provides in ecologically friendly power systems for buses and railway systems. The campus in Heverlee provides in supper cap modules for starts stop recuperation. These are installed on amongst others city buses, see Figure 1.2.

For this they use cylindrical EDLCs. The cooling system consists of several fans for forced convection. The Cells are immediately connected to the drive and BMS circuit PCB. They design tailored BMS systems optimized for reduced Joule losses while respecting EMC design limits. In this way unwanted effects are minimized.

1.3.3 Terminal truck - Cloruyt and Mol

The Company Mol Cy builds many kinds of highly specific heavy duty trucks, see Figure1.3. One example is an electrical terminal truck which serves at Colruyt's distribution center. User profiles of the voltage and current are available.



Figure 1.3: Electric terminal truck

1.3.4 Light electric vehicle - Electric Drive

The REVA L-ion is a small rear-wheel driven three-door hatchback intended for city traffic, as shown in Figure 1.4. The main characteristics of this car can be summarized as follows:

- An estimated range of 80 - 120 km.
- A top-speed of 80 km/h.
- It weighs 565 kg with no occupants.
- Its brakes are hydraulically operated with disc brakes in the front and drum brakes in the back.

The Current battery pack (LiPo_4) is depicted in figure 1.5 and provides an energetic capacity of 640Wh.

Components

Traction battery module The battery pack consists of 16-battery blocks that are connected in a series in order to provide approximately 51 V, 640 Wh and 200 Ah. Each battery block has 10 battery cells that are connected in parallel with the aim to produce 3.2 V and 64 Wh.

The voltage, current and temperature of each battery block is individually monitored. The sensor units can communicate with a central control unit. In addition, 4-fans have



Figure 1.4: LEV REVA - Electric Drive



Figure 1.5: Current battery system

been used for cooling the battery module and these fans are powered by a 12 V battery. This battery module is located under the front seats.

Battery type	LiFePo ₄
Nominal voltage	3.2 V
Number of cells	10
Peak voltage	3.6 - 3.8 V
Cut-off voltage	2.5 V
Capacity	640 Wh / 200 Ah
Manufacturer	Mahindra, India

Table 1.1: Summary of traction battery characteristics

Auxilliary battery module The REVA has a sealed lead-acid battery of 12 V (see Figure 1.6). This battery is used to power the auxiliaries such as the horn, lights, etc.

Charging plugs There are two modes of charging the REVA L-ion. There is an AC-charging plug and a DC-charging plug. On the left side of the REVA L-ion is the male end of an industrial 16 A caravan type socket behind a charge port lid. The cable fitting here should be of the type female industrial 16 A caravan type socket to 13 A3 pin standard 240 V electrical plug.

Charger and DC-DC converter The input of the charger is a 230 Vac at 50 Hz as provided by a standard European electrical socket. It then transforms this current into a 57 Vdc at 2276 W which can be used to recharge the batteries. Incorporated in this system is also a DC-DC converter which transforms the 48 V DC-current of the battery



Figure 1.6: REVA - Pb-acid battery



Figure 1.7: REVA - Motor Control Unit

pack to 13.5 Vdc at 400 W. As a result, 12 Vdc battery can be charged. The charger unit is manufactured by Maini Materials Movement Private Limited which are based in India.

Input	230 Vac, 50Hz
Output charger	2276 W at 57 Vdc
DC-DC converter	400 W at 13.5 Vdc
Manufacturer	Maini Materials movement Pvt. Ltd., India

Table 1.2: Summary of power electronics

Electric motor The electric motor is a three-phase squirrel cage asynchronous motor. It is positioned on the right side of the vehicle under the passenger seats. It is directly connected to the differential on the rear axle which provides a gear reduction of 9.4:1. The motor can provide a maximum power of 14.5 kW at 28 V and 3000 RPM. It is produced by Kirloskar Electric Company Limited in India.

Type of motor	3-phase AC squirrel cage induction motor
Max hourly output	14.5 kW at 3000 RPM
Operating Voltage	28 V
Manufacturer	Kirloskar Electric Co. Ltd., India

Table 1.3: Summary of power electronics

Motor controller The motor controller (illustrated in figure 1.7 is powered by the 48 Vdc coming from the power supply. It then transforms this current into three-phase AC-current. By changing the output voltage and frequency, the motor controller can dictate the speed and torque of the electric motor. The motor controller used in the REVA L-ion is model 1236-5301 produced by Curtis Instruments Incorporated who are located in the U.S.A.

Model	1236-5301
Input battery voltage	36 - 48 V
2 mins RMS current rating arms	350 A
2 mins RMS power rating	19.7 kVA
Communication	CAN bus50 A
Manufacturer	Curtis Instruments Inc., U.S.A.

Table 1.4: Summary of motor controller

1.3.5 SmartRoof

Electrical power generated by the sun and/or wind, and actual power consumption never match. The result is feedback of power into the grid when excess power is generated, and power needed from the grid when power generation is insufficient. As more solar and wind power comes on line, it becomes increasingly difficult, and expensive, to ensure stability of the grid. Intermediate power storage is rapidly becoming an essential tool to keep grid power fluctuations within manageable limits. As a consequence, the Smart Energy Storage System (SESS) offers the solution, and several additional benefits, as follows:

- Li-ion battery system.
- Grid Friendly.
- Ride through a power outage and power independence.
- Flexible and Field upgradable.

The core of the SESS consists of a Li-ion batteries, which are charged in case of excess solar/wind power and discharged when consumption exceeds production. Compared to lead-acid, a Li-ion battery features a much higher charge/discharge efficiency, a longer service-life and reliability.

Grid friendly The SESS will iron out peak demand from the grid (by discharging the battery) as well as supply back to the grid (by recharging the battery). Ride through a power outage and Power independence Energy stored in the battery can be used to provide power to essential equipment during a power outage. With sufficient battery capacity and, if needed, a back-up generator, complete independence from the grid can be achieved. Flexible in the field by it's upgradeable approach, all elements of a SESS can be chosen to specific requirements. Each configuration can be tailored to a particular set of requirements. Additional wind power and battery storage can be connected at a later stage.

Smartroof Energy Storage System The DC electrical power generated by the solar panels is converted to AC by a PV inverter connected to the AC output of an inverter/charger. The AC input of the inverter/charger is connected to the grid and /or Generator. If required by local regulations an anti-islanding device has to be added to the system. Power from the PV inverter is supplied directly to the load. In case of insufficient PV power, the inverter/charger will supply additional power from the battery, or from the grid (battery fully discharged). In case of excess PV power the inverter/charger will use the excess power to recharge the battery, or feed back into the grid (when battery is fully charged). In case of a utility power outage, the SESS will disconnect from the grid and continue to operate as a standalone system. Depending on available solar/wind power, battery storage capacity and inverter/charger rating, all loads, or essential loads only, can be powered for hours or days even when utility power is not available. A generator makes the standalone unit complete!



Figure 1.8: Smart energy storage system.

The main components of the Smartroof Energy Storage System are:

- Smartroof Suntiles peak power rating 120 Wp/m^2 .
- PV inverter: The PV inverter converts DC voltage from the solar array into AC voltage suitable to power the AC loads. In a system without battery, all surplus power will be fed back into the grid, and shortage of power will be supplied by the grid. A normal PV inverter cannot function without an external AC power source/sink (ACpss). The normal PV inverter will therefore shut down when there is no ACpss available (such as a stable grid, suitable inverter or inverter/charger).

Therefore, if we want to work as a standalone unit we need to use PV inverters suitable to work Off and On Grid connected!

- MultiPlus and Quattro inverter/charger: The inverter/charger offering ranges from 800 VA to 10 kVA single phase, and up to six 10 kVA modules can be connected in parallel. All models can also be configured for three phase operation.
- Li-ion battery: (Lithium-iron-phosphate: LiFePO_4 or LFP). It is not small size and less weight that makes Li-ion so much more attractive than lead-acid in grid connected or off grid home systems. The main advantage is efficiency. The round trip energy efficiency (discharge from 100% to 0% and back to 100% charged) of the average lead-acid battery is about 80%. Even worse: the charge process of lead-acid batteries becomes particularly inefficient when 80% state of charge has been reached. Between 80% and 100% charge efficiency is often less than 50%. And these figures become worse in case of high current charging or discharging. The round trip energy efficiency of a Li-ion battery is 92%, under all operating conditions.

Contribution to LBATTS-Project Smartroof invites us to work on one of their systems installed at their offices in Menen. This platform allows for managing an integrated energy solution or off grid system. The system uses a Hybrid EES of LFP batteries and super capacitors to manage PV-, Wind, diesel (75 kVA) and grid power. A PLC system from Siemens software controls the convertors installed for each feeder. Additionally the system features the possibility for off-grid operation and can be applied in mobile as well as in static applications. Through this approach the connected power to the EES can be reduced. The actual applications are at the industrial level.

1.3.6 I-generator and PV-installation - KUL

The I-generator and PV-installation were funded by previous Tetra projects. They are considered as possible applications. Because one the tasks in WP2 consists of performing a techno-economical analysis of these two application, (object of Chapter 2), a detailed description of these applications can be found in Chapter 2.

1.4 Selection of the most interesting casses for LBATTS

The choice of applications is based on several factors, see section 1.1.1.

It is important to reflect on the pro's and con's to asses the potential that a certain

thermal strategy holds for integration on this particular application. PCM can only be used as a heat buffer, thus it can be used to store and release only a finite amount of thermal energy. PCMs can be used to buffer hot as well as cold temperatures, depending on the PCM and environment.

Depending on the heat capacity of the PCM it is possible that PCM's can only buffer the short lasting energy peaks in the temperature profile or long ones.

The following cases are chosen:

PV System: The PV installation is chosen because of the availability of a PV system in our lab, additionally representative users data is readily available from previous measurements and in literature.

Load following cycle The I-generator is chosen for several reasons; the availability of the installation, the load profile depends on the actual use but in combination with the programmable load, any load profile (up to 15 kW) can be easily simulated.

Heavy duty electric vehicle: Heavy duty electric vehicle: the electric terminal puller is chosen because accurate users data is available, additionally the scale of this application allows us to focus strongly on a modular approach.

Light electric vehicle - Electric drive: The light electric vehicle is chosen because useful user data is readily available, additionally we are allowed to keep the application at our lab which facilitates working on it.

These cases will be simulated on prototype battery modules. Accurate users-data and test cycles shall be collected for these in chapter 3. Notice that the last two cases are approximatively the same if scale is not considered.

Chapter 2

Techno economical analysis of the reconversion from lead-acid to Li-ion.

2.1 Set-up for battery benchmarking in hybrid domestic solar systems

2.1.1 Introduction

Recent study shows that installing an energy buffer (i.e. batteries) in a Flemish household is not cost effective [77]. However, rising electricity prices, decreasing prices for energy storage and the present governmental energy policy which tends to financially promote increased self-consumption (possibly from 2017) might change this into a cost effective investment in the near future. This study describes the experimental set-up to benchmark lithium-based battery performance when encapsulated in a phase change material (PCM). The PCM is introduced to provide thermal stability, which should result in better performance and efficiency.

While the test set-up was designed to compare lithium-based batteries in a real-world scenario, it also lends itself to compare performance differences between other battery technologies. As long as the cell voltage stays within the range 0 - 4.096 V and the measuring PCBs (Printed Circuit Board) are mountable on the cells, see figure 2.1.

What follows is the description of a benchmarking set-up for a common real-world installation, a hybrid domestic solar system. The different aspects of a hybrid solar system are visualized in figure 2.2.

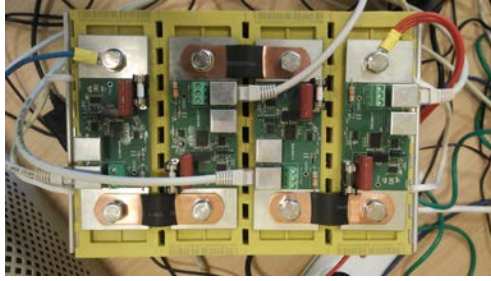


Figure 2.1: PCBs designed to, among other things, measure cell voltage and temperature

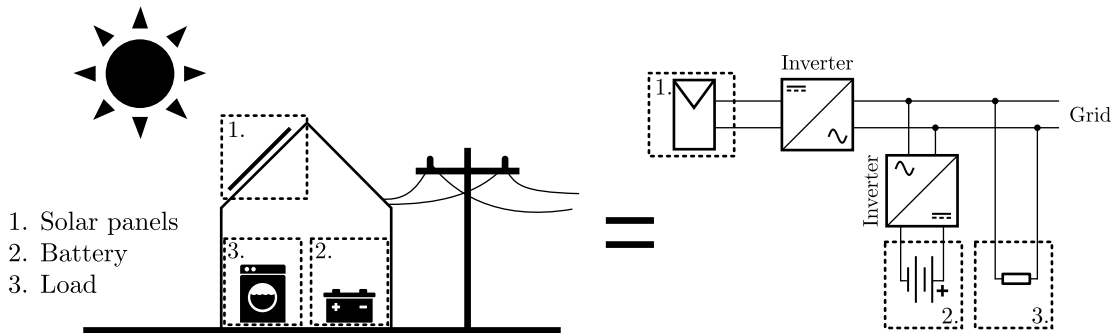


Figure 2.2: Different aspects of a hybrid domestic solar system

2.1.2 Solar panel

The electrical energy produced by a (inverter tied) solar panel is directly related to solar irradiance. Since the irradiance of the sun fluctuates with varying atmospheric conditions (clouds, dust, pollution,...), so does the electrical energy produced by the solar panel, see figure 2.3. When benchmarking different battery technologies, one needs to be able to reproduce the test circumstances in order to make a comparison. Since (exactly) reproducing atmospheric conditions is impossible, this implies the need to emulate the solar panel in order to achieve reproducibility.

Since the behavior of solar panels is well described and simple analytic models are widely available, the first thought is to emulate the solar panel given the input of measured solar irradiance (data available from [74]). This is done by using a programmable DC power supply, which acts as a current controlled voltage source, to implement the exponential approximation of a solar panel’s IV-curve. Specifications of the of the programmable power supply (PPS) can be found in table 2.1.

Model	Current range [A]	Voltage range [V]	Power range [W]	Extensions
EA-PSI 8720-15	0-15	0-720	0-3000	EA-IF-U1

Table 2.1: Programmable power supply specifications

The process of implementing the analytic IV-curve can be split into steps as shown in table 2.2. If the latency between measuring the current and setting the corresponding

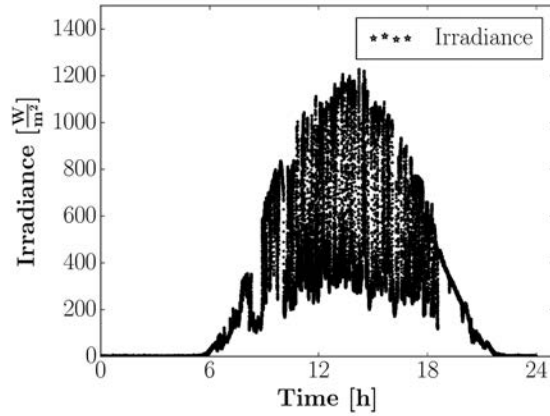


Figure 2.3: Solar irradiance in function of time for 08-06-2015

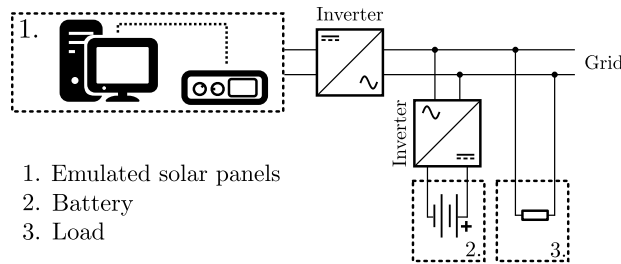


Figure 2.4: Solar panels are emulated by a PC and a programmable power supply (PPS)

voltage is greater than the latency of the inverter’s maximum power point (MPP) tracking (i.e. pull more/less current and check if the power rises), undesirable fluctuations will arise.

Step	Time needed [ms]
PC requests current measurement	5
PPS measures current	≈ 1
PPS transmits current	≈ 4
PC calculates voltage set value	0
PC sends set value voltage	5
PPS sets voltage	≈ 2

Table 2.2: Communication timing between PC and programmable power supply (PPS)

To test this, a linear IV-curve is implemented with function rule shown in equation 2.1. The MPP-tracker of the inverter should stabilize at (3 A, 125 V). Experiments with two different inverters were conducted, the results are shown in figures 2.5 and 2.6. As can clearly be seen, one can hardly speak of a stabilization. The inverter’s MPP tracking is faster than the control loop for implementing the linear IV-curve. Thus this method disqualifies for battery benchmarking due to the lack of reproducibility.

$$v(i) = \frac{i - 6 \text{ A}}{6 \text{ A}} \cdot 250 \text{ V} \quad (2.1)$$

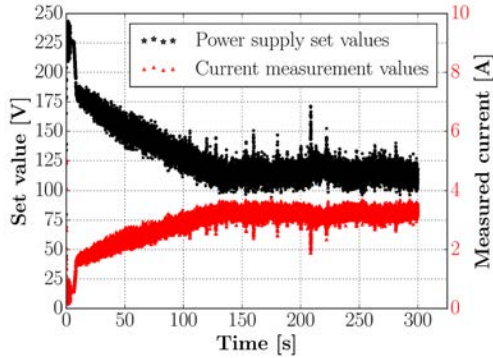


Figure 2.5: Archaic model of a mastervolt inverter

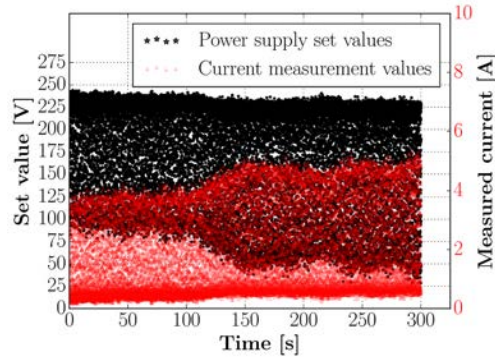


Figure 2.6: More recent model of a sunny boy inverter

Figure 2.7: Current measurements and voltage setpoints with linear IV-curve

Since a feature of the PPS is setting upper boundaries for any of the set (V, I, P), another approach is taken. If data of MPPs (I_{MPP}, V_{MPP}) should be available, one can program the PPS to set the voltage to V_{MPP} and set the current upper boundary to I_{MPP} . In this way, the MPP tracker will migrate and stabilize at the simulated (from the previously measured) MPP. In a recently completed test setup on campus, (V_{MPP}, I_{MPP}) and irradiance G is measured for different strings of solar panels [74]. I_{MPP} and V_{MPP} associated with the previously shown irradiance (see figure 2.3) are shown in figures 2.8 and 2.9.

With this method, reproducibility is not being jeopardized. It will be used for the battery benchmarking set-up.

Solar energy input in test set-up

Now that the solar panel can be emulated, one has to choose the energy input profile for emulating real-world conditions. Should the benchmarking be made for the most extreme conditions imaginable, or for the most common? The benchmarking in this study will be conducted under the most common solar irradiance conditions based on historical data for Ghent, Belgium. The available dataset spans 343 consecutive days, measured between May 2015 and April 2016.

In order to determine the most common irradiance conditions for a day, three parameters are considered, clearness index, fractal dimension and average irradiance. The clearness

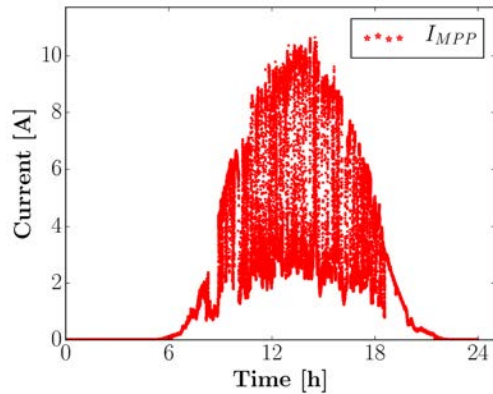


Figure 2.8: Measured I_{MPP} for 08-06-2015

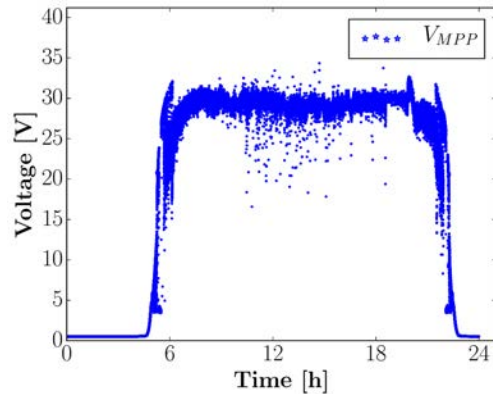


Figure 2.9: Measured V_{MPP} for 08-06-2015

Figure 2.10: I_{MPP} and V_{MPP} for a solar panel coupled to grid-tied inverter with MPP tracking

index is the fraction of the extraterrestrial solar radiation (before it passes through the atmosphere) that makes it through to the earth's surface, it quantizes the daily average atmospheric conditions (cloudy day, pollution, etc.). The fractal dimension quantizes the variation of solar irradiance on the earth surface, it is a measure of the fluctuation in atmospheric conditions (clear sky, fast passing clouds, etc.) [106]. Average irradiance is a measure of the amount of energy reaching the earth's surface. In order to find the most common day, a histogram with equal (variable) bin size is made for the three parameters. The number of bins is incremented until but one day, the so defined most common one, is found in the three histograms' highest frequency bin. The process is illustrated in figure 2.11, nbins is the number of bins, ndays is the number of days found in both histograms' highest frequency bin. As such, the 6th of April 2016 is found to be the most common day and will be used for the experimental set-up. The solar irradiance and corresponding values for (I_{MPP}, V_{MPP}) are given in figures 2.12, 2.13 and 2.14.

2.1.3 Battery

The individual cells will be monitored on cell voltage and temperature to estimate the impact on battery performance. Temperature is measured using the Dallas DS18B20 digital thermometer which has an accuracy of $\pm 0.5^\circ\text{C}$ within a -10 to 85°C temperature range.

For the purpose of conducting continuous voltage measurements with high accuracy (± 1 mV), custom-made measurement PCBs were designed and tested on 4 individual LiFePO₄ battery cells (see figure 2.1). The voltage measurement accuracy of the measurement PCBs (before calibration) is compared to a calibrated DMM4050 precision

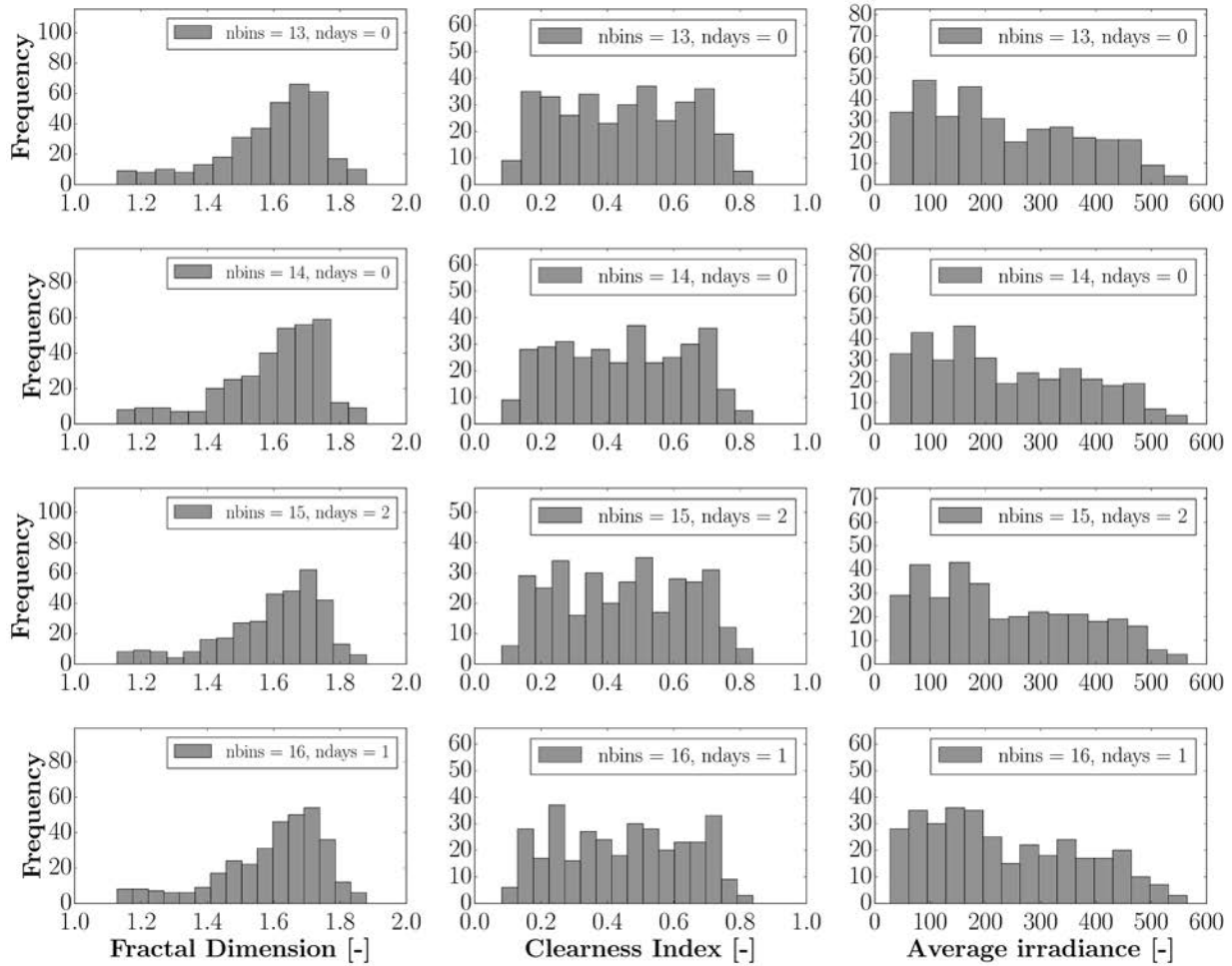


Figure 2.11: Illustration of the process for finding the most common day

multimeter (accuracy of $\pm 130 \mu\text{V}$), results are shown in figure 2.17 and table 2.3. Even without calibration, the accuracy of the custom-made measurement PCBs is better than 1 mV.

2.1.4 Load

The electrical load-profile for Flemish households is the time varying total power consumption. The total (momentary) power used by a household is determined by the sum of the power consumption of all active electrically powered devices. Simulating the load-profile is done by a programmable load bank, a device which allows to dissipate a programmable amount of power.

The load-profile for a Flemish household is determined from historical data (2011-2014) from Eandis' trial projects on smart meters. In these projects, total power consumption

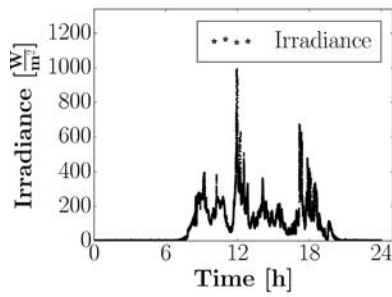


Figure 2.12: Solar irradiance for 06-04-2016

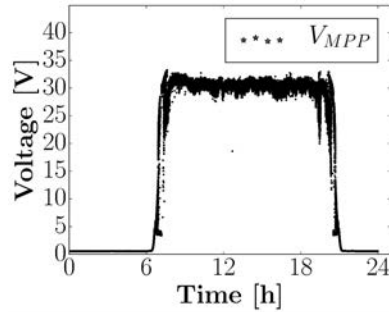


Figure 2.13: Measured V_{MPP} for 06-04-2016

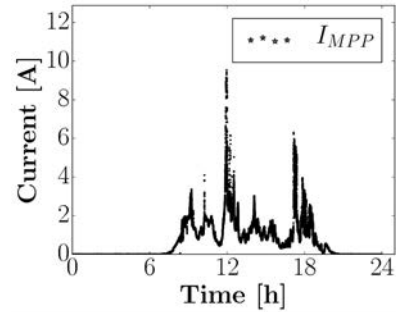


Figure 2.14: Measured I_{MPP} for 06-04-2016

Figure 2.15: G , I_{MPP} and V_{MPP} for a solar panel coupled to grid-tied inverter with MPP tracking

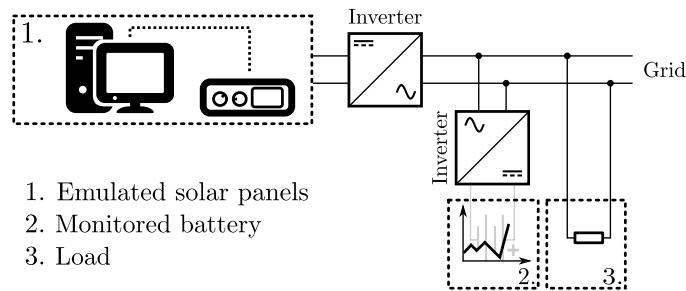


Figure 2.16: Battery is monitored by custom-made measurement PCBs

of Flemish households is measured on a quarter-hour basis. Since the energy input profile was determined for Wednesday 6th of April 2016, several profiles of different households for Wednesday 6th of April 2011 were compared and one was selected. The selected load-profile is shown in figure 2.19.

2.2 Set-up for battery benchmarking in a hybrid genset

2.2.1 Introduction

In spite of a widespread electrical grid, the use of stand-alone electric power generators or gensets in Europe is quite common on remote sites and as temporarily power supply. Due to the bad efficiency of gensets at low load conditions, a substantial amount of primary energy can be saved by combining the genset with a battery pack, a hybrid genset. For illustrative purpose, consider the electrical load profile of the on campus construction site

	Slave 1		Slave 2		Slave 3		Slave 4	
	DMM	BMS	DMM	BMS	DMM	BMS	DMM	BMS
Mean [V]	3.3012	3.3007	3.3009	3.3002	3.3014	3.3006	3.3015	3.3010
Std [μ V]	3.49	4.77	3.71	8.06	3.07	4.70	3.38	27.43

Table 2.3: Mean value and standard deviation of the measurements shown in figure 2.17

in figures 2.20, 2.21. Dimensioning the genset on peak power would result in a load factor of less than 30 %. In fact, extensive field loggings of the E&A research group learned that the load factor of a typical genset at construction sites does not exceed 20 % of the nominal power during 90 % of the time [7]. When comparing a properly sized hybrid genset to a classic genset, research shows a reduction in fuel consumption of up to 40 % and 24 % for respectively a household’s and base transceiver station’s load profile [102],[103]. Recent advances in control strategies lead to a further decrease in fuel consumption per produced kWh [238].

This study describes the experimental set-up to benchmark lithium-based battery performance in hybrid gensets when encapsulated in a phase change material (PCM). The PCM is introduced to provide thermal stability, which should result in better performance and efficiency. While the test set-up was designed to compare lithium-based batteries in a real-world scenario, it also lends itself to compare performance differences between other battery technologies. As such, the currently installed lead-acid batteries will be included in the battery benchmarking. Since the on-campus hybrid generator, the IGenerator, was built in 2009, the installed lead-acid batteries suffer from outdoor conditions and many service hours. The accompanied performance degradation will be mapped and considered when benchmarking against other battery technologies.

Battery type	Nominal voltage [V]	Nominal capacity [Ah]	Nominal power genset [kVA]	Fuel type
AGM	48	240	25	PPO

Table 2.4: Technical specifications of the on-campus IGenerator

2.2.2 Battery

The individual cells will be monitored on cell voltage and temperature to estimate the impact on battery performance. The same set-up as in hybrid domestic solar system will be used, see section 2.1.3 for more information.

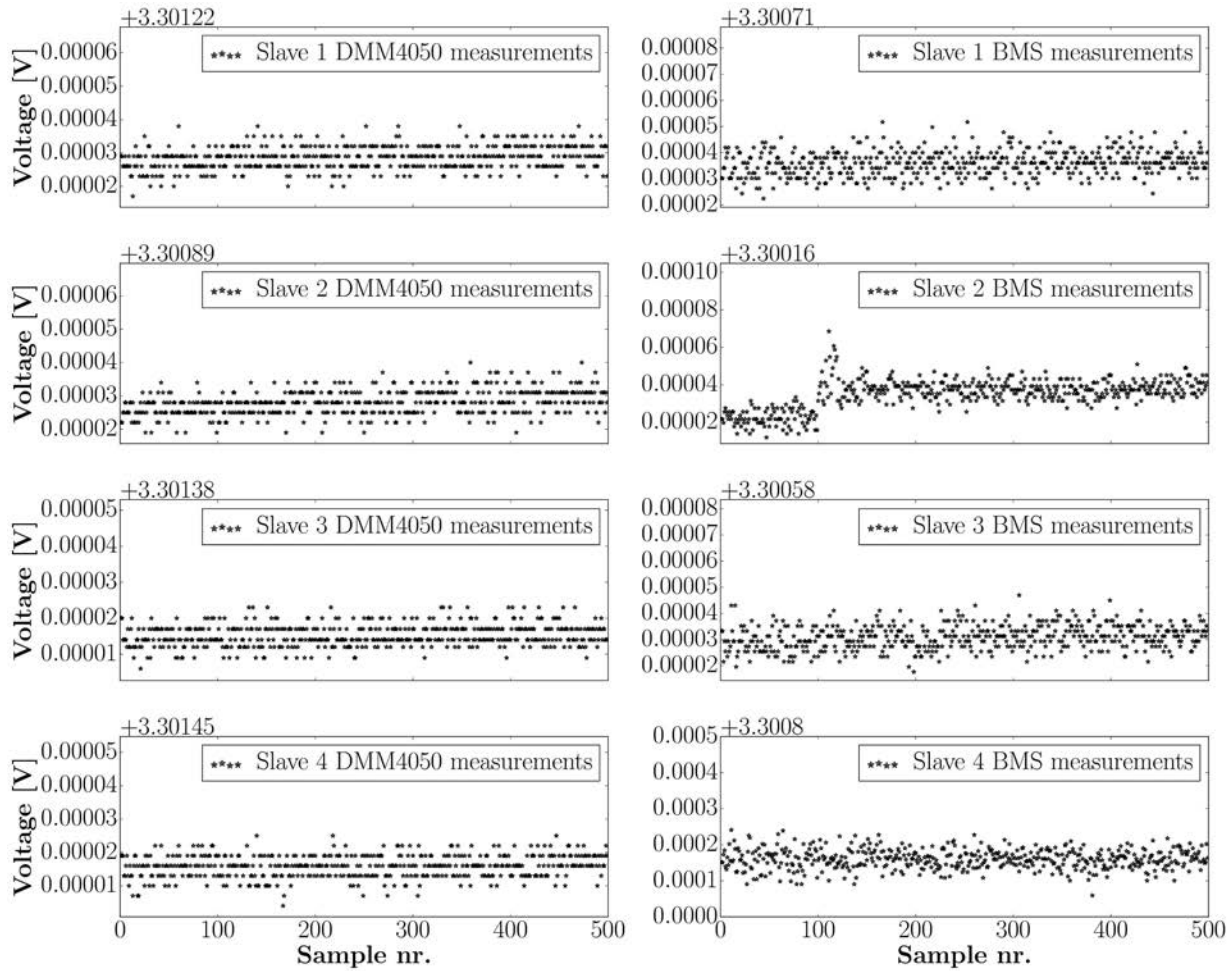


Figure 2.17: Voltage measurement performance of uncalibrated, custom-made BMS compared to calibrated DMM4050 precision multimeter

2.2.3 Load

Reproducibility of the load profile in order to benchmark different battery technologies is achieved by a custom made, programmable load bank (the so called “R&D2”, see figure 2.27). The programmable load ranges from 0 kW to 13.8 kW with a minimum step-size of 100 W. The maximum load of 13.8 kW is well below the maximum power supplied by the IGenerator’s DC buffer since the upper direct current limit of the IGenerator’s integrated inverters is 210 A. Variance of load in function of time is achieved by configuring the relevant relays through a Siemens S7-1214c PLC. All the loads have a power factor of 1.

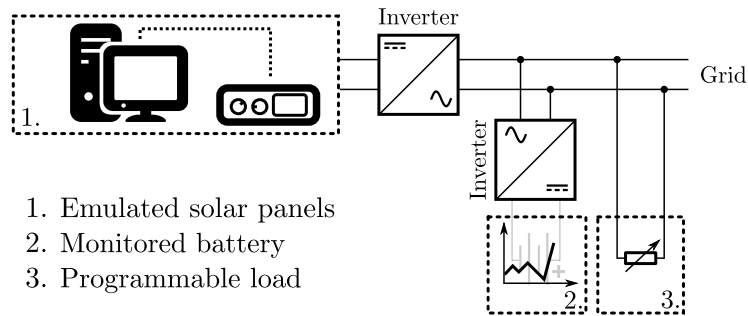


Figure 2.18: The electrical load is emulated by a programmable load bank

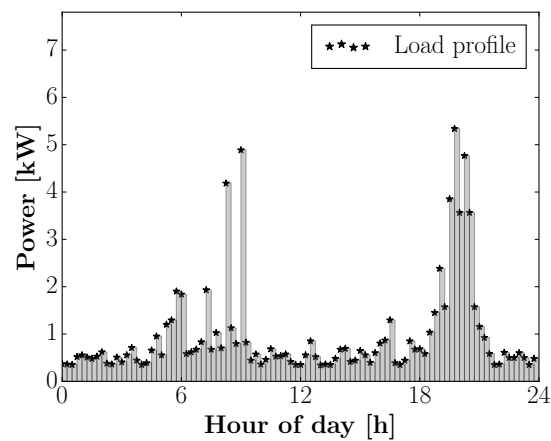


Figure 2.19: Load profile for a Flemish household on Wednesday 6th of April

Different load profiles

Field measurements for two stationary hybrid genset applications are delivered by Locquet Power & Light. The data from these applications will be used in the benchmarking of the batteries.

Hybrid genset on a construction site

The load profile of a construction site is shown in figure 2.30. High variation of the load and a small base load compared to the peak load is typical for these profiles.

Quarter-hour values are introduced to allow the battery to reach a local steady-state and as such measure the battery response on the load variation.

Quarter-hour maximum changes in the current drawn from the battery for one day is given in figure 2.31.

As with the load-profile for a Flemish household, the load-profile is scaled so the RMS (Root Mean Square) value of the load-profile is unity, see figure 2.34.

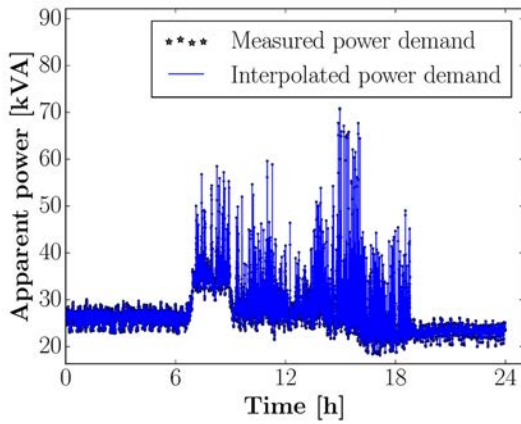


Figure 2.20: Load profile for construction site

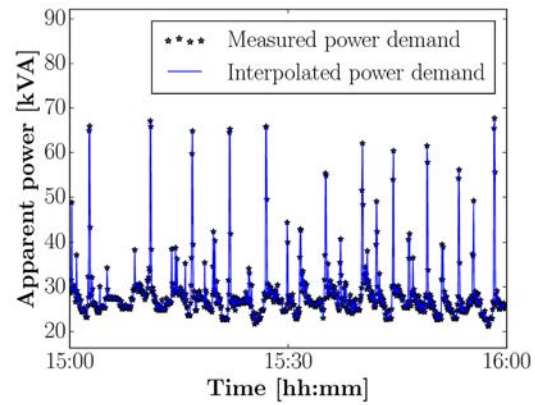


Figure 2.21: Same load profile magnified

Figure 2.22: Electrical load profile for construction site



Figure 2.23: The IGenerator, an on-campus hybrid genset

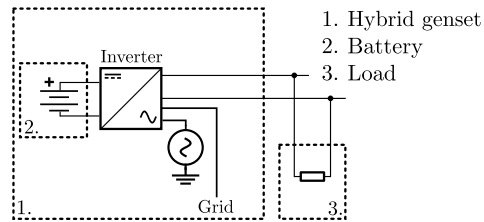


Figure 2.24: Sketch of the target set-up

Figure 2.25: Different aspects of the target hybrid genset set-up

Hybrid genset on a telecom site

The load profile for the battery of a telecom site is shown in figure 2.32. The load is typically quasi constant. As with the load-profile for a Flemish household, the load-profile is scaled so the RMS (Root Mean Square) value of the load-profile is unity, see figure 2.35.

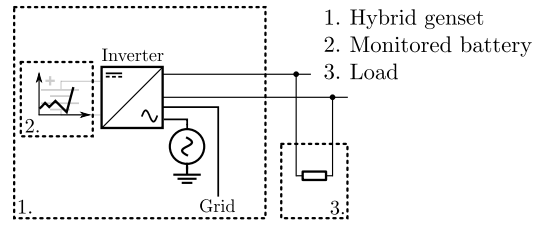
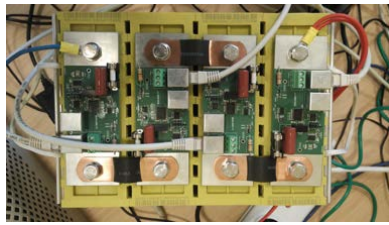


Figure 2.26: The battery is monitored by custom-made measurement PCBs

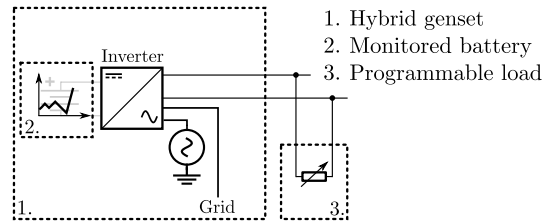


Figure 2.27: The electrical load is emulated by the programmable load bank, the R&D2

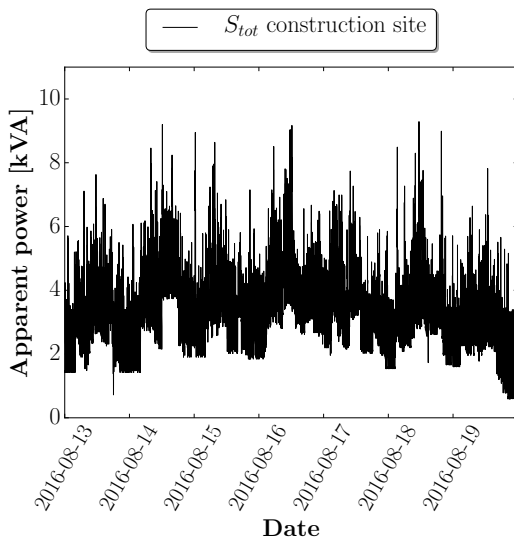


Figure 2.28: Field measurements

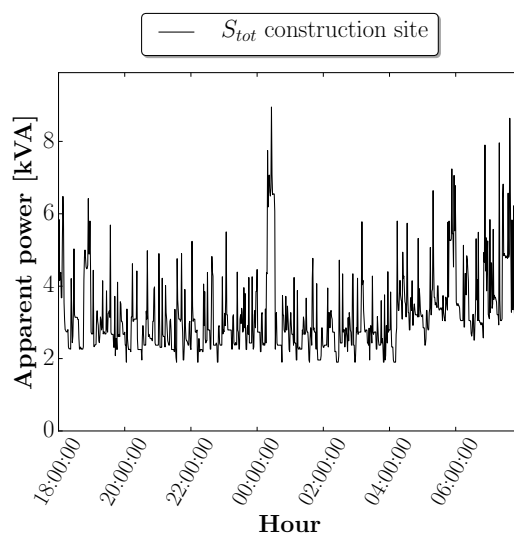


Figure 2.29: Detailed view

Figure 2.30: The electrical load of a construction site, courtesy of Locquet

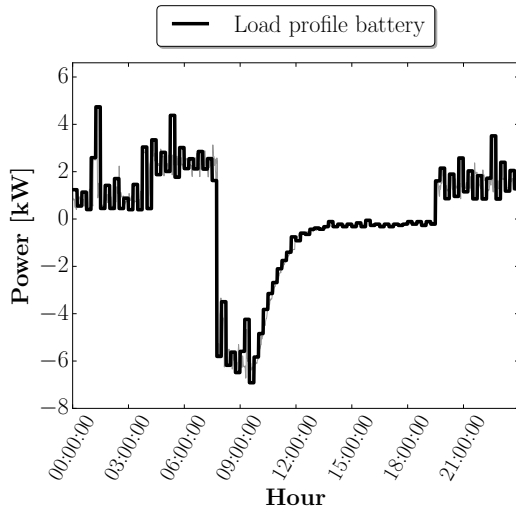


Figure 2.31: Load profile construction site

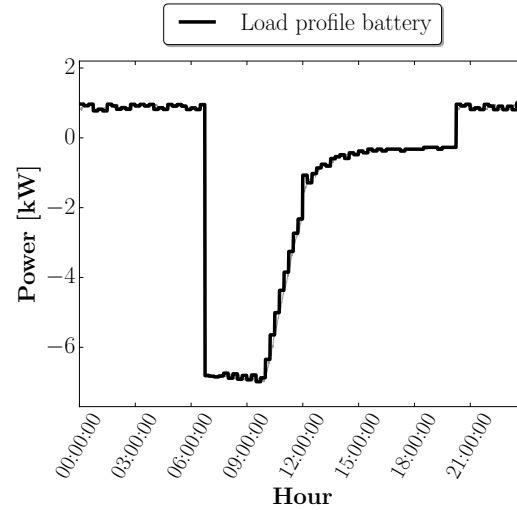


Figure 2.32: Load profile telecom site

Figure 2.33: The battery load of a construction and telecom site, courtesy of Locquet

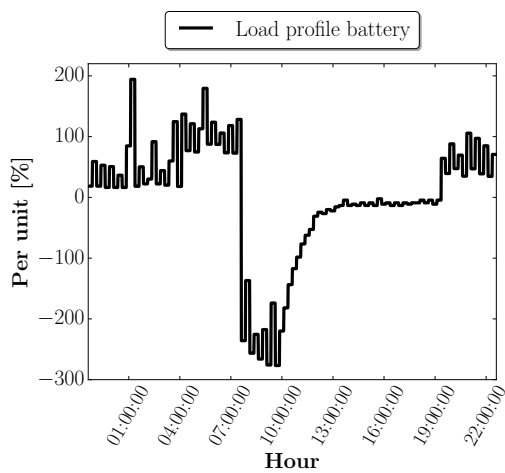


Figure 2.34: Scaled load profile construction site

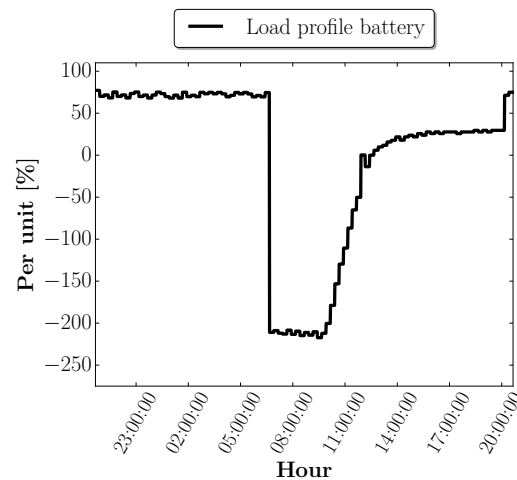


Figure 2.35: Load profile telecom site

Figure 2.36: Scaled battery-load of a construction and telecom site, courtesy of Locquet

Chapter 3

Load cycles

3.1 Introduction

As readily expressed in chapter 1, we are interested in the load cycles the battery goes through in real conditions. By this we mean not only electrical, but also thermal.

In this chapter we will discuss:

The environment The ambient temperature affects the battery in a pertinent way. Based on available historical thermal data, we have constructed a mock up function to simulate the ambient temperature, see section 3.2.

User profiles from international standards Because real data was not always easy to obtain and because it is not always representative for a whole group of applications (one of the primary targets in Tetra dissemination), we will also resolve to alternative literature based methods. For static applications such as load following, PV-generation and frequency regulation user profiles are well defined in standards.

Static applications Several static applications are targeted and their representative load cycles are discussed. Applications. For real test data of static applications see Chapter 2.

Mobile applications We will see that the characteristic discharge of an application is strongly related to the actual drive system. A user profile from a start stop vehicle used in industrial setting (at Colruyts truck terminal) is presented as well as a user profile from a LEV with direct DC drive system.

In the context of TETRA, where a case refer to a class of applications, it is important to use generally representative profiles.

3.2 Environment

A first distinction can easily be made between in- and outside conditions. In some cases however the reality is a combination of both.

3.2.1 Outdoor-applications

The outdoor temperature profile is difficult to predict. However, based on historical data and climate change one can easily erect a probable temperature profile. In Europe, weather stations have been installed gradually in the past 50 years. Reference [45] makes it possible to easily create accurate maps that depict typical climatic characteristics (see figures 3.1 - 3.2 - 3.3 - 3.4)

In the context of this project, temperature buffering a is studied in thermal management systems. For this reason it is important to not only capture the extreme temperatures but also visualize the oscillation of the temperature at different time scales.

Figures 3.1 and 3.2 allow to study the amplitude of the oscillation in summer period. Figures 3.3 and 3.4 provide the same information for the lower temperature limit.

In Belgium for example following approximations; the minimal measured temperature is $-15^{\circ}C$, the minimum value of daily maximum temperature is about $-8^{\circ}C$, the maximal measured temperature is $33^{\circ}C$, the maximum value of daily minimum temperature is about $17^{\circ}C$. These values can be combined to form the Temperature profile as depicted in figure 3.5.

3.2.2 Indoor-applications

Indoor applications take place in a temperature (partially) controlled environment, depending on a specific case the ambient temperature can take on very unique profile, this is illustrated in figure 3.6.

- UPS systems are one of the main applications for battery technology in the industry. Typically the batteries are installed in a room where temperature is controlled to some degree. The cooling and ventilation of these rooms is typically controlled by the building HVAC system.

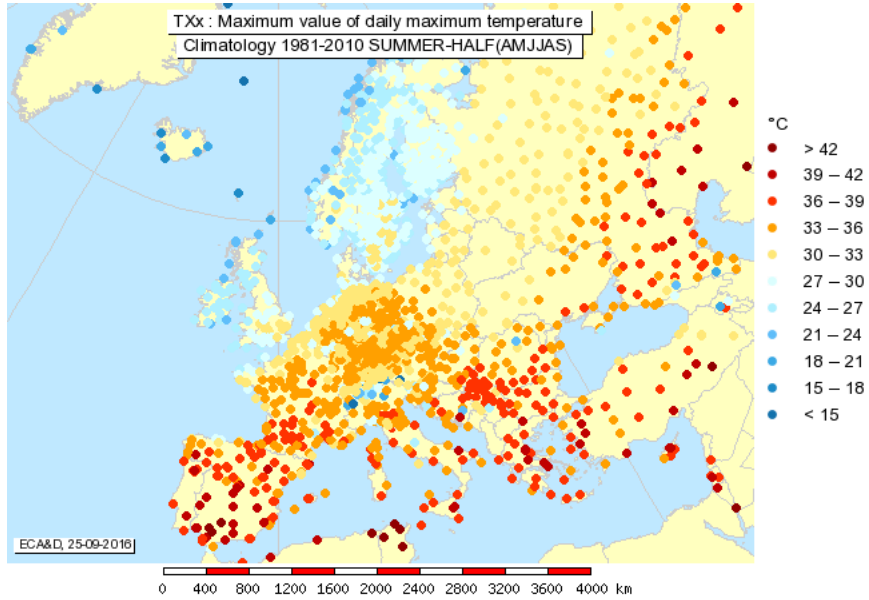


Figure 3.1: Maximal measured temperature during the summer period from 1981 to 2010. Each dot represents a measuring station.

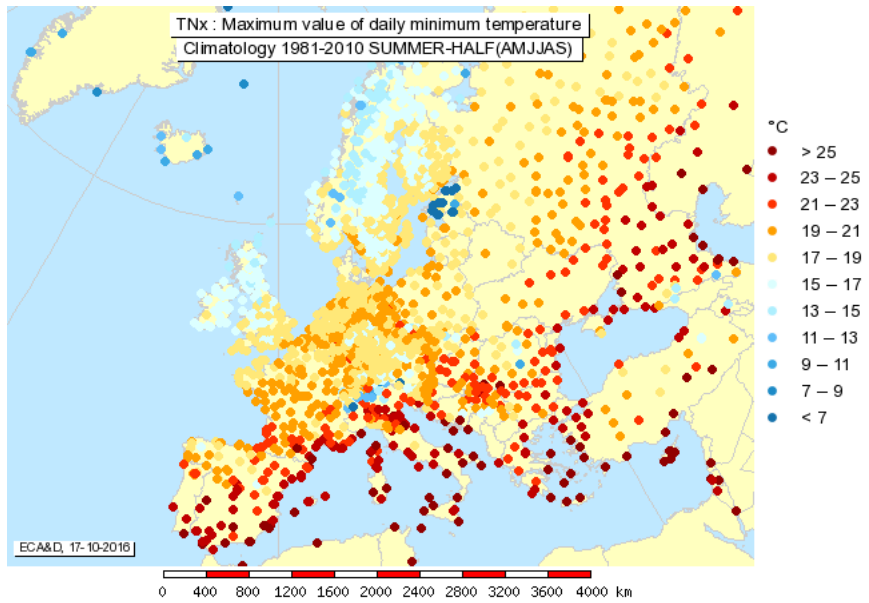


Figure 3.2: Maximal temperature of daily minima during the summer period from 1981 to 2010.

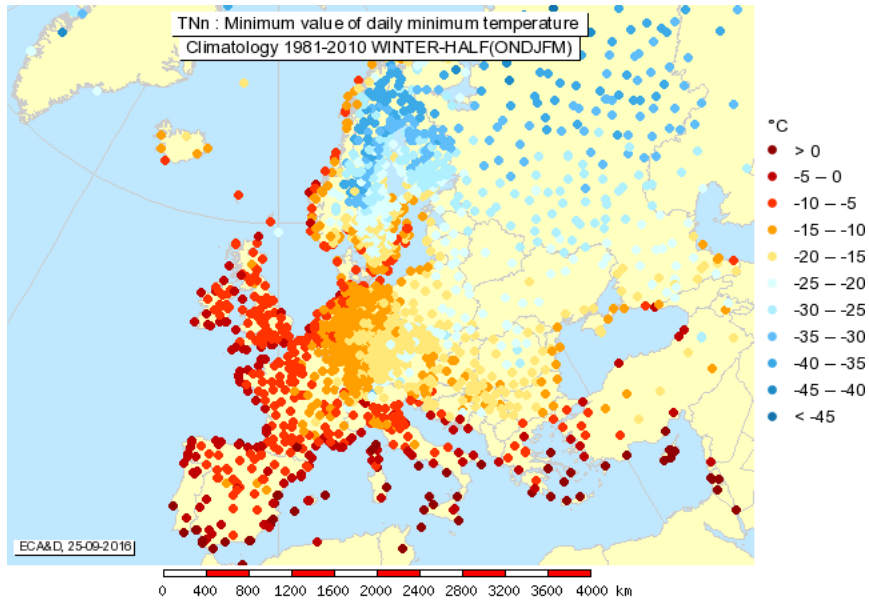


Figure 3.3: Minimal measured temperature during the winter periods from 1981 to 2010.

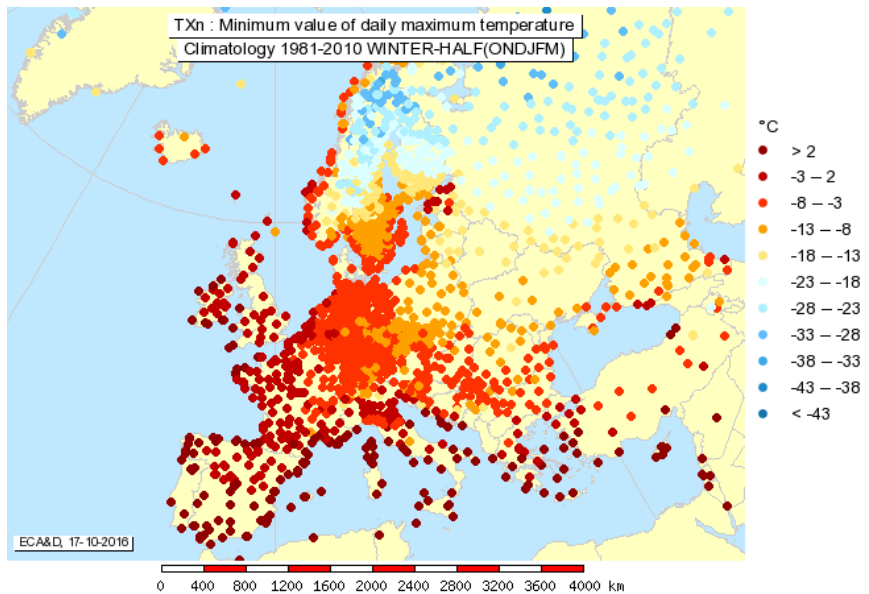


Figure 3.4: Minimal temperature of daily maxima during the winterperiod from 1981 to 2010.

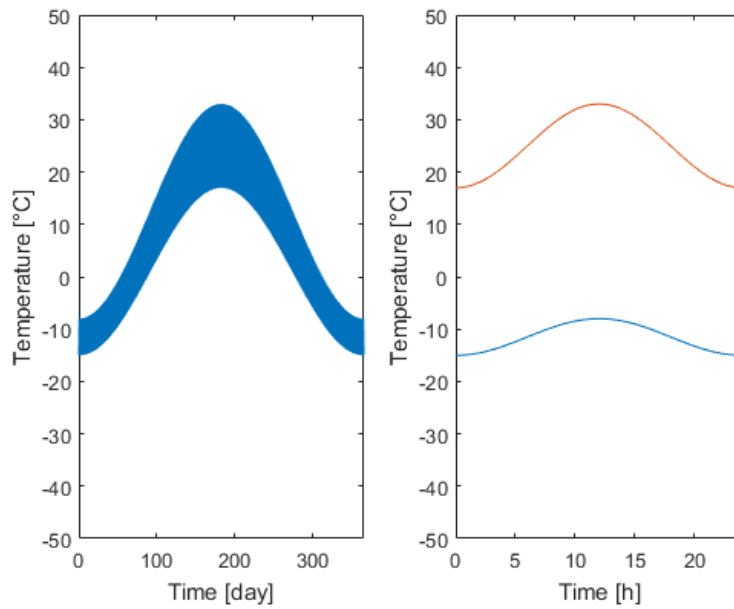


Figure 3.5: Belgian outdoor temperature profile; left: yearly dependence, right: the red and blue curve respectively represent the hottest and coldest day.

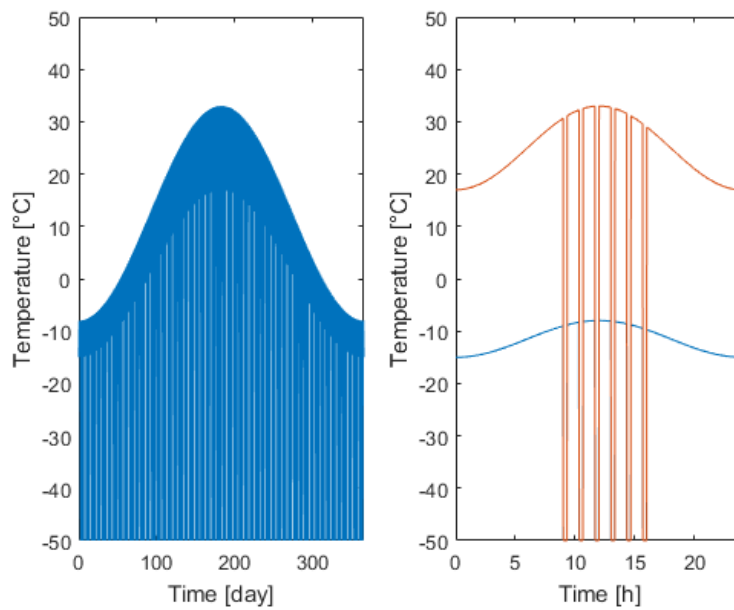


Figure 3.6: Possible temperature profile for LEV in the frozen food industry

- Imagine that a LEV is used for bringing food from a truck to the cooled freezing area and back. In these cases, the application becomes very user specific. Assuming the LEV repetitively goes inside the freezing area (at $-50^{\circ}C$) where it stays for 10 min after which it goes back outside for one hour. The ambient temperature will evolve like depicted in figure 3.6.
- An infinity of other temperature profiles exist.

It is clear that a thermal management system based on passive buffering is tailored on these environmental conditions. Some concepts will allow for short duration peaks in ambient conditions, other might prefer a smoother evolution in the profile.

3.3 User profiles from international standard

Within the user profiles one can easily distinct between generator and load influences. Standardization of these profiles would lead to many combinations.

Therefore some specific applications have been defined in the literature taking into account both the generating and load influences to come too a specific charge and discharge cycle. These are the profiles that we are interested in.

Accelerated testing These tests can be performed in accelerated as well as non accelerated conditions. For this Arrhenius is usually used. However, for several reasons this does not always lead to representative results. Perhaps estimation of the activation energy as function of the state of charge as well as accurate analysis of the cell bulk and hot spot temperatures might make the equivalence more fitting. Another remark around the use of Arrhenius is the fact that multiple chemical reactions take place at the same time. In the case of battery aging, the products of one reaction may fuel a second reaction and represent only one step in the cascade of reactions responsible for cell aging. Because Arrhenius only applies to one single reaction, it should be applied to each one of these reactions separately. In our case, analyzing the PCMs renders Arrhenius's approach even more complicated due to the phase change occurring at a fixed temperature.

3.3.1 Static Applications, profiles from standard

The International Electro technical Commission has defined several representative user profiles that capture our attention in the following applications:

- Frequency regulation, see figure 3.7

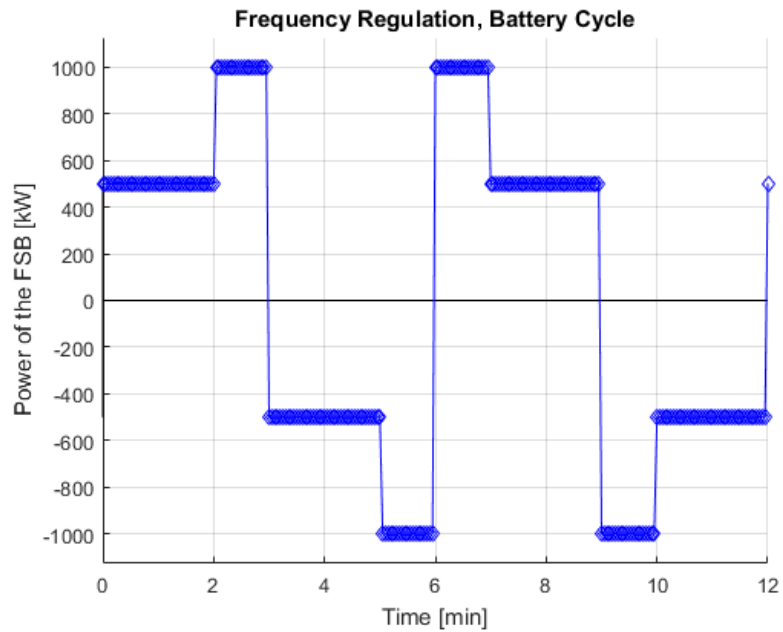


Figure 3.7: A representative users profile in frequency regulation applications. Reproduced from [3].

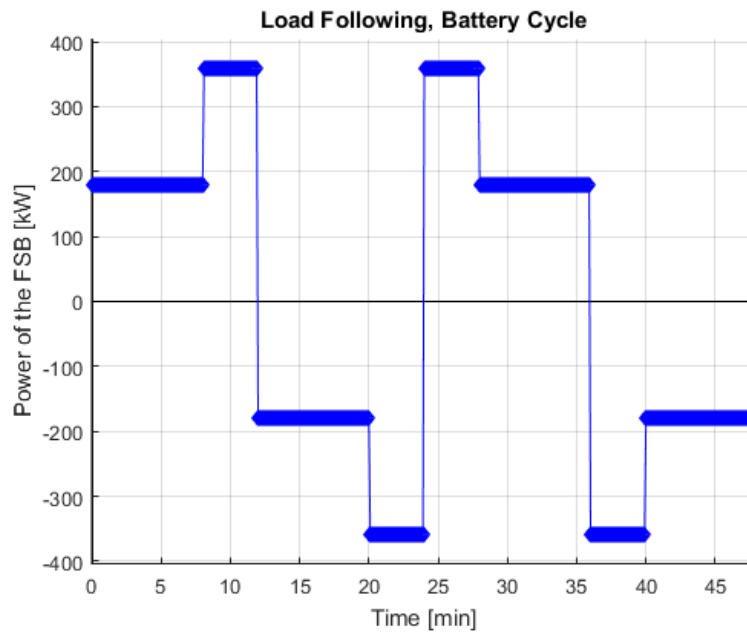


Figure 3.8: Representative users profile in load following applications. Reproduced from [3]

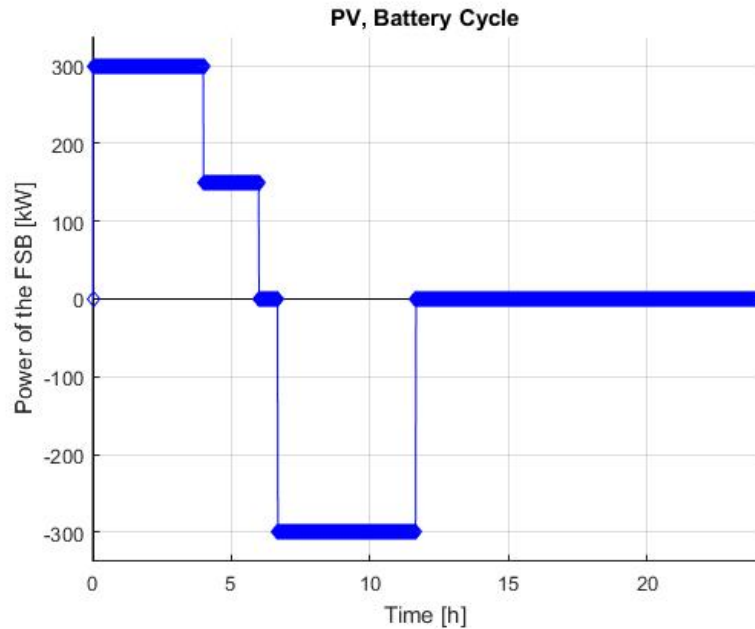


Figure 3.9: Representative cycle in PV instalations. Reproduced from [3].

- Load following, see figure 3.8
- PV generation, see figure 3.9

These profiles are defined in the context of standardization of test procedures for analyzing the battery endurance, that will eventually allow to compare cell technologies in function of the application. Needles to say that these profiles should be one of the most representative we can find. The power is fixed since it is specified for a standardized Full Sized Battery or FSB which is designed by the manufacturers to cycle through the defined load profiles many times without much degradation. The cell manufacturers can then perform aging tests on a scaled down version called the TOB Test object battery, more information on this can be found in [3].

3.3.2 Mobile applications, profiles from standard

Figure 3.10 depicts a similar test profile used for BEV applications.

The analysis for BEV applications can be done using the standardized, dynamic load profile as presented in figure 3.10 [2], which represents the battery behavior in a typical BEVs application.

The standard specifies that the cell should be subjected to the micro-cycle until the depth of discharge capacity is 80%. The standard specifies that the test should be performed at

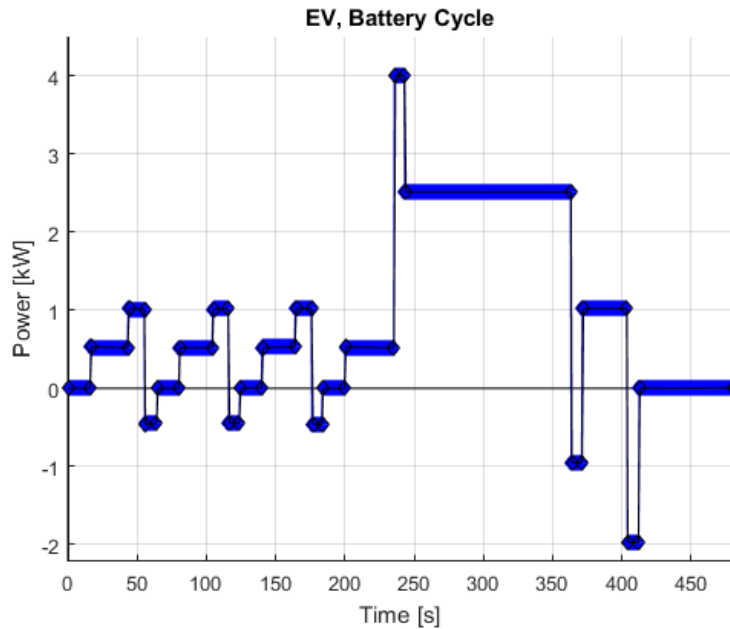


Figure 3.10: EV Driving cycle, reproduced from reference [2]

45°C in order to accelerate the aging mechanism of the battery. However, the numbers of commercial lithium-ion batteries that can operate at this charge temperature are very limited. For most batteries, the maximum charge temperature is 40 °C.

the standard proposes to convert the obtained cycle life value at 45 °C into a calculated value at room temperature by using the Arrhenius law. However, as we explained at the beginning of this section the use of Arrhenius without anything more is rather misleading.

3.4 Static applications

The static applications we will consider (and simulate) in this project are the:

- I-generator
- PV-system system
- Frequency regulation

3.4.1 I-generator

Common sense tell us that the I-generator is just a hybrid EES. The functional relation between capacitors and electrochemical cells of a hybrid battery capacitor system is

rather similar to the relation between electrochemical cells and the combustion engine in the I generator system.

The application only refers to the storage/generating aspect, therefore some assumptions with respect to the usage must be made. The load following profile seems the only representative candidate and can therefore be assumed further on when designing a module for these applications (figure 3.8). Depending on the chosen batteries we might be able to test the battery systems on a frequency regulation cycle as well (figure 3.7).

The I-generator can be used as power supply for powering events, construction works and others. The generated power is constant and corresponds to nominal power of the IC engine. The I-generator is typically used outside.

- Ambient temperature profile (in Belgium) is depicted in figure 3.5.
- The electrical user profile is assumed very similar to the load-following cycle as defined in figure 3.8.
- Measured load- and generator cycles are combined to form a battery cycle, these profiles can be found in Chapter 2.

PV-installation

In the same way as with the I-generator, this application only refers to the generating character. No universal information is available with respect to the actual loading of battery. Assuming the cycle has a daily period, causes the SoC to attain the initial level after a complete cycle.

The ambient temperature profile is not universally defined, because the environment is not always the same. For instance, in some cases the batteries are housed outside in special casings. In other cases however the battery system is housed in a specially dedicated room, in this project we will assume the latter.

- The ambient temperature profile will typically correspond to an indoor profile. Constant temperatures of 5, 15, 25, 35 and 45°C may be of interest.
- The electrical user profile is assumed very similar to the load-following cycle as defined in figure 3.9.
- Representative data (measured cycle) can also be found in Chapter 2.

3.5 Mobile applications

Two ways that mobile applications can be ordered is by their degree of mobility, very long range like the Tesla model S compared to short range industrial start stop applications (characterized by a high amount of regenerative braking), and by their scale, for instance LEV compared to heavy duty electric vehicles.

In summary mobile applications can be ordered in the following way:

- Scale, for instance Heavy Duty EV versus LEV
Battery systems are known to be scalable however at a certain point, adequate thermal management is needed in order to sustain the scalability.
- Degree of mobility:
 - Short range
 - Full DC Power train
 - Regenerative braking
 - Long range
 - Regenerative braking

The drive train and power electronic systems powering the vehicle are in a strong way related to the actual application and its corresponding electric user profile.

If thermal management is no issue, battery technology scales well. Therefore the scale has little to no influence on the electric user profile

3.5.1 Heavy duty Vehicles

The dispatching truck at Colruyts terminal is a good example of a purely electric heavy duty vehicle. Its load cycle is not so different from many LEV used in industrial applications (characterized by many start and stop cycles).

Figure 3.11 represents the data measured by Colruyts, the original cycle is only 16h long and the SoC at the end of the cycle was different from the initial state of charge. For this reason, the extract was prolonged with the needed charging period (to achieve a balanced profile) and resting hours to come to a 24h representative cycle. Figure 3.12 represents the a 5 min extract of the same measurement

Additionally the second and third graphics in figure 3.11 illustrate the normalization process. More information on this can be found in section 3.6.

Power of motor	150 kW 1800rpm
Torque of motor	790 Nm from 0 - 1800rpm
Max vehicle speed	40 km/h (limited to 25 on site)
Semitrailer weight	36 ton
Battery technology	92 large format (2.38kWh) Winston LFP cells.
Battery voltage	312 Vdc
Mean Cell Voltage	3.4Vdc
Voltage range	2.8 Vdc to 4 Vdc,
Battery capacity	209kWh
Mean annual working hours	3000h/year
Mean consumption	21kWh/h
Charging time	4h at charge station on site Dassenveld

Table 3.1: Characteristics of the truck

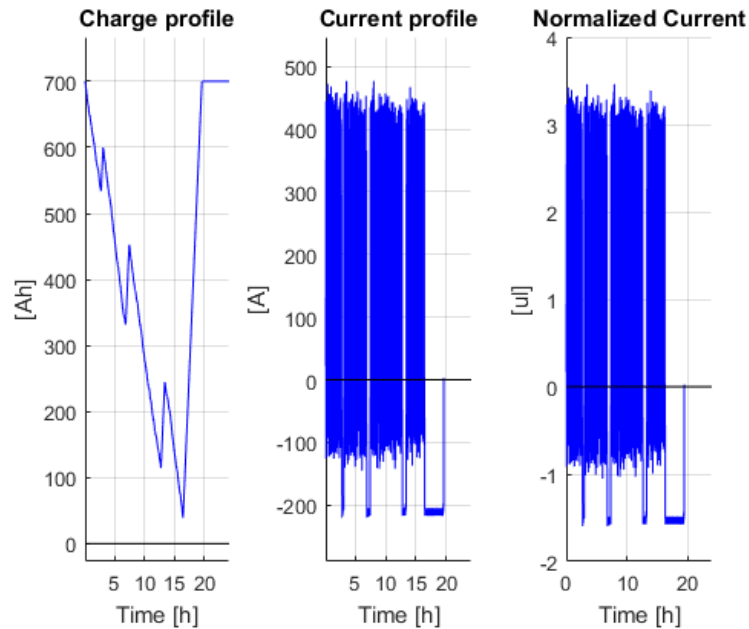


Figure 3.11: 24 hour battery cycle and normalisation

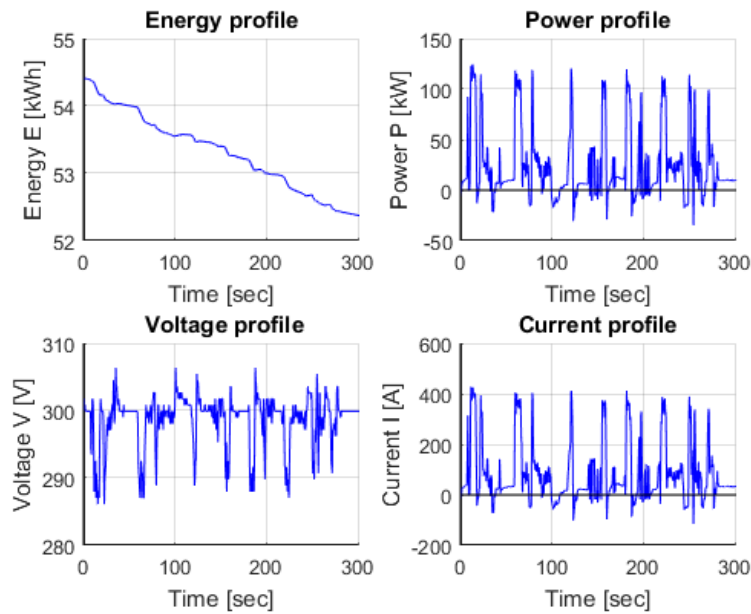


Figure 3.12: 5 min cycle of terminal truck

3.5.2 Light electric Vehicle

In the framework of the Thermie project "E.V.D.-Post", supported under the European Commission, measurements have been performed on postal vehicles used on different sites.

This section describes the measurements held in Nacka, Sweden, in February 2000 [26]

Background: Electric Vehicles in Swedish post has a total delivery fleet of 5900 vehicles (bicycles not included). During one year, 100 million kilometers are driven, for typical delivery duties once a day, 258 days a year.



Figure 3.13: LEV, Postal delivery



Figure 3.14: Tugger vehicle

- 2700 thermal-engined vehicles are used for delivery in city areas, their average delivery route is 45 km per vehicle and day.
- 2700 thermal-engined vehicles are used for delivery in the countryside; their average delivery route is 100 km per vehicle and day.
- 500 electric vehicles, three- or four wheelers, are used for delivery in city areas; their average delivery route is 15 km per vehicle and per day.

The use of electric vehicles in Swedish postal services is clearly aimed at local delivery, using appropriate vehicles which represent a technology comparable with industrial electric vehicles. Two main types of vehicles are used: the fourwheel type (as the subject of this measurements) and the specially developed three-wheel Tugger vehicle illustrated in Figures 3.13 and 3.14 respectively. These vehicles are all of a quite conventional technology, featuring lead-acid batteries and direct current series-excited motors. This technology is proven, reliable and well suited for the stop-and-go local service they are deployed for the Swedish Post. The service has a strong resemblance to the usage pattern of industrial vehicles, where electric traction has proven very strong [26].

Vehicle characteristics The Club Car Carryall II is an electric utility vehicle which finds a variety of uses, both in the industrial field (light utility or personal carrier) as for leisure applications. The vehicles used by Swedish Post are fitted with a purpose-built body [26].

The average weight of the vehicle during the tests can be estimated at 650 kg (including postal load and the measurement system).

Traction characteristics The vehicle is powered by a series-excited DC motor acting on the rear axle through a fixed transmission. The motor is fed through a Mosfet chopper; energy regeneration is not provided. The traction battery consists of 6 monoblocs (of the rather unusual block voltage of 8 V), to obtain a nominal voltage of 48 V. The batteries are fitted under the drivers seat, allowing for easy access and watering. The vehicle comes with an off-board charger; the plug is located in front of the vehicle.

Driving behaviour - Acceleration The traction circuit of the vehicle consists of a series DC motor, fed by a chopper and connected to the wheels via a fixed transmission. The high starting torque of the series motor gives a good acceleration well suited for stop and go traffic. The maximum speed of the vehicle is limited however, the Carryall is not really to be considered a road-going vehicle.

Characteristic	Unit	17-Feb.	18-Feb.	21-Feb.	Average
Trip length	m	14003	13940	13877	13940
Total time spent	h:m:s	02:23:37	02:22:33	02:21:29	02:22:33
Stop time	h:m:s	01:07:56	01:08:34	01:09:12	01:08:34
%stop	%	47	48	49	48
Run time	h:m:s	01:15:41	01:13:59	01:12:17	01:13:59
%run	%	53	52	51	52
Number of stops		328	319	311	319
Stops per km		23,4	22,9	22,4	22,9
Average interval	m	43	44	45	44
Commercial speed	km/h	5,9	5,9	5,9	5,9
Maximum speed	km/h	32,7	35,3	31,9	33,3
Average speed	km/h	11,1	11,3	11,5	11,3
Consumption	Ah/km	6,1	6,1	6,1	6,1

Table 3.2: Summary of delivery routes

Practical realisation: Table 3.2 summarizes the main characteristics of the delivery route measured during a single day. From this data it is easy to determine some typical characteristics of the postal delivery traffic in Nacka [26]:

- A daily distance is driven of about 14 km.
- The actual stop time is about 50 % of total mission time¹.
- The average distance between stops is only about 44 m, with a total number of stops on the round exceeding 300.
- The commercial (end-to-end) speed is very low, of the order of walking speed, due to the frequent stops times.
- The average speed when running is about 11 km/h
- The maximum speed of the vehicle is just about 33 km/h, consistent with the characteristics of the vehicle
- Instantaneous energy consumption is consistent at 6,1 Ah/km.

Figure 3.15 shows a 5-minute extract of a typical delivery run. One can clearly see the progress between the stops, as well as the stop time between them [26].

¹This refers to the time spend in the delivery round proper. The stop time taken by the driver to take his lunch break, at the middle of the delivery round, has not been taken into account.

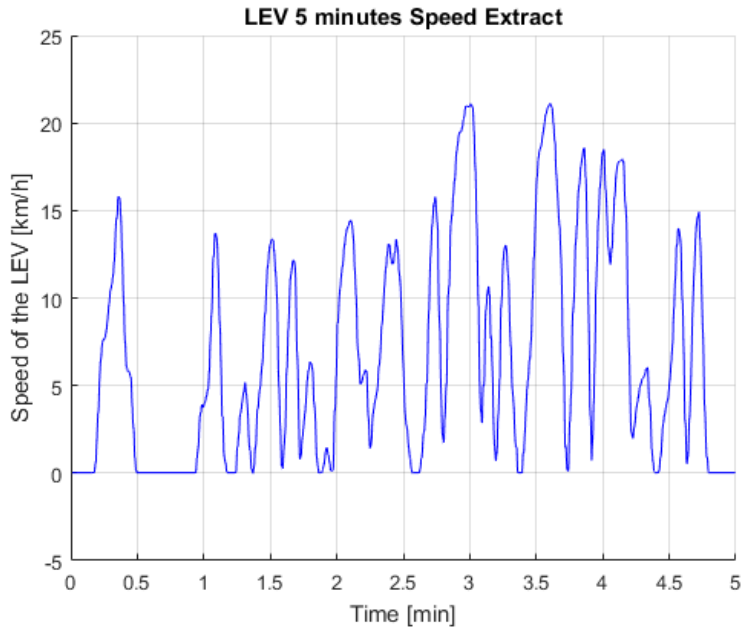


Figure 3.15: Speed/time profile

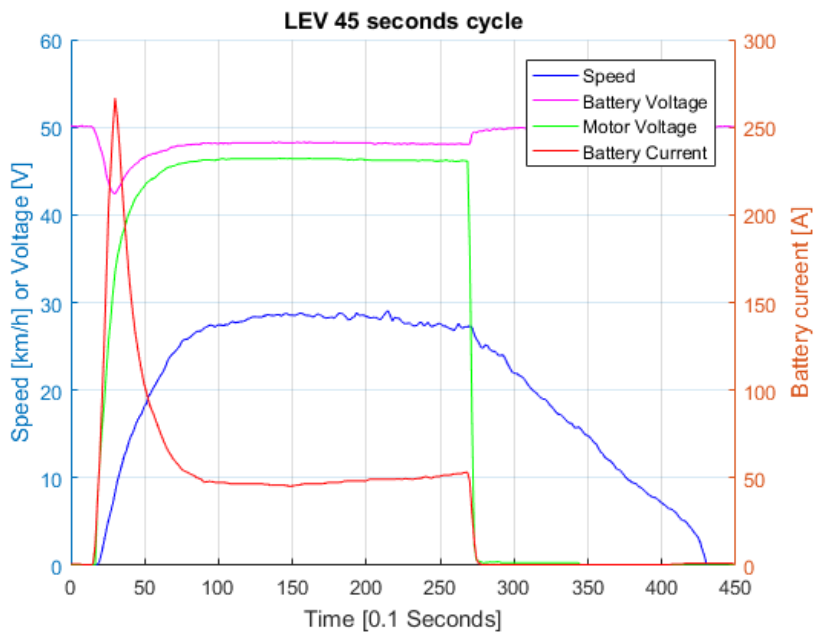


Figure 3.16: Energy flows

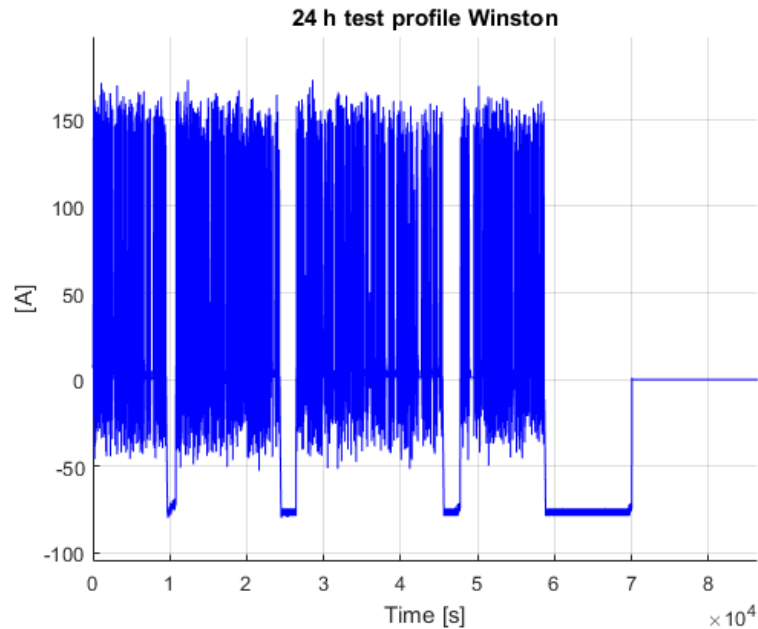


Figure 3.17: Test profile for 100Ah Winston cells.

The energy flows during a typical start-stop cycle are illustrated in figure 3.16. One can see the typical high acceleration current of the series motor, which allows the high starting torque, and allows the vehicle to reach a speed of 25 km/h in just five seconds. This makes the vehicle very suitable for frequent stop and go traffic at low top speeds like encountered in postal delivery.

Only during the first few seconds of the acceleration the chopper is actually at work; after this phase, the motor and battery currents become equal, and the difference between motor and battery voltage represents the voltage drop over the chopper which is now in full conduction mode. Since the system voltage is relatively low, this voltage drop can be clearly seen in this example. The battery voltage drops quite significantly when a high current is absorbed during acceleration.

This phenomenon will become more obvious when the battery discharges; at end-of-discharge, battery voltage during acceleration can drop as low as 36 V (i.e. 1,5 V per cell) which is to be considered a minimum value for the preservation of the battery [26].

3.6 Normalisation of the user profile

As a finishing remark in this work package, let us focus a little on the post processing of all this data.

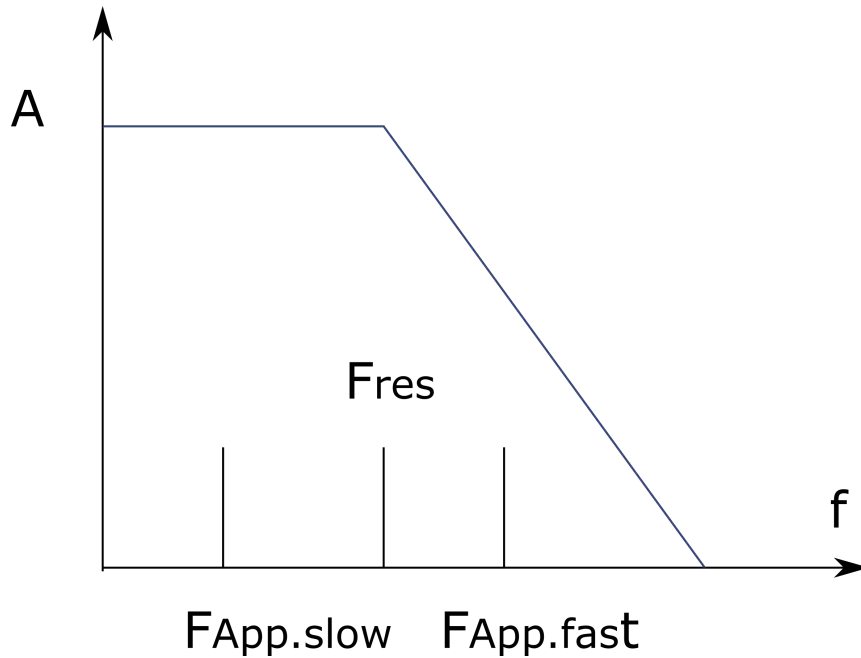


Figure 3.18: RC frequency response of thermal behavior versus ground frequency of the application.

Normalization The measured profiles correspond to a specific application. These applications were designed with a specific safety factor. Because this safety factor does not characterize the application we must conclude that the above user profiles only yield a useful shape.

The Amplitudes of the different user profiles must be normalized to a certain value for enabling comparison. For this reason we will first normalize the signal to its RMS value (see the last graphic in figure 3.11).

Needed Time extract To understand how long a certain profile must last to ensure representativeness, we first have to understand a little more on the module's thermal behavior. Every module has a thermal capacity and when implemented in its application, shows a specific thermal resistance towards the environment. The thermal process can be characterized by the RC behavior of the thermal equivalent circuit. The frequency response of such a system is depicted in figure 3.18.

$$\tau_{Therm} = \frac{1}{R_{Therm} \cdot C_{Therm}} \quad (3.1)$$

Just like the resonance frequency of the battery system, the user profile has also a ground frequency (typical ones can consider a day, week or year due to the cyclic nature of this period).

- If the resonance frequency of the thermal system is (significantly) higher, then the ground frequency of the user profile, the cell temperature will follow the user profile and we may conclude that the influence of the user profile must be considered in life time analysis.
- On the other hand if the ground frequency of the user profile is higher than the resonance frequency of the thermal behavior, the life time analysis becomes independent of the user profile. (this is typically the case for very large scale systems)

Once the normalized profile got erected, simple multiplication with the nominal discharge current (value from DS) can be used to rescale the profile for use in a test setup in laboratory environment. For example figure 3.17 depicts the battery profile scaled to the nominal discharge current (in this case 50 A) of the Winston cells bought for this project.

Part III

Electrical characterisation and modeling

Chapter 1

Introduction

Relevant literature sources describe several battery technologies (i.e., lithium-ion, lead-acid, nickel cadmium, and nickel metal-hydride) that are either in use and/or potentially suitable for stationary and traction applications [78]. Among the available battery technologies, lithium-ion batteries possess significant characteristics, which in turn encourage manufacturers to rely on this technology in the upcoming future. These characteristics can be summarized as:

- High energy density (200-500 Wh/L) and a high power density (1500-10,000 W/L) [121]. This characteristic leads to widespread uses of lithium-ion batteries in portable devices and promising potential in transportation and stationary applications due to small size.
- High specific energy (75-200 Wh/kg) and specific power (500-2000 W/kg) [121]. Thus, lithium-ion batteries are suitable for light weight applications (portable devices).
- Discharge time could vary within the range from seconds to several hours (10 hours) [121].
- Energy efficiency of lithium-ion batteries recorded the highest percentage (75% - 97%) compared with other technologies [121].
- Long life cycles (20,000 cycles), no memory effect and low daily self-discharge (0.1-0.3 %) [121].

Accordingly, it is expected that approximately 80% of the produced lithium-ion batteries will be used in the vehicular services industry and in the renewable energy applications until 2020 [201]. Although Li-ion battery systems are becoming more and more the primary energy source in high power systems, without a proper Battery Management

System (BMS), usually electrical and/or thermal problems will cause the battery to fail prematurely, or even worse, cause the batteries to blow up. In order to prevent this, the BMS should be designed based on models that try to emulate battery cells electrical and/or thermal behavior. In particular, they focus on the SoC (State of Charge - amount of capacity still present on the battery, usually expressed in percentage) and the SoH (State of Health - amount of time passed/left in the batteries life, usually also expressed in percentage) as this are the most important values in order to maximize efficiency and minimize energy consumption, while also preventing malfunctions and accidents. Before building four battery modules in WP5, this report aims to provide a complete information about:

- Characterization of battery cells in order to thoroughly investigate their specific characteristics, such as discharge capacity, internal resistance, and energy as a function of different current rates (I_t), State-of-Charge (SoC) and temperature levels.
- Optimization of electro-thermal model by evaluating the performance of battery cells (electrical and thermal), and contribute in developing thermal management system of the battery modules.

The testing protocols and simulation models should be precisely developed to design and integrate reliable and high-performing battery systems for automotive and stationary applications. The simulation model should provide an accurate and simple model in order to limit the consumed time for the simulation. In addition, the capability of the simulation model for integration with interface circuits (i.e., battery management system, and power electronic converters). Indeed, among battery simulation models (i.e., electrical, electrochemical, and mathematical models), the electrical battery models have been selected, because these models can describe the battery behavior by using electrical elements such as resistor, inductors and capacitors.

As reported in the literature, the accuracy of the battery model increases when increasing the amount of RC circuits to achieve the lowest possible error between measured and estimated data. Currently, different battery models (i.e., Rint, RC, Thevenin, and PNGV model) have been developed and widely used, especially in electric vehicle applications [121]. Among the battery models, the Thevenin model (first-order) can provide an accurate simulation with minimum error ($\leq 1\%$) for dynamic load profiles provided that the model parameters are accurately estimated. In addition, this model has one RC circuit, and thus it can be easily implemented by using Matlab/Simulink and integrated with interface circuits (i.e., battery management system and power electronic converters). An accurate model of the battery cell / module with the consideration of thermal and aging effect is shown in figure 1.1. This model is composed of three interconnected sub-models:

- Electrical model: predict battery cell voltage and SoC in response to current, the output is influenced by temperature and cycle numbers;

- Thermal model: predict the cell temperature in response to current, voltage and ambient temperature;

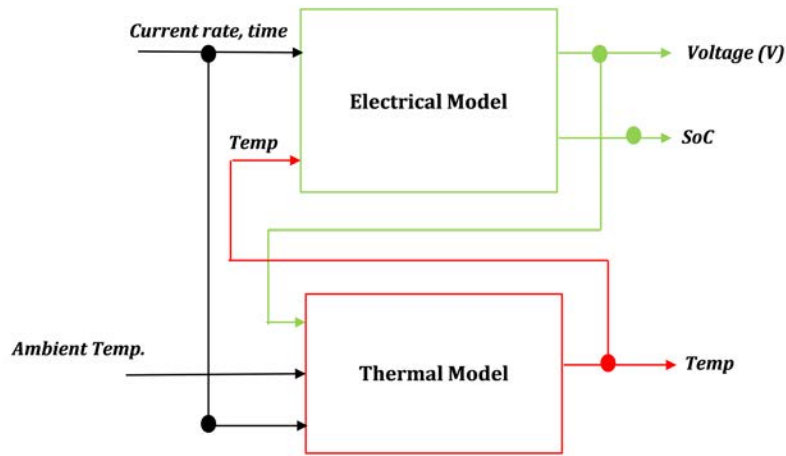


Figure 1.1: Schematic of the electrical battery model with ageing model

As shown in Figure 1.2, the first order model consists of open-circuit voltage V_{OCV} , Ohmic resistance R_o , Thevenin resistance R_{Th} and equivalent capacitance C_{Th} . The R_{Th} and C_{Th} are mainly used to describe the transient response. In order to estimate the model parameters, the charge/discharge pulses of the extended-HPPC test (from 100% till 0% SoC) is used at different temperature degrees [201]. Based on the estimated parameters, for every parameter, two lookup tables (charge and discharge) are developed in Matlab/Simulink. The output of these lookup tables mainly depends on the input charge/discharge current rates, temperature, lifetime and the SoC levels.

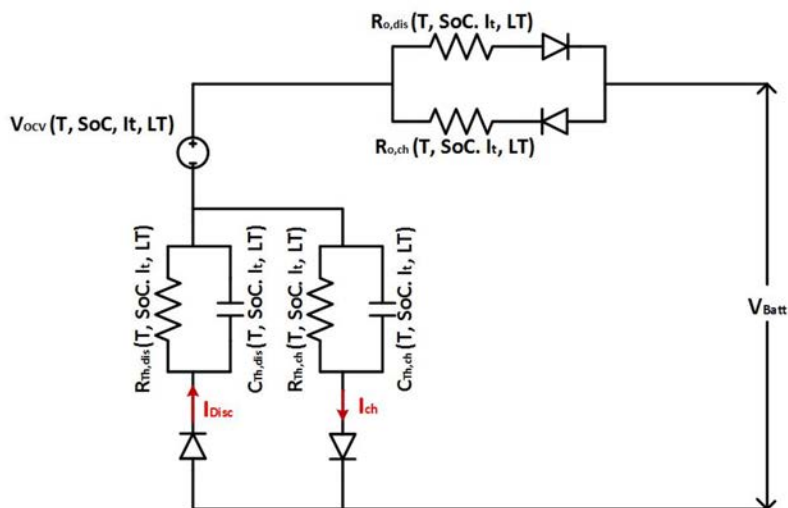


Figure 1.2: Thevenin model (first-order) (adapted from [156])

Chapter 2

Battery specifications

2.1 Toshiba 20Ah LTO

Toshiba released a lithiumtitanate battery, dubbed Super Charge Ion Battery (SCiB). The battery is designed to offer 90% charge capacity in just 10 minutes. The lithiumtitanate battery is a type of rechargeable battery, which has the advantage of being faster to charge than other lithium-ion batteries. Titanate batteries are used in certain Japanese-only versions of Mitsubishi's i-MiEV electric vehicle and Honda uses them in its EV-neo electric bike and Fit EV. Opportunity charging in public transportation, such as large capacity electric bus project TOSA, is using the Titanate batteries high charging capability to partly recharge the battery in 15 seconds while passengers are disembarking and embarking at bus stops.

A lithiumtitanate battery is a modified lithium-ion battery that uses lithium-titanate nanocrystals on the surface of its anode instead of carbon. This gives the anode a surface area of about 100 square meters per gram, compared with 3 square meters per gram for carbon, allowing electrons to enter and leave the anode quickly. This makes fast recharging possible and provides high currents when needed. A disadvantage of lithium-titanate batteries is that they have a lower inherent voltage (2.4 V) than conventional lithium-ion battery technologies (which have an inherent voltage of 3.7 V), which leads to a lower specific energy of about 30-110 Wh/kg.

2.2 Winston 100Ah LFP

This battery cell has a lithium Iron Phosphate chemistry, which is designed for power applications. This battery is used for traction applications (EV, industry, etc..) But also for stationary batteries (Off Grid, Smart Grid, standalone applications, etc..). One of the most safe lithium-ion battery chemistries is the lithium iron phosphate battery, which is

attractive compared with other chemistries due to: low cost, low toxicity, flat charge/discharge voltage, relatively good cycle life and high structural stability.



Figure 2.1: Toshiba cell (left) and Winston cell (right) (figure not on scale)

Chapter 3

Characterization methodology

In WP3 of the LBATTS project, an electro-thermal characterization has been performed followed by the application of an electro-thermal model to obtain a simulated surface heat for both the Toshiba 20Ah LTO cells and the Winston 100Ah LFP cells. A full outline of the electro-thermal model methodology is illustrated in figure 3.1. Notice that the electro-thermal model exists of a separate electrical- and thermal model that have been connected. This approach requires the knowledge of various model parameters which are obtained experimentally during a process called characterization. The followed characterization methodology during this project is shown in figure 3.2 and elaborated further in section 3.1. Hereafter, sections 4.1 and 4.2 discuss the electrical- and thermal model respectively.

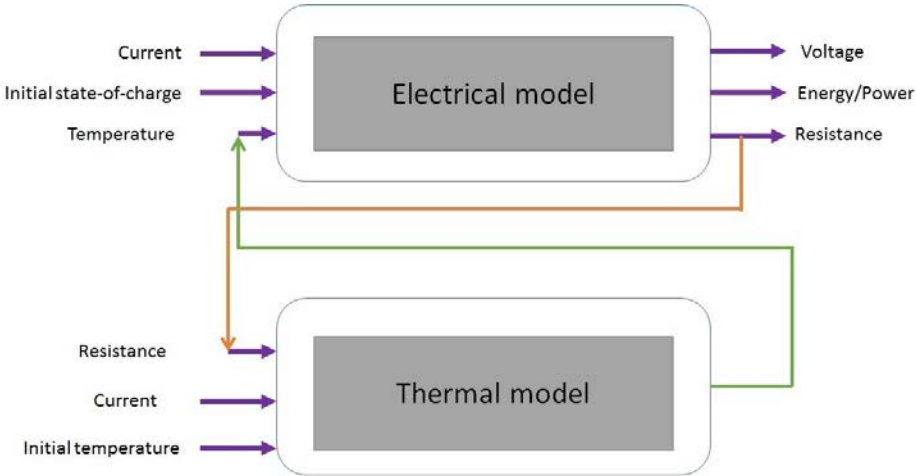


Figure 3.1: Principle schematic of applied electro-thermal model

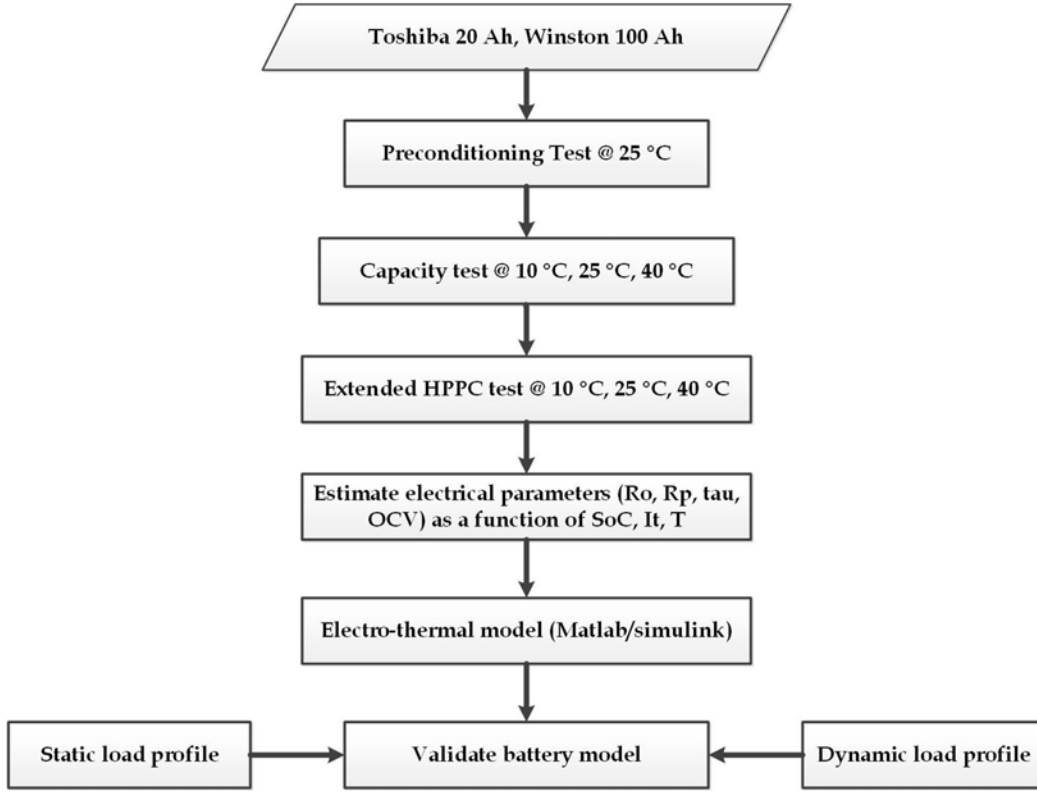


Figure 3.2: Flow chart of the battery testing procedure

3.1 Characterization tests

All battery cells have first been subjected to a preconditioning test at 25 °C, which consists of four standard charge/discharge cycles, as defined by the manufacturer recommendations [156] [155].

An OCV test follows after the preconditioning test, where the cell is fully charged by means of a CC-CV profile, after which the cell is discharged in 5% SoC steps from 100% SoC to 0% SoC with a constant current at a low C-rate. Between every discharge a sufficient relaxation time of two hours is implemented to allow the cell to reach its open circuit voltage.

Secondly, in order to obtain the capacity of the cells at varying temperatures and current rates, a standard capacity test was performed. The capacity test profile consists of constant current (CC), performed at four current rates, followed by constant voltage (CV) technique for charging and CC technique for discharging. According to the international standard IEC61434 [156], $I_t(A)$ is the reference test current, which is expressed as $\frac{C_n(Ah)}{n(h)}$ where C_n is the rated capacity of the cell and n is the time base (h). Hereafter an extended Hybrid Pulse Power Characterization (Extended HPPC) test is

performed on every cell at varying temperatures to obtain the ECM model parameters. The test consists of equal charge and discharge pulses at different current rates with 5 min rest time between every two pulses, followed by CC discharge ($1I_t$) and then 30 min rest time to change the State-of-Charge (SoC) from 100% to 0% SoC with 5% steps.

Chapter 4

Battery Model

4.1 Electrical battery model

4.1.1 Equivalent circuit model

Electrical equivalent circuit models (ECM) are extensively used to describe the electrical behaviour of batteries. They represent the battery with an electrical equivalent circuit composed of electrical components such as an ideal voltage source, resistors and capacitors. The values of these electrical components are paramount for the effectiveness of the model and are often referred to as model parameters. Generally these parameters have to be identified by performing characterization tests on the battery as described in various standardization documents [5]-[4]. Three characterization tests are of great importance for this work package, as explained in section 3.1:

- **Capacity Test** : Used to determine the charge and discharge capacity of the battery.
- **OCV test** : Relates Open Circuit Voltage (OCV) to State of Charge (SoC) for both charging and discharging.
- **HPPC test** : Used to determine the equivalent circuit parameters of the battery model.

The selected electrical model for this project is the first order model, sometimes referred to as the Thevenin model, which consists of four electrical components as can be seen in figure 4.1: an ideal voltage source U_{oc} , a resistor R_{int} and a parallel RC circuit consisting of a resistor R_{th} and a capacitor C_{th} . It can be said that the first order model connects a R_{int} model in series with an RC network. It is this RC network that enables the first

order model to describe the dynamic behaviour of the battery as it describes the chemical reactions at the electrodes and the ion transfer inside the electrolyte [73].

R_{int} is often called the ohmic resistance of the battery. This resistance is due to the battery contacts, electrolyte and electrodes. The resistor R_{th} in the RC network is often called the polarization resistance. This resistance arises due to the different chemical reactions at the electrodes during charging and discharging. Together these two resistors describe the total internal resistance of the battery [148].

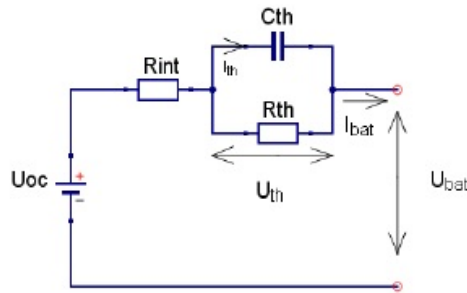


Figure 4.1: Schematic diagram of the First order model [148]

The electrical behaviour of the first order model can be described by equations 4.1 and 4.2:

$$\dot{U}_{th} = -\frac{U_{th}}{R_{th}C_{th}} + \frac{I_{bat}}{C_{th}} \quad (4.1)$$

$$U_{bat} = U_{oc} - U_{th} - I_{bat}R_{int} \quad (4.2)$$

As mentioned before, the values of these model parameters have to be identified by performing different characterization tests. Furthermore, in order to be able to model dynamic loading profiles the model parameters should vary with SoC [148]. Two methods are available to implement this in our battery model: using look-up tables and linear dependency parametrization. In this project only the former is used because it is more accurate than the latter [1]. When using the look-up table method a look-up table is created containing the different values of the model parameter for various SoC and C-rate breakpoints.

Regarding the capability of the first order model to model dynamic behaviour it was found in [73] that the maximum error on the simulated voltage was only 0.52% compared to a maximum error of 2.82% for the simpler R_{int} model. Also in [73] it was found that the more complex second order model showed a maximum error of 0.38%. This minor increase in accuracy compared to the added complexity and required computational power of the second order model lead us to opt for the first order model for this project.

4.1.2 Electrical characterization

The procedure to determine the equivalent circuit model parameters, often referred to as electrical battery characterization, is based on the accurate analysis of characterization tests. These characterization tests are described in various standardization documents ([5]-[4]) and, as mentioned before in section 4.1.1, in order to perform a conclusive electrical characterization for the goals of this work package, three characterization tests were performed: capacity test, OCV test and HPPC test. All three tests were performed on the 24-channel SBT0550 battery tester accompanied by the Lifetest software. The Lifetest software can be used off-line and is fully programmable, which means that an enormous variety of test profiles can be created and performed. The software also provides a graphical user interface to start and stop tests on the different channels, display and export measurement data and many other features. Battery tester and software communicate through an Ethernet connection. Every one of the 24 channels is independently controlled by a microprocessor which ensures very accurate measurements and control. Voltage measurements are possible between -3V and 5V DC with a resolution of $100\mu\text{V}$ and an accuracy of $\pm 0.03\%$. Current measurements are possible between 0A and 50A DC with an accuracy of $\pm 0.02\%$. Through auxiliary modules on every channel it is possible to add both analog and digital in- and outputs such as temperature sensors [160]. After performing all necessary tests, all relevant data (such as time, temperature, current, voltage, capacity etc) can be exported to a .csv file. Hereafter, the appropriate .csv file is loaded into a matlab script that extracts the data of interest and saves it as a .mat file for further analyses. Finally, the .mat file of each type of test (Capacity test, OCV test and HPPC test) is loaded individually into MatLab, which is then analysed by a dedicated script, depending on the information we want to acquire.

It should be noted that every characterization test performed during this work package, was performed at three different temperatures controlled by a climate chamber: 10°C , 25°C and 40°C . Since the battery model parameters are temperature dependent, repeating the tests at different temperatures within the working temperature range is necessary to obtain good simulation results at different working temperatures.

Firstly, we performed a capacity test on both the Toshiba 20Ah LTO and Winston 100Ah LFP at different temperatures to determine their actual capacity, rather than relying on the capacity given in the datasheet, which may vary from cell to cell. The extraction of the capacity values from the characterization test is rather straight forward. Since the SBT0550 battery tester is capable of measuring charged/discharged capacity during a test, we can just extract the capacity at the corresponding temperature and C-rate from the charged/discharged capacity curve. While the results of the capacity tests are shown graphically in figures 4.2 and 4.3. The exact numeric values are shown in tables 4.1 and 4.2.

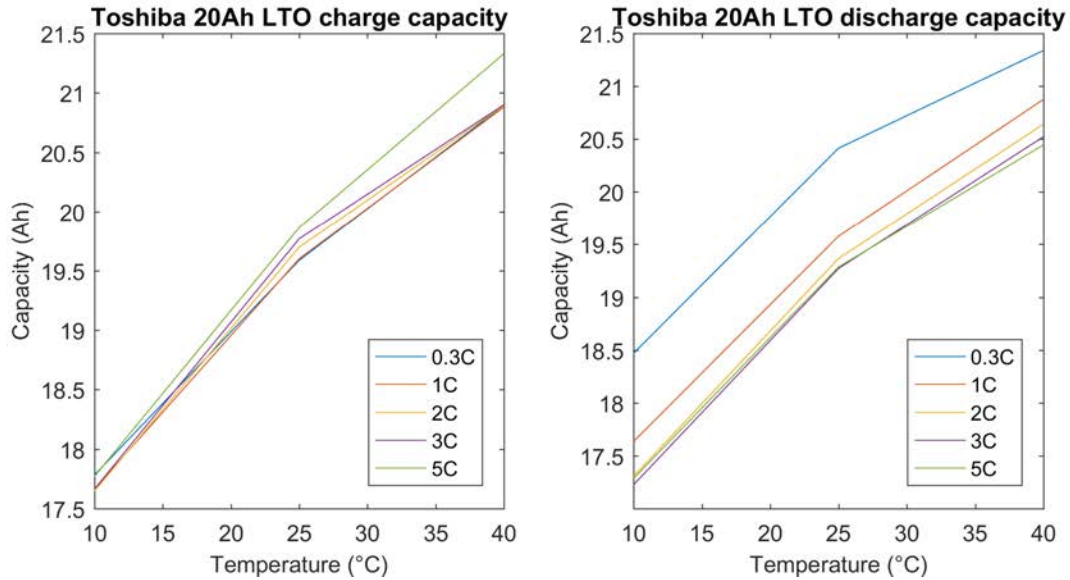


Figure 4.2: Determined charging and discharging capacity for Toshiba 20Ah cell

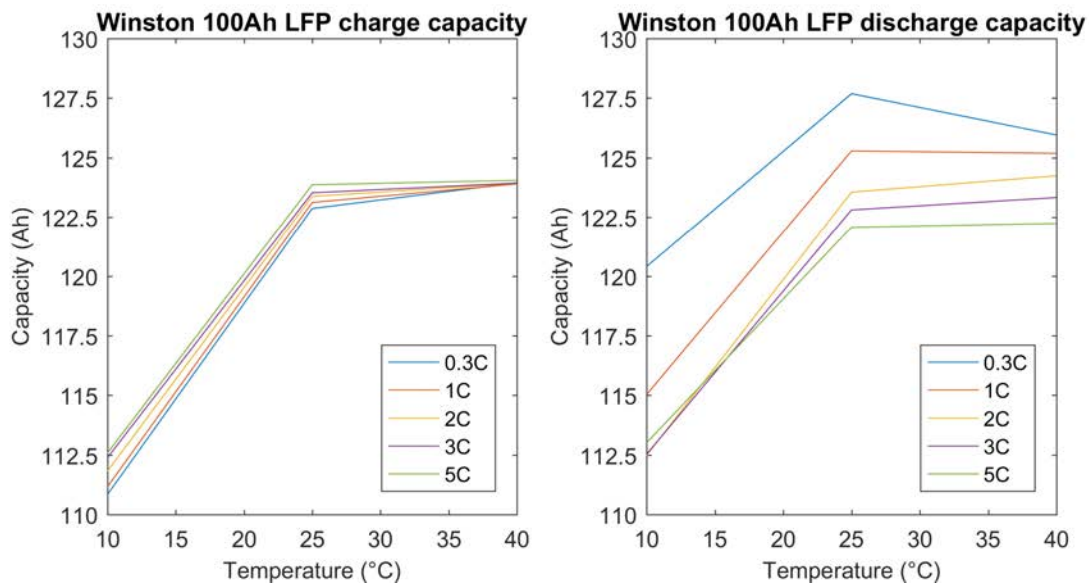


Figure 4.3: Determined charging and discharging capacity for Winston 100Ah cell

Secondly, we performed the OCV test as described in section 3.1. The difficulty of analysing the characterization results of the OCV test lies in correlating the values of the Open Circuit Voltage to the correct State of Charge values. The latter have to be calculated with reference to the discharge/charge capacity value, as obtained and measured during the Capacity test. The resulting OCV-SoC relationship is shown in

Table 4.1: Capacity of Toshiba LTO (Ah)

	10 degC	25 degC	40 degC
0.3C	17.8	19.6	20.9
1C	17.7	19.6	20.9
2C	17.6	19.7	20.9
3C	17.7	19.8	20.9
5C	17.8	19.9	21.3

Table 4.2: Capacity of Winston LFP (Ah)

	10 degC	25 degC	40 degC
0.2C	110.8	122.9	123.9
0.5C	111.2	123.1	123.9
1C	111.8	123.4	123.9
1.5C	112.4	123.5	123.9
2C	112.6	123.9	124.0

figure 4.4 for both chemistries. The most advanced analysis is needed for the analyses of the HPPC test. The main information extracted from the HPPC test depends on the topology of the selected electrical model. In our case this is the internal resistance R_0 , polarization resistance R_{th} and the time constant τ of the first order model, as described in 4.1.1). The method used during the HPPC analysis for the calculation of the parameters consists of combining the model equation (equations 4.1 and 4.2 with the Least Square Fitting method. This method then calculates the relevant set of parameters by finding the best-fitting curve to the set of measured voltage points by minimizing the sum of the squares of the offsets of the points from the curve. This procedure is performed for pulses of varying C-rates and repeated at different SoC levels, resulting in a set of model parameters related to different C-rates and SoC. Finally, in order to address the variation of the parameters at different temperatures the whole characterization procedure is repeated at different temperatures, as mentioned before. In figures 4.5 and 4.6 the obtained model parameters at 25°C can be observed for respectively the Toshiba 20Ah cell and the Winston 100Ah cell. Figures 4.7 to 4.12 show the discharge ohmic resistance in greater detail at the varying tested temperatures for both the Toshiba and Winston cells.

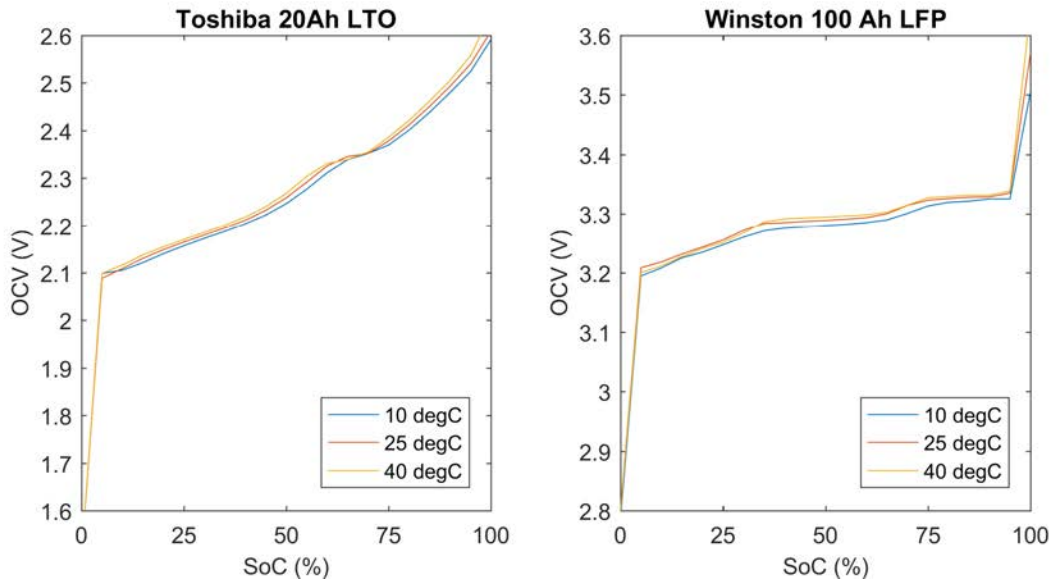
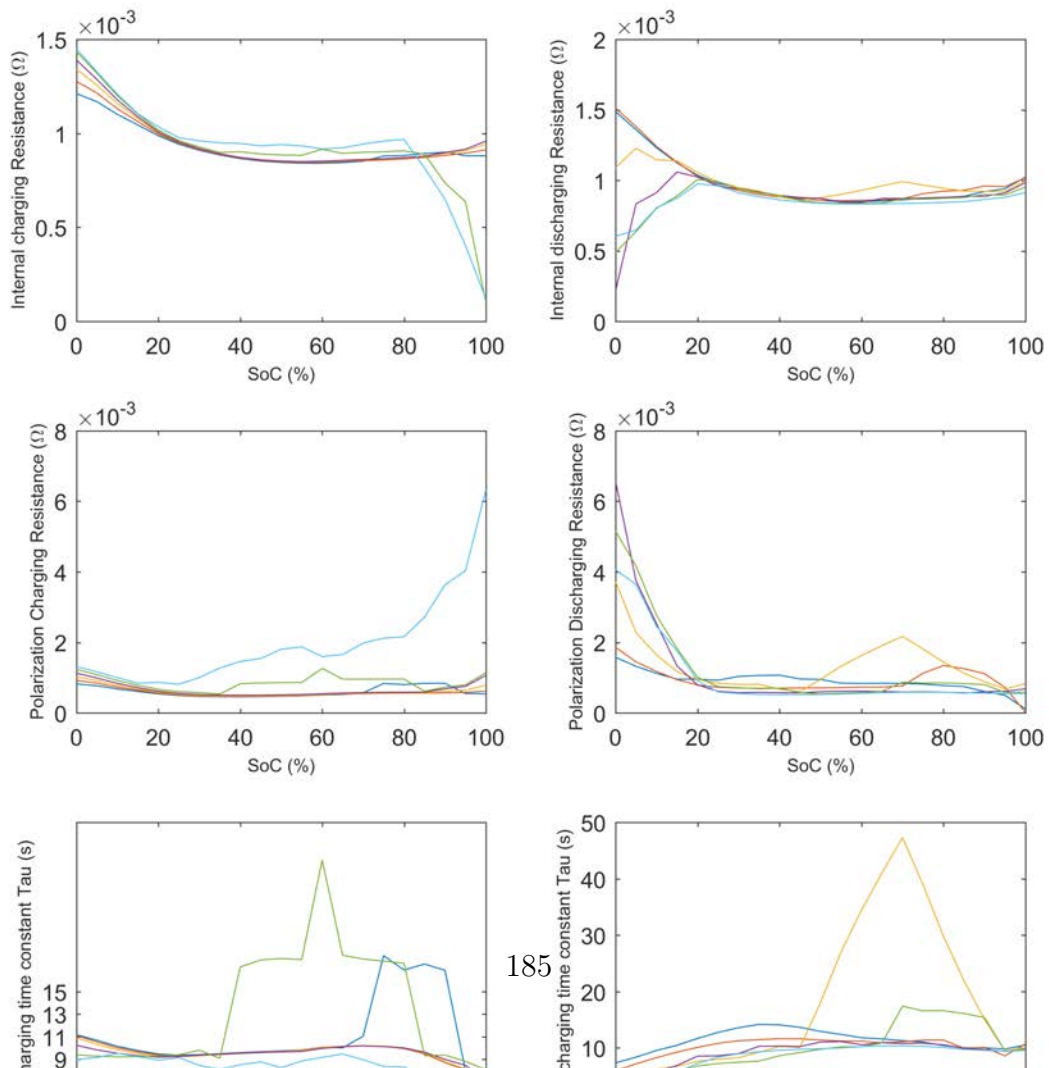


Figure 4.4: Determined OCV-SoC curves at different temperatures



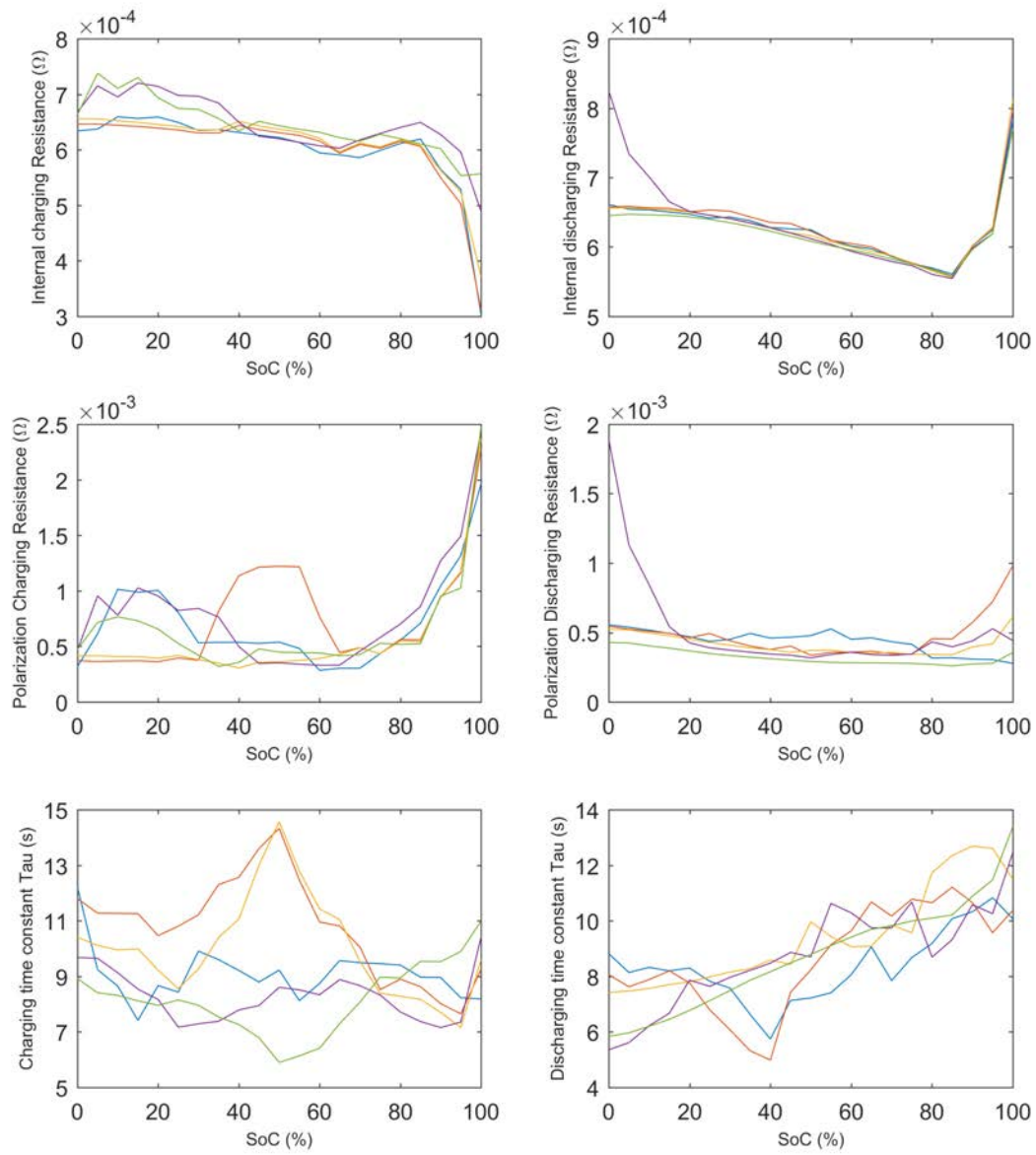


Figure 4.6: Determined parameters for Winston 100Ah LFP cell at 25°C

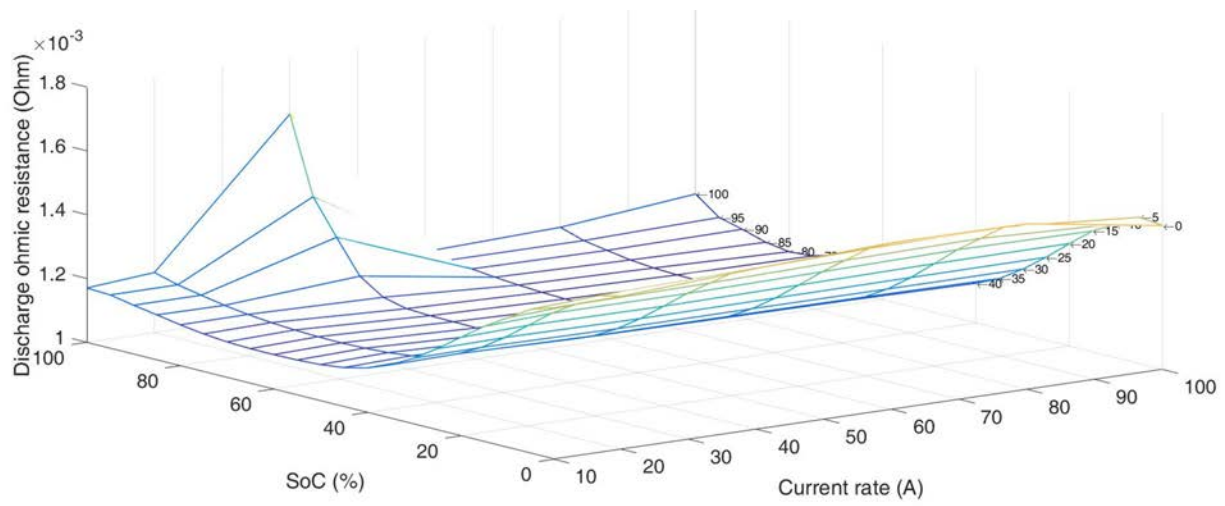


Figure 4.7: Discharge Ohmic Resistance for Toshiba 20Ah cell at 10°C

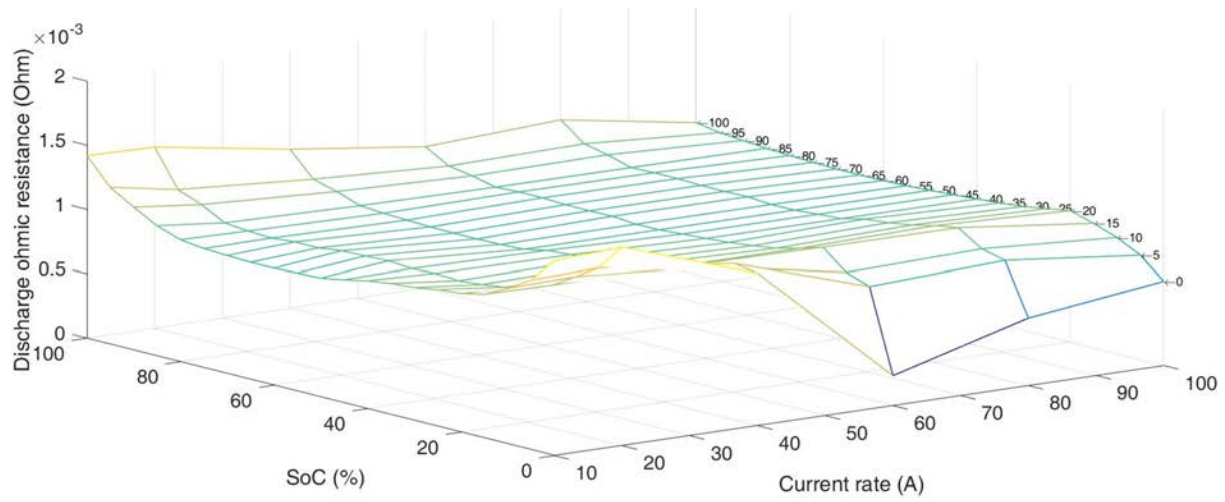


Figure 4.8: Discharge Ohmic Resistance for Toshiba 20Ah cell at 25°C

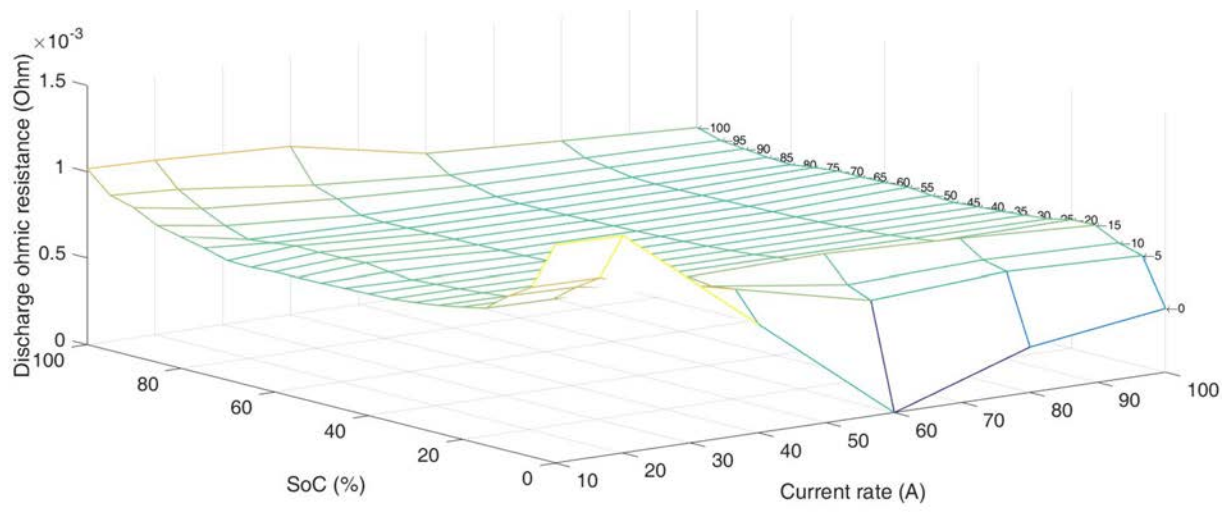


Figure 4.9: Discharge Ohmic Resistance for Toshiba 20Ah cell at 40°C

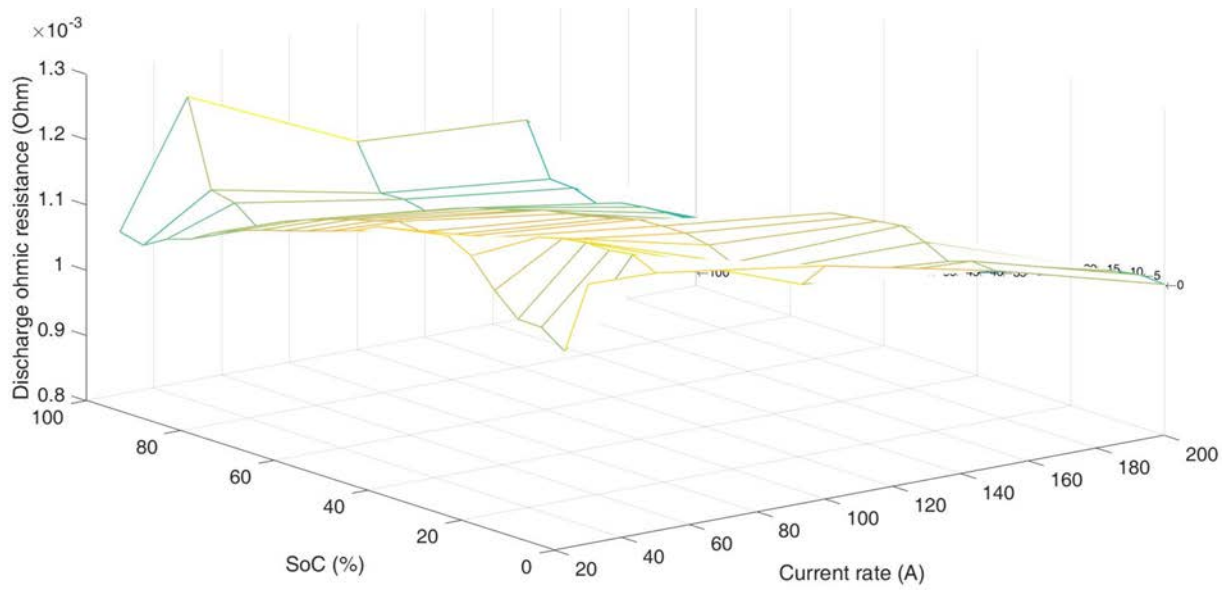


Figure 4.10: Discharge Ohmic Resistance for Winston 100Ah cell at 10°C

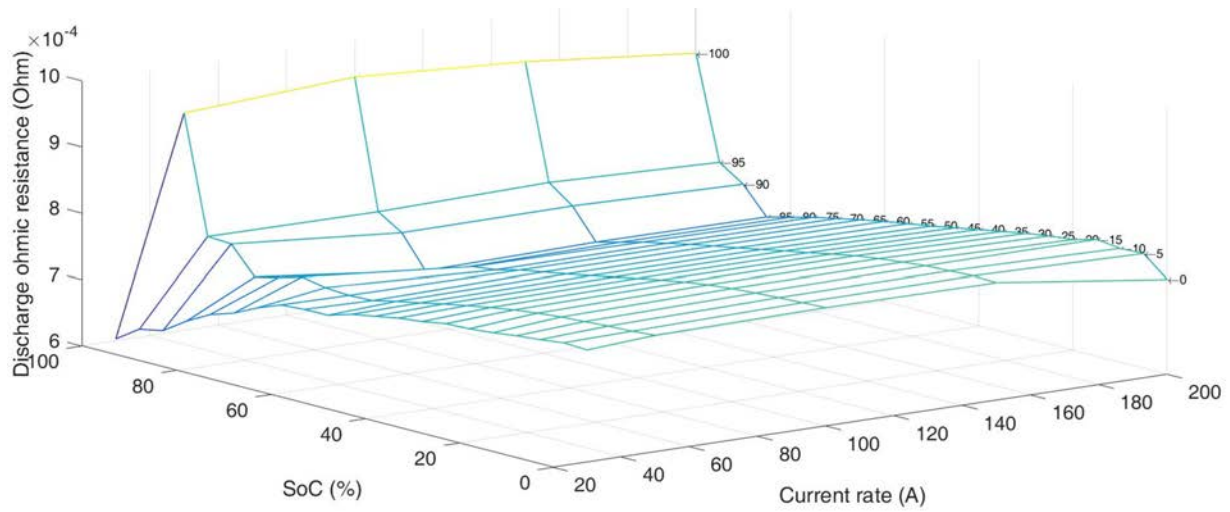


Figure 4.11: Discharge Ohmic Resistance for Winston 100Ah cell at 25°C

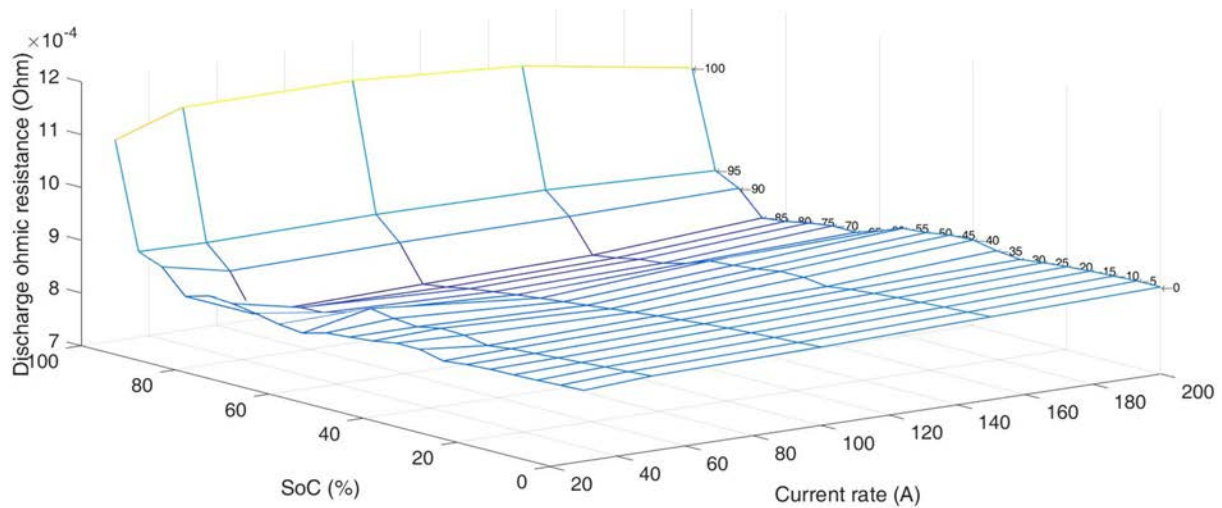


Figure 4.12: Discharge Ohmic Resistance for Winston 100Ah cell at 40°C

4.1.3 SoC estimation

Generally, State of Charge (SoC) is defined as the ratio between the remaining charge of the battery and its total possible charge. In other words, the ratio between the current capacity (Q) and the nominal capacity (Q_n) [196]. The nominal capacity is defined by the manufacturer of the battery and can be found in the data sheet. However, the real nominal capacity of a battery may vary from this defined capacity. Hence the need to

perform a capacity test (see section 3.1). We define the SoC as follows:

$$SoC(t) = \frac{Q(t)}{Q_n} \quad (4.3)$$

Currently there are various methods to estimate SoC, all with their individual advantages and disadvantages. In the literature these methods are often classified according to methodology. Even though different classifications are proposed in the literature, the most common classification allows division into four categories [137] [216].

1. Direct measurements : estimation is based on direct measurements of physical properties of the battery, generally impedance or voltage.
2. Book-keeping estimation : estimation is based on measuring discharging/charging current, which is used as input to calculate the gained/used charge.
3. Adaptive models : estimation is automatically adjusted for different conditions.
4. Hybrid methods : estimation is based on a combination between different methods allowing a globally better performance.

For the electrical modelling performed in WP3 of LBATTS two SoC estimation methods have been selected: Coulomb Counting and Extended Kalman Filter. Both methods will be discussed briefly in sections 4.1.3 and 4.1.3 respectively.

SoC estimation methods	
Direct Measurements	Discharge Method Open Circuit Voltage Method Impedance Measurement
Book keeping estimation	Coulomb Counting method Modified Coulomb Counting method
Adaptive models	Kalman filters Artificial Neural Networks Fuzzy Logic Sliding Mode Observer Least squares
Hybrid methods	Combinations of the above

Figure 4.13: State of charge estimation methods divided into four categories

Coulomb Counting

Coulomb Counting, sometimes also referred to as Ah counting method, relies heavily on the charging/discharging current $I(t)$. This current is used to calculate the amount of load charged or discharged to and from the battery. When an initial SoC value $SoC(t_0)$ is

given, this can be used to estimate the next SoC value with the following equation where a discharging current is negative and a charging current is positive:

$$SoC(t) = SoC(t_0) + \frac{1}{Q_n} \int_{t_0}^t I(\tau) d\tau \quad (4.4)$$

where SoC(t) is the SoC at time t, SoC (t₀) is the initial SoC of a battery, Q_n is the battery nominal capacity, and I(t) is the charging/discharging current at time t. From 4.4 it is obvious that three parameters are needed to perform coulomb counting: initial SoC(t₀), capacity Q_n(I,T) and current I(t). It should be noted that the battery capacity is influenced by temperature and current rate, therefore, the real-time battery capacity during the operation is given by a lookup table defined by the two parameters. Additionally, the battery capacity values are different during charging and discharging. Coulomb counting has two main drawbacks: (a) it requires an initial SoC value for calculation, and a fault initial SoC values can automatically induce estimation error; (b) it requires very accurate current measurement, since the errors accumulated from current measurement will also induce inaccurate SoC estimation. The magnitude of the error is dependent on sensor accuracy, current and testing times. However, the main advantages of coulomb counting are its simplicity and open loop functionality.

Extended Kalman Filter

Kalman filters have shown to be a very accurate and robust method for state of charge estimation [167] [241] [240] [6]. A big advantage of the kalman filters is that apart from estimating the SoC, they also estimate the uncertainty on this SoC estimation. Therefore the Kalman Filter was chosen as the SoC estimation method for the second SoC estimator model.

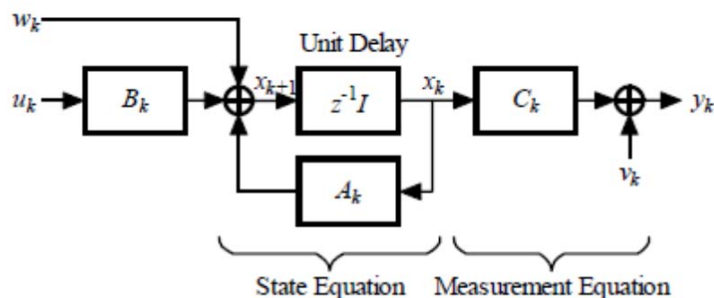


Figure 4.14: Schematic representation of Linear Discrete Time System [167]

Kalman Filter Theory In order to understand the workings of the Extended Kalman Filter SoC estimator one must start from the theory of linear Kalman filtering. In figure

4.14, a schematic representation of a linear discrete time system is shown where A_k , B_k and C_k are time-varying matrices, $z^{-1}I$ is a unit delay block, input and output of the system are respectively u_k and y_k , w_k represents the process noise and v_k represents the noise on the measurements. Finally and most importantly: x_k is the state of the system, which cannot be directly measured. Both the input u_k and the output y_k must be used to estimate the value of the system state. The schematic shown in figure 4.14 can be described by the following two equations.[167] [6]

$$x_{k+1} = A_k x_k + B_k u_k + w_k \quad (4.5)$$

$$y_k = C_k x_k + v_k \quad (4.6)$$

Equation 4.5 is called the state equation of the system, describing the system dynamics. Equation 4.6 is called the output equation, describing the output of the system as a linear combination of system states. The Kalman filter theory offers a solution to the following problem: using measured data u_k and y_k find the best estimate \hat{x}_k of the true state x_k [167]. This solution is a set of recursive equations that are widely accepted and available in the literature [241], where an over-line indicates the prior estimation and the caret indicates the posterior estimation:

$$\bar{x}_{k+1} = A_k \hat{x}_k + B_k u_k \quad (4.7)$$

$$\bar{P}_{k+1} = A_k \hat{P}_k x_k^T + Q_k \quad (4.8)$$

$$K_k = \bar{P}_{k+1} C_k^T [C_k \bar{P}_{k+1} C_k^T + R_k]^{-1} \quad (4.9)$$

$$\hat{x}_{k+1} = \bar{x}_{k+1} + K_k [y_k - \bar{y}_k] \quad (4.10)$$

$$\hat{P}_{k+1} = \bar{P}_{k+1} - K_k C_k \bar{P}_{k+1} \quad (4.11)$$

This recursive set of equations can be broken down into three steps. Firstly, in equation 4.7 and 4.8 the state of the system and the error covariance respectively are predicted for the next time step (k+1). Secondly, in equation 4.9 the Kalman Gain K_k is calculated. Thirdly, this Kalman gain acts as a weighted correction factor in equation 4.10 and 4.11. The Kalman gain determines how trustworthy the prior state estimate and error covariance estimate are. When the prior state estimate and error covariance estimate are very trustworthy, the Kalman gain will be small and thus result in a small update of the prior estimates in equation 4.10 and 4.11. If the uncertainty on the prior estimates is large, the Kalman gain will be large thus resulting in a large update of the prior estimates.

Now, in order to use Kalman filtering theory for SoC estimation one must realise that a battery is not a linear system. Thus, a linearization process is performed at every time step to approximate the non linear system with a linear system. This approximated linear system can then be used to perform the Kalman filter on, which is referred to as the Extended Kalman Filter [241].

Extended Kalman Filter for SoC estimation The first step to implement the Extended Kalman Filter for SoC estimation is to model the non linear battery by a state equation and an output equation as explained in section 4.1.3.

$$x_{k+1} = f(x_k, u_k) + w_k \quad (4.12)$$

$$y_k = g(x_k, u_k) + v_k \quad (4.13)$$

Where x_k , y_k , w_k , v_k and u_k are defined as in section 4.1.3. However, $f()$ and $g()$ are functions that describe the battery behaviour depending on the used battery model. As mentioned in section 4.1.1, a first order battery model is used in this project. The electrical equivalent circuit of this battery model is shown in figure 4.1. As mentioned before in section 4.1.3 a linearization process (first order Taylor series expansion) is performed at every time step to approximate the non linear system with a linear system, which allows to rewrite the model equations [241]:

$$x_{k+1} = A_k x_k + B_k u_k + w_k \quad (4.14)$$

$$y_k = C_k x_k + D_k u_k + v_k \quad (4.15)$$

Where the state of the battery at time step k is taken to be:

$$x_k = \begin{pmatrix} SoC(k) \\ U_{th}(k) \end{pmatrix} \quad (4.16)$$

Where $U_{th}(k)$ is the voltage over the RC block in the first order model at time step k (see figure 4.1). The voltage across this RC block at time step k are defined to be [227]:

$$U_{th}(k) = I_{bat}(k) R_{th} (1 - e^{-\frac{T}{\tau_{th}}}) \quad (4.17)$$

where T is the sample period, τ_{th} is the time constant for the RC block, R_{th} is the concentration polarization resistance. With the knowledge of equations 4.16,4.17 and the definition of SoC (equation 4.3) it is possible to rewrite the state equation 4.14 and the output equation 4.15 as follows.

$$\begin{pmatrix} SoC(k+1) \\ U_{th}(k+1) \end{pmatrix} = \begin{pmatrix} 1 & 0 \\ 0 & e^{-\frac{T}{\tau_{th}}} \end{pmatrix} \cdot \begin{pmatrix} SoC(k) \\ U_{th}(k) \end{pmatrix} + \begin{pmatrix} -\frac{\eta T}{Q_n} \\ R_{th}(1 - e^{-\frac{T}{\tau_{th}}}) \end{pmatrix} I_{bat}(k) \quad (4.18)$$

$$U_{bat} = U_{OC}(SoC(k)) - U_{th}(k) - R_0 I_{bat}(k) + v_k \quad (4.19)$$

where η is the coulombic efficiency of the battery and Q_n is the nominal capacity. These equations mean that the matrices A_k , B_k , C_k and D_k are defined as follows:

$$A_k = \begin{pmatrix} 1 & 0 \\ 0 & e^{-\frac{T}{\tau_{th}}} \end{pmatrix} \quad (4.20)$$

$$B_k = \begin{pmatrix} -\frac{\eta T}{Q_n} \\ R_{th}(1 - e^{-\frac{T}{\tau_{th}}}) \end{pmatrix} \quad (4.21)$$

$$C_k = (U_{OC}(SoC(k)) \quad -1) \quad (4.22)$$

$$D_k = -R_0(k) \quad (4.23)$$

Table 4.3: Inputs and outputs required for EKF implementation

EKF Output	
Estimated SoC	Error Covariance
EKF Input	
OCV	Current, I
Ohmic Resistance, R_0	Sample time, Ts
Resistance, R_{th}	Coulombic efficiency, η
Time constant, τ_{th}	Measured terminal voltage, V_{meas}
Capacity, Q	Simulated terminal voltage, V_{sim}
Error Coveriance	SoC

Implementation of EKF in electrical model The EKF function requires twelve inputs and generates two output values, which are listed in the Table 4.3.

4.2 Thermal battery model

The thermal battery model relies on both the electrical battery model and the energy balance equation. The former provides both the state of charge and the electric battery parameters to the thermal model. While the latter, the energy balance equation, is used to calculate the dynamic temperature response of the cell as follows:

$$mC_p \frac{\delta T}{\delta t} = q_g - q_{conv} \quad (4.24)$$

where m is the mass of the cell (kg), C_p is the specific heat of cell (J/kg.K), T is the cell temperature (K), q_g is the internal generation heat (W), and q_{conv} is the convective flux with surrounding air (W). The internal heat generation rate depends on the thermodynamic properties of the reactions inside a cell, the potential-current characteristics of the cell, and the rates of charge and dis-charge. In this work package, the heat sources can be distinguished in two terms: a) the ohmic heat q_{ohmic} generated by the internal resistances given by equation 4.26 and b) the reversible heat q_{rev} resulting from the entropy heat given by equation 4.27 [?]. The entropic heat coefficient, $\frac{\delta V_{OCV}}{\delta T}$, is determined experimentally using the data gathered from the OCV tests described in section 4.1.2. At every SoC value the corresponding OCV value is taken at varying temperatures (10°C, 25 °C, 40°C) where-after a simple linear regression is applied through the OCV points. The slope of the fitted line is the entropic heat coefficient. The resulting entropic heat coefficient for both Toshiba and Winston cells is shown in figure 4.15. It should be noted that in ideal circumstances the ambient temperature should vary during testing at a fixed SoC to determine the entropic heat coefficient [?]. However, since we used OCV-test values, we are in essence using values acquired with a varying SoC at a fixed temperature. However, since the contribution of the reversible heat is rather small

compared to the ohmic heat, it was deemed sufficient [22]. Finally, the heat loss q_{conv} is given by the convection heat with surrounding air, as defined in equation 4.28 where S is the cross-section area (m^2), and h is the convective heat transfer coefficient (W/m^2).

$$q_g = q_{ohmic} + q_{rev} \quad (4.25)$$

$$q_{ohmic} = R_{int} \cdot I^2 + R_{th} \cdot I^2 \quad (4.26)$$

$$q_{rev} = -T \cdot I \cdot \frac{\delta V_{OCV}}{\delta T} \quad (4.27)$$

$$q_{conv} = h \cdot S \cdot (T_{amb} - T) \quad (4.28)$$

Hereafter, we can solve equation 4.24 for $\frac{\delta T}{\delta t}$ to estimate the cell surface temperature variation over time as follows:

$$\frac{\delta T}{\delta t} = \frac{q_g - q_{conv}}{mC_p} \quad (4.29)$$

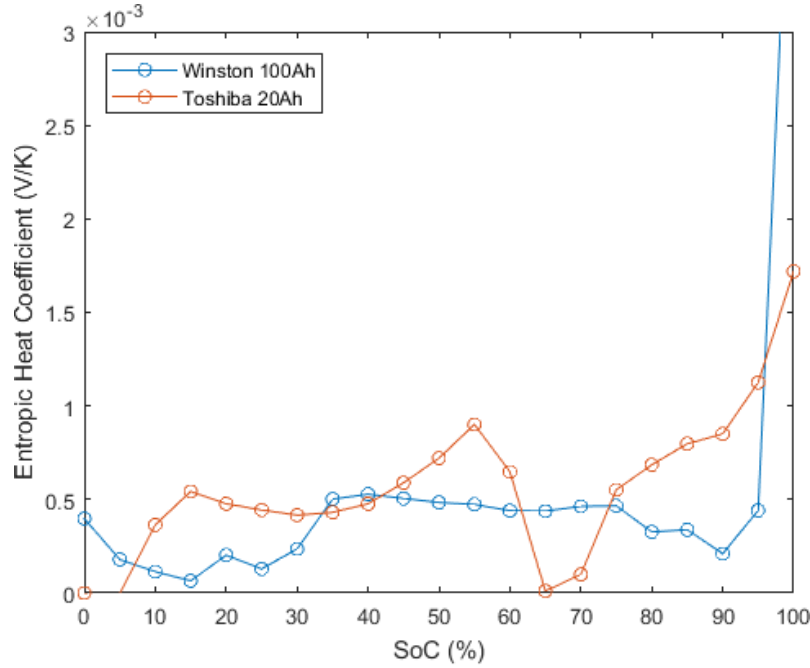


Figure 4.15: Experimentally defined entropic heat coefficient for Winston and Toshiba cells

4.2.1 Thermal characterization and thermal model calibration

In order to estimate the surface temperature of the given cells with equation 4.24, seven parameters are required: width, length, thickness, surface area, weight, specific heat capacity and convective heat transfer coefficient. The dimensions and the weight of the

cells could easily be retrieved from their respective data sheets. However, the specific heat capacity (C_p) and the convective heat transfer coefficient (h) had to be determined experimentally. This was done using the parameter estimation tool on the electro-thermal model in Simulink. Given the measured voltage, current and surface temperature during a test cycle the electro-thermal model outputs an estimated surface temperature based on equation 4.24. However, since both C_p and h are still initial guesses, the estimated cell temperature does not yet approximate the measured cell temperature during the test cycle. The parameter estimation tool in Simulink will now tune the model parameters (C_p and h) to obtain a simulated cell temperature that tracks the measured temperature as good as possible. To do so, the solver minimizes the cost function or estimation error ($e(t)$), a measure of the difference between the simulated and measured responses. For this project we used the sum squared error as cost function given by equation 4.30. The obtained thermal model parameters for both the Toshiba 20Ah and Winston 100Ah cells are shown in table 4.4.

It has to be noted that both C_p and h for the Winston 100Ah cell are exceptionally high. This can be explained by the plastic casing around the cells: since the surface temperature during testing was measured on the surface of this plastic casing, C_p and h not only represent the cell itself but also the casing. However, the argument can be made that this is irrelevant for the project since the cell can only be used with the casing. Thus, the model still provides a good estimate of the cell surface temperature all be it with thermal parameters that have a different physical interpretation.

$$F(x) = \sum_{t=0}^{t_N} e(t)^2 \quad (4.30)$$

Table 4.4: Thermal characteristics of tested cells

	Toshiba 20Ah LTO	Winston 100Ah LFP
Width (mm)	116	143
Length (mm)	106	218
Thickness (mm)	22	67
Surface Area (m^2)	0.0282	0.0312
Weight (kg)	0.515	3.300
Cp (J/kg.K)	1819.3	7317,7
h (W/m^2)	13.927	193.25

Chapter 5

Simulations and discussion

5.1 Dynamic Discharge Pulse Test

The performed test to validate the electro-thermal model is the Dynamic Discharge Pulse test. As the name implies, this test has a more dynamic profile thus poses a great opportunity to evaluate the accuracy of the electrical model. An example of a full DDP test profile is shown in figure 5.1. It has to be noted that this is an example, as the current of the pulses has to be scaled to the rated capacity of each specific cell. The DDP test requires the battery to be fully charged (100% SoC). Upon starting the test the battery is first fully charged with a constant current constant voltage (CCCV) charge cycle to ensure the battery is fully charged when starting the DDP test, as can be seen in the first 500 seconds of the profile in figure 5.1. Hereafter the battery tester idles for 30 minutes to allow the battery to relax before starting the DDP test.

A detail of seven DDP cycles is shown in figure 5.2. A DDP cycle starts with a discharge at 1.6C for 10 seconds, after which a discharge at 0.4C is performed for 20 seconds. Hereafter the battery is charged at 0.8C for 5 seconds, after which the test iddles (0C) for 25 seconds. This cycle is continued until the battery terminal voltage reaches 3V. In other words, the battery is completely discharged from 100% SoC to 0% SoC using these DDP cycles.

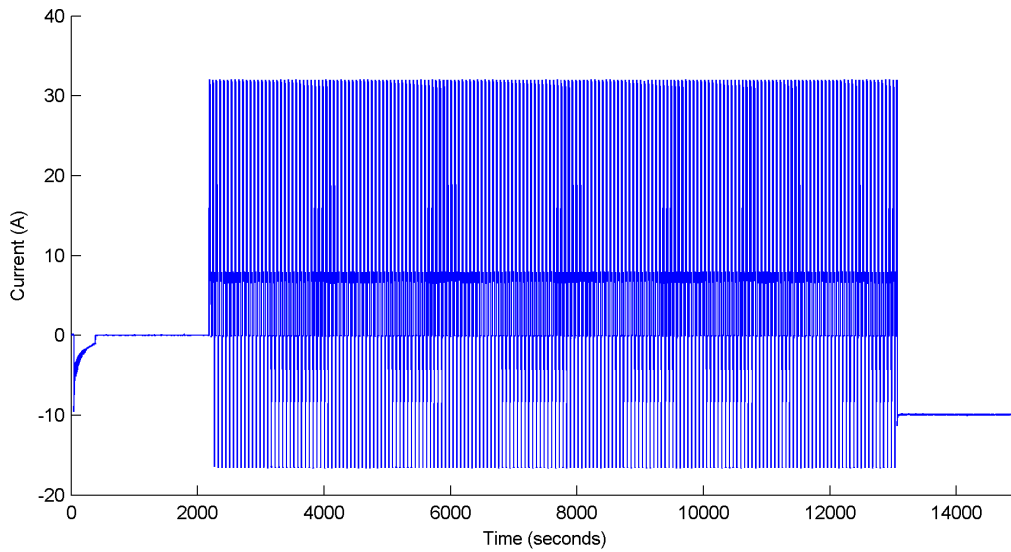


Figure 5.1: Example of a complete DDPT current profile

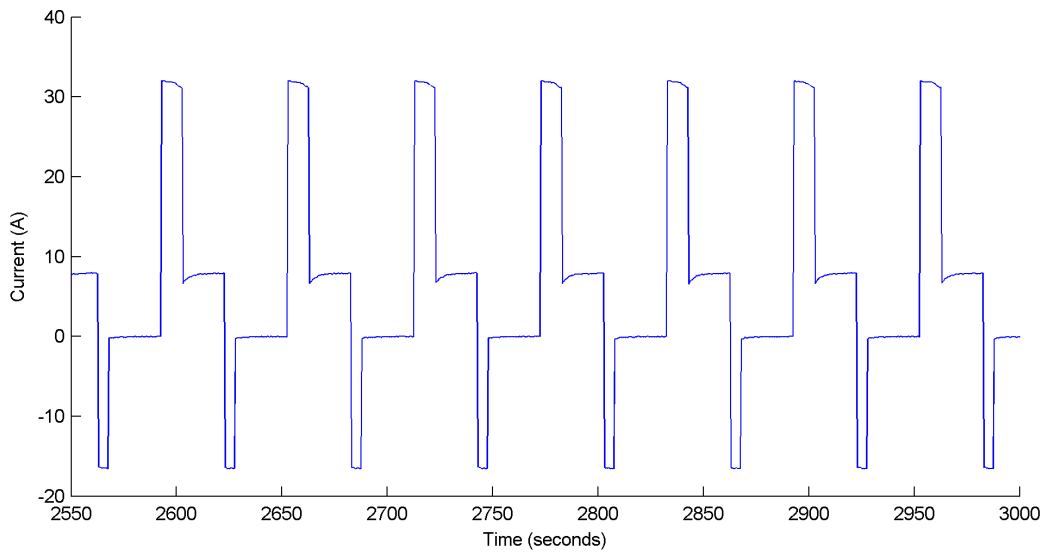


Figure 5.2: Detail of seven DDP cycles

5.2 Simulation results

The previously described DDP test load current was applied to all four tested cells: two Toshiba cells and two Winston cells. The responding terminal voltage and cell surface

temperature were measured during this load profile. Hereafter, in order to validate the electro-thermal model, the DDPT load profile was used as an input for the electro-thermal model. The response of the model, the simulated terminal voltage and the simulated surface temperature, are then compared to the measured terminal voltage and temperature respectively. This validation process is repeated for the two tested cells of both chemistries, at varying ambient temperatures and with both EKF and CC as the SoC estimator in the electrical model. In order to provide a clear overview of simulation accuracies, the maximum electrical- and thermal- simulation errors for all cases are provided in tables 5.1 to 5.4. More detailed simulation results of both chemistries at varying temperatures, using the EKF SoC estimator, are shown in figures 5.3 to 5.20. The maximum electrical error represents the maximum relative error on the simulated terminal voltage compared to the measured terminal voltage. The maximum thermal error represents the maximum deviation of the simulated cell temperature to the measured cell temperature in celsius. Note that the maximum electrical error is given for two SoC windows: 100% to 0% and 90% to 10%.

From tables 5.1 to 5.4 it is observed that, regarding the electrical modelling, using the EKF as an SoC estimator increases overall accuracy. While the EKF improvement on the simulated voltage accuracy is more noticeable at the top and bottom 10% SoC window, it also improves the voltage accuracy in the 90%-10% SoC window. It is also observed that the electrical model for the Toshiba cells is overall more accurate than for the Winston cells. This is specific to the different chemistry of both cells: the Winston LFP cell has a very flat OCV curve while the Toshiba LTO hasn't, as can be seen in figure 4.4. From a thermal standpoint the Toshiba cells also provide a more accurate simulation due to the plastic casing surrounding the Winston cells. This casing made accurate temperature measurements and simulations difficult on the Winston cells.

Table 5.1: Maximum electrical- and thermal- simulation error for Winston cells using EKF

Winston 100 Ah (LFP)						
Ambient Temperature	Cell 1			Cell 2		
	Electrical	Thermal	Thermal	Electrical	Thermal	Thermal
10 °C	100% >SoC >0% <2.8 %	90% >SoC >10% <3.8 %	<1.43 °C	100% >SoC >0% <2.4 %	90% >SoC >10% <2.05 %	<1.9 °C
25 °C	<3.9 %	<1.1 %	<1.12 °C	<1.3 %	<0.85 %	<1.85 °C
40 °C	<1.28 %	<0.5 %	<1.25 °C	<1.1 %	<0.9 %	<1.45 °C

Table 5.2: Maximum electrical- and thermal- simulation error for Toshiba cells using EKF

Toshiba 20Ah (LTO)						
Ambient Temperature	Cell 5			Cell 7		
	Electrical	Thermal	Thermal	Electrical	Thermal	Thermal
10 °C	100% >SoC >0% <2.76 %	90% >SoC >10% <1.1 %	<0.74 °C	100% >SoC >0% <1.51 %	90% >SoC >10% <0.68 %	<0.91 °C
25 °C	<3.1 %	<0.73 %	<0.99 °C	<3 %	<0.92%	<0.79 °C
40 °C	<1.04%	<0.4 %	<1.27 °C	<1.32 %	<1.07 %	<1.37°C

Table 5.3: Maximum electrical- and thermal- simulation error for Winston cells using CC

Winston 100 Ah (LFP)						
Ambient Temperature	Cell 1			Cell 2		
	Electrical	Thermal	Thermal	Electrical	Electrical	Thermal
10 °C	100% >SoC >0% <6.7 %	90% >SoC >10% <5.5 %	<1.43 °C	100% >SoC >0% <6.5 %	90% >SoC >10% <5.4 %	<1.88 °C
25 °C	<5.6 %	<2.95 %	<1.0 °C	<6.0 %	<3.25 %	<1.54 °C
40 °C	<6.8 %	<1.6 %	<1.24 °C	<6.7 %	<1.46%	<1.23 °C

Table 5.4: Maximum electrical- and thermal- simulation error for Toshiba cells using CC

Toshiba 20Ah (LTO)						
Ambient Temperature	Cell 5			Cell 7		
	Electrical	Thermal	Thermal	Electrical	Electrical	Thermal
10 °C	100% >SoC >0% <28 %	90% >SoC >10% <2.2 %	<0.84 °C	100% >SoC >0% <28 %	90% >SoC >10% <1.72 %	<0.78 °C
25 °C	<28 %	<1.6 %	<0.98 °C C	<28 %	<1.1 %	<0.90 °C
40 °C	<26.6 %	<2%	<0.85 °C C	<26.6 %	<0.7 %	<1.41 °C

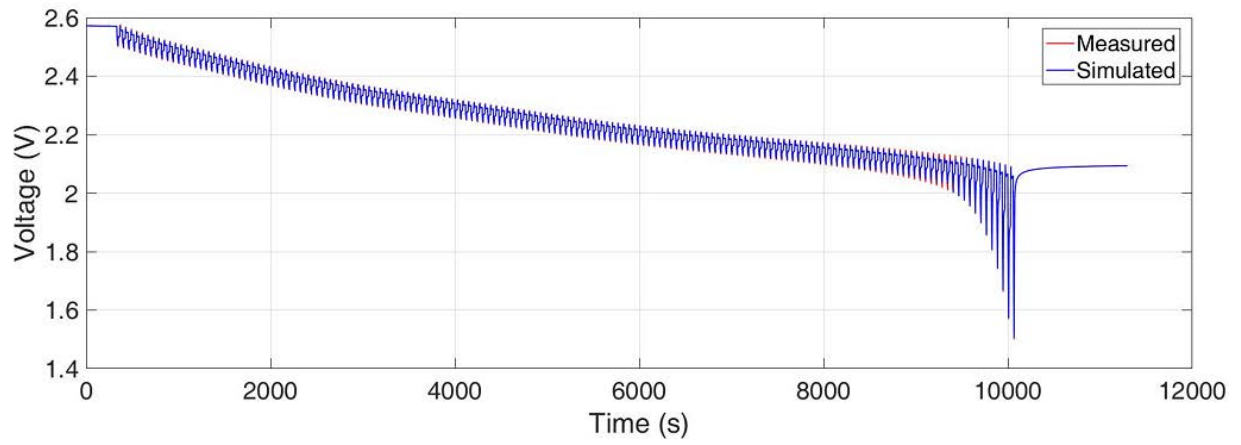


Figure 5.3: Simulated terminal voltage of Toshiba 20Ah cell at 10°C C

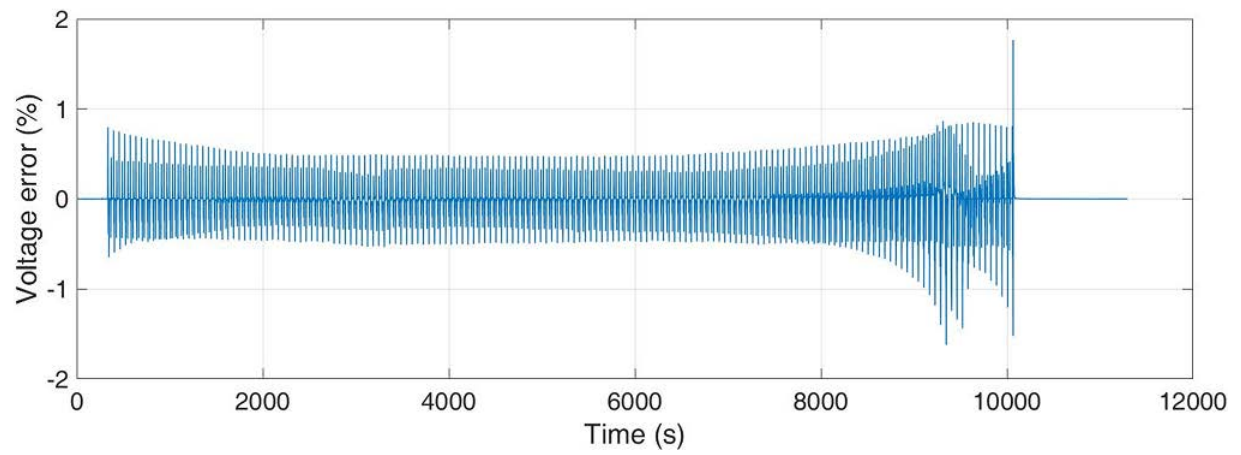


Figure 5.4: Relative error on the simulated terminal voltage of Toshiba 20Ah cell at 10°C C

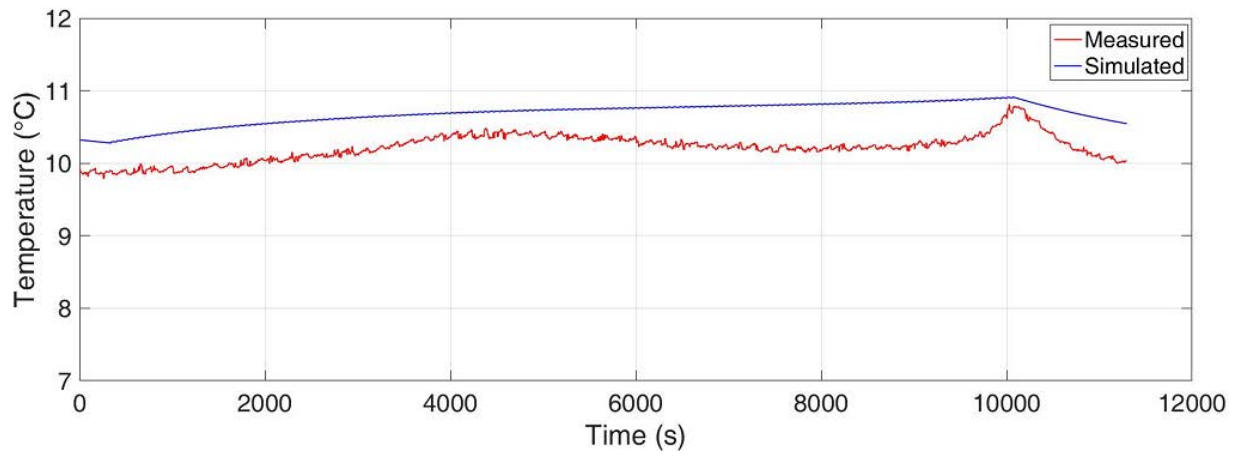


Figure 5.5: Simulated cell temperature of Toshiba 20Ah cell at 10°C C

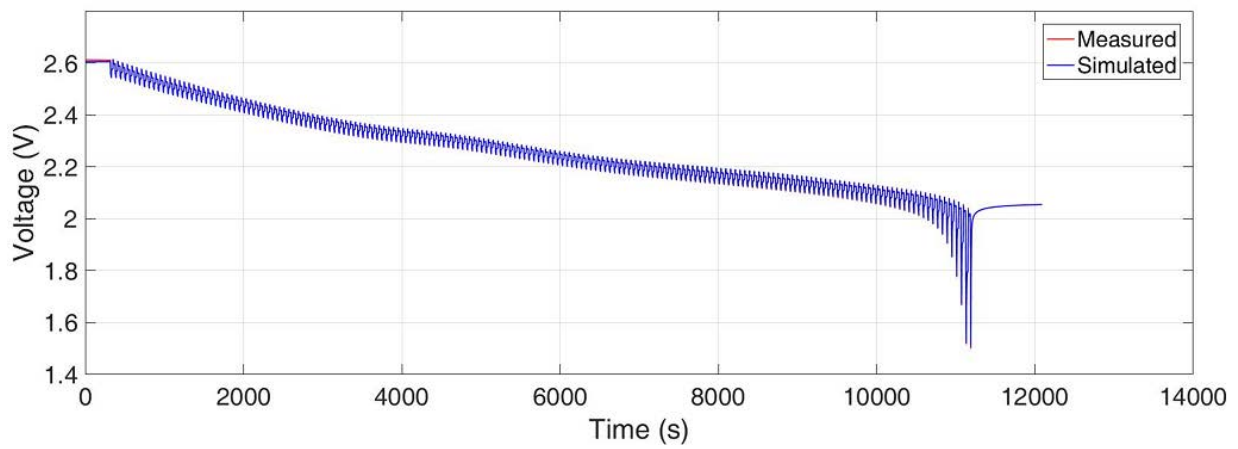


Figure 5.6: Simulated terminal voltage of Toshiba 20Ah cell at 25°C C

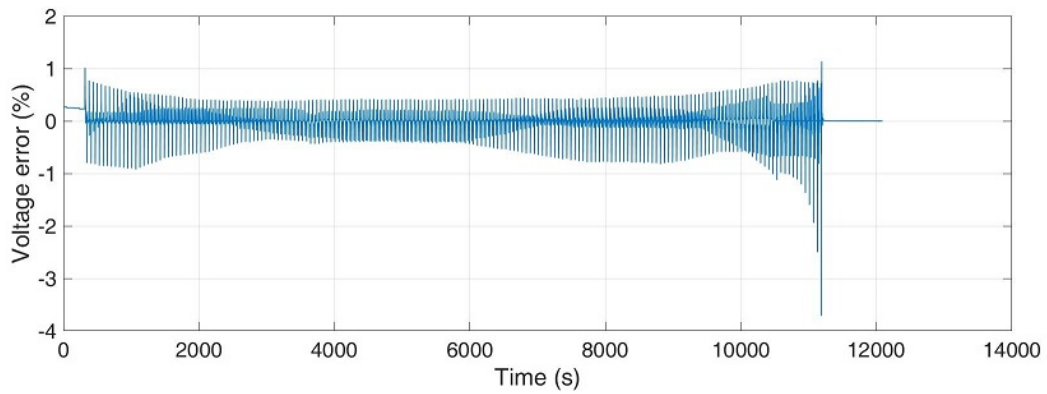


Figure 5.7: Relative error on the simulated terminal voltage of Toshiba 20Ah cell at 25°C C

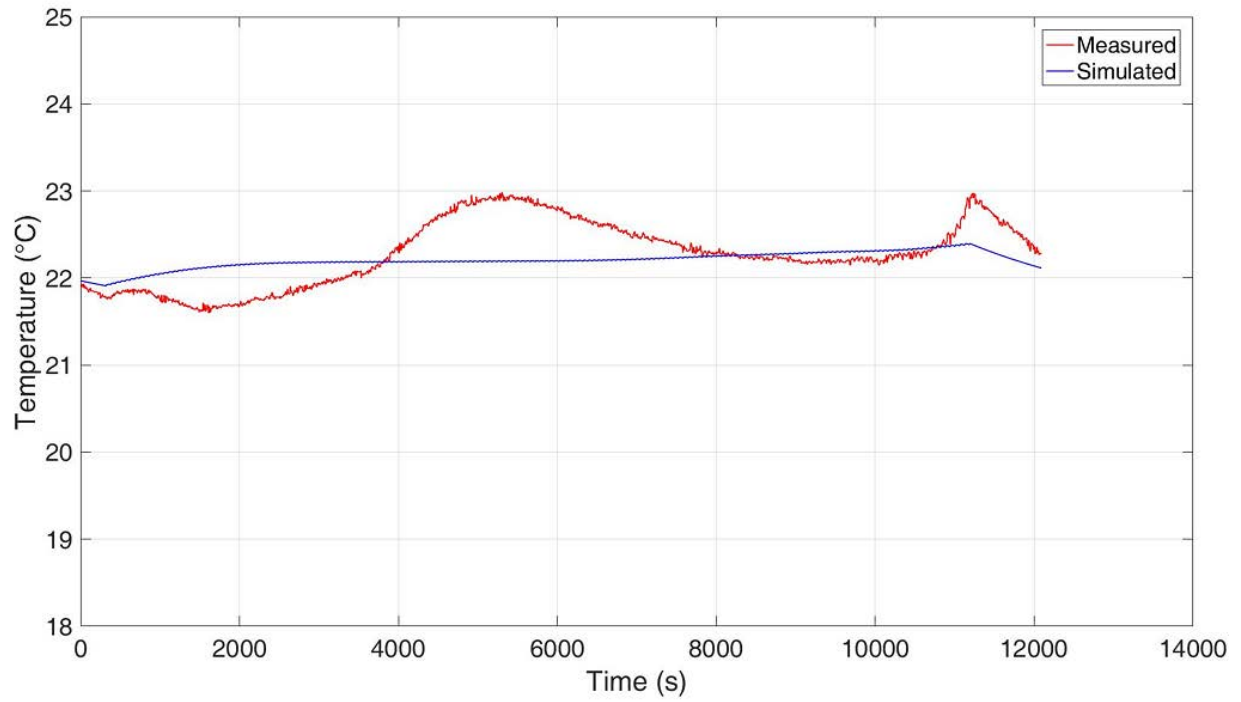


Figure 5.8: Simulated cell temperature of Toshiba 20Ah cell at 25°C C

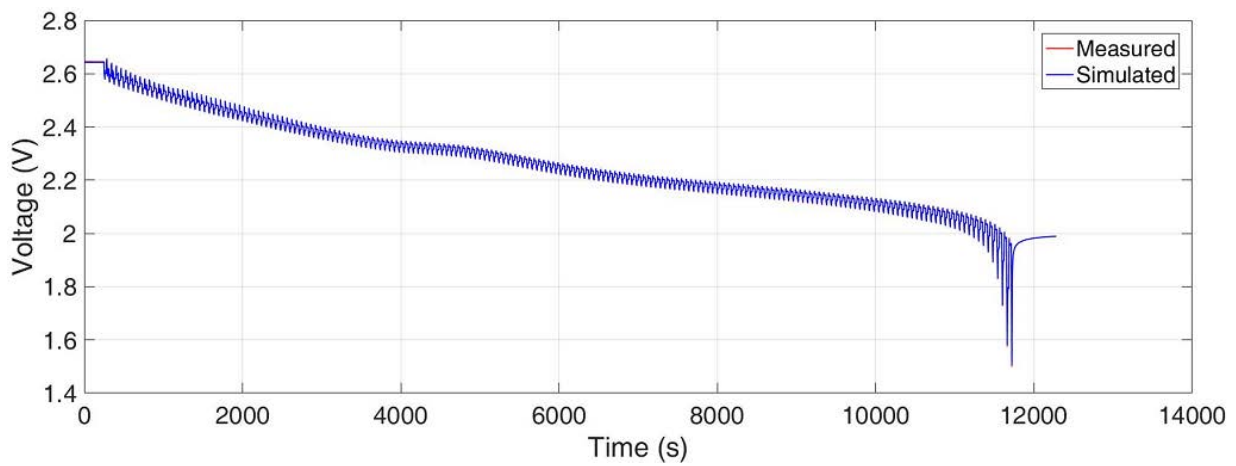


Figure 5.9: Simulated terminal voltage of Toshiba 20Ah cell at 40°C C

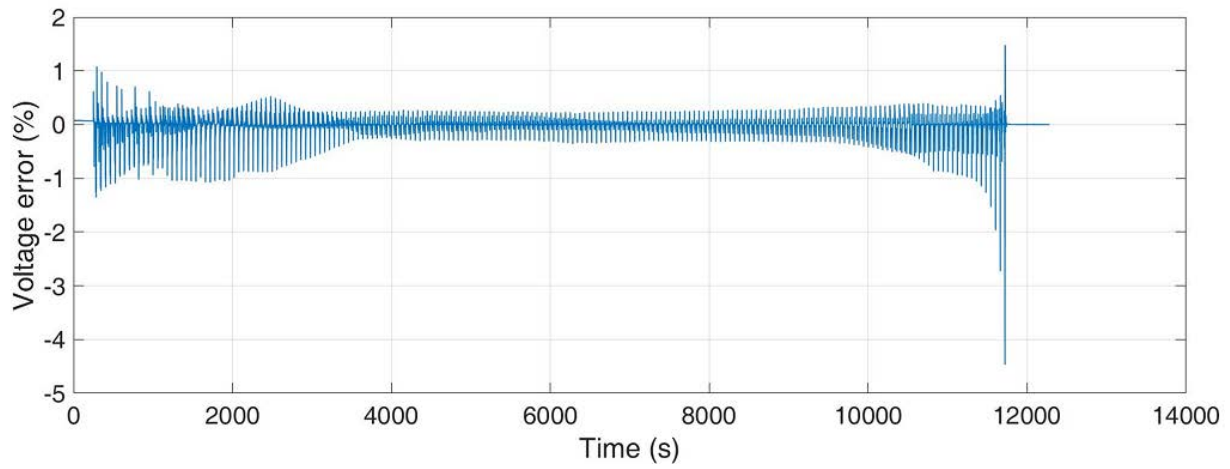


Figure 5.10: Relative error on the simulated terminal voltage of Toshiba 20Ah cell at 40°C C

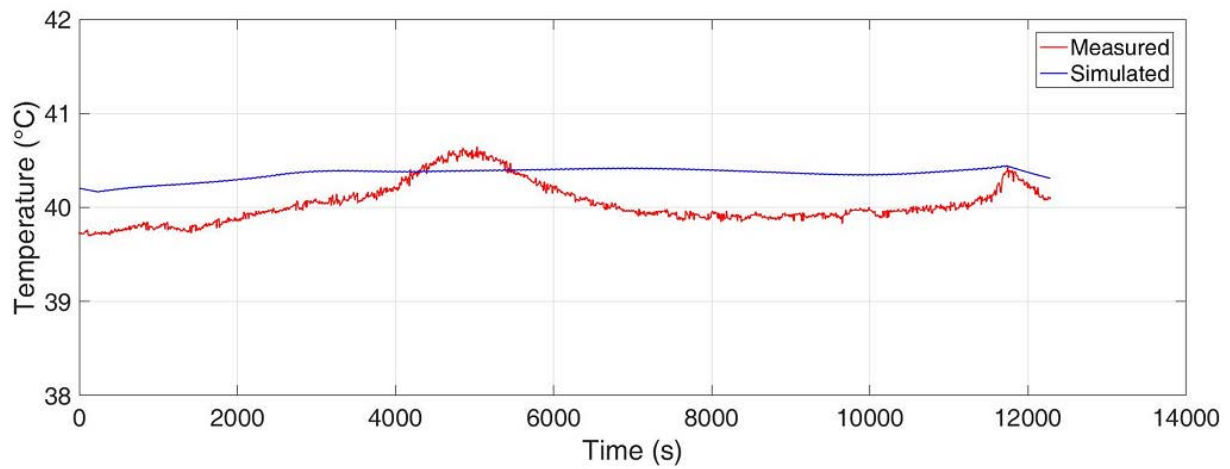


Figure 5.11: Simulated cell temperature of Toshiba 20Ah cell at 40°C C

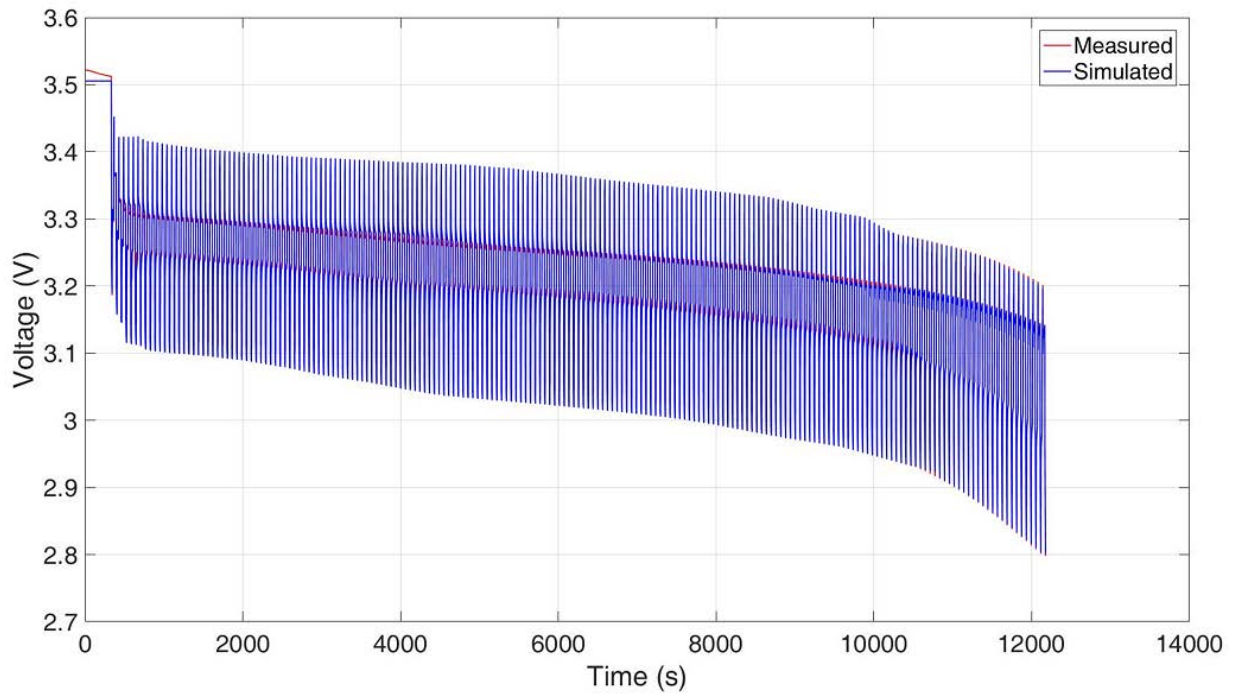


Figure 5.12: Simulated terminal voltage of Toshiba 20Ah cell at 10°C C

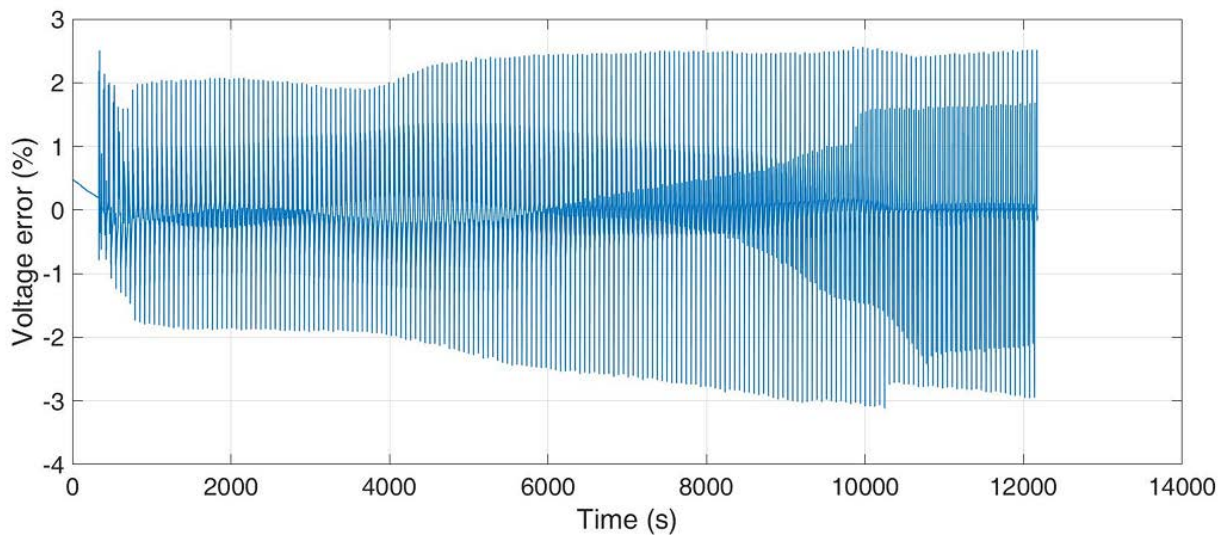


Figure 5.13: Relative error on the simulated terminal voltage of Winston 100Ah cell at 10°C C

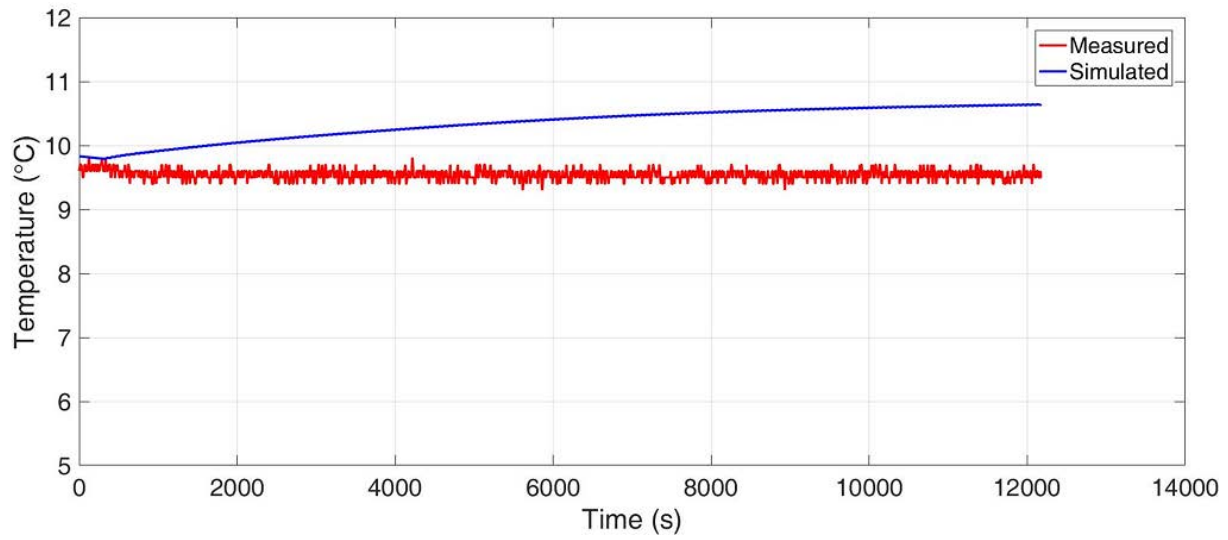


Figure 5.14: Simulated cell temperature of Winston 100Ah cell at 10°C C

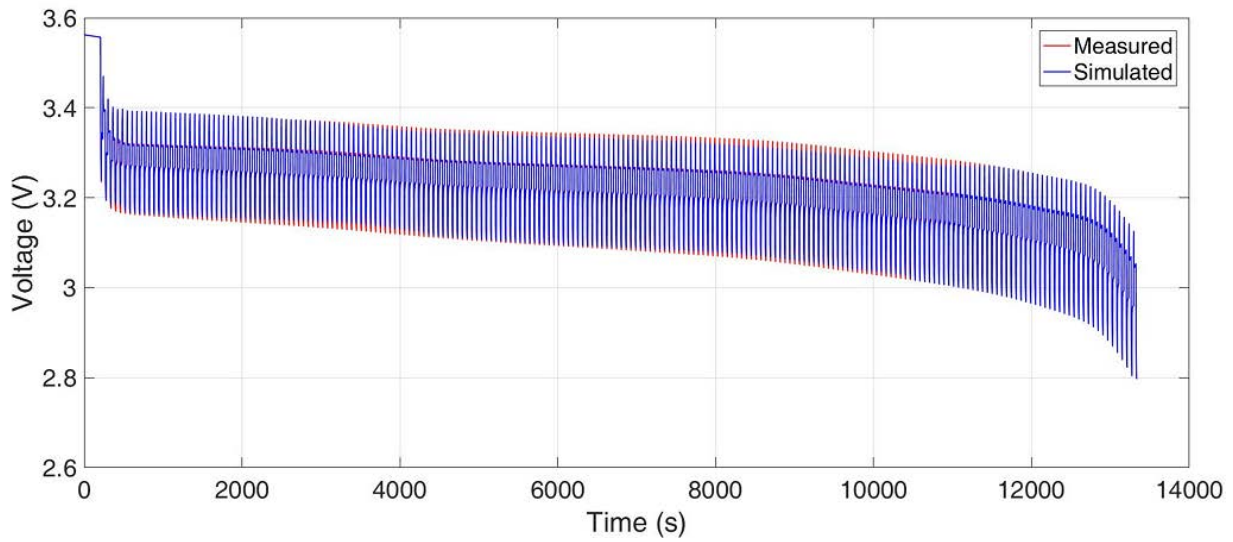


Figure 5.15: Simulated terminal voltage of Toshiba 20Ah cell at 25°C

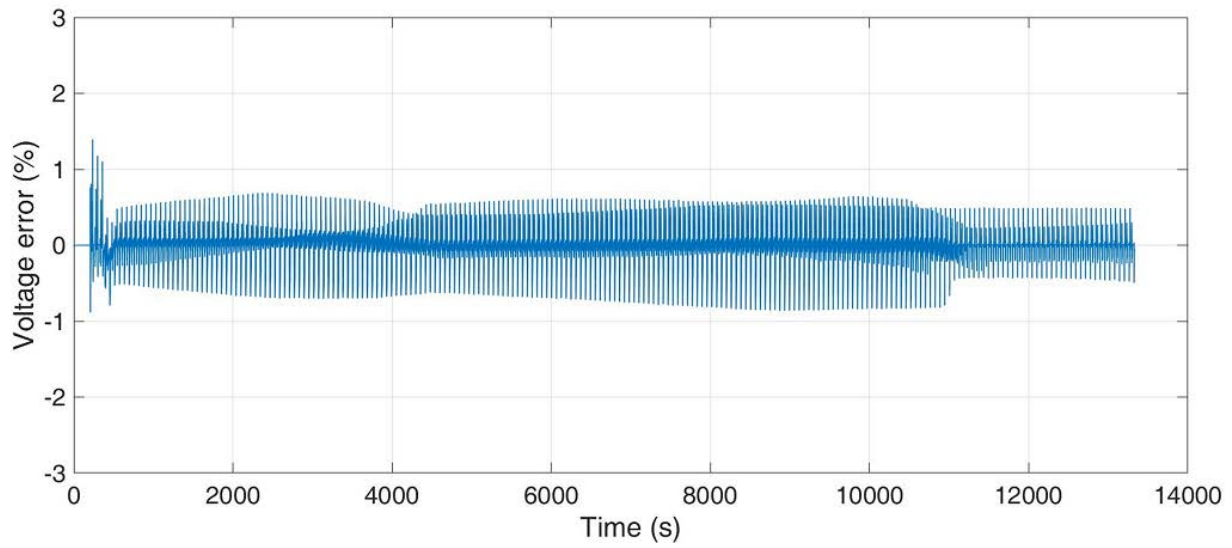


Figure 5.16: Relative error on the simulated terminal voltage of Winston 100Ah cell at 25°C

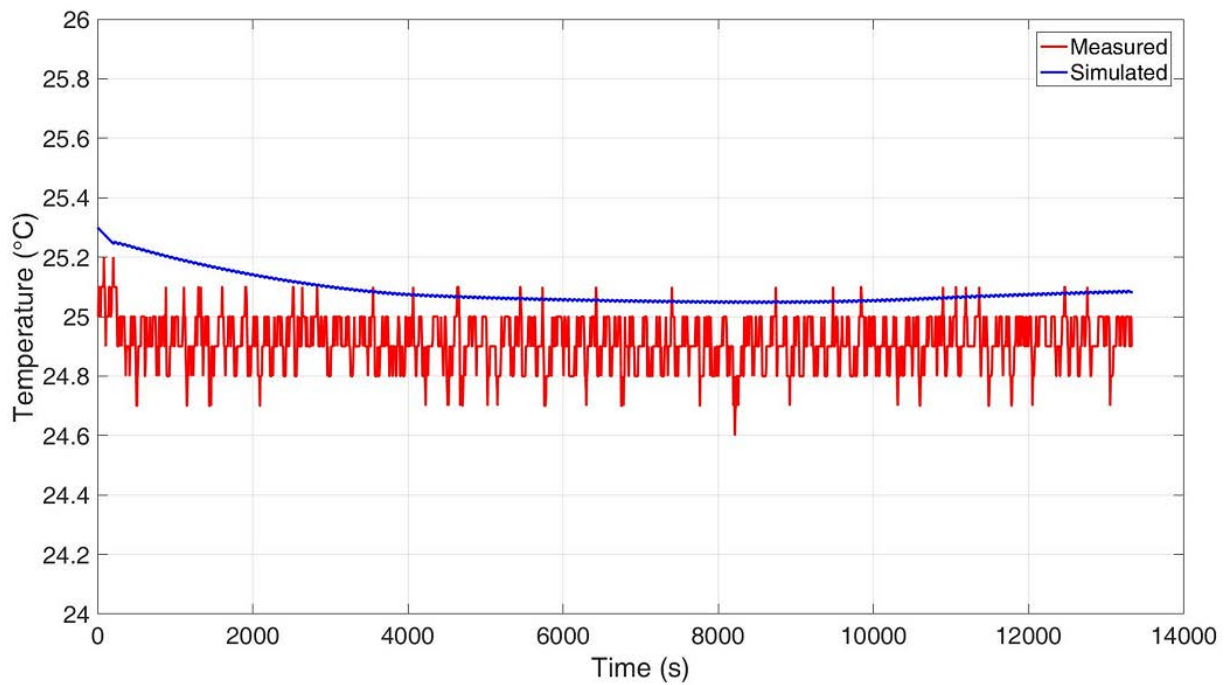


Figure 5.17: Simulated cell temperature of Winston 100Ah cell at 25°C

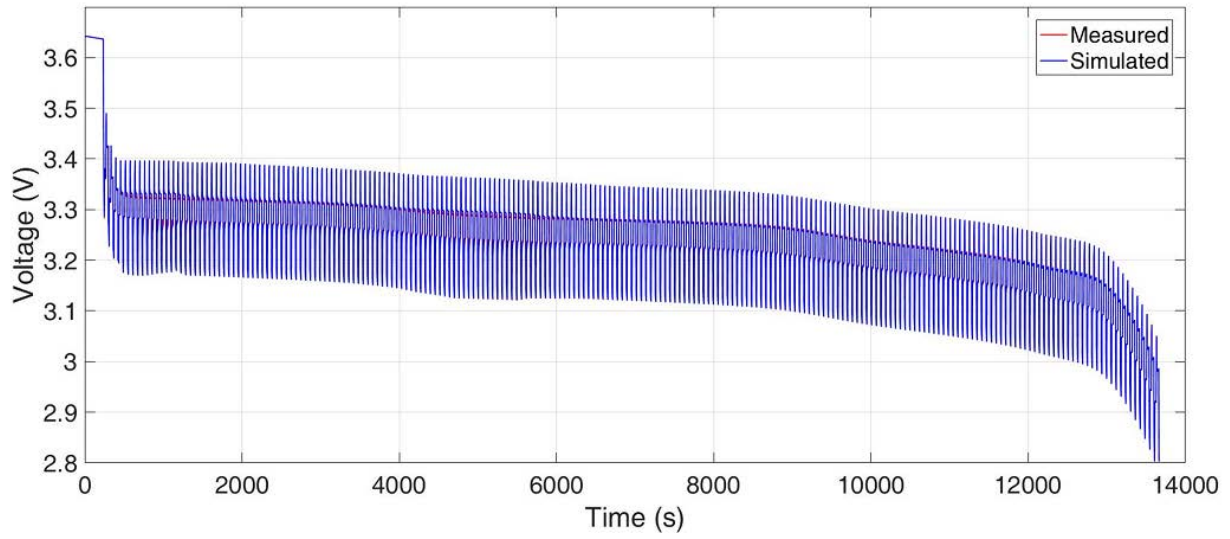


Figure 5.18: Simulated terminal voltage of Toshiba 20Ah cell at 40°C

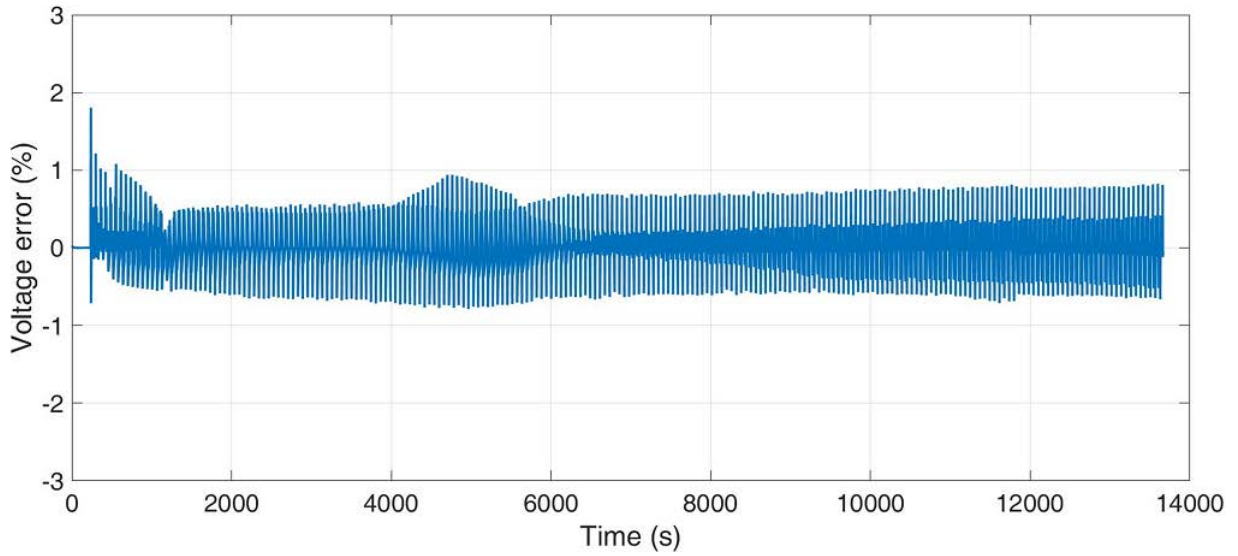


Figure 5.19: Relative error on the simulated terminal voltage of Winston 100Ah cell at 40°C

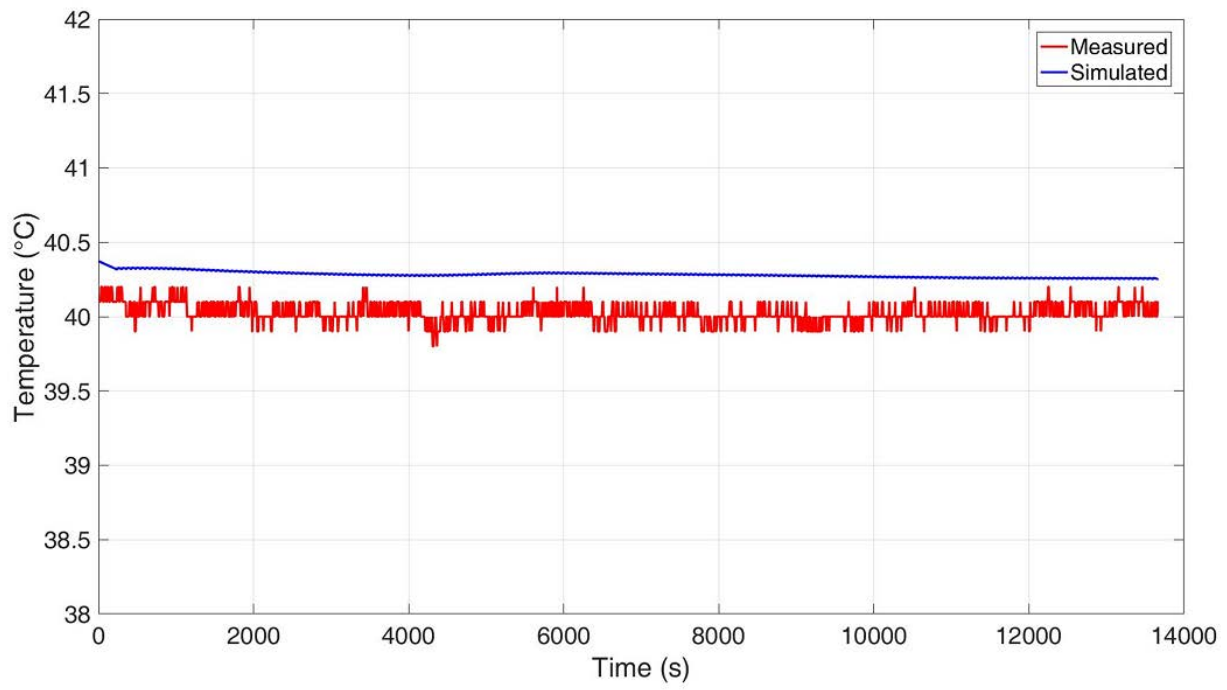


Figure 5.20: Simulated cell temperature of Winston 100Ah cell at 40°C

Part IV

Thermal characterisation and modeling

Chapter 1

Introduction

This document is the report of Work Package 4 (WP4) of the LBATTS project (Lithium ion batteries for Traction and Stationary Applications). The scope of this work package is to analyse in detail the thermal management of a Li-ion battery pack, focusing on module level. This indicates that the analysis does not include a detailed investigation of the thermal phenomena inside the battery, but rather focuses on the heat transfer phenomena outside the battery and its influence on the overall battery temperature. These heat transfer phenomena include cooling of the battery pack through natural or forced convection, but also thermal buffering through the addition of phase change materials (PCMs).

Chapter 2 introduces the concept of thermal buffering and elaborates on the types of PCM and on the methods through which they can be utilized. An overview of commercially available PCMs is provided. The next chapter revolves around thermal simulations of battery packs with different thermal management systems. The different parameters and the used modelling equations are discussed in detail, while the influence of the parameters is simulated and discussed for cases with and without thermal buffering. In chapter 4, a methodology is provided for the selection of an adequate thermal management system, taking into account different boundary conditions, based on the results of the simulations in chapter 3. The final chapter summarizes the conclusions of Work Package 4.

Chapter 2

Battery thermal management with heat buffering

During operation, batteries generate (or absorb) heat, which leads to a change of battery temperature. An adequate thermal management system is needed to ensure that the temperature of the battery remains within a selected range. This management system always comprises of a form of cooling to remove the generated heat from the batteries. Heating may be needed to avoid very low temperatures in low ambient temperature environments. A third option for a thermal battery management system is heat buffering. Heat buffering can be advantageous when the heat flow from the battery is highly fluctuating. A very high heat flow for a short period of time would require a large cooling system. By adding a heat buffer, the heat can be temporarily stored and removed over a longer time at a lower heat flow, requiring a smaller cooling system.

Heat buffering can be done by adding a thermal mass. Sensible heat is stored in any material, by which the temperature of the material will increase. A more interesting possibility is latent heat storage. Latent heat storage is obtained by using the heat that is absorbed when changing phase (solid to liquid or liquid to gas). There are two major advantages of using latent heat storage compared to sensible heat storage. Firstly, the amount of heat that can be stored per mass or volume of storage material is an order higher for latent heat storage. Secondly, the process of melting or evaporating occurs at (quasi) constant temperature, thereby reducing the temperature increase (or decrease) of the battery compared to sensible heat storage.

Phase change materials for thermal storage are often referred to as PCM(s). Liquid to gas transition is not commonly used for these applications. Although the latent heat of this transition is higher, practically the implementation is more difficult. This relates to the high volume or pressure increase by evaporation and problems with sealing or entrapment of the liquid or gas. Only solid to liquid PCMs will be discussed in the following sections.

2.1 Phase Change Materials (PCMs)

2.1.1 Organic PCMs

Organic PCMs can be paraffins and fatty acids but also several other structures. They are stable, safe and compatible with most construction materials. They are however flammable, can be toxic and have low thermal conductivity. Examples are paraffin wax, several vegetable oils and organics like dodecanol.

Table 2.1: Organic PCM properties

Property	Min	Max	
Melting temperature	-10	160	°C
Thermal conductivity	0.15	0.25	W/mK
Latent heat	140	270	kJ/kg
	30	60	kWh/m ³

2.1.2 Salt hydrates

Salt hydrates are structures formed by the addition of water to salt molecules. They have high thermal conductivity and latent heat and are non-flammable. They can however be unstable and corrosive and can have substantial super cooling. Some examples are calcium chloride hexahydrate and sodium sulphate decahydrate.

Table 2.2: Salt hydrate PCM properties

Property	Min	Max	
Melting temperature	-30	120	°C
Thermal conductivity	0.5	1.3	W/mK
Latent heat	70	270	kJ/kg
	40	180	kWh/m ³

2.1.3 Eutectic mixtures

A eutectic mixture is a mixture of a specific atomic ratio of two products at which the mixture melts as a whole. Due to this they have very sharp melting points (close to pure substances) and they are available at a wide range of melting temperatures. Examples are mixtures of acids (for example lauric and stearic acid) and salt hydrates.

Table 2.3: Eutectic mixture PCM properties

Property	Min	Max	
Melting temperature	-115	125	°C
Thermal conductivity	0.14	0.6	W/mK
Latent heat	70	340	kJ/kg
	20	95	kWh/m ³

2.2 Enhanced PCM with structures

When considering a thermal buffering management strategy, next to the thermal mass or capacity, also thermal conductivity is important to be able to transfer heat from the heat source to the thermal buffer and, in the case of overall heat generation, to the environment. The previous section offers a range of typical values for the thermal conductivity of PCMs used in practical applications. These values vary from 0.14 W/mK to 1.3 W/mK. The thermal conductivity of these materials is several orders of magnitude smaller when for example compared to aluminium (200 W/mK). For thermal buffering systems, PCMs act as a thermal insulator and a large temperature difference exists over a small layer of PCM when heat is added. The temperature increase due to this effect can negate the positive effects of the thermal buffering. To increase the thermal conductivity while maintaining the thermal buffering capacity, several hybrid systems of PCMs contained in a solid structure has been proposed. Of these structures, three types stand out because of their beneficial characteristics and they have been widely researched: metal foams, expanded graphite and carbon fibres.

2.2.1 Metal foam

A metal foam (MF) is a cellular metal structure. The structure is filled with several cells or pores. Two types of metal foam can be distinguished: open-cell and closed-cell metal foam. Cells in open-cell foam are made up of struts, which are connected in several ways, but allow free transport of different fluids through the pores. In closed-cell metal foam, the cells are completely surrounded by the metal, and the fluid (air) is trapped inside. For applications with thermal buffering or storage using PCMs, open-cell metal foam is used because closed-cell metal foam cannot be produced with PCMs inside the cells. Open-cell metal foam can be produced in the standard manner, afterwards PCMs can be poured into the open cells.

Open-cell metal foam can be made up of either aluminium or copper. The resulting metallic struts have high thermal conductivity, thereby increasing the conductivity of the combination of metal foam and PCM. Metal foams can be highly porous, with porosities ranging from 75% to 95%. This results in the latent heat capacity of the hybrid material

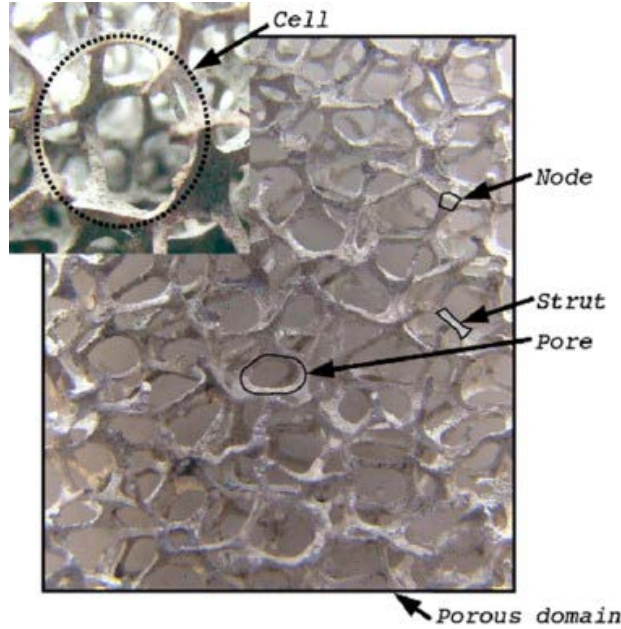


Figure 2.1: Metal foam sample [49]

to go down by 5% to 25%, since this part of the volume can not be taken up by PCM material.

Numerous numerical [131, 100] and experimental [243, 171] studies have been performed on metal foam saturated with PCM. Thermal buffering for Li-ion batteries has also been studied [170, 112]. Boomsma & Poulikakos present an advanced model to determine the effective thermal conductivity of fluid-saturated metal foams [25]. However, they state that using a first order estimate using a weighted average of the thermal conductivity of both components is valid if the structure is uniform, natural convection and radiation can be neglected, the physical properties of the structures are constant throughout the sample and the two structures are in thermal equilibrium. Bhattacharya et al. present an empirical correlation which is a weighted average of the two limiting values (complete series or complete parallel configuration) and is more accurate than the weighted average of the thermal conductivities [23]. This empirical correlation is shown in equation 2.1, where k_{eff} is the effective thermal conductivity of the foam-PCM structure, ϵ is the porosity of the foam, k_{PCM} is the thermal conductivity of the PCM and k_s is the thermal conductivity of the solid metal foam material. The weighing factor A is determined to be equal to 0.35 and this equation is used to determine the effective thermal conductivity in the thermal simulations. Zhao et al. report that the effective thermal conductivity of a metal foam-PCM structure can be 3-10 times higher when compared to pure PCM [243].

$$k_{eff} = A [\epsilon k_{PCM} + (1 - \epsilon)k_s] + \frac{1 - A}{\frac{\epsilon}{k_{PCM}} + \frac{1-\epsilon}{k_s}} \quad (2.1)$$

2.2.2 Expanded graphite

Expanded graphite (EG) is created by intercalating flake graphite with another material, in this case PCM. After intercalating, the PCM material resides in between the graphite layers, whereby the material properties of the PCM expanded graphite are influenced both by the graphite and PCM properties. The highly thermally conductive graphite contributes to an improved thermal conductivity of the structure, while the latent heat of the PCM is used for thermal buffering. Figure 2.2 shows both a pure PCM and a PCM expanded graphite structure. One of the advantages of PCM expanded graphite is that it can be form-stable, which means liquid PCM will be contained within the structure due to capillary forces, regardless if the structure is placed in a container or not.

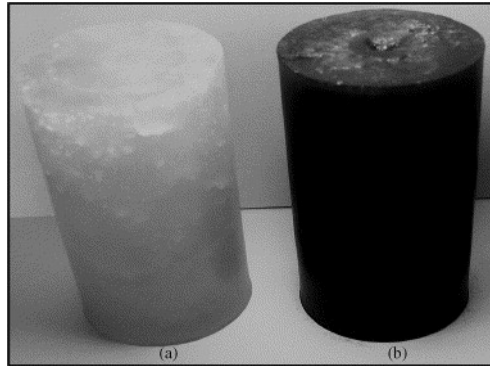


Figure 2.2: Pure PCM (left) and PCM expanded graphite (right) [192]

Sarı & Karaipekli experimentally tested the thermal conductivity of paraffin expanded graphite in 2007 [192]. Mass fractions of EG varied from 2% to 10%. Only the 10% EG structure was form-stable. The results of the measurements are shown in table 2.4. In 2009, Sarı & Karaipekli reported on measurements of a 80%-20% palmitic acid-EG structure [193]. This was the highest mass fraction of palmitic acid for which the structure was form stable. The thermal conductivity was 2.5 times higher when compared with pure palmitic acid. Zhao & Wu compared PCM enhancement with expanded graphite and metal foam, and concluded that both structures can enhance heat transfer, but that metal foams perform better than expanded graphite [244].

Table 2.4: Paraffin (n-docosane) expanded graphite thermal conductivity [192]

EG mass fraction	Thermal conductivity
0 %	0.22 W/mK
2 %	0.40 W/mK
4 %	0.52 W/mK
7 %	0.68 W/mK
10 %	0.82 W/mK

2.2.3 Carbon fibre

Highly thermally conductive carbon fibres (CF) can be mixed with PCMs to increase the thermal conductivity. An example of carbon fibre-PCM composites with different fractions can be seen in figure 2.3. Frusteri et al. tested the influence of mass fraction and fibre length on the thermal conductivity of PCM44 mixed with carbon fibres with a diameter of $6\mu m$ [63]. They concluded that a linear relationship exists between the mass fraction of carbon fibres and the thermal conductivity. Lower fibre lengths resulted in higher thermal conductivity, which the authors related to the higher homogeneity of the composite. Thermal conductivity enhancement up to a factor five were measured. Babapoor et al. analysed the thermal management of Li-ion batteries with paraffin PCM enhanced with carbon fibres with an average diameter of $10\mu m$ [19]. The same conclusions were found concerning the influence of the fibre length, but their results also showed an optimal mass fraction 0.46%, where the thermal conductivity is maximal. However, the reported mass fractions are very small compared to other studies, cfr. [63, 92]. Karaipekli et al. compared the performance of expanded graphite and carbon fibre (diameter $6\mu m$) structure [92]. The thermal conductivity of the structure increases linearly with the mass fraction for both EG and CF. The increase of thermal conductivity for EG was slightly higher than for CF.

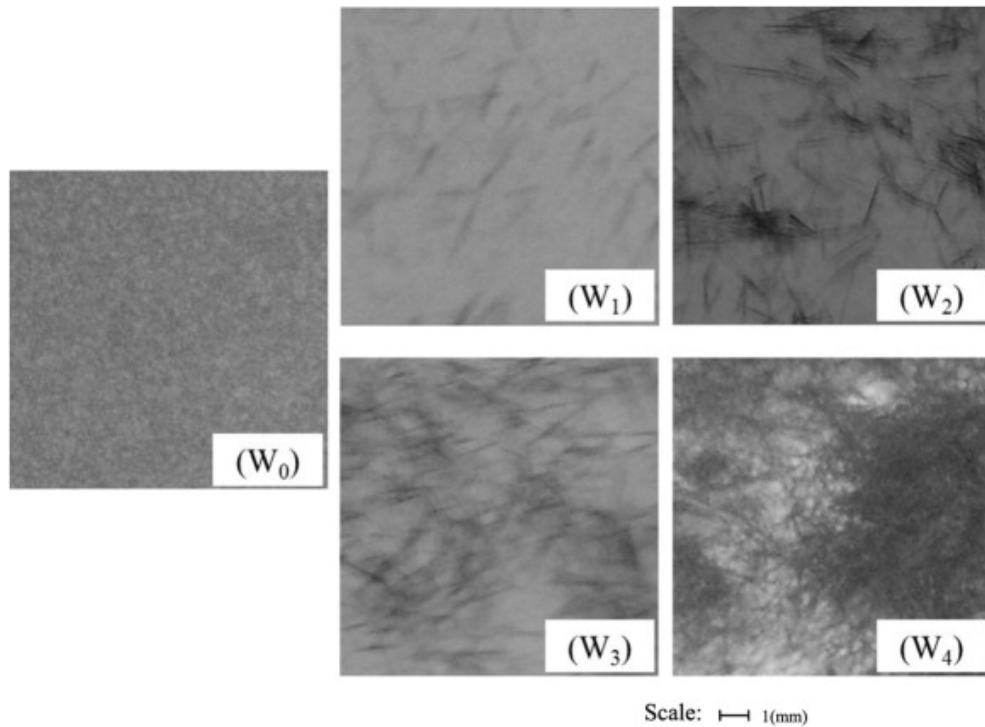


Figure 2.3: Carbon fibre-PCM composites with different weight fractions. Carbon fibre mass fractions: (W1) 0.32%, (W2) 0.46%, (W3) 0.56%, (W4) 0.69% [19].

2.3 Overview PCMs

Table 2.5 gives an overview of PCM °. Tables 2.6 to 2.11 give an overview of the commercially available PCMs from a selection of these °.

Table 2.5: PCM manufactures

Rubitherm
PCM Products
PureTemp
Climator
Micronal
RGEES
Cristopia
Microtek
Mitsubishi Chemicals
PCM Energy

Table 2.6: Selection of commercially available PCMs

Supplier	Product name	Melting range	Latent heat	Type
Rubitherm	RT - 9 HC	-9 °C	250 kJ/kg	Organic
	RT - 4	-4 °C	180 kJ/kg	Organic
	RT 0	0 °C	175 kJ/kg	Organic
	RT 2 HC	2 °C	200 kJ/kg	Organic
	RT 3 HC_1	3 °C	190 kJ/kg	Organic
	RT 4	4 °C	175 kJ/kg	Organic
	RT 5	5 °C	180 kJ/kg	Organic
	RT 5 HC	5 °C	250 kJ/kg	Organic
	RT 8	8 °C	175 kJ/kg	Organic
	RT 8 HC	8 °C	190 kJ/kg	Organic
	RT 9	9 °C	175 kJ/kg	Organic
	RT 10	10 °C	160 kJ/kg	Organic
	RT 10 HC	10 °C	200 kJ/kg	Organic
	RT 11 HC	11 °C	200 kJ/kg	Organic
	RT 12	12 °C	155 kJ/kg	Organic
	RT 15	15 °C	155 kJ/kg	Organic
	RT 18 HC	18 °C	260 kJ/kg	Organic
	RT 21	21 °C	155 kJ/kg	Organic
	RT 21 HC	21 °C	190 kJ/kg	Organic
	RT 22 HC	22 °C	190 kJ/kg	Organic
	RT 24	24 °C	160 kJ/kg	Organic
	RT 25	25 °C	170 kJ/kg	Organic
	RT 25 HC	25 °C	230 kJ/kg	Organic
	RT 26	26 °C	180 kJ/kg	Organic
	RT 28 HC	28 °C	250 kJ/kg	Organic
	RT 31	31 °C	165 kJ/kg	Organic
	RT 35	35 °C	160 kJ/kg	Organic
	RT 42	42 °C	165 kJ/kg	Organic
	RT 35 HC	35 °C	240 kJ/kg	Organic
	RT 44 HC	44 °C	250 kJ/kg	Organic
	RT 47	47 °C	165 kJ/kg	Organic
	RT 50	50 °C	160 kJ/kg	Organic
	RT 54 HC	54 °C	200 kJ/kg	Organic
RT 55	55 °C	170 kJ/kg	Organic	
RT 60	60 °C	160 kJ/kg	Organic	
RT 64 HC	64 °C	250 kJ/kg	Organic	
RT 65	65 °C	150 kJ/kg	Organic	

Table 2.7: Selection of commercially available PCMs

Supplier	Product name	Melting range	Latent heat	Type	
Rubitherm	RT69HC	69°C	230 kJ/kg	Organic	
	RT 70 HC	70°C	260 kJ/kg	Organic	
	RT 82	82°C	170 kJ/kg	Organic	
	RT 80 HC	78°C	220 kJ/kg	Organic	
	RT 90 HC	90°C	170 kJ/kg	Organic	
	SP - 21	-21 <>-19°C	285 kJ/kg	Salt hydrate	
	SP - 13	-13 <>-11°C	300 kJ/kg	Salt hydrate	
	SP - 7.2	-7 <>-5°C	290 kJ/kg	Salt hydrate	
	SP 5	4 <>6°C	170 kJ/kg	Salt hydrate	
	SP 21 E	21 <>23°C	170 kJ/kg	Salt hydrate	
	SP 24 E	24 <>25°C	180 kJ/kg	Salt hydrate	
	SP 25 E2	24 <>26°C	180 kJ/kg	Salt hydrate	
	SP 26 E	25 <>27°C	180 kJ/kg	Salt hydrate	
	SP 29 Eu	29 <>31°C	200 kJ/kg	Salt hydrate	
	SP 31	31 <>33°C	210 kJ/kg	Salt hydrate	
	SP 58	56 <>59°C	250 kJ/kg	Salt hydrate	
	SP 70	67 <>73°C	150 kJ/kg	Salt hydrate	
	SP 90	88 <>90°C	150 kJ/kg	Salt hydrate	
	PCM Products	S117	117°C	160 kJ/kg	Salt hydrate
		S89	89°C	151 kJ/kg	Salt hydrate
S83		83°C	141 kJ/kg	Salt hydrate	
S72		72°C	127 kJ/kg	Salt hydrate	
S70		70°C	110 kJ/kg	Salt hydrate	
S58		58°C	145 kJ/kg	Salt hydrate	
S50		50°C	100 kJ/kg	Salt hydrate	
S46		46°C	210 kJ/kg	Salt hydrate	
S44		44°C	100 kJ/kg	Salt hydrate	
S34		34°C	115 kJ/kg	Salt hydrate	
S32		32°C	200 kJ/kg	Salt hydrate	
S30		30°C	190 kJ/kg	Salt hydrate	
S27		27°C	183 kJ/kg	Salt hydrate	
S25		25°C	180 kJ/kg	Salt hydrate	
S23		23°C	175 kJ/kg	Salt hydrate	
S21		22°C	170 kJ/kg	Salt hydrate	
S19		19°C	160 kJ/kg	Salt hydrate	
S17		17°C	160 kJ/kg	Salt hydrate	
S15	15°C	160 kJ/kg	Salt hydrate		

Table 2.8: Selection of commercially available PCMs

Supplier	Product name	Melting range	Latent heat	Type
PCM Products	S13	13°C	160 kJ/kg	Salt hydrate
	S10	10°C	155 kJ/kg	Salt hydrate
	S8	8°C	150 kJ/kg	Salt hydrate
	S7	7°C	150 kJ/kg	Salt hydrate
	A164	164°C	290 kJ/kg	Organic
	A155	155°C	100 kJ/kg	Organic
	A144	144°C	115 kJ/kg	Organic
	A133	133°C	126 kJ/kg	Organic
	A118	118°C	340 kJ/kg	Organic
	A95	95°C	205 kJ/kg	Organic
	A82	82°C	155 kJ/kg	Organic
	A70	70°C	173 kJ/kg	Organic
	A62	62°C	145 kJ/kg	Organic
	A60H	60°C	212 kJ/kg	Organic
	A60H	60°C	145 kJ/kg	Organic
	A58H	58°C	243 kJ/kg	Organic
	A58	58°C	132 kJ/kg	Organic
	A55	55°C	135 kJ/kg	Organic
	A53H	53°C	166 kJ/kg	Organic
	A53H	53°C	130 kJ/kg	Organic
	A52	52°C	222 kJ/kg	Organic
	A50	50°C	218 kJ/kg	Organic
	A48	48°C	234 kJ/kg	Organic
	A46	46°C	155 kJ/kg	Organic
	A44	44°C	242 kJ/kg	Organic
	A43	43°C	165 kJ/kg	Organic
	A42	42°C	105 kJ/kg	Organic
	A40	40°C	230 kJ/kg	Organic
	A39	39°C	105 kJ/kg	Organic
	A37	37°C	235 kJ/kg	Organic
	A36	36°C	217 kJ/kg	Organic
	A32	32°C	130 kJ/kg	Organic
	A29	29°C	225 kJ/kg	Organic
A28	28°C	155 kJ/kg	Organic	
A26	26°C	150 kJ/kg	Organic	
A25H	25°C	226 kJ/kg	Organic	
A25	25°C	150 kJ/kg	Organic	

Table 2.9: Selection of commercially available PCMs

Supplier	Product name	Melting range	Latent heat	Type
PCM Products	A24	24°C	145 kJ/kg	Organic
	A23	23°C	145 kJ/kg	Organic
	A22H	22°C	216 kJ/kg	Organic
	A22	22°C	145 kJ/kg	Organic
	A17	17°C	150 kJ/kg	Organic
	A16	16°C	213 kJ/kg	Organic
	A15	15°C	130 kJ/kg	Organic
	A9	9°C	140 kJ/kg	Organic
	A8	8°C	150 kJ/kg	Organic
	A6	6°C	150 kJ/kg	Organic
	A4	4°C	200 kJ/kg	Organic
	A3	3°C	200 kJ/kg	Organic
	A2	2°C	200 kJ/kg	Organic
	E0	0°C	332 kJ/kg	Eutectic
	E-2	-2°C	306 kJ/kg	Eutectic
	E-3	-3,7°C	312 kJ/kg	Eutectic
	E-6	-6°C	275 kJ/kg	Eutectic
	E-10	-10°C	286 kJ/kg	Eutectic
	E-11	-11,6°C	301 kJ/kg	Eutectic
	E-12	-12,3°C	250 kJ/kg	Eutectic
	E-14	-14,8°C	243 kJ/kg	Eutectic
	E-15	-15°C	303 kJ/kg	Eutectic
	E-19	-18,7°C	282 kJ/kg	Eutectic
	E-21	-20,6°C	263 kJ/kg	Eutectic
	E-22	-22°C	234 kJ/kg	Eutectic
	E-26	-26°C	260 kJ/kg	Eutectic
	E-29	-29°C	222 kJ/kg	Eutectic
	E-32	-32°C	243 kJ/kg	Eutectic
	E-34	-33,6°C	240 kJ/kg	Eutectic
	E-37	-36,5°C	213 kJ/kg	Eutectic
	E-50	-49,8°C	218 kJ/kg	Eutectic
	E-75	-75°C	102 kJ/kg	Eutectic
	E-78	-78°C	115 kJ/kg	Eutectic
E-90	-90°C	90 kJ/kg	Eutectic	
E-114	-114°C	107 kJ/kg	Eutectic	

Table 2.10: Selection of commercially available PCMs

Supplier	Product name	Melting range	Latent heat	Type
PureTemp	PureTemp -37	-37°C	145 kJ/kg	Organic
	PureTemp -21	-21°C	239 kJ/kg	Organic
	PureTemp -15	-15°C	301 kJ/kg	Organic
	PureTemp -2	-2°C	277 kJ/kg	Organic
	PureTemp 1	1°C	301 kJ/kg	Organic
	PureTemp 4	4°C	187 kJ/kg	Organic
	PureTemp 6	6°C	220 kJ/kg	Organic
	PureTemp 7	7°C	185 kJ/kg	Organic
	PureTemp 8	8°C	178 kJ/kg	Organic
	PureTemp 12	12°C	181 kJ/kg	Organic
	PureTemp 15	15°C	182 kJ/kg	Organic
	PureTemp 18	18°C	192 kJ/kg	Organic
	PureTemp 20	20°C	171 kJ/kg	Organic
	PureTemp 23	23°C	227 kJ/kg	Organic
	PureTemp 25	25°C	187 kJ/kg	Organic
	PureTemp 27	27°C	202 kJ/kg	Organic
	PureTemp 28	28°C	190 kJ/kg	Organic
	PureTemp 29	29°C	202 kJ/kg	Organic
	PureTemp 37	37°C	210 kJ/kg	Organic
	PureTemp 42	42°C	218 kJ/kg	Organic
	PureTemp 48	48°C	230 kJ/kg	Organic
	PureTemp 53	53°C	225 kJ/kg	Organic
	PureTemp 58	58°C	225 kJ/kg	Organic
PureTemp 60	60°C	220 kJ/kg	Organic	
PureTemp 63	63°C	206 kJ/kg	Organic	
PureTemp 68	68°C	213 kJ/kg	Organic	
PureTemp 108	108°C	180 kJ/kg	Organic	
PureTemp 151	151°C	217 kJ/kg	Organic	

Table 2.11: Selection of commercially available PCMs

Supplier	Product name	Melting range	Latent heat	Type
Climator	Climsel C -21	-21°C	288 kJ/kg	Salt hydrate
	Climsel C -18	-18°C	288 kJ/kg	Salt hydrate
	Climsel C 7	7°C	126 kJ/kg	Salt hydrate
	Climsel C 10	10,5°C	126 kJ/kg	Salt hydrate
	Climsel C 21	21°C	112 kJ/kg	Salt hydrate
	Climsel C24	24°C	151.3 kJ/kg	Salt hydrate
	Climsel C28	28°C	162.3 kJ/kg	Salt hydrate
	Climsel C32	32°C	162.3 kJ/kg	Salt hydrate
	Climsel C48	48°C	180 kJ/kg	Salt hydrate
	Climsel C58	58°C	288.5 kJ/kg	Salt hydrate
	Climsel C70	70°C	282.9 kJ/kg	Salt hydrate
Micronal	DS 5000	26°C	45 kJ/kg	Organic
	DS 5007	23°C	41 kJ/kg	Organic
	DS 5030	21°C	37 kJ/kg	Organic
	DS 5001	26°C	110 kJ/kg	Organic
	DS 5008	23°C	100 kJ/kg	Organic
	DS 5029	21°C	90 kJ/kg	Organic
RGEES	PCM-HS26N	-26°C	205 kJ/kg	Salt hydrate
	PCM-HS23N	-23°C	200 kJ/kg	Salt hydrate
	PCM-HS10N	-10°C	220 kJ/kg	Salt hydrate
	PCM-OM06P	5.5°C	252 kJ/kg	Organic
	PCM-OM18P	18°C	233 kJ/kg	Organic
	PCM-HS22P	22°C	185 kJ/kg	Salt hydrate
	PCM-OM37P	37°C	218 kJ/kg	Organic
	PCM-OM65P	65°C	210 kJ/kg	Organic

Chapter 3

Thermal simulations

3.1 Simulation setup

To analyse the thermal behaviour of batteries with different thermal management strategies, a simulation model is built. In the model three different parts can be distinguished: the battery model (heat generation), the PCM model (heat buffering) and the convective heat transfer modelling (heat transfer), as shown in figure 3.1.

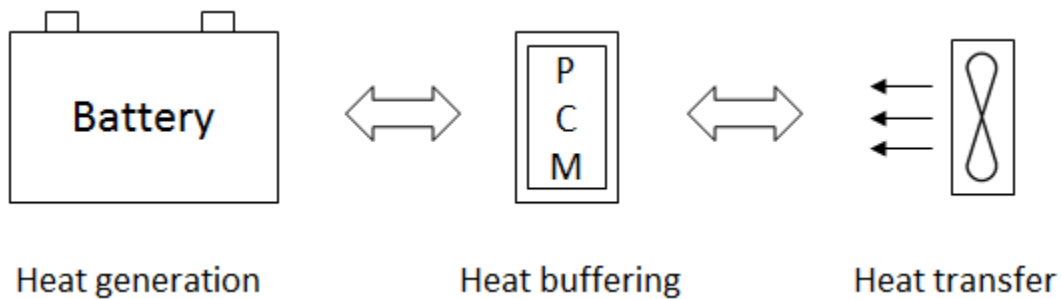


Figure 3.1: Overview of the thermal management model

3.1.1 Battery and load characteristics

A simple thermal battery model for the internal heat generation Q was used for the following simulations, based on the two heat generating effects, as shown in equation 3.1. The first effect is the irreversible heat Q_{irr} , which are the Joule losses and are modelled by an internal electrical resistance. The second effect is the reversible heat Q_{rev} , which is due to entropy change related to the chemical reactions in the battery during charging and discharging. The irreversible heat is always positive, which means heat is generated

by the battery. The irreversible heat can be positive or negative, which means heat can be generated or absorbed by the battery. In most cases, batteries generate heat during discharge and absorb heat during charge.

$$Q_{bat} = Q_{irr} + Q_{rev} \quad (3.1)$$

The irreversible heat generation is modelled according to equations 3.2 and 3.3. The internal resistance R is modelled based on the measurements reported in WP3. The internal resistance can be slightly dependent on the state of charge (SOC) and the current rate, in this simple model however it was only modelled to be dependent on the battery temperature T . In the following equations, I is the current and R_0 and T_0 are fitting constants that are determined from the measured values.

$$Q_{irr} = R(T)I^2 \quad (3.2)$$

$$R(T) = R_0 \exp\left(-\frac{T}{T_0}\right) \quad (3.3)$$

The reversible heat is modelled as in equation 3.4. The entropic coefficient $\frac{dE}{dT}$ is derived from the measurements, dependent on the SOC of the battery. It is determined from linear interpolation between the measured values, and is plotted in figure 3.2.

$$Q_{rev} = -\frac{dE}{dT} T I \quad (3.4)$$

Two battery cells have been used in the simulations: the Toshiba SCiB 20Ah cell and the Winston Thundersky 100Ah cell. Their geometric characteristics and the constants in equation 3.3 for both cells are given in table 3.1. In this table, q is the electric charge, I_{max} is the maximal continuous discharge current, H is the battery height, L is the battery length, W is the battery width or thickness, m is the cell mass and R_0 and T_0 are the constants used in equation 3.3.

Table 3.1: Battery cell characteristics

	$q[Ah]$	$I_{max}[A]$	$H[m]$	$L[m]$	$W[m]$	$m[kg]$	$R_0[m\Omega]$	$T_0[^\circ C]$
Toshiba	20	60	0.106	0.116	0.022	0.515	2.497	64
Winston	100	300	0.143	0.218	0.067	3.300	1.847	62

The amount of heat generated by the batteries is dependent on the current that is drawn from the batteries. Several different load cycles are used in the simulation to model real-life applications. The load cycles are divided in three groups: long (daily) cycles, medium duration cycles and short cycles. In the modelling, it is assumed that the battery

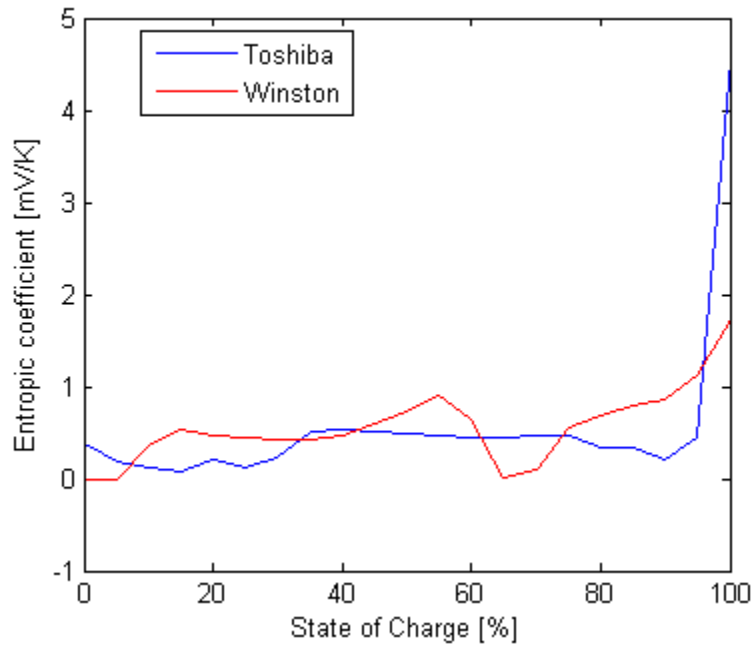


Figure 3.2: Entropic coefficient for the Toshiba and Winston battery cell as a function of SOC

pack runs through the cycle continuously or in other words that the battery is always cycling: when the load cycle has ended, it starts again at the beginning.

Long (daily) load cycles

These cycles are characterized by a long time period: the battery is charged and discharged in a sufficiently long time such that the current drawn from the battery is significantly lower than the rated maximal continuous discharge current. In the following simulations, three daily (full charging and discharging in 24 hours) cycles are used (construction, household and telecom). Figure 3.3 shows the current and the corresponding state of charge during the cycle.

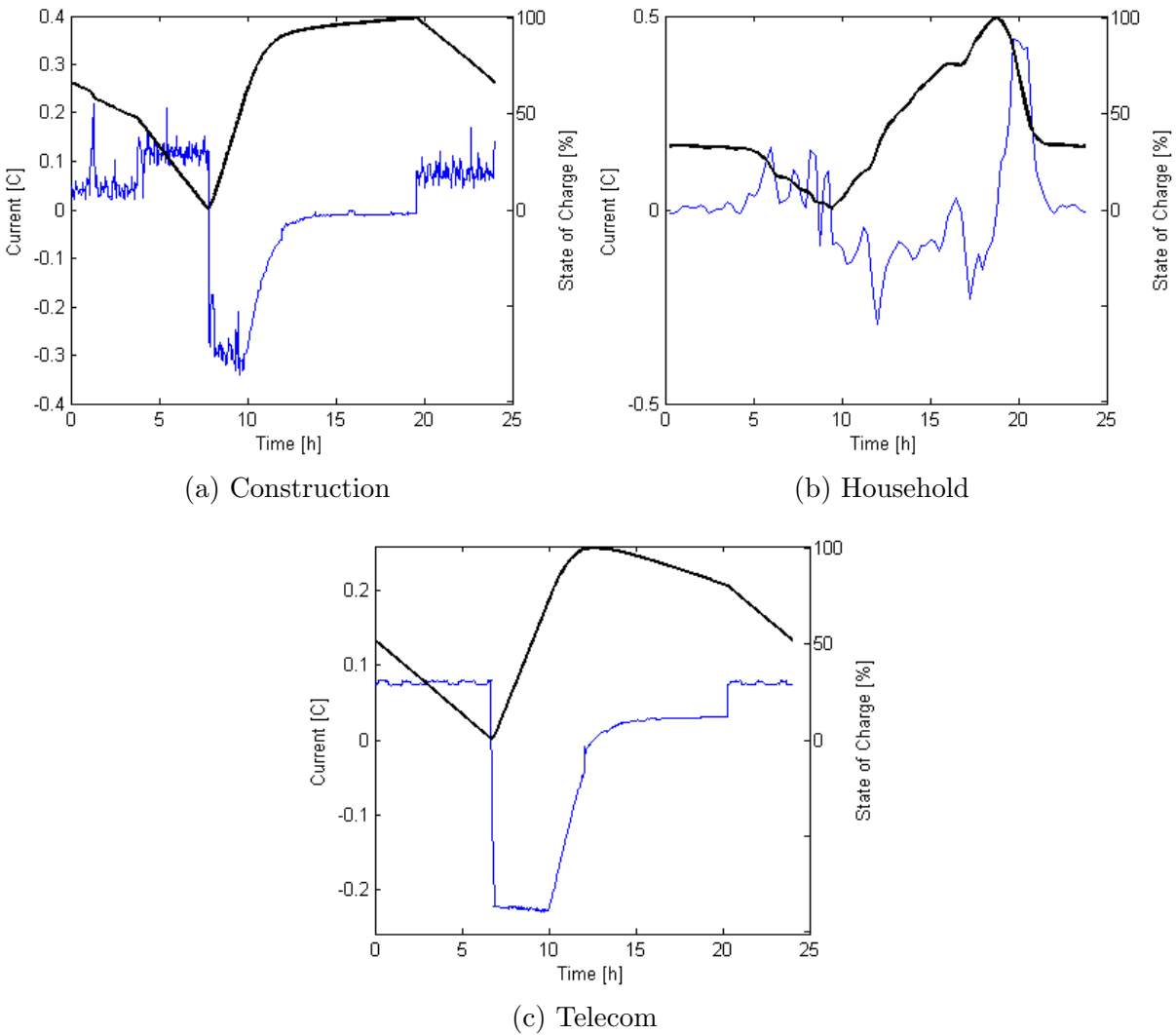


Figure 3.3: Daily load cycles for different applications (current in blue and SOC in black)

Medium duration load cycles

For medium duration cycles, the battery is fully charged and discharged in a shorter time period and the current is closer to the rated current. The current is scaled using the RMS value of the signal. Three current rates are used in the simulations: RMS current equal to the maximal discharge current (3C), 1C and 0.5C. Practically, one load profile of about seven hours is used and the charge and discharge periods are shortened such that the capacity of the battery is not exceeded. The duration of these cycles is in the range of (several) hours. Figures 3.4a and 3.4b show the current and state of charge for respectively the maximal current and 0.5C load cycle.

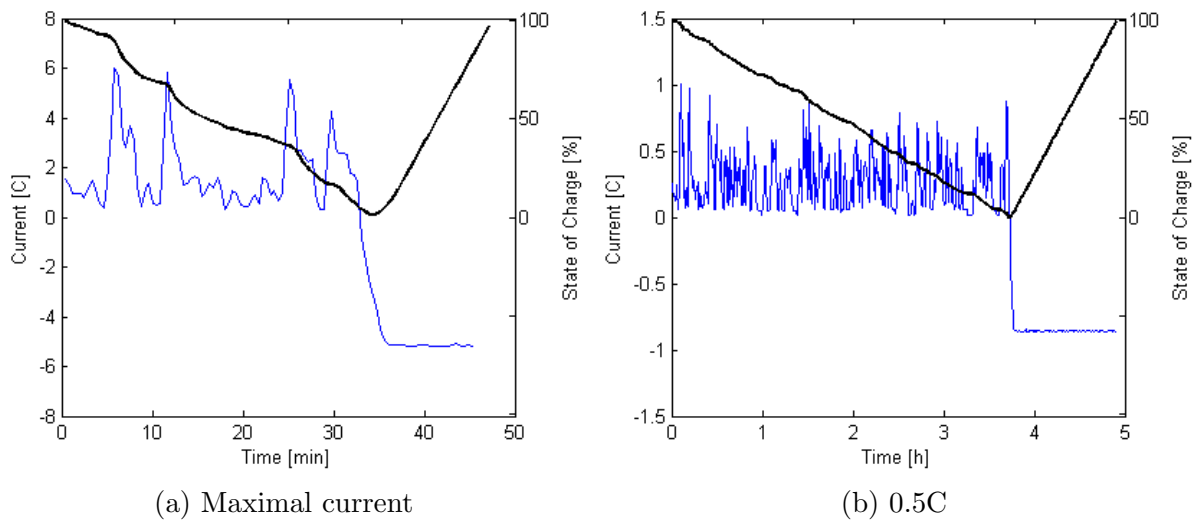


Figure 3.4: Maximal current and 0.5C medium duration load cycle (current in blue and SOC in black)

Short load cycles

The short cycles go through charging and discharging in a time period too short to fully charge and discharge the battery. For this cycle, the current is again scaled to the RMS value. The same current rates are used: RMS current equal to the maximal discharge current (3C) and RMS current equal to 1C and 0.5C. Since the cycle is very short, the same time period is used for all current rates, which is about seven minutes. The load current and corresponding state of charge for the maximal current and 0.5C case are shown in figures 3.5a and 3.5b respectively.

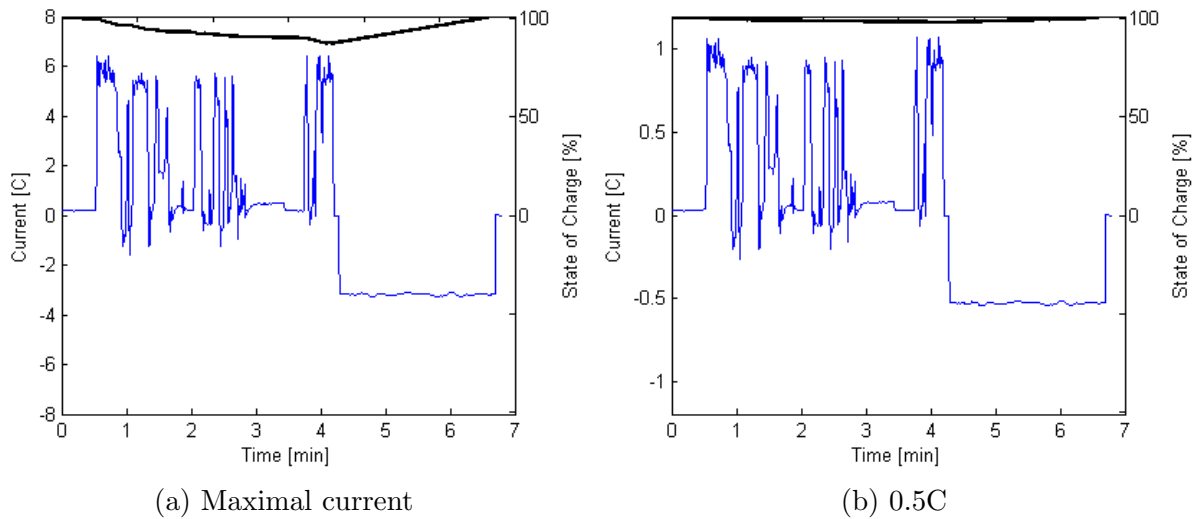


Figure 3.5: Maximal current and 0.5C short duration load cycle (current in blue and SOC in black)

3.1.2 PCM characteristics

The model assumes that both sides of the battery are covered with a layer of PCM material for heat buffering. The PCM considered in the calculations is 'RT35HC' by Rubitherm. This choice is mostly related to the melting temperature. Firstly, the optimal battery temperature for most batteries is around 30°C to 40°C, which is a trade-off between better efficiency at higher temperatures and lower ageing at lower temperatures. The melting point of 35°C is compliant with this range. Secondly, for the Belgian climate, even on the hottest days, the PCM will not melt due to heating by the ambient, so the heat buffering with latent heat is still maintained even with high ambient temperatures. The material properties of 'RT35HC' are given in table 3.2.

Table 3.2: Rubitherm 'RT35HC' organic PCM characteristics

Melting range	34-36	$^{\circ}C$
Latent heat	240	kJ/kg
Solid specific heat capacity	2000	J/kgK
Liquid specific heat capacity	2000	J/kgK
Solid density	880	kg/m^3
Liquid density	770	kg/m^3
Solid thermal conductivity	0.2	W/mK
Liquid thermal conductivity	0.2	W/mK

As for most PCMs, 'RT35HC' is not a pure substance and has a melting range rather

than a single melting point. This is taken into account by the model, dividing the latent heat in the temperature range between 34°C and 36°C, as shown in figure 3.6.

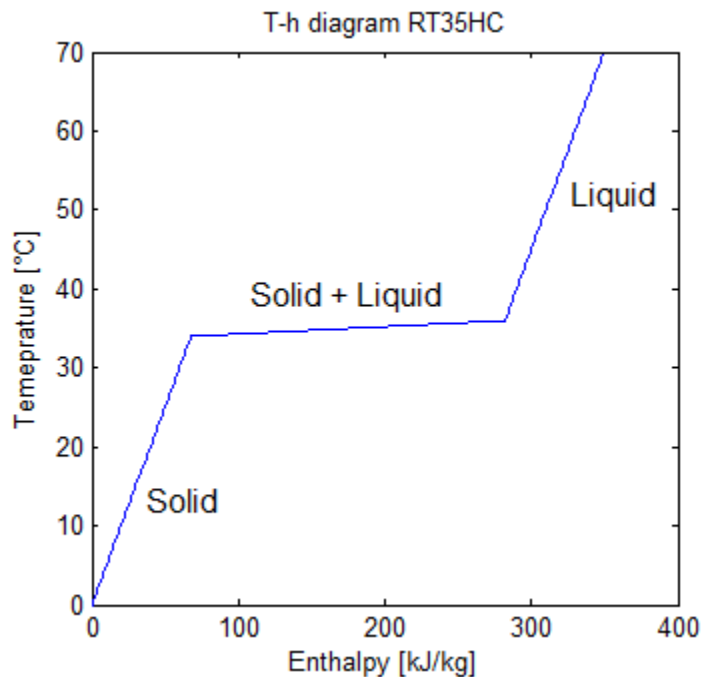


Figure 3.6: Simplified temperature-enthalpy diagram used in the simulations

For both the thermal conductivity and the density of the PCM in the melting range, a weighted average between the solid and liquid property based on the enthalpy is used.

Since the influence of the melting temperature is studied, also other kinds of PCM are needed in the simulations. To be able to compare the systems with different PCM melting temperatures, without having the influences of differing material properties, the same material properties as these in table 3.2 are used for all PCMs. The same melting range of 2°C is also used: if the melting temperature is stated as 40°C, the melting range will be 39-41°C.

The PCM is usually contained inside a closed structure. A metallic container is assumed in the model. The thermal resistance of the wall of this container R_{casing} is calculated by equation 3.5, taking into account a 1 mm thick (t_{casing}) aluminium plate with thermal conductivity (k_{casing}) equal to 200 W/mK. The thermal resistance of the contact area between the battery and the container is calculated by equation 3.6, assuming a 0.5 mm thickness ($t_{contact}$) thermal paste layer with thermal conductivity ($k_{contact}$) of 2 W/mK.

$$R_{casing} = \frac{t_{casing}}{k_{casing}A} \quad (3.5)$$

$$R_{contact} = \frac{t_{contact}}{k_{contact}A} \quad (3.6)$$

3.1.3 Convective thermal resistance

For the convection of the heat from either the battery in the simulation case with no PCM or from the container in the simulation case with PCM to the air, two possibilities are compared. Either the battery cells are passively cooled (natural convection) or fans are used to force air through the battery pack (forced convection). Both natural and forced convection thermal resistances are calculated according to Nusselt number correlations. All air properties are calculated using the open-source fluid property database CoolProp.

For natural convection, the equations are only valid for laminar flow, which is a valid assumption for the dimensions and temperature differences encountered in battery packs.

$$Ra = \frac{g\beta(T_w - T_a)H^3}{\nu\alpha} \quad (3.7)$$

$$Nu = 0.59Ra^{1/4} \quad (3.8)$$

$$h = \frac{k Nu}{H} \quad (3.9)$$

In these equations Ra is the Rayleigh number, g is the gravitational acceleration, β is the thermal expansion coefficient, T_w is the wall temperature, T_a is the ambient air temperature, H is the height of the battery, ν is the kinematic viscosity, α is the thermal diffusivity, Nu is the Nusselt number, h is the convection coefficient and k is the thermal conductivity.

For forced convection, the Gnielinski correlation (equation 3.13) is used, combined with the Petukhov correlation (equation 3.12) for the friction factor. These correlations are only valid for transitional and turbulent flows, which is valid from a certain value for the air velocity. The air velocities used in these simulations are sufficiently high for turbulent flow.

$$D_h = \frac{4Ht}{2H + 2t} \quad (3.10)$$

$$Re = \frac{vD_h}{\nu} \quad (3.11)$$

$$f = (0.79\ln(Re) - 1.64)^{-2} \quad (3.12)$$

$$Nu = \frac{(f/8)(Re - 1000)Pr}{1 + 12.7(f/8)^{1/2}(Pr^{2/3} - 1)} \quad (3.13)$$

$$h = \frac{k Nu}{D_h} \quad (3.14)$$

In these equations D_h is the hydraulic diameter, t is the thickness of the gap between the battery cells, Re is the Reynolds number, v is the air velocity, f is the Darcy friction factor and Pr is the Prandlt number.

From the convective heat transfer coefficient, the thermal resistance R_{conv} is calculated using the side area of the battery A :

$$R_{conv} = \frac{1}{hA} \quad (3.15)$$

3.2 Model governing equations

3.2.1 Overview

A schematic of a battery pack in combination with PCM heat buffering is shown in figure 3.7. The model assumes both sides of the battery are covered with a layer of PCM, contained in a casing. The model simulates half a battery, since the battery is assumed to be symmetric. A close-up of one battery cell with PCM is shown in figure 3.8. This figure also shows the equivalent electrical network that is used to calculate the thermal behaviour of the battery. To calculate the thermal behaviour of the PCM, the PCM layer is discretized to a 1D-model of n PCM elements.

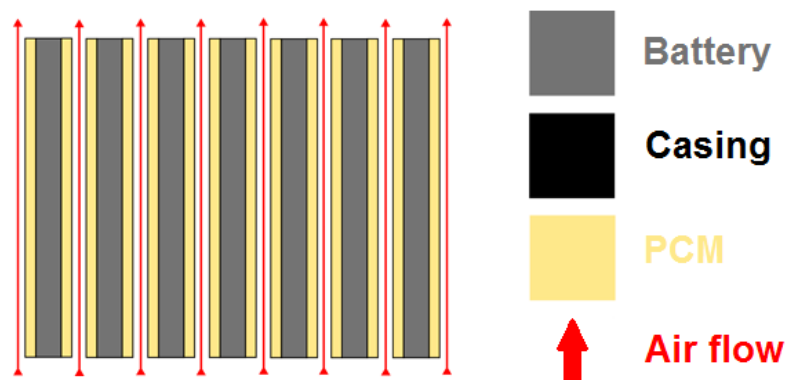


Figure 3.7: Schematic of a battery pack with PCM heat buffering

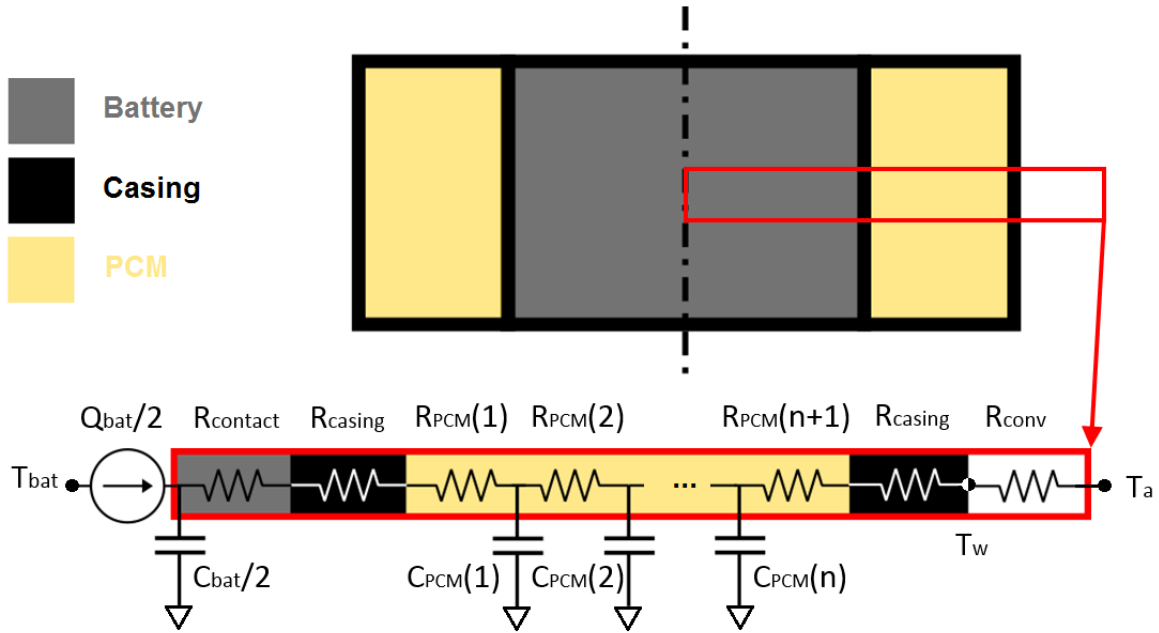


Figure 3.8: Equivalent electrical network for the temperatures and heat flow in a battery with PCM heat buffering

3.2.2 Equations

From the equivalent electrical network shown in figure 3.8, a system of $n + 2$ equations (equations 3.16, 3.18, $n - 2$ times 3.19, 3.20 and 3.21) and consequently $n + 2$ variables is derived. Two of the variables are temperatures: the battery temperature T_{bat} and the wall temperature T_w (the ambient temperature T_a is an input). The other n variables are used to calculate the thermal behaviour of the PCM layer. The enthalpy method is used to simulate this behaviour. Rather than solving for temperatures, the enthalpies of the different PCM layers are used as variables. This allows the model to also solve problem with a PCM with a fixed melting point, since the temperature is derived from the enthalpy.

For each of the $n + 2$ elements, a heat balance is formulated. Thermal inertia is taken into account by discretizing the time in small time steps and calculating the amount of heat stored in this time step.

For the battery, the heat balance at time t is:

$$\frac{Q_{bat}}{2} + \frac{T(H_{PCM}(1, t)) - T_{bat}(t)}{R_{contact} + R_{casing} + R_{PCM}(1)} + \frac{C_{bat}}{2} \frac{T_{bat}(t - dt) - T_{bat}(t)}{dt} = 0 \quad (3.16)$$

$$R_{PCM} = \frac{dx}{k_{PCM}A} \quad (3.17)$$

The first term is the heat generation from the battery, calculated as explained in section 3.1.1. The second term is the heat transfer with the neighbouring element, where the temperature of the neighbouring element is calculated from the enthalpy H_{PCM} , using the curve from figure 3.6. The thermal resistance of the PCM layer R_{PCM} is defined by equation 3.17, with dx the thickness of the discretized PCM layer and k_{PCM} the thermal conductivity of the PCM layer, dependent on the enthalpy as explained in 3.1.2. The third term is the heat stored in (half of) the battery, by multiplying the heat capacity of (half of) the battery C_{bat} with the temperature difference of the battery between the current and the previous time step and dividing by the time step dt . The heat capacity of the battery is determined by multiplying the mass of the battery with a specific heat capacity of 1015 J/kgK.

For the first PCM element, the heat balance is given by:

$$\frac{T_{bat}(t) - T(H_{PCM}(1, t))}{R_{contact} + R_{casing} + R_{PCM}(1)} + \frac{T(H_{PCM}(2, t)) - T(H_{PCM}(1, t))}{R_{PCM}(2)} + \rho_{PCM} dx A \frac{H_{PCM}(1, t - dt) - H_{PCM}(1, t)}{dt} = 0 \quad (3.18)$$

The first two terms are heat transfer to the neighbouring elements, the third term is the heat stored in the PCM element. This is calculated by multiplying the mass of the PCM element (product of density ρ_{PCM} , thickness dx and surface A) with the enthalpy difference and dividing by the time step dt .

For a PCM element i between element two and $n - 1$, the following heat balance is used:

$$\frac{T(H_{PCM}(i - 1, t)) - T(H_{PCM}(i, t))}{R_{PCM}(i)} + \frac{T(H_{PCM}(i + 1, t)) - T(H_{PCM}(i, t))}{R_{PCM}(i + 1)} + \rho_{PCM} dx A \frac{H_{PCM}(i, t - dt) - H_{PCM}(i, t)}{dt} = 0 \quad (3.19)$$

For PCM element n , the heat balance is:

$$\frac{T(H_{PCM}(n - 1, t)) - T(H_{PCM}(n, t))}{R_{PCM}(n)} + \frac{T_w(t) - T(H_{PCM}(n, t))}{R_{PCM}(n + 1) + R_{casing}} + \rho_{PCM} dx A \frac{H_{PCM}(n, t - dt) - H_{PCM}(n, t)}{dt} = 0 \quad (3.20)$$

For the PCM casing, the heat balance is:

$$\frac{T(H_{PCM}(n, t)) - T_w(t)}{R_{PCM}(n + 1) + R_{casing}} + \frac{T_a - T_w(t)}{R_{conv}} = 0 \quad (3.21)$$

The thermal inertia of the casing is not taken into account, since it is assumed to be negligible compared to the thermal inertia of the PCM.

3.2.3 Assumptions and limitations of the model

To reduce the computational load of the simulation and to allow for easy adaptation and optimization of the design parameters, several simplifications were made during the conception of the model:

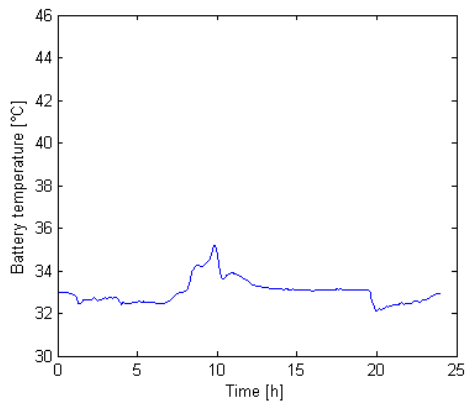
- The heat transfer in the model is assumed to be one-dimensional. This means no heat is transferred in other directions than perpendicular to the battery. In practice, there will be heat dissipation from these other sides of the battery, however the surface is small compared to the larger side surface.
- To allow for the one-dimensional modelling, the temperature in a cross-sectional plane perpendicular to the direction of the heat transfer is assumed to be constant. This is not completely true for the battery, where more heat will be generated in proximity of the electrodes. This results in a higher temperature near the electrodes.
- The heat transfer in the PCM is assumed to be solely by conduction. In the liquid phase of the PCM, also heat transfer by convection is possible. Since the thickness of the PCM layers in the simulation is very small, conduction is assumed to be the primary heat transfer mechanism.
- The model does not take into account the internal thermal resistance of the battery, but assumes a quasi constant temperature in the entire battery. This is valid if the internal thermal resistance is an order of magnitude smaller than the external thermal resistance. For more accurate simulations, the model can be expanded to take into account the internal thermal resistance.

3.3 Reference case: no heat buffering

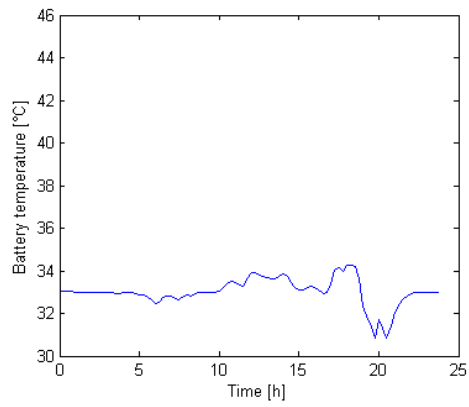
3.3.1 Comparison of load cycles

As reference cases, the different load cycles are used as input for the battery model with no PCM added and with forced convective cooling. The RMS value of the current is set to 1C. The battery used for these simulations is the Toshiba battery. The ambient temperature is set to 33°C (maximal daily value for Belgium). Figure 3.9 shows the temperature profile of the battery for the different load cycles. For the daily cycles, the battery temperature is within 3°C of the ambient temperature, since the load current is very low. For the medium duration case, the average temperature is about 34°C, but the variation in temperature during the cycle is higher with a maximal temperature of 46°C. For the seven minute cycle, the load current is the same as for the medium duration cycle which results in a similar average temperature. Since the cycle is shorter, the thermal

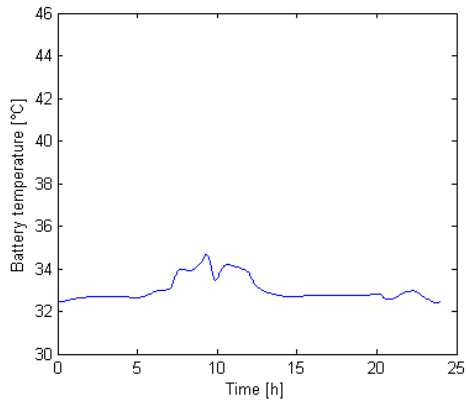
mass of the battery acts as a buffer for the cyclic heating. This results in a lower cyclic variation of the battery temperature. Since the variation of the temperature is highest in the medium duration case, this case will be most suited for thermal management with heat buffering.



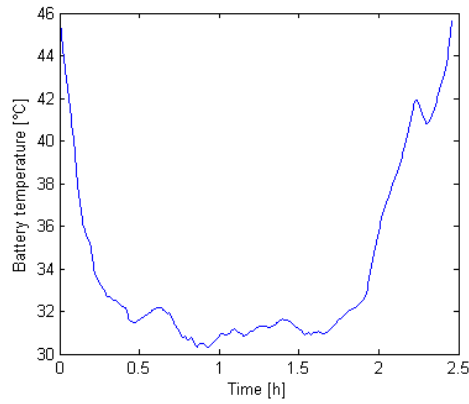
(a) Daily: construction



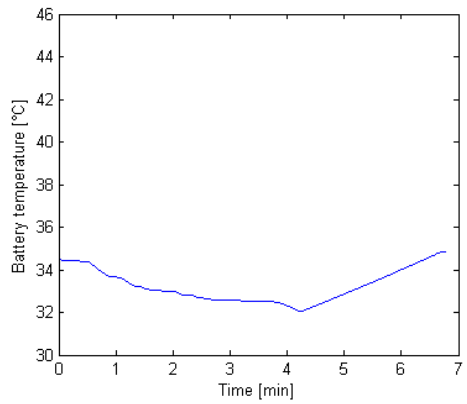
(b) Daily: household



(c) Daily: telecom



(d) Medium



(e) Short

Figure 3.9: Battery temperature with no heat buffering and forced convection with the Toshiba battery for different load cycles, ambient temperature is 33°C

3.3.2 Comparison of batteries

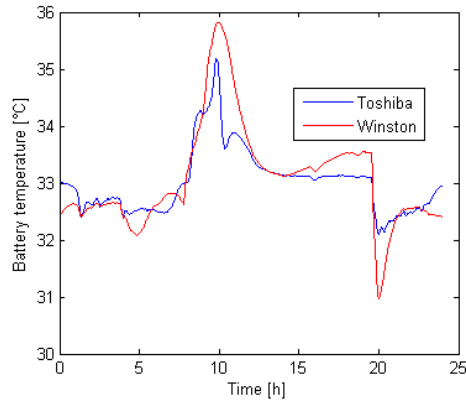
The two battery types, Toshiba and Winston, are compared. It is important to note that the load cycles are scaled to the capacity of the battery. So for both batteries to deliver the same current, one 100Ah Winston cell should be compared with five 20Ah Toshiba cells. Consequently, the current from a single Winston cell is five times higher than the current from a single Toshiba cell. The comparison of the battery temperature for both cells and the different load cycles can be found in figure 3.10. For the daily cycles, the current is small and the reversible heat is the largest part of the battery heat generation, since it varies linear with current. Since the current is larger for the Winston battery, the reversible heat factor is higher and the temperature variation is higher. For the medium duration and short cycle, the current is higher and the irreversible heat will become more important, since it varies quadratically with the current. Also here it is clear that the higher current causes higher temperature variation, but also the average temperature is higher for the Winston cells. To reduce the maximal temperature of the battery, five Toshiba batteries are preferred to one Winston battery, since the surface to transfer the heat to the environment is higher for the combination of the five batteries. However regarding space requirements, one Winston cell may be more compact than five Toshiba cells.

3.3.3 Comparison of natural and forced convective cooling

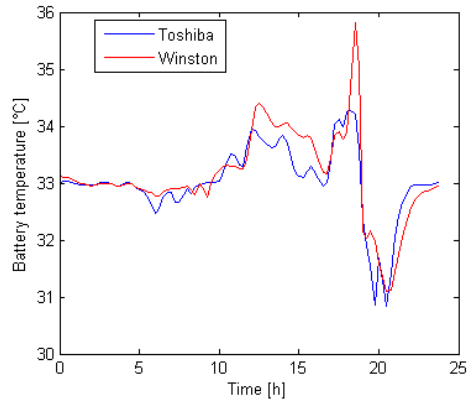
The heat transfer to the ambient air can be due to forced convection with a fan system, or through natural convection. Natural convection has a higher thermal resistance, which results in higher average temperatures and higher temperature variations. The results of the simulations for the different load cycles with both cooling methods are shown in figure 3.11. The Toshiba cells are used, with the same boundary conditions as in the previous paragraphs. The increase in cyclic temperature variation is most prominent in the daily cycles, while the increase in average temperature is more notable for the short cycles.

3.3.4 Comparison of current rates

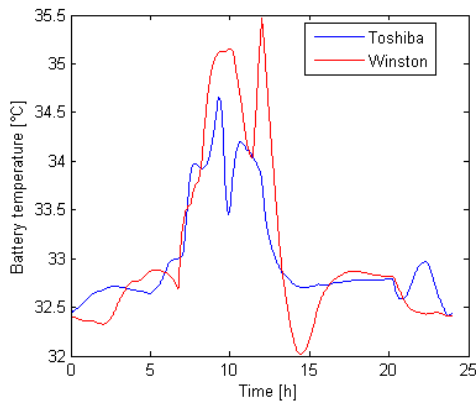
For the medium duration and short cycles, the RMS value of the current is varied between 0.5C, 1C and 3C which is the maximal continuous discharge current. The battery temperature for the two load cycles are shown in figure 3.12. For the medium duration cycle, the cycle length is dependent on the current, higher current result in shorter cycles. As concluded before, higher current rates lead to higher average battery temperatures and higher cyclic temperature variations.



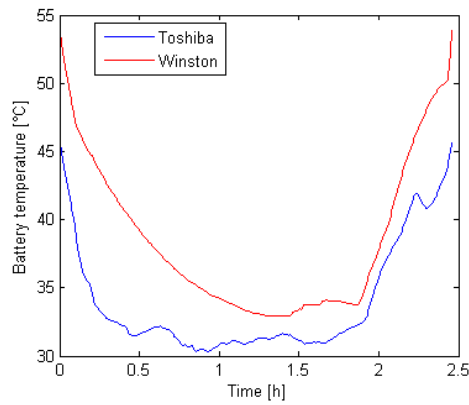
(a) Daily: construction



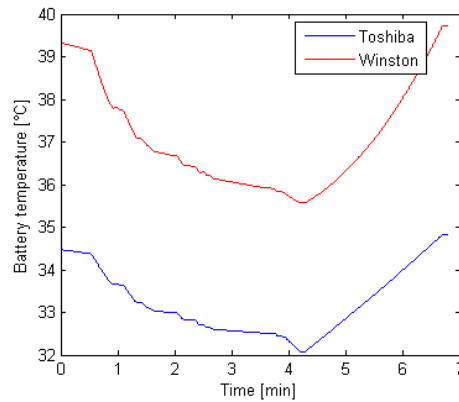
(b) Daily: household



(c) Daily: telecom

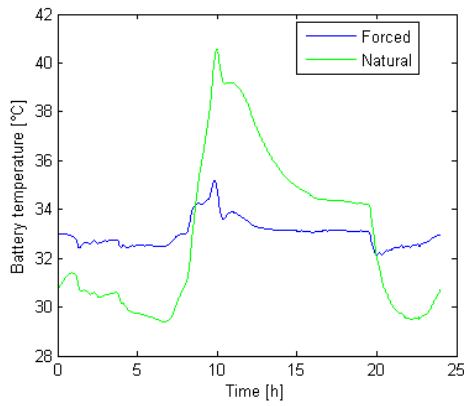


(d) Medium duration

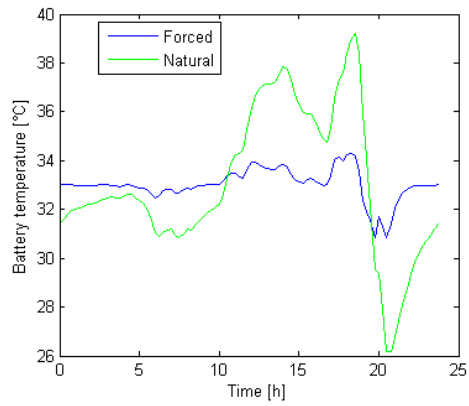


(e) Short cycle

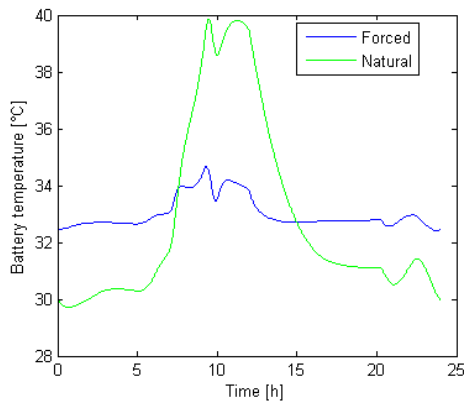
Figure 3.10: Battery temperature with no heat buffering and forced convection for the Toshiba and Winston battery for different load cycles, ambient temperature is 33°C



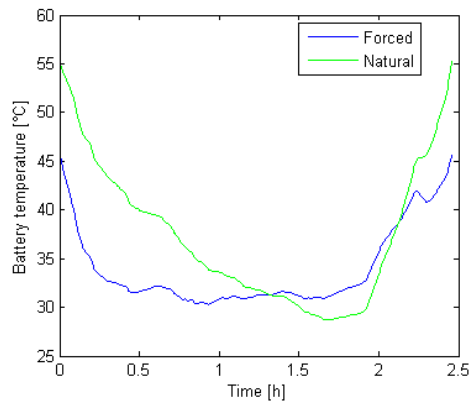
(a) Daily: construction



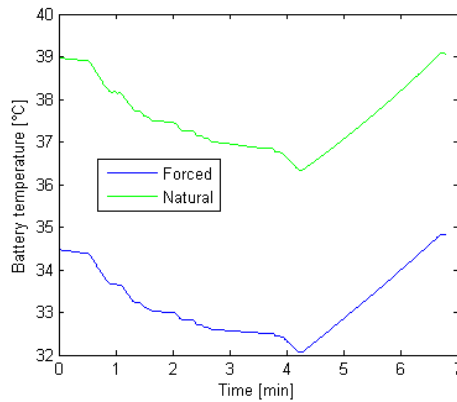
(b) Daily: household



(c) Daily: telecom



(d) Medium duration



(e) Short cycle

Figure 3.11: Battery temperature with no heat buffering and natural or forced convection with the Toshiba battery for different load cycles, ambient temperature is 33°C

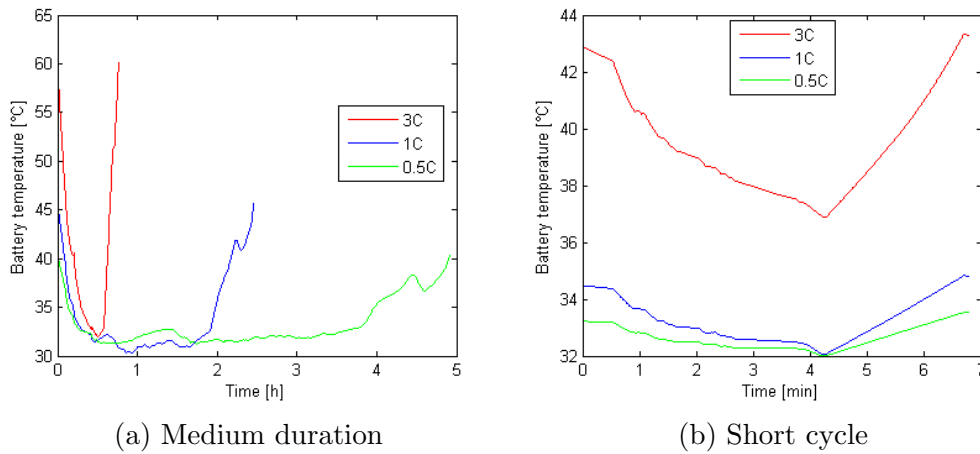


Figure 3.12: Battery temperature with no heat buffering and forced convection for the Toshiba battery for different load cycles and current rates, ambient temperature is 33°C

3.4 Sensitivity study: thermal management with heat buffering

This section presents the results of simulations of thermally buffered battery packs and the sensitivity of the battery temperature to different parameters. First, the influence of the discretization size of the PCM layer in the model is assessed. In further paragraphs, the influence of the PCM melting temperature, amount of PCM added, load cycle, battery type, current rate and cooling method is discussed. In the last section, the influence of adding thermally conducting structures to the PCM layer is simulated.

3.4.1 PCM layer discretization

In a finite element model, increasing the number of elements improves the accuracy of the model, but also increases the computational time needed for a simulation. An optimal amount of nodes is wanted, for which adding extra nodes results in a negligible improvement of the accuracy. Figure 3.13 shows the differences in the simulated battery temperature when adding an extra node in the PCM discretization. These simulations are for a Toshiba battery cell with 'RT35HC' PCM added. Both sides of the battery are enclosed in a layer of 3.1 mm thickness, which is representative for the thickness of the PCM layers that will be used in the following simulations. The outside of the PCM layer is cooled by natural convection. The load cycle used is the medium duration load cycle and the RMS current rate is 1C. By increasing the amount of nodes from three to four, the maximal difference in the simulated battery temperature is 0.11°C. If the number of nodes is increased from four to five, the maximal difference is 0.05°C or 0.35% of the

cyclic temperature variation. Variations in these orders of magnitude are not significant for the results and conclusions of these simulations, therefore the number of nodes in the following simulations is set to four.

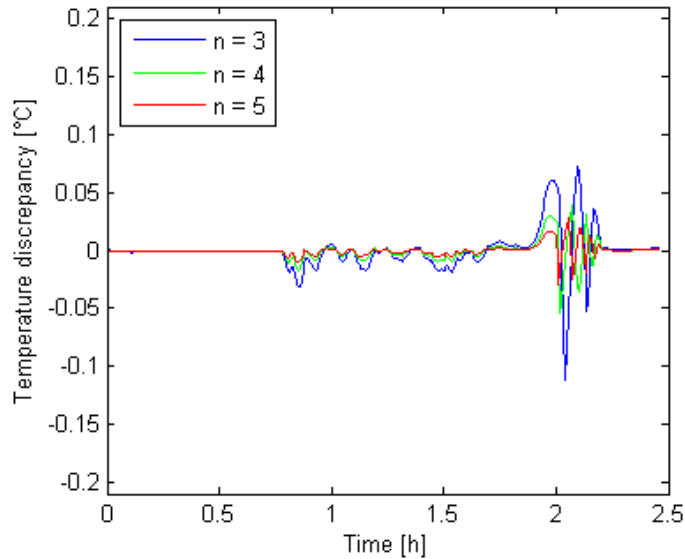


Figure 3.13: Difference in simulated battery temperature when increasing the number of nodes by one. Natural convection cooled Toshiba battery with a 'RT35HC' PCM layer of 3.1 mm thickness for medium duration load cycle, ambient temperature is 33°C.

3.4.2 Parameter sensitivity study

The base case for the sensitivity study is the Toshiba battery case with the medium duration load cycle. It is cooled by natural convection with an ambient temperature of 33°C and the RMS current rate is equal to 1C. The nominal thickness of the PCM layer t_{nom} used in the calculations is based on the heat generated by the battery. It is chosen such that the cyclic heat generated during the cycle is equal to the heat that is used to melt and solidify a PCM layer of that thickness. This is equivalent to full melting and solidification of all the PCM in an ideal case with the entire PCM mass in its melting range and negligible thermal capacitance of the battery. In the simulation, heat will also be buffered by changes in battery temperature and by sensible heat in changes in PCM temperature outside of the melting range. The nominal PCM thickness is thus dependent on the battery characteristics, PCM characteristics, load cycle and current rate.

To analyse the reduction in peak temperature, the difference between the peak temperature during a load cycle with no PCM and the peak temperature during a load cycle with PCM is used. Next to the absolute temperature difference, the relative reduction is also used which is defined as the the ratio of the absolute peak temperature

reduction to the temperature difference between the peak temperature in the cycle without PCM and the ambient temperature. Both absolute and relative peak temperature reductions can provide different insights, dependent on the boundary conditions (battery type, load cycle, etc.) of the simulation.

Melting temperature

The melting temperature (range) of the PCM used for thermal buffering is an important design parameter. Averaging over an entire cycle, the battery pack will generate heat and the system will be at a higher temperature than the ambient temperature. To take advantage of the latent heat of the PCM, it should therefore melt at a (at least slightly) higher temperature than ambient. Furthermore, if the melting point is chosen too low, all the PCM can be in liquid phase during the entire cycle. The latent heat is not used, and the PCM layer only acts as an additional thermal resistance for the cooling of the batteries. If the melting point is too high, the PCM will remain in its solid phase and a similar situation with little buffering and only an additional thermal resistance will occur.

Figure 3.14 illustrates the results of a simulation covering a range of PCM melting temperatures. The setup is a Toshiba battery with a nominal thickness PCM layer, natural cooling and the medium duration load cycle with RMS current 1C. The ambient temperature is 33°C. The peak battery temperature and the maximal cyclic temperature variation are also listed in table 3.3. The thermal buffering of the battery temperature is clearly visible by the plateau in the battery temperature around the PCM melting temperature. Both the peak temperature and temperature variation are reduced by adding any kind of PCM. The lowest peak temperatures are achieved with a PCM melting temperature near 39-40°C. For the lower melting temperatures, the peaks in temperature are buffered less than for the higher melting temperatures (7.4°C reduction at 37°C and 10.2°C at 42°C). Lower melting temperatures are better to buffer the lowest temperatures, while higher melting temperatures are better to buffer the highest (peak) temperatures, which is more useful for the batteries. For this reason, it is better to use a slightly higher PCM melting temperature in the design, since this will still offer adequate buffering and peak temperature reduction, even with higher battery loads than the design load. PCM with a melting temperature of 40°C is chosen as the standard for the following simulations with Toshiba cells, natural convection and the medium duration load cycle at 1C.

Table 3.3: Peak and temperature variation in function of PCM melting temperature

Melting T [°C]	No PCM	35	36	37	38	39	40	41	42
Peak T [°C]	55.3	50.5	49.7	47.9	45.2	43.8	43.9	44.5	45.1
T variation [°C]	26.6	15.5	13.8	11.3	7.9	6.1	8.8	10.7	12.1

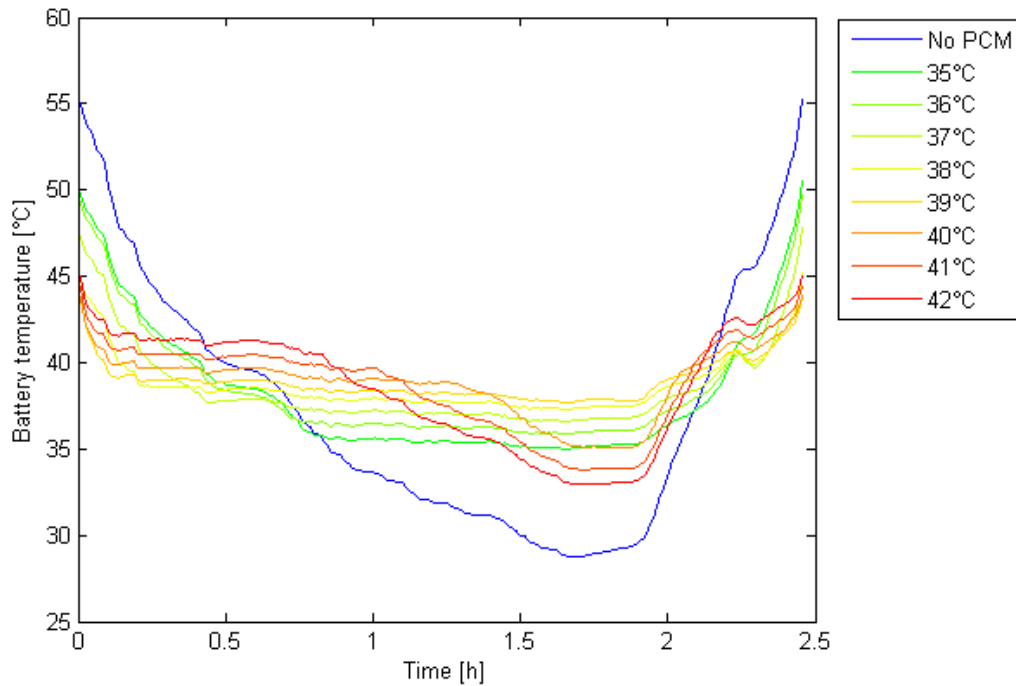


Figure 3.14: Battery temperature when using different PCM melting temperatures. Natural convection cooled Toshiba battery with a PCM layer of 3.1 mm thickness for medium duration load cycle, ambient temperature is 33°C.

PCM layer thickness

Next to the melting temperature of the PCM, the amount of PCM that is added to the battery pack is the most important design parameter. The battery temperature during a cycle for different amounts of PCM added to the sides of the battery is plotted in figure 3.15. The amount of PCM added is described as a function of the nominal thickness, as defined previously, which is in this case 3.1 mm. With a layer smaller than the nominal thickness, the PCM attains temperatures above and below its melting range during the load cycles, thereby reducing the thermal buffering effect. With the thickness higher than the nominal thickness, the additional PCM will stay in one phase (solid or liquid) during the entire cycle, not taking advantage of the latent heat of the phase change. The optimal thickness is thus close to the nominal thickness. For the lowest peak temperature, slightly less than the nominal thickness (90%-95%) is optimal. Adding up to twice the amount of PCM increases the peak temperature by less than 1°C, but reduces the compactness of the system. If more PCM would be added, thereby increasing the thickness to several centimetres, the thermal resistance of the PCM layer would cause the battery temperature to increase again.

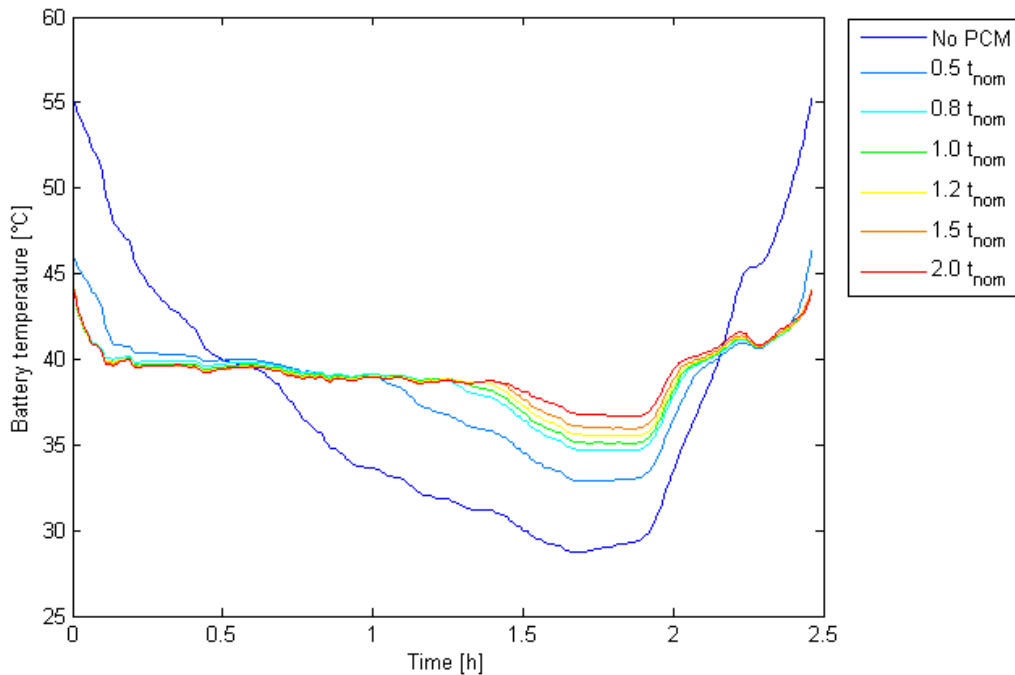


Figure 3.15: Battery temperature when using different PCM layer thicknesses. Natural convection cooled Toshiba battery with a 40°C melting point PCM for medium duration load cycle, ambient temperature is 33°C.

Battery type

The results of the medium duration load cycle simulation with the Winston battery are shown in figure 3.16. Natural convection is used for cooling, the ambient temperature is 33°C and a layer of nominal thickness of PCM is added, which is in this case 7.7 mm. As discussed before, the Winston battery heats up more due to the increased compactness (volume to outside surface). This results in more heat going through a smaller surface or a higher heat flux. Consequently, PCMs with a higher melting range have to be used for the thermal buffering system. Simulations with three different melting temperatures are shown in figure 3.16: 58°C, 60°C and 62°C. The PCM reduces the temperature variation during the cycle by 5°C or more, but the peak temperatures are only slightly decreased, up to 2.6°C. The smaller gains for the Winston battery compared to the Toshiba battery can also be explained by the low surface-to-volume ratio and the resulting higher heat fluxes. To buffer the higher heat fluxes, a larger layer of PCM is needed (7.7 mm compared to 3.1 mm for the Toshiba cells). This results in a larger thermal resistance between the battery and the ambient. This thermal resistance can be reduced by adding thermally conducting structures to the PCM, which is simulated in section 3.4.3. Furthermore, it might be more useful to use forced convection cooling (with or without

the addition of thermal buffering through PCMs) to reduce the average temperature of battery to a more optimal range.

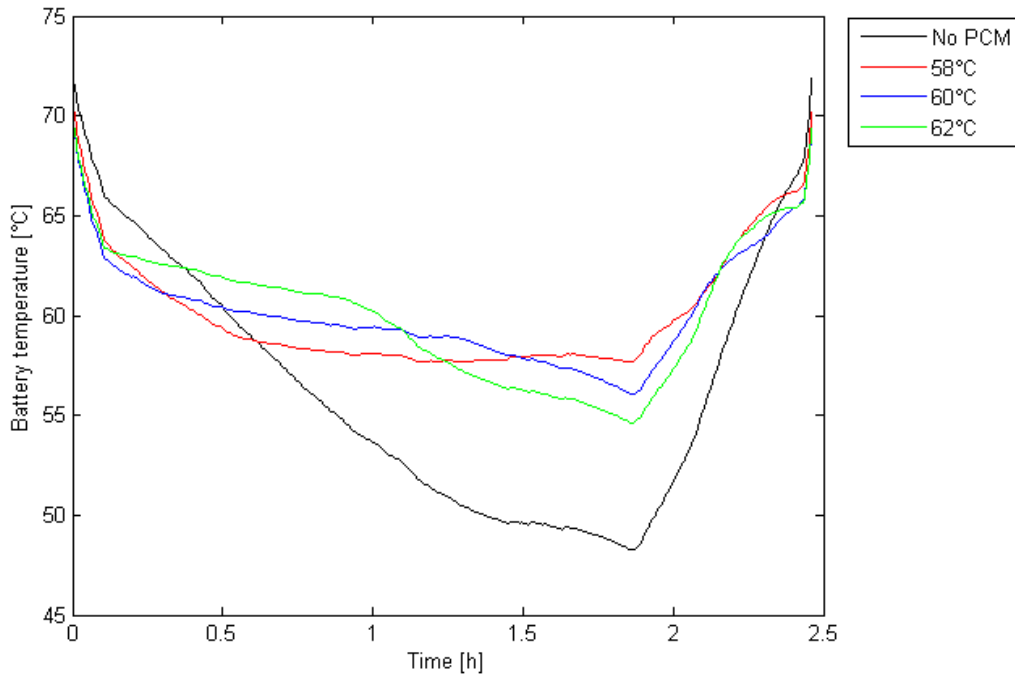


Figure 3.16: Battery temperature of thermally buffered natural convection cooled Winston battery with three different PCM melting points and the nominal PCM layer thickness for the medium duration load cycle, ambient temperature is 33°C.

Load cycle

For the medium duration load cycle, a well designed thermal buffer can reduce the peak temperature by 11.5°C or a reduction 52% of the peak temperature difference with the ambient, as shown in the previous sections. For the daily cycles, the absolute temperature differences are smaller because of the lower current, so less gains in absolute temperature differences are possible. However, since the main heat generation mechanism will be the reversible heat in these systems, buffering should be more useful when looking at the relative temperature gains. Figures 3.17 plot the battery temperature of a Toshiba battery cell with PCM thermal buffering and natural convective cooling. The PCM melting point is 34°C and the ambient temperature 33°C. The PCM layer thickness is nominal, which is respectively 2.6 mm, 2.6 mm and 2.7 mm for the construction, household and telecom load cycles. The peak temperatures are reduced by 5.5°C, 3.8°C and 4.4°C or relatively by 72%, 61% and 64% respectively.

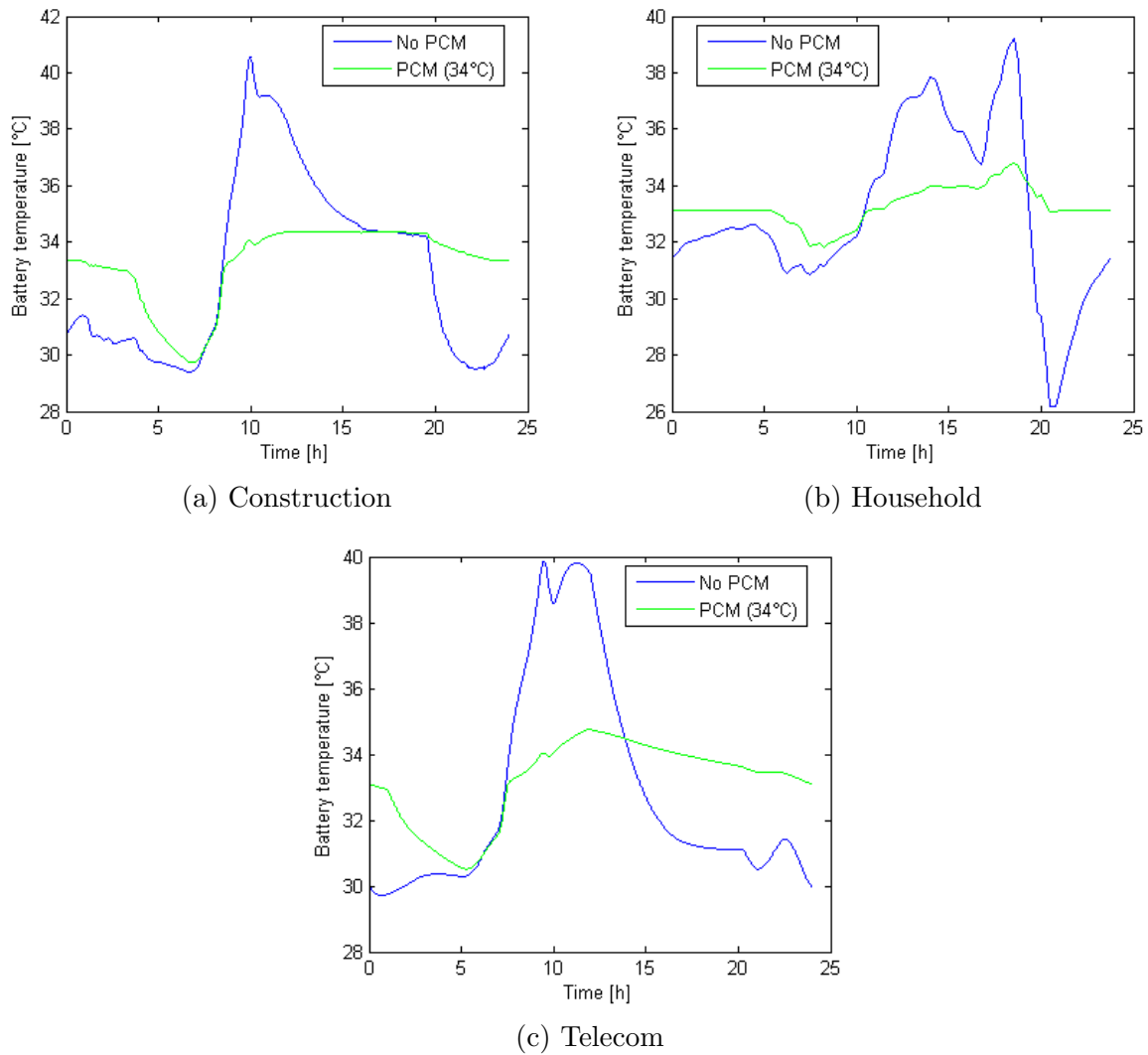


Figure 3.17: Battery temperature of thermally buffered natural convection cooled Toshiba battery with a 34°C melting point PCM and the nominal PCM layer thickness for three daily load cycles, ambient temperature is 33°C.

For the seven minute load cycle, the temperature variation during the cycle with no buffering is less than 3°C, so the absolute gains that can be achieved are smaller than for the other cycles. The battery temperature with and without a PCM layer is shown in figure 3.18. Adding the PCM layer decreases the battery temperature variation during the cycle but also increases the average temperature during the cycle. In this case, this results in an increase of the peak battery temperature. For the short cycle, adding a PCM layer is not beneficial to reduce the peak temperature.

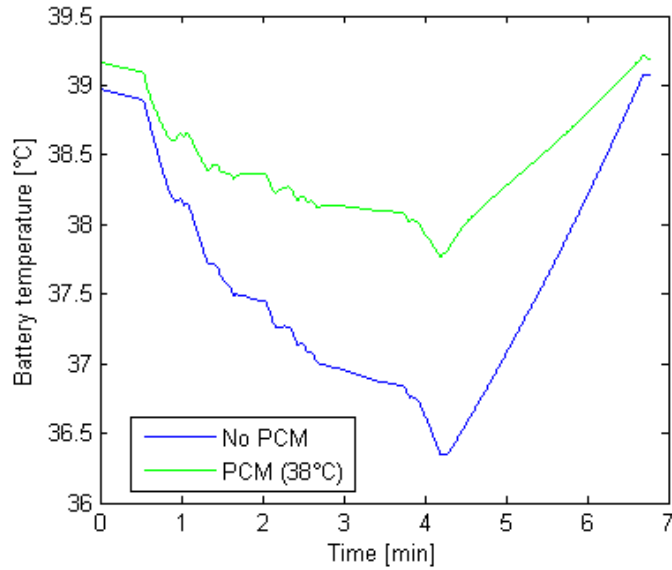


Figure 3.18: Battery temperature of thermally buffered natural convection cooled Toshiba battery with a 38°C melting point PCM and the nominal PCM layer thickness for the short load cycles, ambient temperature is 33°C.

Current rate

Altering the current rate has two major effects on the heat generation behaviour of the battery. When increasing the current, both the irreversible and reversible heat increase, leading to a larger heat flux. Next to this, since the irreversible heat varies with the current squared while the reversible heat varies linearly with the current, the irreversible heat will become more dominant with increasing current. Figure 3.19 illustrates the effect of the current rate on the thermal buffering system design. For the maximal current rate (3C), the optimal melting temperature of the PCM is around 65°C. The peak temperature can be reduced by 6.6°C. The relative reduction (scaled to the difference between peak and ambient temperature for the simulation with no heat buffering) is only 14%, since the average temperature of the battery is around 58.7°C due to the high irreversible heat. For the cycles with high current, using forced convection (with or without PCM thermal buffering) is more suited to reduce the temperatures closer to the optimal range for batteries. When regarding the low current (0.5C) cycle, The melting temperature that is used is 35°C, which is a lot closer to the ambient temperature. The peak temperature is reduced by 11.9°C and relatively by 69%. The higher percentage of reduction is related to the higher fraction of reversible heat that is generated, which is more suitable for buffering.

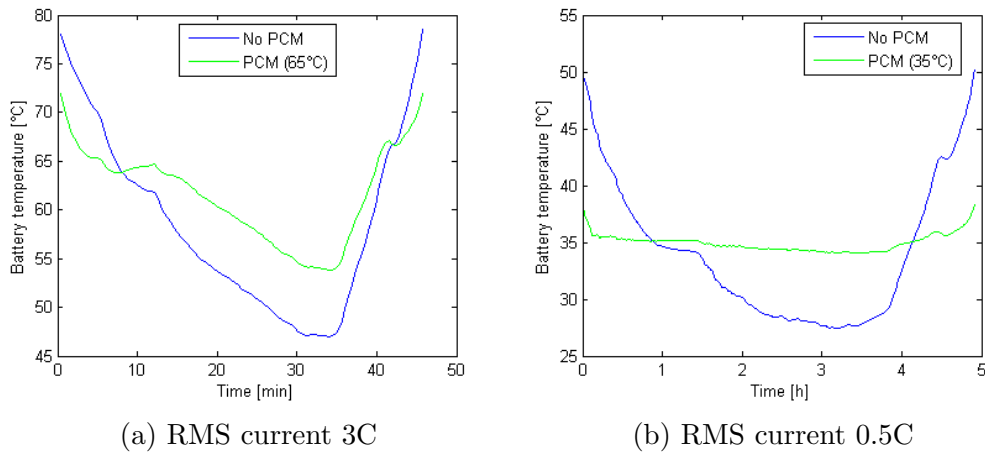


Figure 3.19: Battery temperature with nominal thickness PCM layer and natural convection for the Toshiba battery for the medium duration load cycles and varying current rate, ambient temperature is 33°C

Natural and forced convective cooling

By using forced convection instead of natural convection, the peak and average temperature are reduced by 9.7°C and 3.5°C respectively. However, the temperature variation during the cycle is still 15.3°C, so adding PCM can still be beneficial. This is valid for the medium duration load cycle, whereas in the other cycles the temperature variations are always smaller than 3°C. Figure 3.20 shows the results of the simulation with forced convection cooling and the addition of PCM with a melting point of 35°C. Compared to the forced cooling case without buffering, the peak temperature is reduced by 6.3°C or relatively by 50%. For this case, a combination of thermal buffering through PCMs and forced convection cooling can be effective to reduce peak and average temperatures.

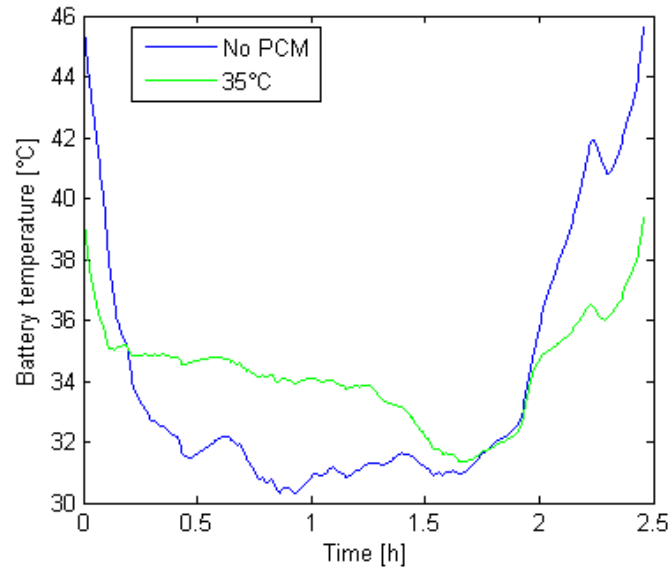
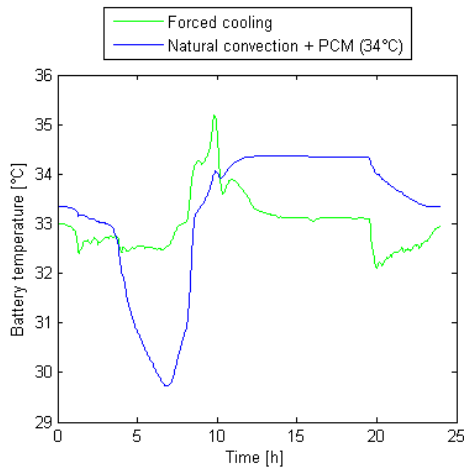


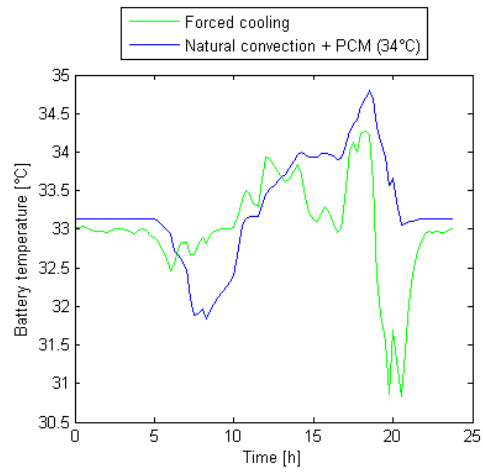
Figure 3.20: Battery temperature of thermally buffered forced convection cooled Toshiba battery with a nominal PCM layer thickness with 35°C melting point for the medium duration load cycles, ambient temperature is 33°C.

Comparing simulations of natural convection cooled batteries with thermal buffering to forced convection cooled batteries with no buffering is done to see if PCM thermal buffering can be an effective alternative for a forced cooling system. This can be beneficial because it eliminates the need for maintenance of a fan, does not require an energy input and can be more compact. Figure 3.21 plots the battery temperature for the three daily load cycles and the medium duration load cycle (the short cycle is omitted since adding PCM is not beneficial for the battery temperature). For the daily cycles, the peak temperatures of the battery are within 1°C when comparing forced cooling to PCM thermal buffering. For these load cycles, using forced cooling or PCM thermal buffering is interchangeable. For the 2.5 hour cycle, the peak temperature when using PCM thermal buffering is 1.7°C lower than the peak temperature with forced convection cooling. The average battery temperature in the thermally buffered system is 4.9°C higher than in the forced convection cooled system, due to the difference in thermal resistance. Also for the medium duration load cycle, both forced cooling and thermal buffering with natural convection cooling are effective to reduce the battery peak temperatures.

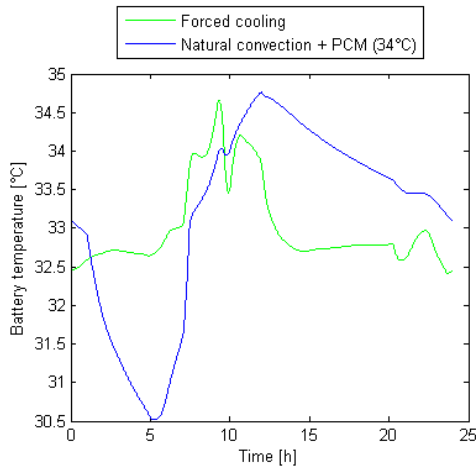
A side remark to be made when comparing forced cooling with PCM thermal buffering is that the design and performance of the buffering system is very dependent on the load cycle and current rate. This makes the PCM system less flexible. If the battery load and current rates are highly variable, it might be more opportune to utilize forced convection cooling over PCM thermal buffering.



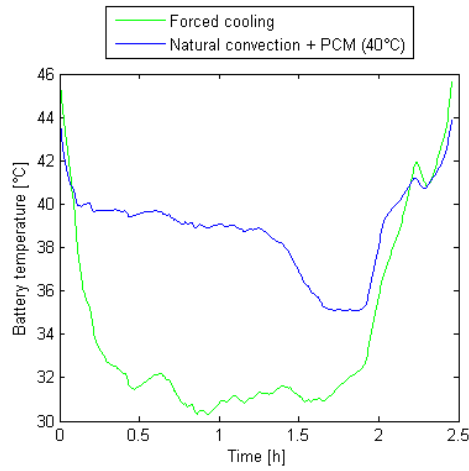
(a) Daily: construction



(b) Daily: household



(c) Daily: telecom



(d) Medium duration

Figure 3.21: Comparison of battery temperature with no heat buffering and forced convection cooling with heat buffering and natural convection cooling. Toshiba battery for different load cycles with a nominal thickness PCM layer with different melting temperatures, ambient temperature is 33°C

3.4.3 Thermal conductivity enhancement

As stated in chapter 2, thermally conducting structures can be used to reduce the thermal resistance created by the PCM layer. Three structures are studied here: metal foam, expanded graphite and carbon fibres. The base case (Toshiba cell, natural convection, medium duration load cycle, RMS current 1C and ambient temperature 33°C) is simulated with a thermal buffer with the three structures, as well as three other cases. These cases result from the previous simulations, having the most challenging boundary conditions for the thermal buffering system. These three simulations include: utilizing the Winston battery instead of the Toshiba battery, loading the battery with the short load cycle instead of the medium duration cycle and using the maximal current rate instead of 1C.

Base case

The battery temperature for the base case is shown in figure 3.22. The different cycles shown are no buffering, buffering with pure PCM and buffering with a combination of PCM and metal foam, expanded graphite and carbon fibres. The PCM layer with a nominal thickness is used, which is 3.1 mm for the pure PCM layer and 3.3 mm, 3.5 mm and 3.4 mm for the metal foam, expanded graphite and carbon fibre mixture respectively. The thickness of the layer has to be increased to achieve equal latent heat, since less PCM is present in a layer with equal thickness. As shown in the previous sections, thermal buffering with PCM reduces the peak temperature by 11.4°C. Adding a MF, EG or CF structure to the PCM causes an additional reduction of the battery temperature by 2.9°C, 2.4°C and 2.4°C respectively.

Winston battery

Adding thermal buffering reduced the peak battery temperature of the Winston battery cell with 2.6°C. Figure 3.23 plots the battery temperature during the cycle with structures added to the PCM. The nominal thickness is 7.7 mm for the pure PCM buffering, while it is 8.2 mm, 8.6 mm and 8.3 mm for the MF, EG and CF PCM mixtures. An additional peak temperature reduction of 7.2°C, 4.8°C and 4.8°C is acquired with the three respective mixtures.

Short load cycle

The peak temperature of the battery under the seven minute load cycle was not reduced by adding PCM, instead it increased. Adding structures to the PCM slightly reduces the temperatures compared to the pure PCM case, but it does not reduce the peak

temperature when compared to the case without thermal buffering.

High current rate

When the battery is loaded with the maximal current rate, the peak temperature is reduced by 6.6°C by the addition of thermal buffering with pure PCM. Figure 3.25 displays the battery temperature with no thermal buffering, thermal buffering with pure PCM and thermal buffering with a mixture of PCM and MF, EG and CF. The thickness of the PCM layer is 3.9 mm for pure PCM, while it is 4.1 mm, 4.3 mm and 4.2 mm for the mixture of PCM and MF, EG and CF respectively. By adding a structure to the PCM, the peak battery temperature can be reduced by another 5.7°C, 4.3°C, 4.3°C for the MF, EG and CF respectively.

Summary

The addition of a thermally conducting structure to a PCM layer reduces the peak temperature and average temperature of the battery. This is related to the reduction of the temperature gradient over the PCM layer by the increase of the effective thermal conductivity of the PCM-structure combination. The benefits of using the structure are highest for the cases where the PCM layer is thickest, since this relates to the highest thermal resistances introduced by the PCM layer. This is most clear in the simulation with the Winston battery, where the PCM layer thickness is around 8 mm, compared to 3-4 mm in the other cases. In the other cases the benefits when compared to pure PCM are less outspoken. For the seven minute load cycles, thermal buffering does not reduce the peak temperature with or without structure. Even with the enhanced thermal conductivity, the PCM layer reacts too slowly to the variations of temperature in this time-scale to be able to buffer it sufficiently.

Another remark to be made about the feasibility of implementing these structures is the stability in thin layers (< 10 mm). For metal foam, the pores should be smaller than the thickness or the foam loses its structural strength. Metal foam layers with a thickness smaller than 10 mm will be hard to manufacture. For the expanded graphite, the structural strength will also decrease with the thickness. A thickness of 10 mm is the minimal commercially available. For carbon fibres, care has to be taken that the fibres are equally distributed in the PCM layer when using such thin layers. For all the possible structures with thin PCM layers, the benefits of temperature reduction may not outweigh the disadvantage of increased complexity and cost when compared to pure PCM.

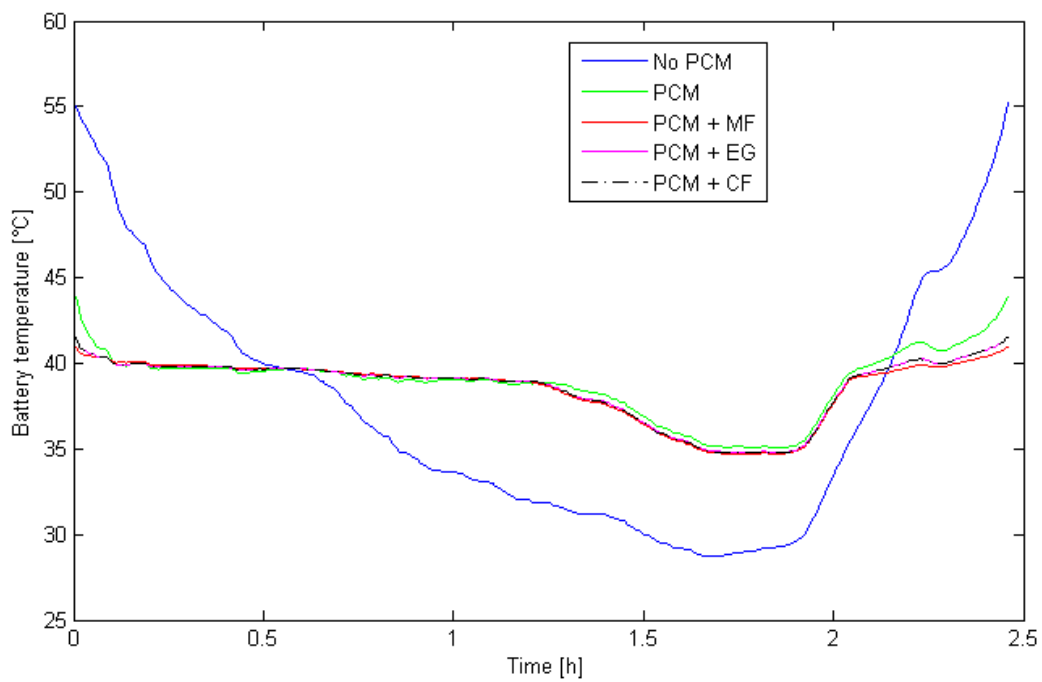


Figure 3.22: Battery temperature with no thermal buffering, PCM thermal buffering and PCM with conducting structure (MF, EG and CF) thermal buffering. Natural convection cooled Toshiba battery with nominal thickness PCM with melting point 40°C and medium duration load cycle with RMS current 1C, ambient temperature is 33°C.

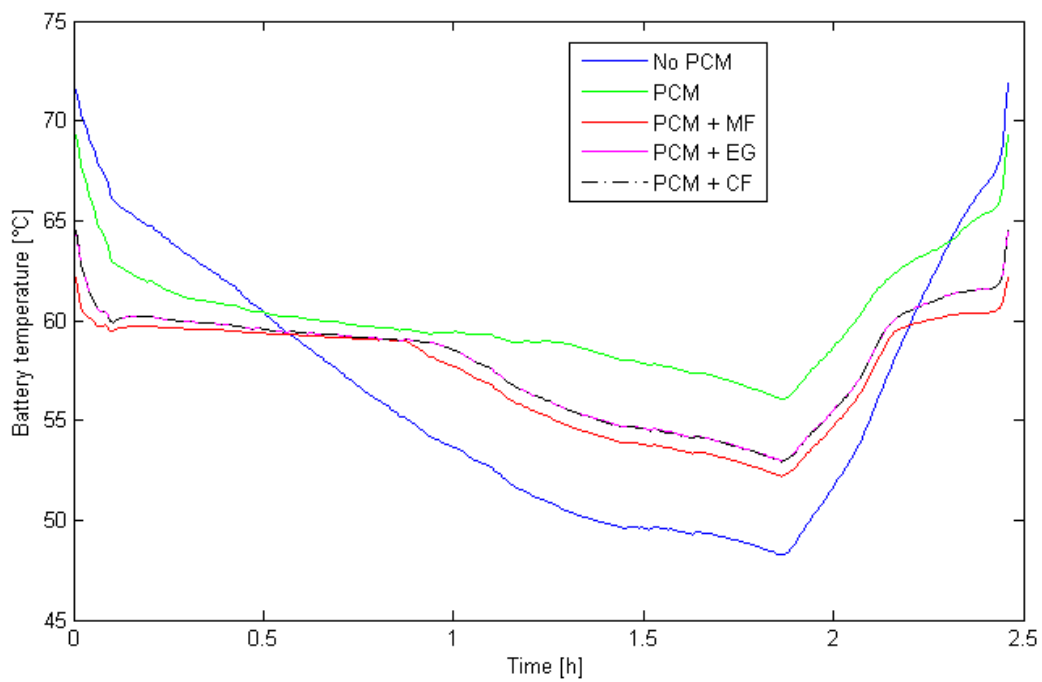


Figure 3.23: Battery temperature with no thermal buffering, PCM thermal buffering and PCM with conducting structure (MF, EG and CF) thermal buffering. Natural convection cooled Winston battery with nominal thickness PCM with melting point 60°C and medium duration load cycle with RMS current 1C, ambient temperature is 33°C.

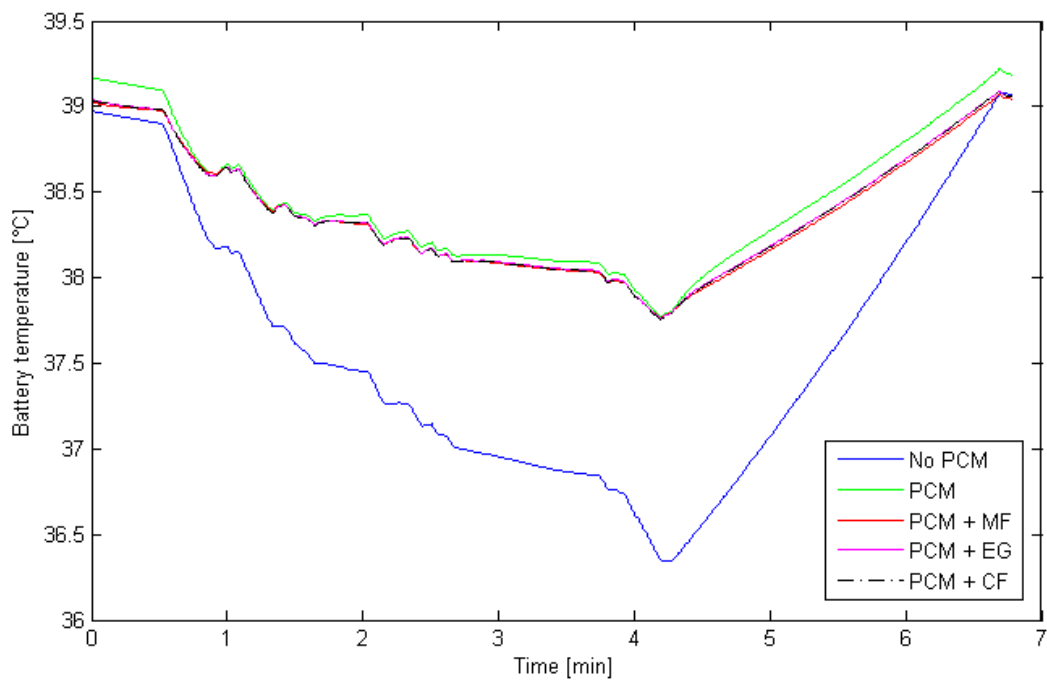


Figure 3.24: Battery temperature with no thermal buffering, PCM thermal buffering and PCM with conducting structure (MF, EG and CF) thermal buffering. Natural convection cooled Toshiba battery with nominal thickness PCM with melting point 60°C and seven minute load cycle with RMS current 1C, ambient temperature is 33°C.

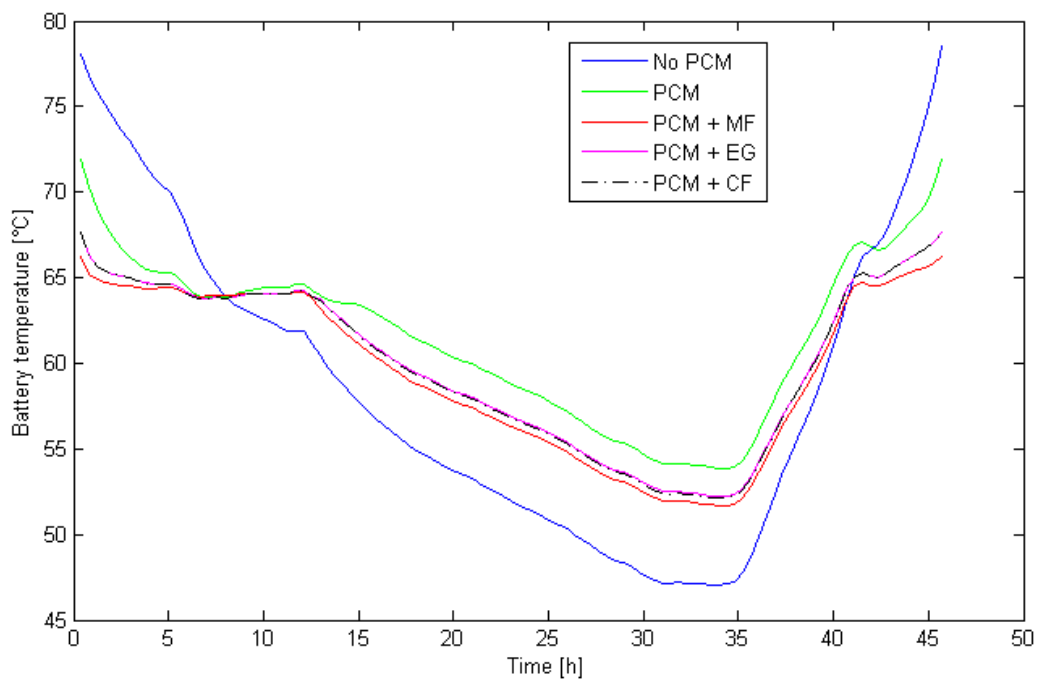


Figure 3.25: Battery temperature with no thermal buffering, PCM thermal buffering and PCM with conducting structure (MF, EG and CF) thermal buffering. Natural convection cooled Toshiba battery with nominal thickness PCM with melting point 40°C and medium duration load cycle with RMS current 3C, ambient temperature is 33°C.

Chapter 4

Selection of battery thermal management system

Using the results from the battery simulations of the previous chapter and general knowledge on heat transfer phenomena, a methodology to design the thermal management system for a battery pack is formulated. The methodology aims to provide guidelines and straightforward calculations to design the thermal management system, removing the need for complex and time-consuming simulations as were done in the previous chapter. The goal of this design methodology is to reduce the peak battery temperature, although a design with thermal buffering can have several other advantages. Other benefits can be reducing the temperature variation, avoiding very low temperatures and improving the safety of the battery pack. These effects are not the goal of this methodology, but can be positive side effects of adding a PCM thermal buffering system.

The methodology takes into account the possibility of natural or forced convection and possible thermal buffering through the use of PCMs with or without thermally conducting structure. It is aimed at prismatic cells with one of the dimensions (thickness) typically being smaller than the others two (length and height). However, it can also be expanded to cylindrical battery cells with some restrictions. In the case of the addition of a PCM thermal buffer, guidelines are provided for the choice of the melting temperature and for the amount of PCM that should be added. At the end of this chapter, a flowchart of the methodology is provided in figure 4.1. In the following sections, next to the general guidelines, a representative example will be elaborated on.

4.1 Determine cell type and configuration

The load characteristics should be known to determine the battery type and configuration (number of cells, series and/or parallel). The battery pack can be limited by either the

instantaneous power needed or by the energy needed during one cycle. If the load is very variable or not well known, the electrical and thermal design should be based on the worst case, which is the highest power and/or energy use. If the design is limited by the thermal behaviour (excessive temperatures), it is advisable to choose a battery cell with a high outer surface to power or energy rate. The battery choice can be reiterated after the thermal calculations if this is required to achieve acceptable battery temperatures.

Example

The load cycle in the example is chosen as the medium duration load cycle with RMS current rate equal to 20 A. This cycle is chosen to be able to compare the example with the simulations, since most simulations were done with this load cycle. The Toshiba cells are chosen since they have a large surface to energy ratio. The number of cells and configuration of the cells is not further specified, since this only influences the electrical design, not the thermal.

4.2 Determine battery properties

Several battery characteristics are readily available from the data sheet: the outside surface, the battery mass and usually the internal resistance. Next to these parameters, the entropic coefficient and specific heat capacity of the battery have to be known. If there is no data from the manufacturer, data can either be gathered for a similar battery from scientific literature or it can be measured.

Nieto et al. measured the thermal characteristics of a prismatic Li-ion cell (model TENERGY 30123) [147]. The values for the specific heat capacity (1015 J/kgK) and the average value of the entropic coefficient (-0.36 mV/K) can be used as an estimate for design calculations.

For more accurate simulations, the internal resistance and the entropic coefficient can be determined experimentally for the battery type used in the system. The internal resistance can be determined as the difference of the open-circuit voltage and the cell voltage during discharge divided by the discharge current. The entropic coefficient can be determined by measuring the variation of the open-circuit voltage when the temperature of the battery is varied in a climate chamber. The entropic coefficient is the ratio of the open-circuit voltage difference to the temperature difference. For an accurate representation of the entropic coefficient, measurements should be done for varying state of charge, since this will have an effect on the entropic coefficient.

Example

The outside surface (246 cm^2 , assuming only the side surface are used for cooling) and mass (515 g) of the Toshiba battery are known from the data sheet. The internal resistance is measured and equal to $1.3 \text{ m}\Omega$ at one temperature. The used specific heat capacity and average entropic coefficient are gathered from literature [147].

4.3 Determine cooling method

For cooling of the battery pack, two possibilities are taken into account: through natural or free convection (no fans) or forced convection (with fans). The choice is dependent on the heat transfer coefficient needed, which is higher for forced convection than for natural convection. The needed heat transfer coefficient can be estimated using equations 4.1 and 4.2. In these equations, Q_{irr} is an estimation of the irreversible heat, R is the internal thermal resistance, I_{RMS} is the RMS current rate during the load cycle, h_{req} is the estimated required heat transfer coefficient, A is the surface area of the battery, T_{avg} is the desired average battery temperature and T_{amb} is the ambient temperature. If the load cycle is variable, the estimation should be done for the worst case (highest current and highest ambient temperature).

$$Q_{irr} = RI_{RMS}^2 \quad (4.1)$$

$$h_{req} = \frac{Q_{irr}}{A(T_{avg} - T_{amb})} \quad (4.2)$$

If the estimated heat transfer coefficient is lower than $5 \text{ W/m}^2\text{K}$, natural convection can be used. The actual heat transfer coefficient can be calculated using equations 3.7 to 3.9. Air properties can be gathered using the open-source fluid property database CoolProp. If the calculated heat transfer coefficient is lower than the estimated needed value, forced convection should be used instead.

If the estimated needed heat transfer coefficient is higher than $5 \text{ W/m}^2\text{K}$, forced convection is advisable. In this case, the heat transfer coefficient is dependent on the air velocity. Equations 3.10 to 3.14 can be used to determine the velocity that is required to achieve the desired heat transfer coefficient. Since the accuracy of heat transfer correlations is typically around 20%, it is advisable to choose the air velocity related to a heat transfer coefficient that is 20% higher than the estimated value as a margin of safety.

In further use of the heat transfer coefficient for design calculations, it is best reduced by 20% to take into account the inaccuracies in the heat transfer correlation and thereby creating a safety margin for the design.

Example

The RMS current is 20 A (or 1C) for the Toshiba cell. The estimated irreversible heat generation per cell is 0.52 W. The maximal desired temperature is chosen as 40°C and the ambient temperature as 33°C. This results in a needed heat transfer coefficient of 3.02 W/m^2K . Natural convection should therefore suffice for this case. Calculating the actual natural convection heat transfer coefficient results in 3.95 W/m^2K , reducing this value by 20% for safety results in 3.16 W/m^2K .

4.4 Determine buffering method

4.4.1 Estimate temperature variation

To determine if thermal buffering through PCMs is useful for a specific battery pack application, the temperature variation of the batteries during one cycle should be estimated. The model described in the previous chapter can be used to get an accurate representation of the temperature variation. For design purposes, an estimation can also be made by considering the two limiting factors on this temperature variation: a limitation due to the thermal mass of the battery and a limitation due to the cooling of the battery. The limiting temperature variation by the thermal mass of the battery ΔT_1 can be estimated with equations 4.3 and 4.4. The limiting temperature variation due to the cooling ΔT_2 can be estimated with equation 4.5. Q_{rev} is an estimation of the reversible heat, $\frac{dE}{dT}$ is the entropic coefficient, T an estimation of the battery temperature in K, ΔT is the estimated variation of the battery temperature during the cycle, m is the mass of the battery, c is the specific heat capacity of the battery, t_{cycle} is the length of one charge-discharge cycle and h is the calculated heat transfer coefficient (with safety margin).

$$|Q_{rev}| = \left| \frac{dE}{dT} \right| T I_{RMS} \quad (4.3)$$

$$\Delta T_1 = \frac{|Q_{rev}| \frac{t_{cycle}}{2}}{mc} \quad (4.4)$$

$$\Delta T_2 = \frac{2|Q_{rev}|}{hA} \quad (4.5)$$

Since both temperature variations are limiting cases, only the lower of both calculation should be regarded. Both calculated values should be larger than the actual temperature variation. If the temperature variation is larger than 10°C, adding a thermal buffer with PCM can be useful to reduce the temperature variation and peak temperature.

If the temperature variation is lower than 10°C or the load cycle is highly variable, it is preferred not to use a PCM buffering system. The upper limit for the peak temperature T_{peak} can be estimated with equation 4.6. If this upper limit is too high for the battery cells, the cooling has to be improved. If natural convection was used, the design should be switched to forced convection. The air velocity determination from the previous section has to be renewed, but utilizing equation 4.7 where the sum of the two heat effects is used and the desired average battery temperature is replaced with the desired maximal battery temperature T_{max} .

$$T_{peak} = T_{amb} + \frac{Q_{irr}}{hA} + \frac{\min(\Delta T_1, \Delta T_2)}{2} \quad (4.6)$$

$$h_{req} = \frac{Q_{irr} + |Q_{rev}|}{A(T_{max} - T_{amb})} \quad (4.7)$$

Example

With the battery temperature at 40°C, the reversible heat generation during the charge or discharge cycle is estimated as 2.25 W. The estimated temperature variation limited by the thermal mass of the battery is 19.1°C, while the limitation by cooling is 58.0°C. Since 19.1°C is higher than 10°C, a thermal buffer with PCM will be added in the design.

4.4.2 Determine melting temperature

The melting temperature should be close to the average battery temperature, resulting in a PCM layer that is constantly melting and solidifying. From the simulations in the previous chapter, it results that it is safer to design the PCM melting temperature slightly higher than the average temperature, since this will result peak temperature buffering even if the load is slightly higher than expected. The optimal melting temperature T_m can be estimated using equation 4.8. When using the heat transfer coefficient with the 20% safety margin, the resulting melting temperature will be slightly higher than the average temperature which is recommendable.

$$T_m = T_{amb} + \frac{Q_{irr}}{hA} \quad (4.8)$$

With the determined melting temperature, a PCM can be selected from the list provided in chapter 2 or from other sources.

Example

For the example case, equation 4.8 yields a PCM melting temperature of 39.7°C. The PCM 'A40' of PCM products with melting temperature 40°C is selected.

4.4.3 Determine PCM mass and layer thickness

The mass of the PCM that is needed per battery cell is directly related to the amount of heat that needs to be stored during the cycle by the latent heat h_{lat} of the PCM. The latent heat can be retrieved from the data sheet of the PCM manufacturer. The mass of PCM (m_{PCM}) needed is subsequently estimated using equation 4.9.

$$m_{PCM} = 1.5 \frac{|Q_{rev}| \frac{t_{cycle}}{2}}{h_{lat}} \quad (4.9)$$

The factor 1.5 in equation 4.9 is added to account for two effects. The first effect is that, depending on the current profile, parts of the irreversible heat also need to be buffered. This increases the amount of PCM needed. Secondly, the simulations show that adding more PCM only slightly increases the peak temperature but allows for significantly more buffering. However, if compactness is one of the main concerns in designing the thermal management system, the factor 1.5 can be removed from the equation.

The PCM mass can be applied to the battery pack in several geometries. As in the simulations, it can be used to cover the entire side surfaces of the battery. This is beneficial for the buffering effect, but can also hamper the cooling of the battery cells. A configuration with part of the surface covered by the buffer and the other part in direct contact with the cooling air is also feasible. It is preferred to contain the PCM in a casing, avoiding leaks and possible material incompatibilities. If the PCM is used in direct contact with the battery and other materials, care must be taken to test the compatibility and leak-tightness of all components. Another important aspect of the buffer design is to allow space for the PCM to expand, which will occur during melting (volume increases of 10% are typical).

Adding a conducting structure to the PCM layer is only needed (and feasible) if the thickness of the layer is larger than 10 mm. If the entire side surface of the battery is used, equation 4.10 can be used to determine the thickness t_{PCM} of the PCM layer. This equation can be used for cylindrical cells if the thickness is an order of magnitude smaller than the diameter of the battery. The density ρ of the solid PCM can be retrieved from the data sheet of the specific PCM.

$$t_{PCM} = \frac{m_{PCM}}{\rho A} \quad (4.10)$$

Example

The latent heat of 'A40' is 230 kJ/kg, which results in a needed PCM mass per cell of 65.1 g. When covering the entire side surfaces with a PCM layer, the resulting thickness of the layer is 3.3 mm (with a solid density of the PCM of 810 kg/m^3). The thickness is less than 10 mm, so a thermally conducting structure is not used.

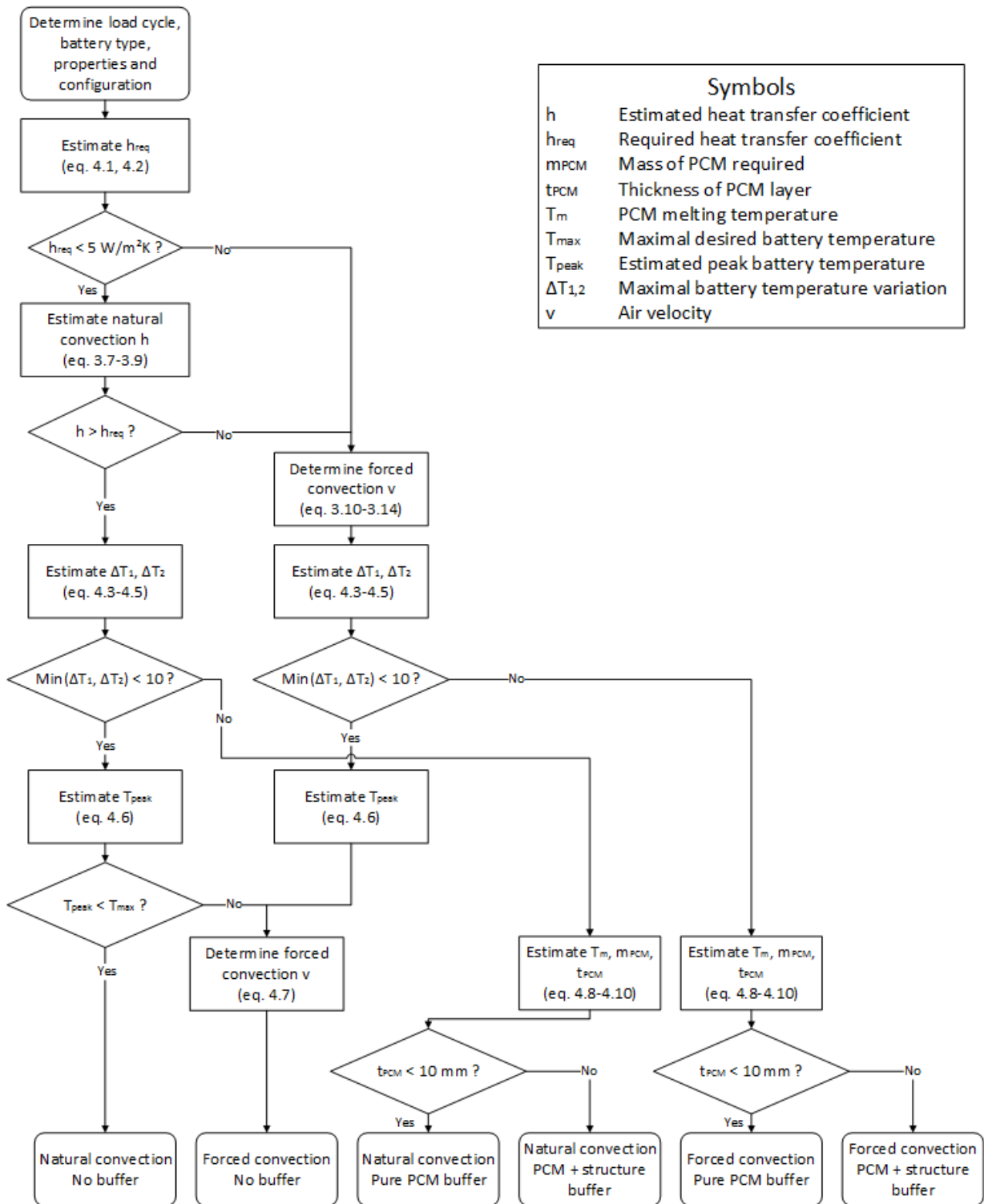


Figure 4.1: Flowchart for the design methodology of a battery thermal management system.

Chapter 5

Conclusion

This document analyses the thermal behaviour or the thermal management of battery packs, with a special focus on heat buffering through the use of phase change materials. Heat buffering is mainly used to reduce peak temperatures of the battery, but also has other advantages such as a reduced temperature variation during the cycle and less extreme cold temperatures. Phase change materials in a wide range of melting temperatures are available on the market, however their thermal conductivity is always limited (usually $< 1 \text{ W/mK}$). Several methods have been proposed to enhance the thermal conductivity, usually through the addition of thermally conducting structures. The most viable structures to use are metal foam, expanded graphite and carbon fibres. All three these structures combined with PCM can increase the effective thermal conductivity by a factor 4-10 compared to the thermal conductivity of pure PCM.

A one-dimensional thermal simulation model has been constructed to analyse the thermal behaviour of battery packs under different boundary conditions and using several thermal management systems. The influence of the different boundary conditions can be summarized as follows:

- From the simulations, it was concluded that the **load cycle** has a big influence on the battery temperature and that it is mainly determined by two factors: the duration of one cycle and the current rating of the cycle. Three categories of the duration of one cycle are determined.
 - The first load cycle is a **long cycle**, in which the battery is fully charged and discharged but the current is lower than maximal allowed current. The low current results in battery temperatures close to ambient, so natural convection is preferred. The temperature variation of the battery can be more than 10° C , which allows for the use of a thermal buffer.
 - Secondly a **medium duration cycle** is analysed, in which the battery is fully charged and discharged and the current is at or close to the maximal current.

The medium duration cycles result in higher battery temperatures and higher temperature variations. A thermal management system with thermal buffering is preferred. Natural or forced convection can be used, depending on the other boundary conditions.

- Finally a **short cycle** is a possibility, which draws the maximal or close to the maximal current from the battery but uses only part of the total battery energy during the cycle. For the short cycles, the temperature variation is small and thermal buffering is not useful. Also here forced or natural convection can be used, depending on the other boundary conditions.
- The simulations also show that using a **battery type** with a large outside surface compared to the power or energy of the battery is better for the thermal management system, both with or without thermal buffering.
- Increasing the **current** increases both the peak and average temperature and the temperature variation during the cycle, which results in a shift in desired thermal management system from natural to forced convection and from no buffering to PCM buffering.

A comparison has been made between forced convection cooling with no thermal buffering and natural convection cooling with thermal buffering. For several sets of boundary conditions, both systems achieve similar results in reduction of the peak battery temperature. It can therefore be feasible to replace an active cooling system with a passive thermal buffering system, which can be advantageous for maintenance and reduction in auxiliary power. Nonetheless, a forced convection cooling system is more flexible relating to variations in load cycle and current rate.

Adding thermally conducting structures to the PCM reduces the thermal resistance of the PCM and thereby reduces the average and peak battery temperature. This effect becomes more significant with thicker PCM layers. From a thermal and practical viewpoint, it is concluded that thermally conducting structures are best used when the thickness of the PCM layer is larger than 10 mm.

Starting from the simulation results, a methodology is derived to design a thermal management system for battery packs, with the aim to keep the average and peak battery temperature within a desired limit. The optimal cooling method can be chosen based on the estimate heat generation of the batteries. Equations to estimate the temperature variation of the battery are provided to determine the need for a thermal buffering system. If a thermal buffering system is chosen, design guidelines for the PCM melting temperature and amount of PCM are established. When the optimal amount of PCM that should be added is known, it can be decided if the resulting layer of PCM is in a thickness range which requires the addition of a thermally conducting structure. With this methodology and guidelines, thermal management systems for battery packs can be

designed without the need for complex and time-consuming simulations, while still optimizing the temperature response of the batteries.

Part V

Construction of setups

Chapter 1

Introduction

Several test cases were developed based on the outcomes of the analyzes of different applications in WP2. The decision to purchase cells, instead of integrating the applications of the members of the End-users Committee has been taken due to two reasons: in order to avoid favorizing a single Committee member and because the applications of the users are often difficult to access, as also pointed out in the intermediate project report.

For the model validation two setups were made from each type of cells (Toshiba and Winston) and for each cell type one module was equipped with PCM and a second one (with no PCM) was used as a reference.

The modules were built in a straight forward way, i.e. the cells were placed in a casing and PCM has been added around the cells. However the initial validation proved that a hybrid solution would be needed to test more accurately the different user cases. Therefore in agreement with the consortium Committee an additional laboratory set up has been made: the thermal set-up.

Chapter 2

Construction battery modules

2.1 Winston module

The Winston cells were chosen due to the fact that three of the committee members readily used these cells in their applications. In addition these cells use lithium iron phosphate technology which is one of the most widespread technologies. As PCM we used R35HC, from Rubitherm. These cells turned out to be less good than expected. The reason for this is the rather thick plastic casing. This topology has a high thermal resistance, therefore the temperature difference needed for a certain heat flux is rather large. This leads to the conclusion that the PCM had no influence on thermal management.

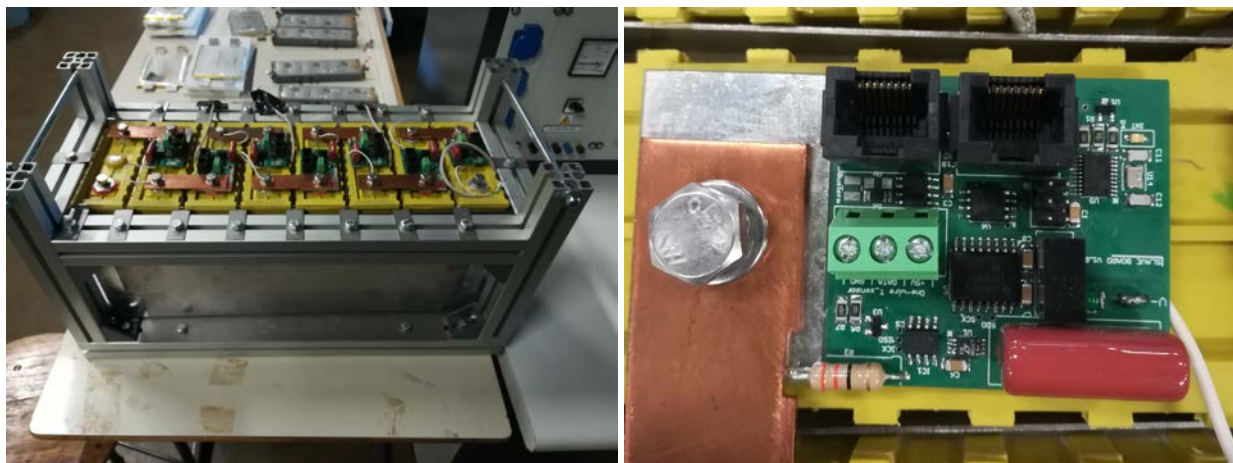


Figure 2.1: Left the Winston battery module with PCM. On the right one of the distributed BMS printed circuit boards

The full image file with the BMS software (*lbatts_bms_software.img*) as well as the

Eagle files for the PCB design and the BOM are available on the LBATTS website (www.LBATTS.com). The Image file should be loaded onto an SD-card and plugged into the RaspBerry Pi.

The main characteristics of the BMS are:

- Distributed BMS, passive balancing
- Programmable local intelligence with ATtiny45 (per cell)
- Allows hot swapping
- CAN-bus communication between cells, virtually unlimited number of slaves
- RPi master, full remote control and data acquisition through flask server with HTTP requests
- High precision measurements $\pm 0.5\%$ on pack current, $< 1mV$ on cell voltage
- Virtually unlimited amount of DS18B20 temperature sensors installable
- Easily extendable python software

The distributed BMS has a main control unit that allows to monitor and control the battery module via a web application (see Figure 2.1).

2.2 Toshiba module

We have build two modules with the Toshiba battery cells. One with PCM buffer and a second one as reference with no PCM.

The cells have $2mm$ of space surrounding them, for the reference module, these spaces remain void, for the second module the voids are filled with PCM. The $2mm$ spacing is based on the optimization process as explained in WP4.

The Toshiba cells are NMC-LTO technology. They are of the prismatic format and are housed in a metal casing.

As PCM we have used di-Sodium hydrogen phosphate dodecahydrate. This PCM has a melting point of approximately $35^{\circ}C$ and a latent heat energy of $200kJ/kg$ making it very useful for this application. No conductive matrix was added due to the small gap. We used a generic BMS of REC power control (see figure 2.3) for the monitoring of cell voltages and current.

The main characteristics of the BMS are:

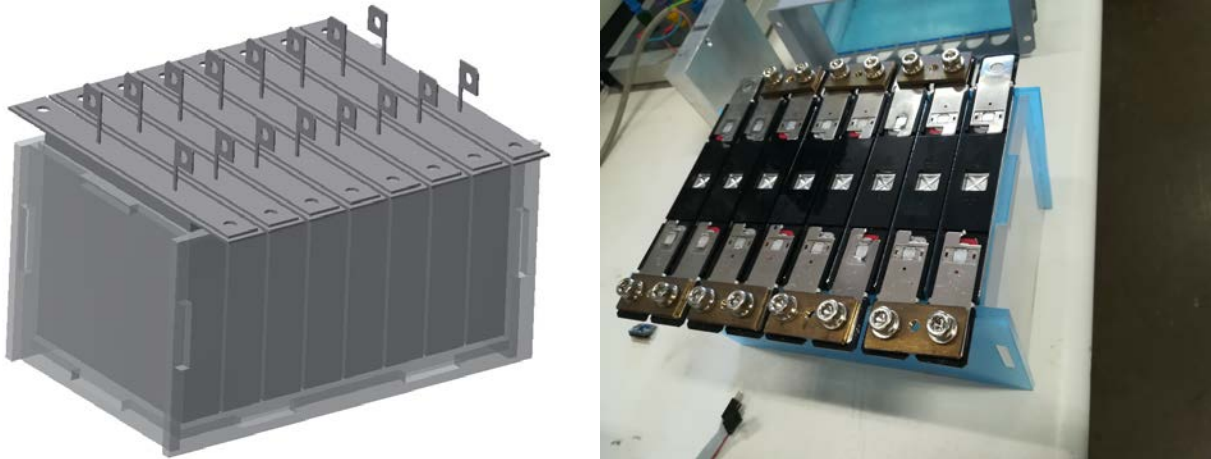


Figure 2.2: Left the CAD module as designed in Inventor, at the right a picture of the same module.

- 5 16 cells
- single cell voltage measurement (0.1 5.0 V, resolution 1 mV)
- single cell - under/over voltage protection
- single cell internal resistance measurement
- SOC and SOH calculation
- over/under temperature protection (up to 4 temperature sensors)
- passive cell balancing with 4.3 Ω
- 18-bit shunt current measurement (resolution 7.8 mA at 200 A)
- galvanically isolated user defined multi-purpose digital output
- programmable relay (normally open)
- galvanically isolated RS-485 communication protocol
- CAN communication
- error LED + buzzer indicator
- PC user interface for changing settings, data-logging and firmware update



Figure 2.3: Generic BMS of power control.

Chapter 3

Construction of dedicated Thermal setup's

3.1 Thermal setup

In WP4 we have proven that the only applications where thermal buffering can play a role are cases where the battery pack is cooled by natural convection. These are typically relatively low power applications.

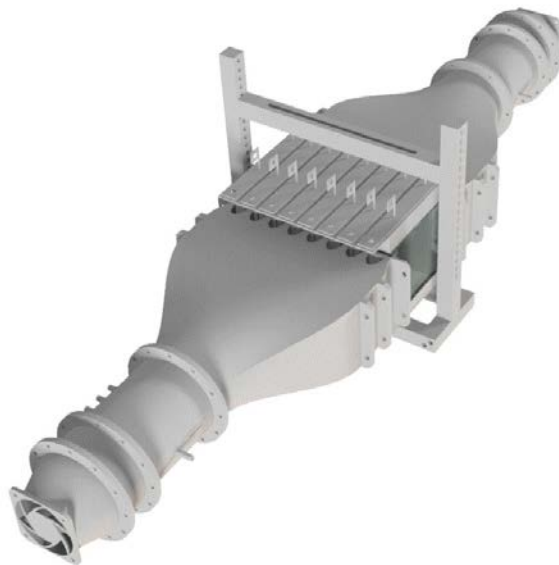


Figure 3.1: Rendering of the thermal setup

Studying performance of high power applications, is more challenging (with high power, we mean power density). The typical case are mobile applications i.e. EVs and others. In

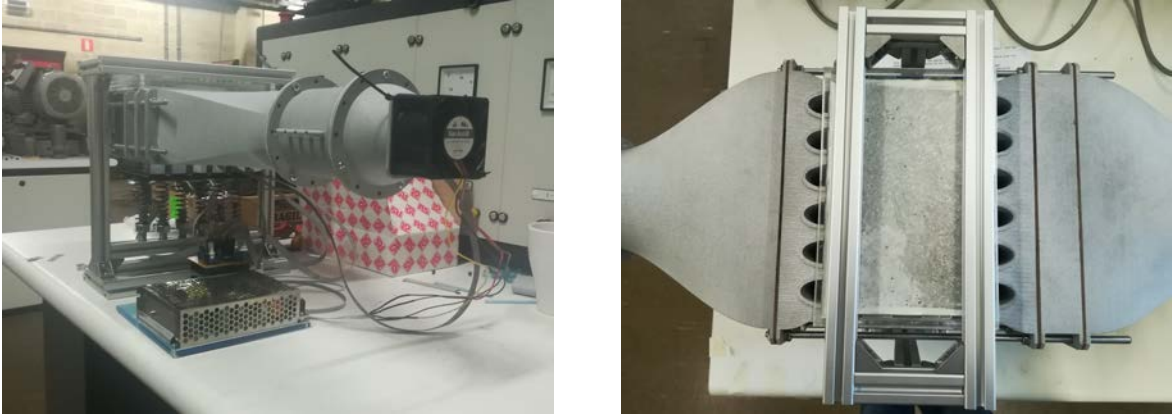


Figure 3.2: a: at the left we can see the thermal set up with spring pushing the cells on a base plate. b: on the right a top view of the base plate equipped with PCM buffer and conductive aluminium mesh.

theory it should be possible to have a complete passive thermal management system. At stand still, the produced heat can be buffered in the thermal buffers (sensible heat of the cell as well as sensible and latent heat of the PCM). Nevertheless a fan for active cooling should always be integrated just in case the cells get too hot and no ambient ventilation is for hand to capture and provide the necessary cooling. Once the vehicle is in movement, the ambient ventilation can be captured (in a controlled way) to provide the necessary cooling.

A set-up with a controllable ventilation in combination with a PCM buffer and that fits within a lot of other available infrastructure and would enable us to determine the effect of a controlled air flow on battery cooling is needed. This set-up had to be designed in a modular way such that the research output it will yield is broader than a single thermal topology. The fact that a high strained application is contemplated means that the cooling should be more effective than what is achievable with a series topology. For this reason we decided to go for a parallel topology.

The set-up can be powered with resistors (Fig.3.4), which makes it much safer to work on and will allow for additional research in hybrid cooling systems. The air flow can be monitored using the Pitot tube. To better understand the flow properties of the cooling media around the battery cells, we can also apply particle imaging velocimetry or PIV. Up to eight thermal sensors (accurate to 1/4K) are distributed over the setup to gather data.

We choose to go for an interchangeable buffering base plate equipped with PCM. This topology would enable us to test different PCM buffers, cells, baseplate configurations, etc. Some new base plates can be constructed, allowing to test different cooling techniques.

The cell base is a strategic place to cool the cell because of the anisotropic topology of separators and electrodes in cells. The cells are pushed on this plate with springs which

allows to regulate the contact force and ensure the same force applies for all cells. In between the cells a void space serves as cooling channel. The forced cooling is provided by an in and outlet fan. These fans can be controlled separately. The set-up allows to simulate a variable in and outlet flow (Fig. 3.1).

When the dynamic pressure $p_{dyn} = \rho \cdot \bar{v}^2 / 2$ and total pressure $p_{tot} = P_{sta} + P_{dyn}$ sum of the dynamic and total pressure are low enough (in case of powered extraction this might be possible), the flow might come into a laminar regime. This allows to decrease the necessary power driving the fans because in this regime the back pressure is proportional with the air velocity. Theoretically, the laminar flow field can be regulated such that the cells are thermally uncoupled. The main advantage of this is that the cells will be at identical temperatures. This in also allows for a nearly identical temperature and as a consequence the aging process should be similar for each cell. Once the velocity reaches the critical Reynolds number, turbulence kicks in. In this case the pressure drop over the cells is proportional to the square of the velocity. The turbulence immediately increases the convection coefficient (because the boundary layer is blown away for the largest part) but due to the vortexes in turbulent flow, the cells are again thermally coupled leading to less uniform aging.

At this point it is difficult to estimate these influences. Dedicated models should be found but also setups which are versatile and modular. Allowing for instance to experimentally visualize and verify the flow field, capture the convection process in real modules would be a step forward.

At this point, the setup is not fully operational but lots of progress has readily been achieved;

- designing more specific and dedicated test equipment,
- 3D printing the aero-dynamically shaped parts,
- integrate temperature, and rpm measurement,
- datalogging on SD card,
- CNC milling of the bottom plate,
- welding of alu foam on bottom plate with tin in an oven,
- laser-cutting of several plastic housings,
- assembly, of components and support structure,
- RS232 communication with lab power source for powering the mock-up cells,
- manual drive for the fans
- assembly of 6 mock-up cells and cnc milling.



Figure 3.3: a: at the left we can see the inside of the airconducts. b: on the right, the plastic transparent covers closing the airduct.

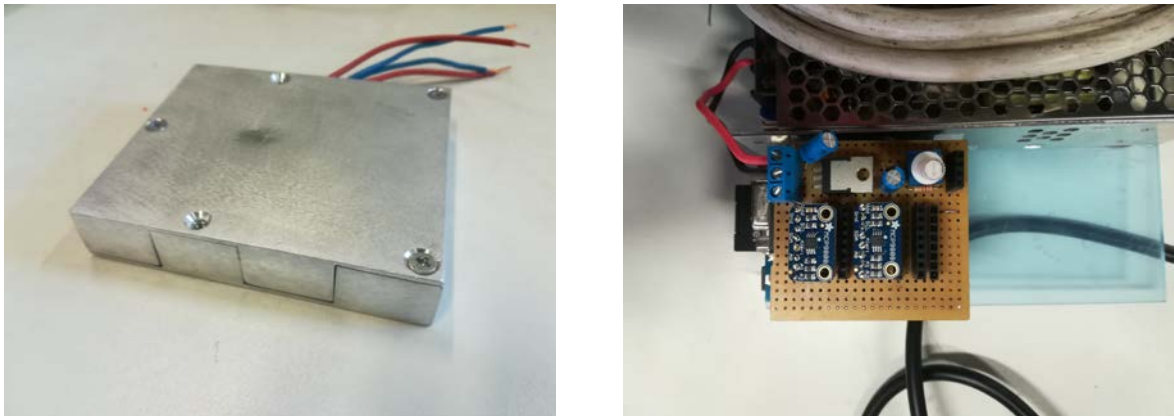


Figure 3.4: a: mockup cell b: PCB for ventiation control and temperature logging for 8 sensor (two visible sensors).

There were some issues with the control of the fans, basically we failed to understand that they had an intrinsic characteristic that would lead to a large and impressive overshoot at start-up, later tests showed that seemingly uncontrollable and impressive getaway of the motor was due to its large inertia and small hub to tip ratio. Because of this, the PCB is not yet in its final state and additional work should be done to reach this goal. Once the mock up cells can be powered automatically by a laboratory power supply, this means automatically drive the signal via RS232 protocol in order to simulate a driving cycle and once the fans are controlled by the micro controller, the set-up will be completely ready.

3.2 Thermal conductivity measurement

Thermal cell characterization is important in this project. For this purpose two setups were build. In Figure 3.5 the first setup is shown. The idea was to have two large thermal buffers of water, one buffer would be brought to 0 deg C while the second one is heated to approximatively 50C. Once the buffers are at temperature, they are pored into a thermally insulated box with two compartments, shielded by the battery cell. The buffers can be assumed to be in thermal equilibrium thanks to the sirring motion of screws in the water. Heat will transmit from one compartment to the other at a exponentially decreasing rate and form temperature measurements of the buffers we should be able to capture the thermal characteristics of battery cells.

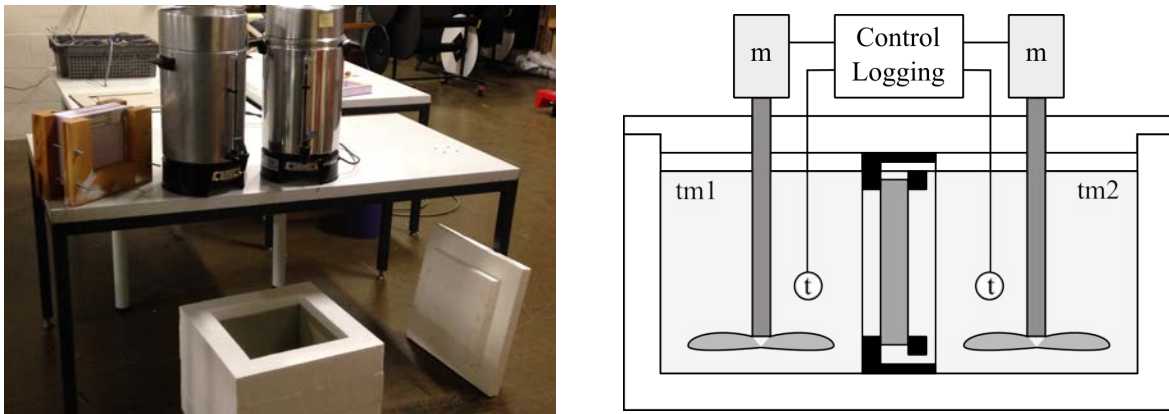


Figure 3.5: a: set up b: schematic representation of the setup.

After dealing with the motors, thermal sensors and logger we faced the problem of making the joints watertight, we planned on using a tire, however this was not enough to stop leakage. Doing a test was also rather labor intensive and so we decided to abandon this approach.

A second set-up based on radiation was build. This is depicted in Figure 3.6. This set-up gave more predictable results. And we were able to measure the thermal conductivity in a transversal and longitudinal plane.



Figure 3.6: Radiation testing for thermal conductivity in the longitudinal direction (6 pouch cells next to each other)

The cell bought in the context of LBATTS were difficult to characterize due their casing and relatively large size.

Part VI

Testing of setups

Chapter 1

Introduction

The applicability of PCMs is not easy to prove, since there are numerous influences that play an important role. Application simulations have the following physical inputs: ambient temperature; electrical load profile; thermal insulation and ventilation profiles. Multidisciplinary simulations can be built to study these setups; a case by case approach is needed.

Chapter 2

Testing of dedicated thermal setups

2.1 Thermal conductivity measurements

As explained in WP5 measurement of the thermal properties is not as straight forward as one might think.

- The first setup did not allow adequate sealing of the compartments. In addition the study of the convective effects was hampered by the geometry.
- The second issue was due to the choice of battery cells. Comparison of the two cells use was not straightforward due to the different characteristics of the shell: thermally isolating for the Winston cell and thermally conductive for the Toshiba cell.

Because of the importance of performing this test, the irradiation test was set up for pouch cells. The cells used are Li-Pos for radio controlled applications. These cells still have a plastic cover but this layer is actually very thin which makes the required test feasible. This cell uses NMC-442 chemistry. From the shape of the pouches we can deduce that the electrodes are folded. We have measured the thermal conductivity in the transversal and longitudinal direction. The test data is compared to a model which allows us to also calculate the thermal capacity. The capacity can be deduced for both tests which gives us a better confidence of the obtained results. The model is based on a one dimensional electro thermal equivalent circuit as developed and discussed in WP4. Because no phase changes are considered, we can use the temperature-voltage equivalent, note in WP4 we used an enthalpy-voltage equivalent.

The equivalent circuit used in this case is depicted in figure 2.1. U_1 , U_2 , R_{nc} , R , C and n represent respectively; the inlet power, the ambient temperature, the natural convection thermal resistance, the cell thermal resistance, the cell thermal capacity, and the number of spatial sample points. Notice the layout of the sample points is not totally symmetric.

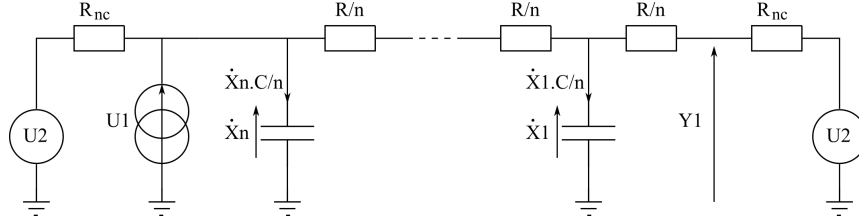


Figure 2.1: Irradiation test, thermoelectric equivalent scheme

It turns out that the numerical computation of the depicted illustration is much more stable and easier than the case where a resistor would be placed between the current source U_1 and capacitor C_n . The numbering of the capacitors in an upstream direction results in a system matrix mostly populated near the first diagonal. Perhaps it could be useful to place an other capacitor at position $Y1$ to restore the symmetric properties of the system. The X 's are the state variables and in this case correspond to the capacitor voltages. $Y1$ is an output corresponding to the surface temperature which is used every time step to calculate the natural convection.

2.1.1 Inlet power calculation

In this system the power reaching the sample should be relatively simple to estimate. The electric power reaching the radiator is $P_{in} = U * I = 380[W]$. The energy transfer is mainly considered as radiation although we consider 10% general losses. The power reaching the sample can be approximated using small point sources. Subdividing the radiator in 9 small segments leads to the following values for the radiator element (see figure 2.2) leads to a $p_{in} = 38.94[W]$ and length $d = 42.2[mm]$. Figure 2.2 represents the set up during the measurement form the "side to side" thermal conductivity. For each element a new set of upper and lower angles is calculated α_h and α_l .

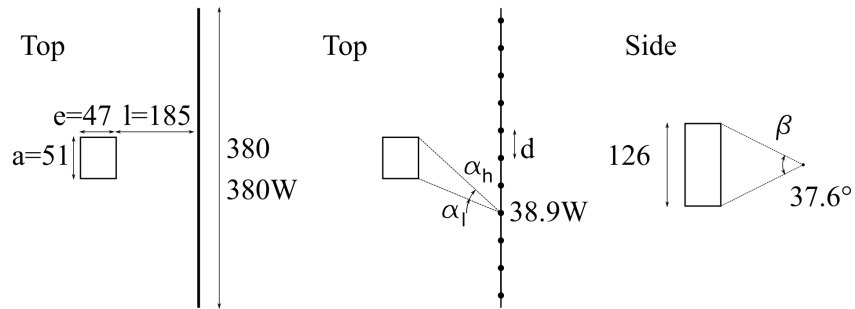
$$\alpha_h(n) = atan\left(\frac{d \cdot n + \frac{a}{2}}{l}\right)$$

$$\alpha_l(n) = atan\left(\frac{d \cdot n - \frac{a}{2}}{l}\right)$$

The total radiation power reaching the sample is:

$$P_{somp} = p_{in} \cdot \frac{\beta}{2 \cdot \pi} \cdot \left(\sum_{n_{min}}^{n_{max}} \frac{\sin(\alpha_h) - \sin(\alpha_l)}{2} \right) = 3.518[W] \quad (2.1)$$

Side to Side



Front to Back

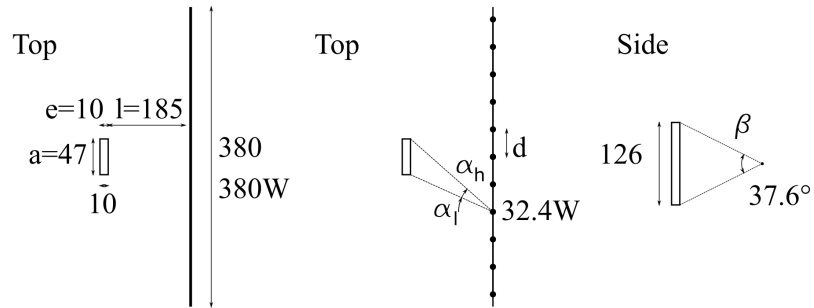


Figure 2.2: Calculation heat generation, side to side experiment above and front to back below.

With n the whole numbers ranging from -4 to $+4$.

The sample was painted black to encourage absorption. The sample radiates also but compared to the radiator this loss is negligible due to the relatively low temperature compared to its environment, this is different for the radiator.

For the side to side experiment we obtain $P_{samp} = U1 = 3.518[W]$.

For the front to back experiment we get P_{samp} was $3.24[W]$.

2.1.2 Natural convection resistance

The principles of natural convection were discussed in WP4. The influence of convection is very important because without it the cell can not cool down. It is also important to realize that those equations are only valid in theoretical cases. Real life situation will only approximate it.

Alternative calculation methods reach deep in the field of CFD computation.

Deviations of the convective term could according to some sources WELKE, citeren! be up to 25%. They depend on the creation of convective flows, which will develop in time and cool the object or not due to obstruction.

In the set-up the cells are fixed in a isolating frame to limit the heat losses through the sides. It does not reach the ground however.

For all these reasons, the analysis should be conducted with a sensibility factor for this resistance to analyze its influence.

2.1.3 Solving process

The solving process requires a state space representation of the from:

$$\vec{X} = [A].\vec{X} + [B].\vec{U} \quad (2.2)$$

$$\vec{Y} = [C].\vec{X} + [D].\vec{U} \quad (2.3)$$

Equation (2.2) is called the system equation and (2.3) is called the output equation. \vec{X} , \vec{Y} and \vec{U} respectively the state, output and input vectors.

The matrices $[A]$ (2.4) and $[B]$ (2.5) are obtained by applying Kirchoff's laws on circuit 2.1. Matrices $[C]$ (2.6) and $[D]$ (2.7) are needed to calculate the surface temperatures, serving as inputs for the calculation of the natural convection resistances.

$$A = -\frac{n^2}{C_{th} \cdot R} \cdot \begin{bmatrix} \left(1 + \frac{1}{1 + \frac{R_{cn} \cdot n}{R}}\right) & -1 & 0 & 0 & 0 \\ -1 & 2 & -1 & 0 & 0 \\ 0 & -1 & 2 & -1 & 0 \\ 0 & 0 & -1 & 2 & -1 \\ 0 & 0 & 0 & -1 & \left(1 + \frac{1}{1 + \frac{R_{cn} \cdot n}{R}}\right) \end{bmatrix} \quad (2.4)$$

$$B = \begin{bmatrix} 0 & \frac{n^2}{C_{th} * R} \cdot \left(1 + \frac{n \cdot R_{cn}}{R}\right)^{-1} \\ 0 & 0 \\ 0 & 0 \\ 0 & 0 \\ \frac{n}{C_{th}} & \frac{n}{C_{th} \cdot R_{cn}} \end{bmatrix} \quad (2.5)$$

$$C = \begin{bmatrix} 1 - \left(1 + \frac{2 \cdot n \cdot R_{cn}}{R}\right)^{-1} & 0 & 0 & 0 & 0 \\ 0 & 0 & 0 & 0 & R_{cn} \cdot \left(R_{cn} + \frac{R}{2n}\right)^{-1} \end{bmatrix} \quad (2.6)$$

$$D = \begin{bmatrix} 0 & \frac{R}{2 \cdot n} \cdot \left(R_{cn} + \frac{R}{2 \cdot n}\right)^{-1} \\ \frac{R * R_{cn}}{2 \cdot n} \cdot \left(R_{cn} + \frac{R}{2 \cdot n}\right)^{-1} & 1 - R_{cn} \cdot \left(R_{cn} + \frac{R}{2 \cdot n}\right)^{-1} \end{bmatrix} \quad (2.7)$$

To be able to integrate this function we replace the left side of equation 2.2 with a 6th order downwind finite difference formula, yielding the following formulation:

$$\vec{X}_{k+1} = f(\vec{X}_k, \vec{X}_{k-1}, \vec{X}_{k-2}, \vec{X}_{k-3}, \vec{X}_{k-4}, \vec{X}_{k-5}) \quad (2.8)$$

And so we are able to compute the states in time $k + 1$ and function of the previous states. In addition, the method allows to change the coefficients in A during the simulation and to take in to account changing R_{nc} . Note: in the computation a different variable was used for the R_{nc} in the front and back.

2.1.4 Results

The results of this analysis are listed in the table below, eight spatial discretization points were used in this analysis.

- The results of the side to side experiment lead to;
 $R = 3.4[W/K]$, $C = 1170[J/K]$ and a sensibility factor = 0.85 .
- The results of the front to back experiment lead to;
 $R = 2.7[W/K]$, $C = 230[J/K]$ and a sensibility factor = 0.87.

Or in other words an in-plane conductivity of $k = 2.15[W/mK]$ and a transversal conductivity of $k = 0.62[W/mK]$. Figure 2.3 illustrates the test data captured by both thermal sensors along with the results obtained with this dedicated model which in turn illustrates the applicability of electro thermal equivalent models.

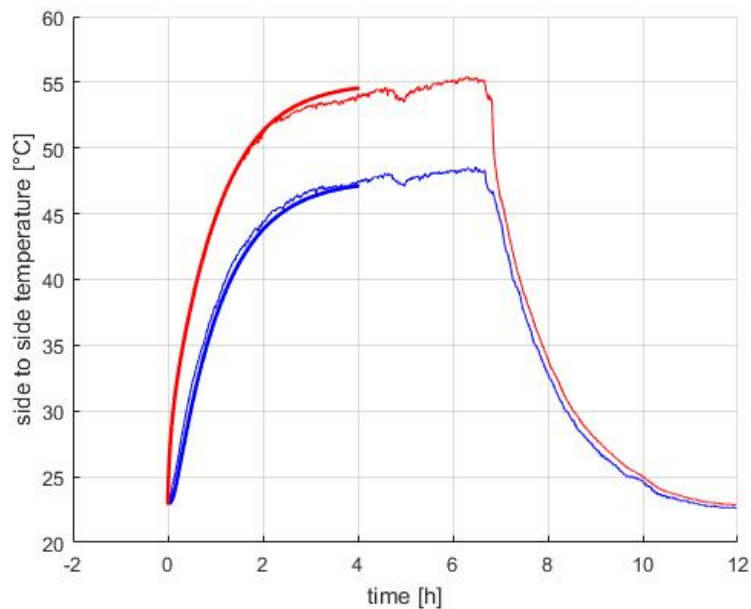


Figure 2.3: Test of the side to side thermal conductivity measurement along with the model data.

2.2 Thermal setup

In WP4 we have proven that the only applications where it could play a role are cases where the battery pack is cooled by natural convection. These are typically relatively low powered applications.

The implementation in this case consists of a series topology i.e., the phase change material encapsulates all battery cells making up the pack and thus heat needs to go through the PCM where it is temporarily stored before it can be evacuated through convection. Adding the PCM improves the temperature gradient but any thermally insulating casing would do this. It also increases the total heat capacity which in turn lowers the mean temperature.

Studying performance of high strained applications, is more challenging because the analysis of the flow around the battery cell should be part of it. In engineering applications (using forced air cooling), the convective coefficient can differ severely, some sources speak of 0.5 to 200 W/m^2K . Depending on the actual design (outer surface, shape of cooling channels, battery cell etc.) the thermal resistance representing the convection can be important leading to higher cell temperatures. This in turn has a direct impact on electric performance.

For testing of high strained applications we choose to implement the PCM in parallel with the convective cooling. This gave us the possibility to get a good and nearly uniform flow field for the cooling but also allows for an interchangeable cassette with PCM buffer while keeping the cooling vanes constant.

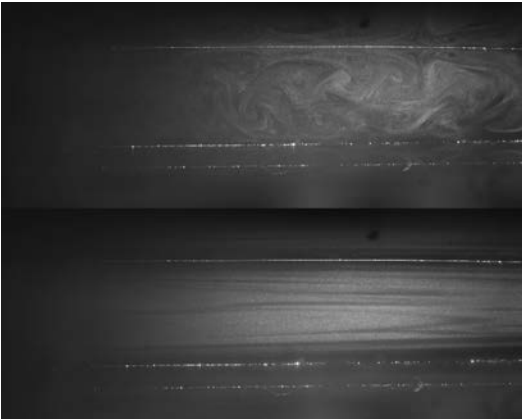


Figure 2.4: Images of laminar and turbulent flow profiles in cooling channels



Figure 2.5: PIV measurement synchronised pulsing lazer and camera

We wanted a setup that integrates well with a lot of other available infrastructure and would also enable us to determine the effect of a controlled air flow on battery cooling along with PCM buffer. The setup readily features several important features:

- The set-up can be fitted with resistors representing the heat output of the battery cells, which makes it much safer to work on and will allow for additional research in hybrid cooling systems without undue stress on real cells.
- The air flow can be monitored using the Pitot tube. To better understand the flow

properties of the cooling media around the battery cells, we can also apply a particle imaging velocimetry.

- Up to eight additional thermal sensors are distributed over the setup to gather additional data.
- The thermal elements can be driven by a regulated power supply. This power-source can be driven via RS232 protocol in order to simulate a driving cycle.

Several features remain to be implemented before testing can begin:

- The power cycle should be launched after a selection procedure.
- The fans should be driven by the central micro controller.

The test possibilities that are enabled because of this are much broader than what was originally intended.

The preliminary results of the thermal setup (see WP5) is depicted in figure 2.4 where we illustrate pictures of a laminar and turbulent flow-fields in the cooling channels.

2.3 PCM properties

As PCM we chose to use the di-Sodium hydrogen phosphate dodecahydrate. This PCM has a melting point of approximately $35^{\circ}C$ and a latent heat energy of $200J/g$ making it very useful for this application however after a few cycles we noticed that the thermal buffer became drastically less effective.

We decided to further investigate this phenomena in a separate test. We filled two glasses with approximately 100 gram of PCM. One was sealed and the other not. Figure 2.6 presents the data. The open glass clearly lost weight during the experiment. We believe the water molecules were disappearing from the mixture.

Lessons learned is that the PCM should be covered and not like in our case in contact with the atmosphere. The PCM changed from a partially translucent mixture to a mat white plaster like material. In the process it loses its beneficial properties due to the evaporation of water.

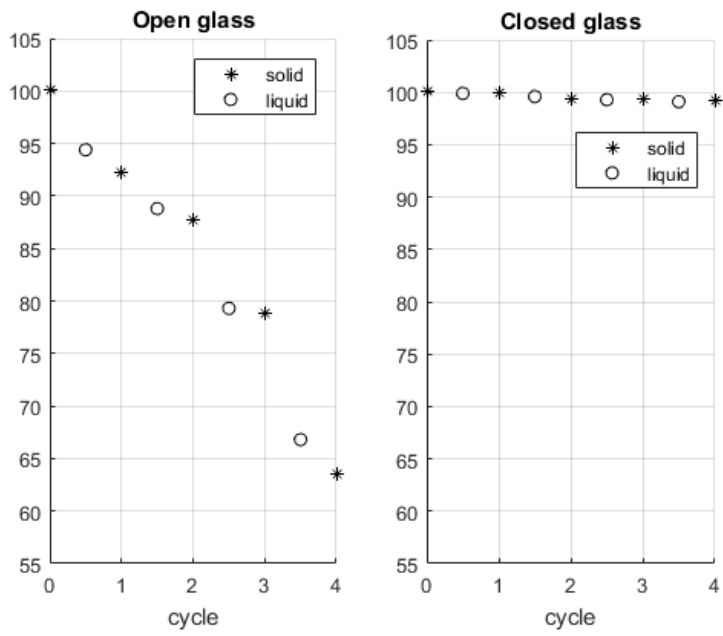


Figure 2.6: PCM weight decrease over a few cycles

Chapter 3

Testing of battery modules

3.1 Winston module

The Winston cells were chosen due to the fact that three of the committee members readily used these cells in their applications. In addition these cells use lithium iron phosphate technology which is one of the most widespread technologies.

The cells turned out to be less good than expected. The reason for this is the rather thick plastic casing. This topology has a high thermal resistance, therefore the temperature difference needed for a certain heat flux is rather large. This leads to the conclusion that the PCM has no influence on thermal management.

Actual tests on the module were also difficult to start. We wanted to connect the module on the testers at the VUB lab but it was impossible to get the BMS operational. At the moment KUL is still using it to conduct field tests.

3.2 Toshiba module

We have built two modules with the Toshiba battery cells. One with a PCM buffer and a second one as reference with no PCM.

The cells have 2mm of space surrounding them, for the reference module, these spaces remain void, for the second module the voids are filled with PCM. The 2mm spacing is based on the optimization process as explained in WP4. The design of these modules does not allow however to apply the 1D model. Cooling channels should have been needed for this.

The Toshiba cells are NMC-LTO technology. They are of the prismatic format and are housed in a metal casing. In contrast to the Winston cells they have a smaller thermal resistance which makes thermal management more effective.

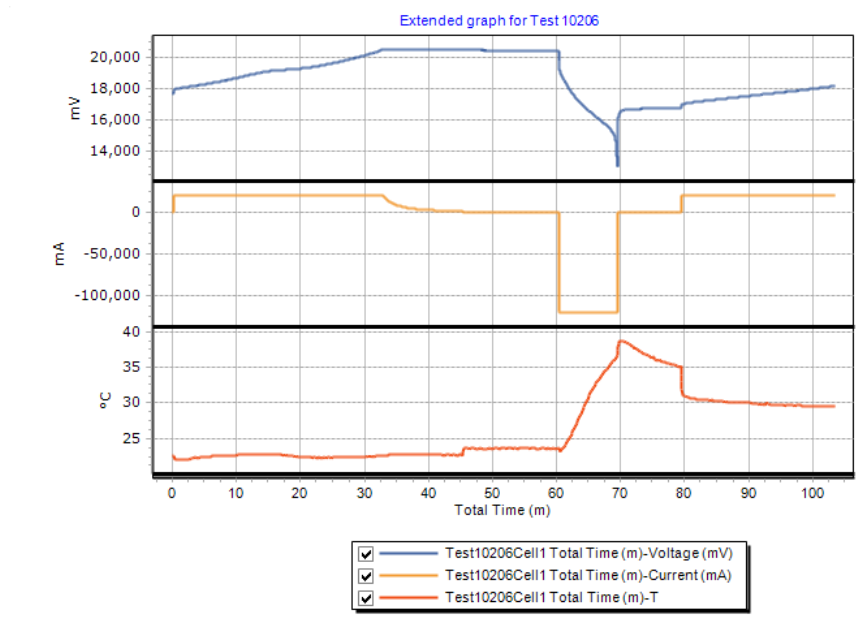


Figure 3.1: $1I_t$ charge, $6I_t$ discharge

During testing several issues became apparent,

- The BMS is a generic component and due to the relatively low cell voltages, the balancing function is rather slow.
- The BMS draws power from the battery with no safeguard.
- The eprom memory got corrupted, we had to constantly reprogram the BMS.
- Issues with the thermal sensor of the tester made a second logging system necessary.

3.2.1 Usage tests

Several conditioning tests, ranging from 1 to $6I_t$ were performed on the modules with and without PCM. Figures 3.2 and 3.1 were performed with the tester temperature logger and the PCM battery module.

Often, the temperature sensor would give faulty results. After the first set of tests, we decided to go for $5I_t$ discharge and charge profiles. The choice of $5I_t$ profiles was made based on the first test results on module level.

The issues with thermal measurement persisted and we turned to a separate logging device.

The figures 3.4 and 3.3 represent respectively the data captured from the PCM module and the reference module.

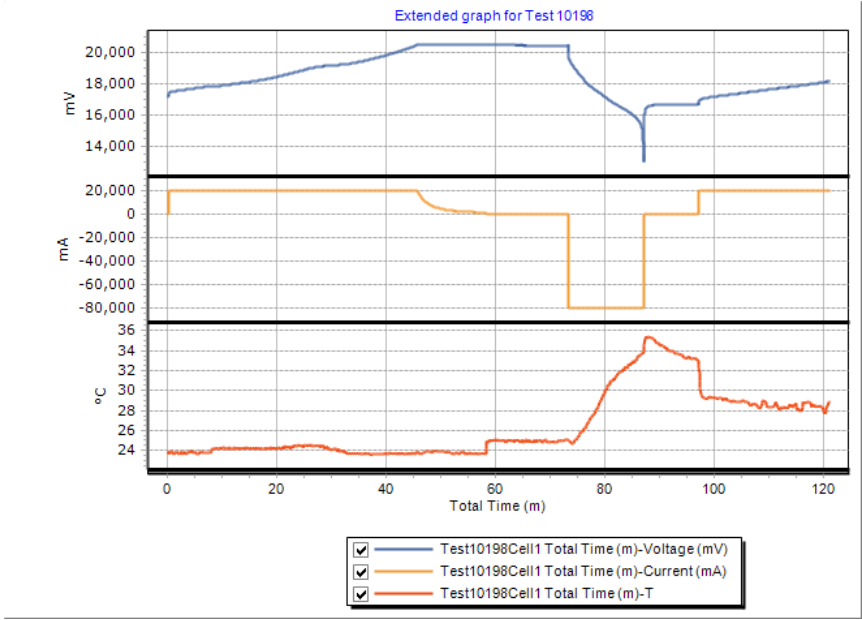


Figure 3.2: $1I_t$ charge, $4I_t$ discharge

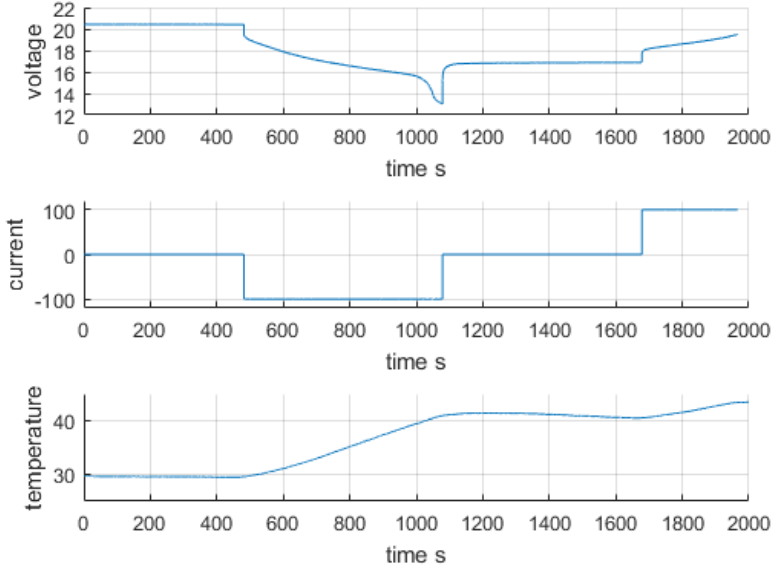


Figure 3.3: Reference module $5I_t$ test

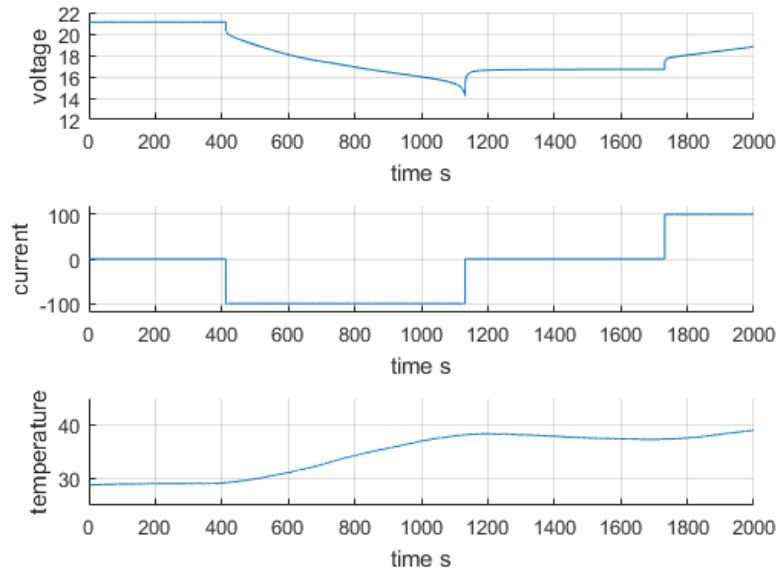


Figure 3.4: PCM infused module $5I_t$ test

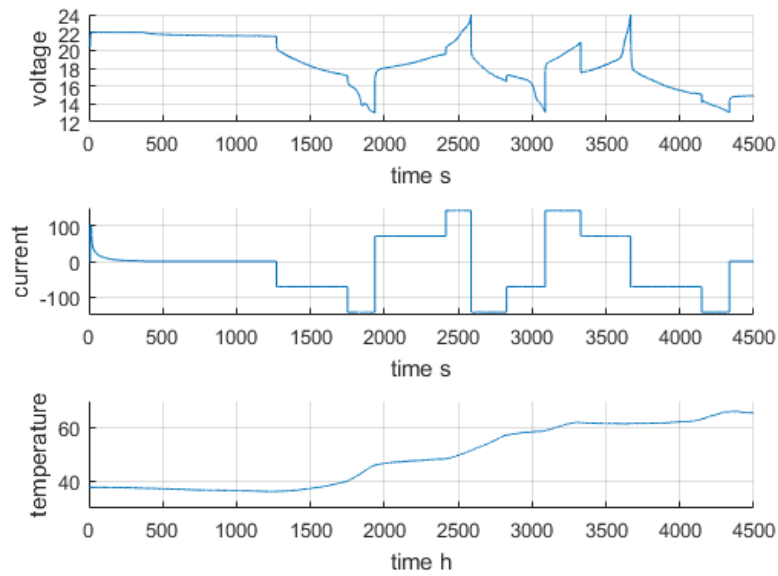


Figure 3.5: $5I_t$ loadFollow with no PCM

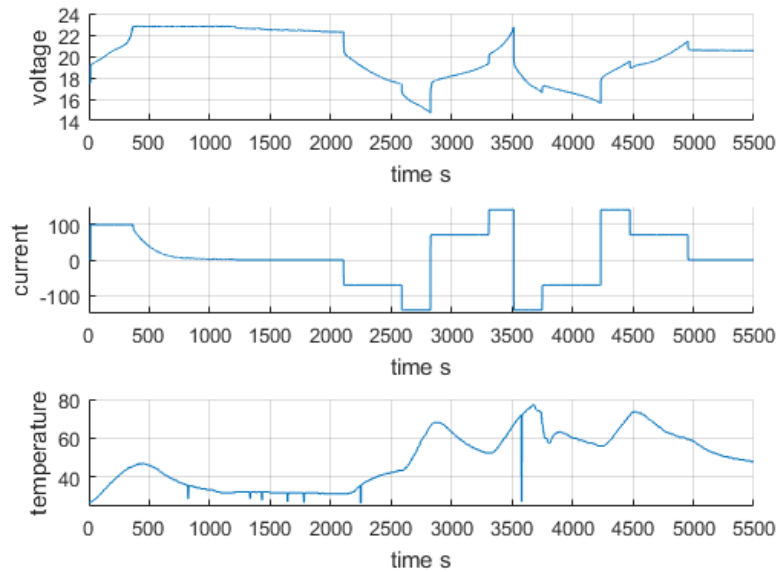


Figure 3.6: $5I_t$ Load following with PCM

We can see that the module with PCM seems to cool down a bit faster than the module without PCM.

The difference in temperature rise is about 10°C for the module with and 12°C for the module without PCM buffer which is explained by the added thermal capacity.

The load following user profile multiplied with $5C$ was the only user profile, that addresses the full battery capacity approximatively 18 Ah out of 20 Ah. For this reason we chose to implement this profile, on the tester. Perhaps it had been better to chose a medium term cycle but LTO cells are known for very high continuous currents.

Figures 3.5 and 3.6 represent the test data during load following test for respectively the module without and the module with PCM. Although the tests were performed, the resulting thermal data was again corrupted. The second logging device began to give erroneous results. Therefore we turned to the bms logging unit and placed some extra thermal sensors. The sensors were connected between the electrode tabs. The Bms was rather uncertain, the data sheet mentioned it would fail to work under 15V which sometimes happened during our tests and made data logging again uncertain.

The sensors were squished in between the electrodes but they would sometimes get lose and make less good contact. Depending on the response of the sensor this could explain the strange perturbation in temperature depicted in figure 3.6. Another explanation for the temperature decrease is due to the current over the junction of the electrode tabs and messing connection rods. Possibly a Peltier like heat pump may be at work.

3.2.2 Thermal imaging

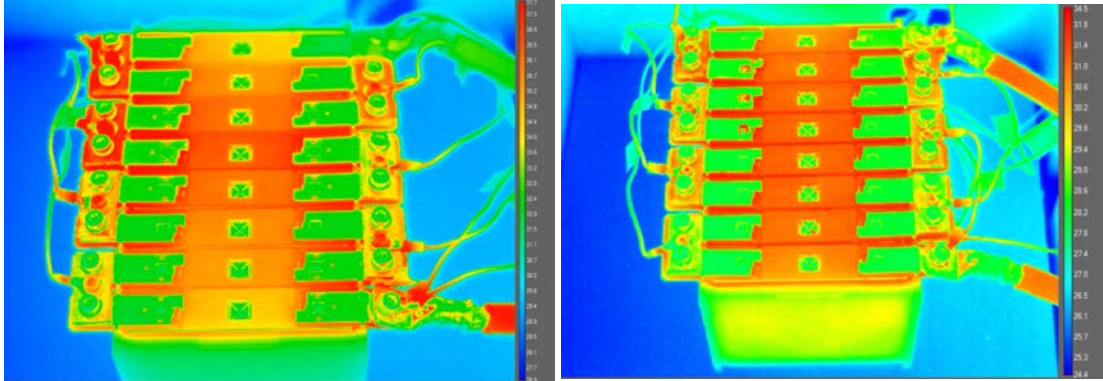


Figure 3.7: Left the toshiba module with no PCM, right the same module with PCM. Both pictures were taken after a constant discharge current of $2I_t$ testing or after $28min$

We have added a thermal camera to look at the module in a different way. Some temperature differences were observed near the electrodes. This is due to a non optimal connection between the electrode tabs and the battery electrodes. The difference between the tabs dissipated after tightening the screw.

Chapter 4

Conclusions

4.1 Lessons learned

There main lessons learned through from this project can be summarized as follows:

1. PCM buffering makes sense for naturally cooled battery modules depending on other boundary conditions.
2. PCM buffering makes sense for medium cycles around 4 to 8h depending on other boundary conditions.
3. PCM can actively buffer heat and keep the cells in a better working range.
4. A laboratory set up has been made that can provide useful insights for hybrid systems.
5. To ensure certain PCMs to maintain their thermal properties, these should be kept in a sealed environment.
6. The 1D model could be applied to the battery cell thermal conductivity measurement.

4.2 General conclusions

The LBATTS project has delivered valuable insights on the thermal management of batteries, and more particularly on the use of phase change materials. It is clear that these materials present specific opportunities for improving the thermal behavior of batteries. However, it is no panacea, and a number of boundary conditions have to be optimized in order to get best results, which can be summarized as follows:

- Selection of the cells

The proper operation of a thermal management system depends on the mechanisms of heat exchange between the battery cell and its surroundings. A low thermal resistance and a low thermal time constant both will facilitate the heat transfer behavior. Hence, compact cells with a thermally conductive housing will be advantaged. Pouch cells and shallow prismatic cells with metal enclosures are particularly well suited for the application, whereas cylindrical cells and large prismatic cells with (thermally insulating) plastic housing can benefit less.

- Structure of the module

The battery cells are grouped together in a battery module or battery pack. The design of such module will have a considerable impact on the thermal behavior, as it encompasses the thermal management system, active or passive cooling, phase change thermal buffers.

- Application cycle

The most significant aspect however to determine the effectiveness of the PCM buffer is whether the buffer can cope with the thermal dynamics of the cell. These are function of the application cycle. For slow cycling applications where the strain on the battery is limited, the natural heat exchange between the cell and the environment can usually cope quite easily with the dynamics of the cycle, and the advantage of the thermal buffer is minimal. Also for extremely high strain applications, the benefits of a buffering system are limited due to the dynamics of the system. The real advantage of the system is shown with those load cycles where the heat production by the cell is easily absorbed by the thermal buffer, and where the latter can dissipate this heat through the cooling system in a way that the cell temperature can be kept in a narrow envelope throughout the cycle.

Bibliography

- [1] Comparison , selection , and parameterization of electrical battery models for automotive applications.
- [2] Iec 12405-2, electrically propelled road vehicles test specification for lithium-ion traction battery packs and systems part 1: High-energy applications.
- [3] Iec 61427-2, secondary cells and batteries for renewable energy storage general requirements and methods of test part 2: On-grid applications.
- [4] Iec 61982-2: Secondary batteries for the propulsion of electric road vehicles - part 2: Dynamic discharge performance test and dynamic endurance test.
- [5] Iso 12405-2: Electrically propelled road vehicles - test specification for lithium-ion traction battery packs and systems - part 2 : High energy application.
- [6] Simplified extended kalman filter observer for soc estimation of commercial power-oriented lfp lithium battery cells.
- [7] Improving the performance of a stand-alone ppo genset while charging your electric car. Proceedings EVS25, International Battery, Hybrid and Fuel Cell Electric Vehicle Symposium, 2010.
- [8] Poullikkas A. A comparative overview of large-scale battery systems for electricity storage. *Renew Sustain Energy Rev*.
- [9] Joos G. Abbey C. Supercapacitor energy storage for wind energy applications. *IEEE Trans Ind Appl*. 43:76976.
- [10] Intrator J Washom B et al. Abele A, Elkind E. 2020 strategic analysis of energy storage in california.
- [11] International Energy Agency. Technology roadmap energy storage, March 2014.
- [12] B.; Hassoun J. Agostini, M.; Scrosati. An advanced lithium-ion sulfur battery for high energy storage. n/a n/a.

- [13] Said Al Hallaj and JR Selman. A novel thermal management system for electric vehicle batteries using phase-change material. *Journal of the Electrochemical Society*, 147(9):3231–3236, 2000.
- [14] Said Al-Hallaj and JR Selman. Novel thermal management of battery systems. *US patent*, 6468689:B1, 2002.
- [15] F.; Du Pasquier A.; Zheng T. Amatucci, G. G.; Badway. An asymmetric hybrid nonaqueous energy storage cell. 148, A930.
- [16] D. Andrea. *Battery Management Systems for Large Lithium-ion Battery Packs*. Power engineering. Artech House, 2010.
- [17] B. Z. J. Aruna Zhamu. Method of producing prelithiated anodes for secondary lithium ion batteries.
- [18] Volodymyr Yartys Asbjorn Ulvestad. Porus silicon as anode material for lithium ion batteries.
- [19] A Babapoor, M Azizi, and G Karimi. Thermal management of a li-ion battery using carbon fiber-pcm composites. *Applied Thermal Engineering*, 82:281–290, 2015.
- [20] L. M. Babu, G.; Reddy Arava. Graphene-decorated graphitesulfur composite as a high- tap-density electrode for lis batteries. 5, 4762147627.
- [21] Research N. Second-Life Batteries. From pevs to stationary applications.
- [22] & Wang X. Bazinski, S. J. The influence of cell temperature on the entropic coefficient of a lithium iron phosphate (lfp) pouch cell. 161(1):168–175.
- [23] A Bhattacharya, VV Calmidi, and RL Mahajan. Thermophysical properties of high porosity metal foams. *International Journal of Heat and Mass Transfer*, 45(5):1017–1031, 2002.
- [24] Strbac G. Black M. Value of bulk energy storage for managing wind power fluctuations.
- [25] K Boomsma and D Poulidakos. On the effective thermal conductivity of a three-dimensionally structured fluid-saturated metal foam. *International Journal of Heat and Mass Transfer*, 44(4):827–836, 2001.
- [26] Prof. Peter Van Den Bossche. E.v.d. post.
- [27] S.; Biensan P.; Kasztejna P.; Nechev K.; Staniewicz R. J. Broussely, M.; Herreyre. Aging mechanism in li ion cells and calendar life predictions. 97-98, 1321.
- [28] B.; Tarascon J.-M. Bruce, P. G.; Scrosati. Nanomaterials for rechargeable lithium batteries. 47, 29302946.

- [29] S. A.; Hardwick-L. J.; Tarascon J.-M. Bruce, P. G.; Freunberger. Li-o₂ and li-s batteries with high energy storage. 11, 1929.
- [30] A. Burke. Randd considerations for the performance and application of electrochemical capacitors. 53, 10831091.
- [31] A. Burke. Ultracapacitor technologies and application in hybrid and electric vehicles. 34, 133151.
- [32] Z.; Zhao H. Burke, A.; Liu. Present and future applications of supercapacitors in electric and hybrid vehicles.
- [33] Soma GG Dal Canto D Pasca E-Quadrelli A. Celli G, Pilo F. Benefit assessment of energy storage for distribution network voltage regulation. Work Integr Renewables into Distrib Grid.
- [34] L. L. Chen, L.; Shaw. Recent advances in lithiumsulfur batteries. 267, 770783.
- [35] T.; Wu F. Chen, R.; Zhao. From historic review to horizon beyond: Lithium-sulphur batteries run on the wheels. 51, 1833.
- [36] Cong TN Cong TN Yang W Yang W et al. Chen H, Chen H. Progress in electrical energy storage system. (19:291312).
- [37] K.-S.; Cho J.-H.; Kim S.-W.; Chin E.-Y.; Kim H.-T. Cheon, S.-E.; Ko. Rechargeable lithium sulfur battery. 150, A796.
- [38] European Commission. Commercialisation of energy storage in europe.
- [39] Contractor. The future value of storage in the uk with generator. URN NUMBER 04/1877.
- [40] Michael R Cosley and Marvin P Garcia. Battery thermal management system. In *Telecommunications Energy Conference, 2004. INTELEC 2004. 26th Annual International*, pages 38–45. IEEE, 2004.
- [41] Pihl J Weinstock I-Symons P. Cready E, Lippert J. Technical and economic feasibility of applying used ev batteries in stationary applications.
- [42] Pihl J Weinstock I-Symons P. Cready E, Lippert J. Technical and economic feasibility of applying used ev batteries in stationary applications. PBD 1 Mar 2003 2003:Medium: ED; Size: 130 pages.
- [43] Rastler D. Electricity energy storage technology options.
- [44] Rastler D. Electricity energy storage technology options. 170.
- [45] Europe Climate Assesment & Dataset. Climatology maps.

- [46] Gomis-Bellmunt O-Bianchi FD. Daz-Gonzlez F, Sumper A. Energy management of flywheel-based energy storage device for wind power smoothing. 110:20719.
- [47] Gomis-Bellmunt O-Villaffila-Robles R. Daz-Gonzlez F, Sumper A. A review of energy storage technologies for wind power applications. (16:215471).
- [48] Gomis-Bellmunt O-Villaffila-Robles R. Daz-Gonzlez F, Sumper A. A review of energy storage technologies for wind power applications. *Renew Sustain Energy Rev* 2012.
- [49] Peter De Jaeger, Christophe TJoen, Henk Huisseune, Sander Van Herzeele, Niels Vorst, and Michel De Paepe. Thermo-hydraulic study of a single row heat exchanger consisting of metal foam covered round tubes. *International Journal of Heat and Mass Transfer*, 53(15):3262–3274, 2010.
- [50] Anming Hu Delong Ma, Zhanyi Cao. Si-based anode materials for li-ion batteries: A mini review. 6(4):347358.
- [51] H. E.; Density. New materials and new configurations for advanced electrochemical capacitors.
- [52] C.; Liaw B. Y. Cell Dubarry, M.; Truchot. Degradation in commercial lifepo4 cells with high-power and high-energy designs. 258, 408419.
- [53] Alboyaci B. Dursun B. The contribution of wind-hydro pumped storage systems in meeting turkeys electric energy demand. *Renew Sustain Energy Rev*.
- [54] C.; Nishimura K.; Fujino T.; Miyashita-K. Endo, M.; Kim. Recent development of carbon materials for li ion batteries. 8, 183197.
- [55] ERP. The future role for energy storage in the uk. Main Report 2011, 1-48.
- [56] L. F. Evers, S.; Nazar. New approaches for high energy density lithium-sulfur battery cathodes. 46, 11351143.
- [57] Corey G. Eyer J. Energy storage for the electricity grid.
- [58] Corey G. Eyer J. Energy storage for the electricity grid. *Contract* 2010;321:232.
- [59] Donal P Finegan, Mario Scheel, James B Robinson, Bernhard Tjaden, Ian Hunt, Thomas J Mason, Jason Millichamp, Marco Di Michiel, Gregory J Offer, Gareth Hinds, et al. In-operando high-speed tomography of lithium-ion batteries during thermal runaway. *Nature communications*, 6, 2015.
- [60] R. Fong. Studies of lithium intercalation into carbons using nonaqueous electrochemical cells. 137, 2009.

- [61] M. J.; Staub J. W.; Ridgley R. D.; Landi B. J. Forney, M. W.; Ganter. Prelithiation of silicon-carbon nanotube anodes for lithium ion batteries by stabilized lithium metal powder (slmp).
- [62] Q.; Bguin F. Frackowiak, E.; Abbas. Carbon/carbon supercapacitors. 22, 226240.
- [63] F Frusteri, V Leonardi, S Vasta, and G Restuccia. Thermal conductivity measurement of a pcm based storage system containing carbon fibers. *Applied Thermal Engineering*, 25(11):1623–1633, 2005.
- [64] A. Fu, Y.; Manthiram. Core-shell structured sulfur-polypyrrole composite cathodes for lithium-sulfur batteries. 2, 5927.
- [65] A. Fu, Y.; Manthiram. Orthorhombic bipyramidal sulfur coated with polypyrrole nanolayers as a cathode material for lithiumsulfur batteries. 116, 89108915.
- [66] M.; Pereira-Ramos J. P.; Baffier N.; Bloch D. Garcia, B.; Millet. Electrochemical behaviour of chemically lithiated $\text{Li}_x\text{V}_2\text{O}_5$ phases (0.9x1.6). 81-82, 670674.
- [67] Said Al-Hallaj Greg Albright, Jake Edie. Acomparision of lead acid to lithium ion in stationary storage applications, March 2012.
- [68] Sebastien Grolleau. Vieillissement calendaire des accumulateurs lithium-ion.
- [69] A.; Chen X.; Wang C.; Manivannan A. Guo, J.; Sun. Cyclability study of siliconcarbon composite anodes for lithium-ion batteries using electrochemical impedance spectroscopy. 56, 39813987.
- [70] W.Yang C. Tan Y. Li Y. Ding H. Chen, T.N. Cong. *Progress in electrical energy storage system*.
- [71] Iwasaki T Atomura N Tsuda M Miyagi D Hamajima T, Amata H. Application of smes and fuel cell system combined with liquid hydrogen vehicle station to renewable energy control.
- [72] Jessica Lyons Hardcastle. Global transportation li-ion battery market to reach 22 billion dollar in 2020.
- [73] R.; Fan J. He, H.; Xiong. Evaluation of lithium-ion battery equivalent circuit models for state of charge estimation by an experimental approach.
- [74] Bert Herteleer. Outdoor thermal and electrical characterisation of photovoltaic modules and systems. 2012.
- [75] Shimizukawa J Iba K Tanaka K Seki T. Hida Y, Yokoyama R. Load following operation of nas battery by setting statistic margins to avoid risks. PES Gen Meet PES.

- [76] H.; Scheifele W.; Novk P.; Petrat F.-M. Holzapfel, M.; Buqa. A new type of nano-sized silicon/carbon composite electrode for reversible lithium insertion. 15661568.
- [77] KU Leuven HoWest. Decongestie van het distributienet door decentrale opslag (d3o). IWT-130187, 2014.
- [78] Chung J. Hu C, Youn BD. A multiscale framework with extended kalman filter for lithium-ion battery soc and capacity estimation.
- [79] Qian Huang, Manming Yan, and Zhiyu Jiang. Thermal study on single electrodes in lithium-ion battery. *Journal of Power Sources*, 156(2):541–546, 2006.
- [80] International Energy Agency IEA. Key electrical trends.
- [81] International Energy Agency IEA. Technology roadmap: Electric and plug-in hybrid electric vehicles.
- [82] IEC. Electrical energy storage.
- [83] IEEE/CSC and ESAS. Superconducting magnetic storage.
- [84] David L. Wood III, Jianlin Li, and Claus Daniel. Prospects for reducing the processing cost of lithium ion batteries. *Journal of Power Sources*, 275:234 – 242, 2015.
- [85] Irena. Battery storage for renewables.
- [86] Irena. *Battery storage for renewables*.
- [87] Sato S Katahira O Fukui F-Okada H et al. Irie F, Takeo M. A field experiment on power line stabilization by a smes system. *IEEE Trans Magn.* 28:4269.
- [88] B. Luerssen F. Hoffmann J. Roggenbuck-M. F. J. Janek, H. Buschmann. o title. 80,1241.
- [89] Ju-Chan Jang and Seok-Ho Rhi. Battery thermal management system of future electric vehicles with loop thermosyphon. In *US-Korea conference on science, technology, and entrepreneurship (UKC)*, 2010.
- [90] L. F. Ji, X.; Nazar. Advances in lis batteries. 20, 9821.
- [91] Tweed K. Uk launches europes largest energy storage trial.
- [92] Ali Karaipekli, Ahmet Sari, and Kamil Kaygusuz. Thermal conductivity improvement of stearic acid using expanded graphite and carbon fiber for energy storage applications. *Renewable Energy*, 32(13):2201–2210, 2007.

- [93] C.; Appleby a. J. Kasavajjula, U.; Wang. Nano- and bulk-silicon-based insertion anodes for lithium-ion secondary cells. 163, 10031039.
- [94] Moghaddam MP. Kazempour SJ, Hosseinpour M. Self-scheduling of a joint hydro and pumped-storage plants in energy, spinning reserve and regulation markets.
- [95] Sparacino AR Kerestes RJ, Reed GF. Economic analysis of grid level energy storage for the application of load leveling.
- [96] Siddique A Khateeb, Shabab Amiruddin, Mohammed Farid, J Robert Selman, and Said Al-Hallaj. Thermal management of li-ion battery with phase change material for electric scooters: experimental validation. *Journal of Power Sources*, 142(1):345–353, 2005.
- [97] Riza Kizilel, Rami Sabbah, J Robert Selman, and Said Al-Hallaj. An alternative cooling system to enhance the safety of li-ion battery packs. *Journal of Power Sources*, 194(2):1105–1112, 2009.
- [98] Zach K. Kloess M. Bulk electricity storage technologies for load-leveling operation.
- [99] Vladimir KORITAROV. Grid-scale energy storage.
- [100] Shankar Krishnan, Jayathi Y Murthy, and Suresh V Garimella. A two-temperature model for solid-liquid phase change in metal foams. *Journal of Heat Transfer*, 127(9):995–1004, 2005.
- [101] Zayegh A. Krishnan KJ, Kalam A. Optimisation and fuel cell as a back-up power for telecommunication sites. Int Conf Circuits, Power Comput Technol.
- [102] K Kusakana. Minimum cost solution of isolated battery-integrated diesel generator hybrid systems. In *South African University Power and Energy conference–SAUPEC*, pages 141–7, 2015.
- [103] K Kusakana. Optimisation of battery-integrated diesel generator hybrid systems using an on/off operating strategy. In *Domestic Use of Energy (DUE), 2015 International Conference on the*, pages 187–192. IEEE, 2015.
- [104] Hayes JG Griffiths J Egan MG. Kyriakopoulos A, Sullivan DO. Kinetic energy storage for high reliability power supply back-up. 115863.
- [105] Guermazi A Troudi A. Lahyani A, Venet P. Battery/supercapacitors combination in uninterruptible power supply (ups).
- [106] Jannes Lambrecht. Emulating the behavior of pv panels in a lab based on actual irradiation data. KU Leuven, 2016.
- [107] M. J.; Cress C. D.; DiLeo-R. A.; Raffaele R. P. Landi, B. J.; Ganter. Carbon nanotubes for lithium ion batteries. 2, 638.

- [108] S.; Morcrette M.; Edström K.; Jumas J.-C.; Tarascon J.-M. Larcher, D.; Beattie. Recent findings and prospects in the field of pure metals as negative electrodes for li-ion batteries. 17, 3759.
- [109] Lazard. Lazard's levelized cost of storage analysis, November 2015.
- [110] R.; Yim T.; Ji X.; Nazar-L. F. Lee, K. T.; Black. Surface-initiated growth of thin oxide coatings for li-sulfur battery cathodes. 2, 14901496.
- [111] S.-M.; Park E.; Scrosati B.; Hassoun J.; Park-M.-S.; Kim Y.-J.; Kim H.; Belharouak I.; Sun Y.-K. Lee, S.-K.; Oh. Highly cyclable lithiumsulfur batteries with a dual-type sulfur cathode and a lithiated si/sio₂ nanosphere anode. 15, 2863 2868.
- [112] WQ Li, ZG Qu, YL He, and YB Tao. Experimental study of a passive thermal management system for high-powered lithium ion batteries using porous metal foam saturated with phase change materials. *Journal of power sources*, 255:9–15, 2014.
- [113] Hiyama T. Li S, Tomsovic K. Load following functions using distributed energy resources. (Cat No00CH37134) 2000;3:175661.
- [114] Chen L. Q. Huang X.J. Li.H Wang, Z. X. Research on advanced materials for li-ion batteries. 21,4593-4607.
- [115] H.; McDowell M. T.; Yao Y.; Wang C.; Cui Y. A Liu, N.; Wu. Yolk-shell design for stabilized and scalable li-ion battery alloy anodes. 12, 33153321.
- [116] Ran Liu, Jonathon Duay, and Sang Bok Lee. Heterogeneous nanostructured electrode materials for electrochemical energy storage. *Chem. Commun.*, 47:1384–1404, 2011.
- [117] Z.-Z.; Young W.-S.; Shieh D.-T.; Wu H.-C.; Yang M.-H.; Wu N.-L. Liu, W.-R.; Guo. Effect of electrode structure on performance of si anode in li-ion batteries- si particle size and conductive additive. 40.
- [118] Rouco L. Lobato E, Sigrist L. Use of energy storage systems for peak shaving in the spanish canary islands. IEEE Power Energy Soc Gen Meet 2013.
- [119] Kim S-I. Lott MC. Technology roadmap: Energy storage.
- [120] Dooner M Clarke J. Luo X, Wang J. Overview of current development in electrical energy storage technologies and the application potential in power system operation. (137:51136).
- [121] Dooner M Clarke J. Luo X, Wang J. Overview of current development in electrical energy storage technologies and the application potential in power system operation.

- [122] Dooner M Clarke J. Luo X, Wang J. *Overview of current development in electrical energy storage technologies and the application potential in power system operation.* Appl Energy 2015, 2014. doi:10.1016/j.apenergy.2014.09.081.
- [123] LuxResearch. Energy storage market rises to 50 billion us d in 2020.
- [124] Rajib Mahamud and Chanwoo Park. Reciprocating air flow for li-ion battery thermal management to improve temperature uniformity. *Journal of Power Sources*, 196(13):5685–5696, 2011.
- [125] S.-H.; Zu C. Manthiram, A.; Chung. Lithium-sulfur batteries: Progress and prospects. n/a -n/a.
- [126] Y.; Chung S.-H.; Zu-C.; Su Y.-S. Manthiram, A.; Fu. Rechargeable lithiumsulfur batteries. 114, 1175111787.
- [127] Y.; Su Y.-S. Manthiram, A.; Fu. Challenges and prospects of lithium-sulfur batteries. 46, 11251134.
- [128] Yangxing Li Y. G. Marina Yakovleva, K.B.Fitch. Stabilised lithium metal powder-material and application technologies for high energy li-ion batteries.
- [129] Greentech Media. Automakers on second-life batteries for the grid.
- [130] Bowler M Melissa Bowler. Clemson u. battery second use.
- [131] Osama Mesalhy, Khalid Lafdi, Ahmed Elgafy, and Keith Bowman. Numerical study for enhancing the thermal conductivity of phase change material (pcm) storage using high thermal conductivity porous matrix. *Energy Conversion and Management*, 46(6):847–867, 2005.
- [132] P. C.; Wiseman P. J.; Goodenough Mizushima, K.; Jones. A new cathode material for batteries of high energy density. 15, 783 789.
- [133] M.L.Patterson. anode materials for lithium ion batteries, November.
- [134] Habibi MS. Model for impact of storage on spinning reserve requirements and distributed generation. Proc 33rd Southeast Symp Syst Theory. (Cat No01EX460) 1615.
- [135] Wheeler N. Voltage regulation application of a kinetic energy storage system. Second IEE Int Conf Power Electron Mach Drives. v2605 v2605.
- [136] L.C. Klein N. Pereira and G. G. A. Abstract 126. 2000-2.
- [137] B. Blunier N. Watrin and A. Miraoui. Review of adaptive systems for lithiumbatteries state-of-charge and state-of-health estimation,. In USA Mich, editor, in *Proceedings of IEEE Transportation Electrification Conference and Expo*, page 1 to 6.

- [138] J.; Dyatkin B.; Presser V.; Taberna P.-L.; Simon P.; Barsoum-M. W.; Gogotsi-Y. Naguib, M.; Come. Mxene: A promising transition metal carbide anode for lithium-ion batteries. 16, 6164.
- [139] Katsuhiko Naoi. *Encyclopedia of Sustainability Science and Technology*, chapter Electrochemical Supercapacitors electrochemical supercapacitors and Hybrid Systems hybrid systems. Springer New York, New York, NY, 2012.
- [140] Onar O Starke MR Andrews G Narula CK, Martinez R. Economic analysis of deploying used batteries in power systems.
- [141] G. Nazri, G.-A.; Pistoia. Lithium batteries: Science and technology;.
- [142] Paul Nelson, Dennis Dees, Khalil Amine, and Gary Henriksen. Modeling thermal management of lithium-ion pngv batteries. *Journal of Power Sources*, 110(2):349–356, 2002.
- [143] Paul A Nelson, KG Bloom, and DW I Dees. Modeling the performance and cost of lithium-ion batteries for electric-drive vehicles. Technical report, Argonne National Laboratory (ANL), Argonne, IL (United States), 2011.
- [144] S.; Yang Y.; Jackson A.; Liu Y.; Wang H.; Dai H.; Andrews J. C.; Cui Y.; Toney-M. F. Nelson, J.; Misra. In operando x-ray diffraction and transmission x-ray microscopy of lithium sulfur batteries. 134, 63376343.
- [145] Pesaran A. Neubauer J. The ability of battery second use strategies to impact plug-in electric vehicle prices and serve utility energy storage applications. 196:103518.
- [146] Williams B. Ferry M. Eyer J. Neubauer JS., Pesaran A. A techno-economic analysis of pev battery second use.
- [147] Nerea Nieto, Luis Díaz, Jon Gastelurrutia, Isabel Alava, Francisco Blanco, Juan Carlos Ramos, and Alejandro Rivas. Thermal modeling of large format lithium-ion cells. *Journal of the Electrochemical Society*, 160(2):A212–A217, 2013.
- [148] De Hoog J Fleurbaey K Timmermans J-M Omar N Van Den Bossche P & Van Mierlo J Nikolian, A. Classification of electric modeling and characterization methods of lithium-ion batteries for vehicle applications.
- [149] B.; Popov B. N. Ning, G.; Haran. Capacity fade study of lithium-ion batteries cycled at high discharge rates. 117, 160169.
- [150] Bjrñ Nykvist and Mans Nilsson. Rapidly falling costs of battery packs for electric vehicles.

- [151] R. J. Ohzuku, T.; Brodd. An overview of positive-electrode materials for advanced lithium-ion batteries. 174, 449456.
- [152] Johnson C Mendelsohn M Neubauer J Pesaran A. OKeefe M, Brooker A. Battery ownership model.
- [153] M.; Hegazy O.; Al Sakka M.; Coosemans T.; Van den Bossche P.; Van Mierlo J. Omar, N.; Daowd. Assessment of lithium-ion capacitor for using in battery electric vehicle and hybrid electric vehicle applications. 86, 305315.
- [154] M.; Smekens J.; Van Mierlo J. Omar, N.; Al Sakka. Electric and thermal characterization of advanced hybrid li-ion capacitor rechargeable energy storage system. pp. 15741580.
- [155] Firouz Y Salminen J Smekens J Hegazy O et al. Omar N, Abdel-Monem M. Lithium iron phosphate based battery - assessment of the aging parameters and development of cycle life model.
- [156] Hegaz O Mulder G Timmermans JM Coosemans T et al. Omar N, Daowd M. Standardization work for bev and hev applications: Critical appraisal of recent traction battery documents.
- [157] Kazuo Onda, Hisashi Kameyama, Takeshi Hanamoto, and Kohei Ito. Experimental study on heat generation behavior of small lithium-ion secondary batteries. *Journal of the Electrochemical Society*, 150(3):A285–A291, 2003.
- [158] Beguin A. Oudalov A, Cherkaoui R. Sizing and optimal operation of battery energy storage system for peak shaving application.
- [159] YongJin Park, Sangook Jun, Sanghun Kim, and Dong-Ho Lee. Design optimization of a loop heat pipe to cool a lithium ion battery onboard a military aircraft. *Journal of mechanical science and technology*, 24(2):609–618, 2010.
- [160] PEC.NV. Sbt0550 battery test system r&d test equipment.
- [161] Ahmad A Pesaran. Battery thermal management in ev and hevs: issues and solutions. *Battery Man*, 43(5):34–49, 2001.
- [162] Ahmad A Pesaran and Matthew Keyser. Thermal characteristics of selected ev and hev batteries. In *Applications and Advances, 2001. The Sixteenth Annual Battery Conference on*, pages 219–225. IEEE, 2001.
- [163] Ahmad A Pesaran, Andreas Vlahinos, and Steven D Burch. *Thermal performance of EV and HEV battery modules and packs*. National Renewable Energy Laboratory Golden, CO, USA, 1997.

- [164] Mathias Petzl, Michael Kasper, and Michael A. Danzer. Lithium plating in a commercial lithium-ion battery a low-temperature aging study. *Journal of Power Sources*, 275:799 – 807, 2015.
- [165] Ben Schweitzer Maryam Yazdanpour Peyman Taheri, Abraham Mansouri and Majid Bahrami. Electrical constriction resistance in current collectors of large-scale lithium-ion batteries. 160(A1731-A1740).
- [166] Wilkes J. Pineda I. Wind in power.
- [167] Gregory Plitt. Kalman-filter soc estimation for lipb hev cells.
- [168] Beacon Power. Frequency regulation and flywheels, 2014.
- [169] Parfomak PW. Energy storage for power grids and electric transportation. (146).
- [170] ZG Qu, WQ Li, and WQ Tao. Numerical model of the passive thermal management system for high-power lithium ion battery by using porous metal foam saturated with phase change material. *International Journal of Hydrogen Energy*, 39(8):3904–3913, 2014.
- [171] ZG Qu, WQ Li, JL Wang, and WQ Tao. Passive thermal management using metal foam saturated with phase change material in a heat sink. *International Communications in Heat and Mass Transfer*, 39(10):1546–1549, 2012.
- [172] Castro M Sainz JA. Quesada J, Sebastin R. Control of inverters in a low voltage microgrid with distributed battery energy storage. 114:12635.
- [173] Rashid MH. Racine MS, Parham JD. An overview of uninterruptible power supplies. Proc 37th Annu North Am Power Symp.
- [174] Zhonghao Rao and Shuangfeng Wang. A review of power battery thermal energy management. *Renewable and Sustainable Energy Reviews*, 15(9):4554–4571, 2011.
- [175] Zhonghao Rao, Shuangfeng Wang, Maochun Wu, Zirong Lin, and Fuhuo Li. Experimental investigation on thermal management of electric vehicle battery with heat pipe. *Energy Conversion and Management*, 65:92–97, 2013.
- [176] Francesco Gattiglio Rene Schroeder. Battery technology for vehicle applications. Roadmap 2030.
- [177] Reneweconomy. Car makers want second-life batteries used on the grid.
- [178] IPHE Renewable Hydrogen Report. Utsira wind power and hydrogen plant.
- [179] Navigant Research. Second-life batteries: From pevs to stationary applications.

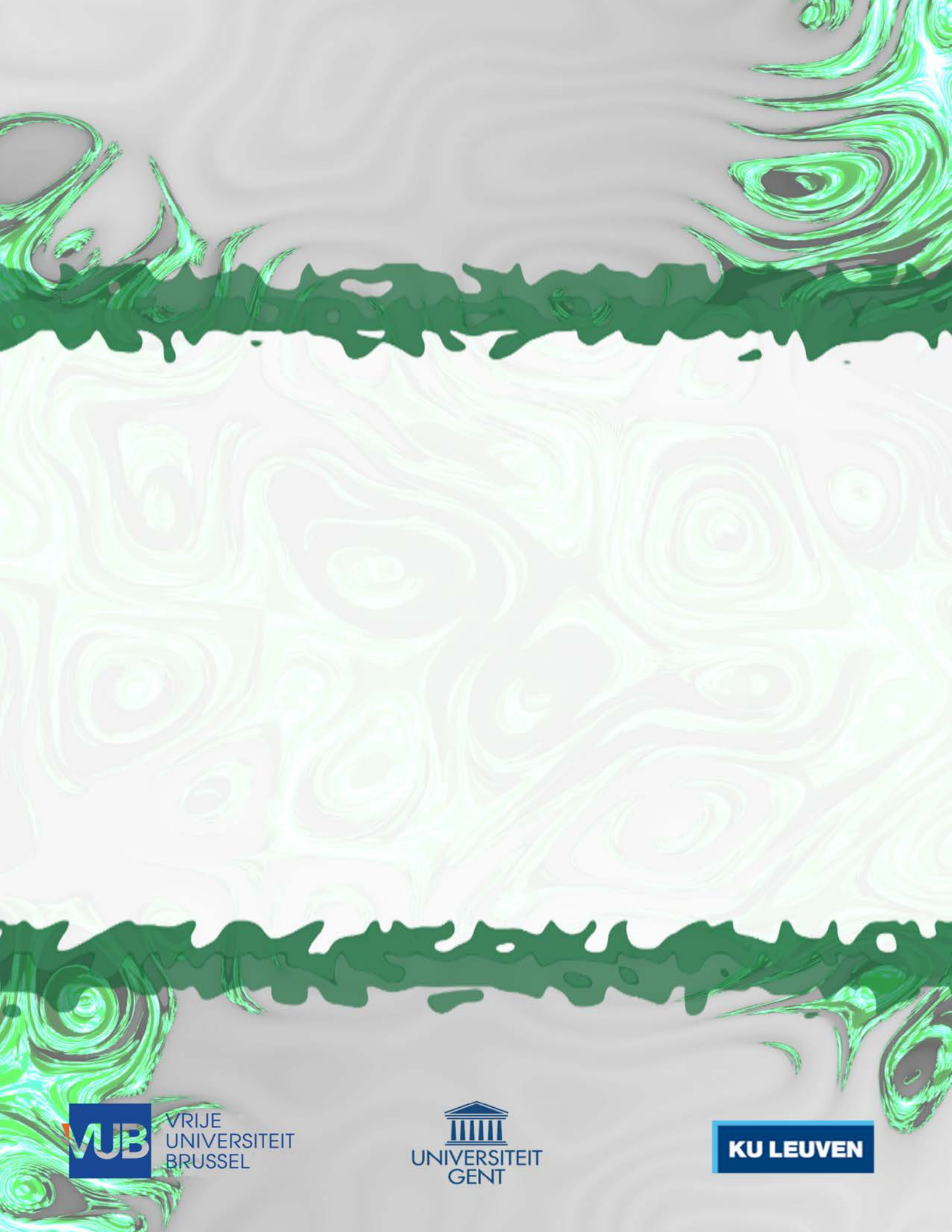
- [180] Taiyou Research. Global market for lithium-ion batteries - forecast, trends and opportunities 2013-2020. ID 2599948.
- [181] Boccaletti C. Ribeiro E, Cardoso a. JM. Fuel cell-supercapacitor system for telecommunications. 5th IET Int Conf Power Electron Mach Drives. (PEMD 2010) PO8PO8.
- [182] Michael Graham Richard. Lithium-sulfur breakthrough could mean safer and more energy-dense batteries.
- [183] McDonagh M. Rittershausen J. Moving energy storage from concept to reality.
- [184] Miller BL Hauer JF Rogers JD, Schermer RI. superconducting magnetic energy storage system for electric utility transmission stabilization. Proc IEEE. 71:1099107.
- [185] J. Ronsmans. Combining energy with power : Lithium ion capacitors.
- [186] Rami Sabbah, R Kizilel, JR Selman, and S Al-Hallaj. Active (air-cooled) vs. passive (phase change material) thermal management of high power lithium-ion packs: Limitation of temperature rise and uniformity of temperature distribution. *Journal of Power Sources*, 182(2):630–638, 2008.
- [187] G. Sachs. Goldman sachs global investment report: Americas clean energy storage battery.
- [188] Professor Donald Sadoway. Unlocking renewables / world economic forum. Website, 10 2015. MIT / Ambri.
- [189] Yoshiyasu Saito, Katsuhiko Kanari, and Kiyonami Takano. Thermal studies of a lithium-ion battery. *Journal of power sources*, 68(2):451–454, 1997.
- [190] H.; Omar N. Sakka, M. Al; Gualous. Batteries and supercapacitors for electric vehicles. 135164.
- [191] Apurba Sakti, Jeremy J. Michalek, Erica R.H. Fuchs, and Jay F. Whitacre. A techno-economic analysis and optimization of li-ion batteries for light-duty passenger vehicle electrification. *Journal of Power Sources*, 273:966 – 980, 2015.
- [192] Ahmet Sarı and Ali Karaipekli. Thermal conductivity and latent heat thermal energy storage characteristics of paraffin/expanded graphite composite as phase change material. *Applied Thermal Engineering*, 27(8):1271–1277, 2007.
- [193] Ahmet Sarı and Ali Karaipekli. Preparation, thermal properties and thermal reliability of palmitic acid/expanded graphite composite as form-stable pcm for thermal energy storage. *Solar Energy Materials and Solar Cells*, 93(5):571–576, 2009.

- [194] Guy Sarre, Philippe Blanchard, and Michel Broussely. Aging of lithium-ion batteries. *Journal of Power Sources*, 127(1):65–71, 2004.
- [195] Hassenzahl W. Schoenung SM. Characteristics and technologies for long-vs. short-term energy storage. SAND2001-0765.
- [196] Liaw BY. Sepasi S, Ghorbani R. Inline state of health estimation of lithium-ion batteries using state of charge calculation.
- [197] R. N. Sharma, R. A.; Seefurth. Thermodynamic properties of the lithium-silicon system. 123, 1763.
- [198] Deguchi H Hara T. Shigematsu T, Kumamoto T. Applications of a vanadium redox-flow battery to maintain power quality. IEEE/PES Transm Distrib Conf Exhib. 2:106570.
- [199] Y. Simon, P.; Gogotsi. Materials for electrochemical capacitors. 7, 845854.
- [200] Brendan Sims. Power technologies review.
- [201] Stroe D-I Teodorescu R Andreassen SJ. Stan A-I, Swierczynski M. Lithium ion battery chemistries from renewable energy storage to automotive and back-up power applications an overview.
- [202] Energy storage association. Energy storage technologies.
- [203] A. Su, Y.-S.; Manthiram. Lithium-sulphur batteries with a microporous carbon paper as a bifunctional interlayer. 3, 1166.
- [204] Bayne SB Giesselmann MG Harral MA Subburaj AS, Kondur P. *Analysis and review of grid connected battery in wind applications*.
- [205] Gerhardus Swanepoel. *Thermal management of hybrid electrical vehicles using heat pipes*. PhD thesis, University of Stellenbosch, 2001.
- [206] J. Long T. Brousse, D.Belanger. To be or not to be pseudocapacitive? 162, A5185A5189.
- [207] D.; Schubert T. J. S. Taige, M.; Hilbert. Mixtures of ionic liquids as possible electrolytes for lithium ion batteries. 226, 129139.
- [208] Xiaopeng Tang, Yujie Wang, and Zonghai Chen. A method for state-of-charge estimation of lifepo4 batteries based on a dual-circuit state observer. *Journal of Power Sources*, 296:23 – 29, 2015.
- [209] Lafoz M Laing D Tamme R Pedersen AS et al. Teller O, Nicolai J-P. *Recommendations for a European Energy Storage Technology Development Roadmap Towards 2030*.

- [210] W. I. F.; Bruce P. G.; Goodenough J. B. Thackeray, M. M.; David. Lithium insertion into manganese spinels. 18, 461472.
- [211] Roadmap lithium x batteries, technological assessment by application. Internally in Mobi, Pleinlaan 2 1050 Brussels, 2015.
- [212] Roadmap lithium x batteries, technological roadmap. Internally in Mobi, Pleinlaan 2 1050 Brussels, 2015.
- [213] Jörn Tinnemeyer. New advances in lithium ion battery monitoring. In *Battery Power conference, Dallas, Texas, 19e20 October*, 2010.
- [214] Moura F. Turton H. Vehicle-to-grid systems for sustainable development.
- [215] Umicore. Rechargeable battery cathode materials:.
- [216] E. J. William et al. V. Prajapati, H. Hess, editor. *A literature review of state of-charge estimation techniques applicable to lithium poly-carbon monoflouride (LI/CFx) battery*, January.
- [217] P.; Wagner M. R.; Veit C.; Mller K. C.; Besenhard J. O.; Winter M.; Wohlfahrt-Mehrens M.; Vogler C.; Hammouche a. Vetter, J.; Novk. Ageing mechanisms in lithium-ion batteries. 147, 269281.
- [218] Wladislaw Waag, Christian Fleischer, and Dirk Uwe Sauer. Critical review of the methods for monitoring of lithium-ion batteries in electric and hybrid vehicles. *Journal of Power Sources*, 258:321 – 339, 2014.
- [219] Gran Wall. Exergetics. <http://exergy.se/ftp/exergetics.pdf>.
- [220] K.; Wan W.; Guo H.; Zhou H.; Chen J.; Zhang X.; Huang Y. Wang, C.; Su. High sulfur loading composite wrapped by 3d nitrogen-doped graphene as a cathode material for lithiumsulfur batteries. 2, 5018.
- [221] Qingsong Wang, Ping Ping, Xuejuan Zhao, Guanquan Chu, Jinhua Sun, and Chunhua Chen. Thermal runaway caused fire and explosion of lithium ion battery. *Journal of power sources*, 208:210–224, 2012.
- [222] W.; Cha J. J.; Zheng G.; Yang Y.; McDowell M. T.; Hsu P.-C.; Cui Y. Wei Seh, Z.; Li. Sulphur-tio2 yolk-shell nanoarchitecture with internal void space for long-cycle lithium-sulphur batteries. 4,1331.
- [223] Sihua Wen. Cell balancing buys extra run time and battery life. *Analogue Applications Journal*, 2009.
- [224] Lipman T. Williams B. Analysis of the combined vehicle.

- [225] J. O.; Spahr M. E.; Novk P. Winter, M.; Besenhard. Insertion electrode materials for rechargeable lithium batteries. 10, 725763.
- [226] G.; Choi J. W.; Ryu I.; Yao Y.; McDowell M. T.; Lee S. W.; Jackson A.; Yang Y.; Hu L.; et al. Wu, H.; Chan. Stable cycling of double-walled silicon nanotube battery anodes through solid-electrolyte interphase control. 7, 310-315.
- [227] Guoliang Wu, Chunbo Zhu, and C. C. Chan. Comparison of the first order and the second order equivalent circuit model applied in state of charge estimation for battery used in electric vehicles. 8(1):1357–1362.
- [228] J.; Tian Y.; Su Y.; Wang J.; Yang W.; Li N. Wu, F.; Li. Doped carbon-sulfur composite for high performance lithium-sulfur batteries. 110.
- [229] Mao-Sung Wu and Pin-Chi Julia Chiang. High-rate capability of lithium-ion batteries after storing at elevated temperature. *Electrochimica acta*, 52(11):3719–3725, 2007.
- [230] Mao-Sung Wu, KH Liu, Yung-Yun Wang, and Chi-Chao Wan. Heat dissipation design for lithium-ion batteries. *Journal of power sources*, 109(1):160–166, 2002.
- [231] L.; Zhao N.-H.; Yin Y.-X.; Zhou L.-J.; Guo Y.-G.; Wan L.-J. Xin, S.; Gu. Smaller sulfur molecules promise better lithium-sulfur batteries. 134, 1851018513.
- [232] Jonathan Clarke Xing Ling. Overview of current development in electrical energy storage technologies and the application potential in power system operation.
- [233] D.; Wang Z.; Meng Y. S. Xu, B.; Qian. Recent progress in cathode materials research for advanced lithium ion batteries. 73, 5165.
- [234] Yanusako. Ultracapacitor product line.
- [235] Bashir N Yekini M, Wazir Mustafa M. Energy storage systems for renewable energy power sector integration and mitigation of intermittency.
- [236] Jinrong Qian Yevgen Barsukov. *Battery Power Management for Portable Devices*. Artech House, 2013.
- [237] L.-J.; Shu J.; Yue-C.-B.; Zhu-R.-S.; Qiao-H.-B. Yi, T.-F.; Jiang. Recent development and application of $\text{Li}_4\text{Ti}_5\text{O}_{12}$ as anode material of lithium ion battery. 71, 12361242.
- [238] H. Yin, C. Zhao, M. Li, C. Ma, and M. Y. Chow. A game theory approach to energy management of an engine x2013;generator/battery/ultracapacitor hybrid energy system. *IEEE Transactions on Industrial Electronics*, 63(7):4266–4277, July 2016.
- [239] S.; Guo Y.-G.; Wan-L.-J. Yin, Y.-X.; Xin. Lithium-sulfur batteries: Electrochemistry, materials, and prospects. 52, 1318613200.

- [240] Ding Xuan Yu and Yan Xia Gao. Soc estimation of lithium-ion battery based on kalman filter algorithm. 347.
- [241] Yanli Liu Ze Cheng, Jikao Lv and Zhihao Yan. Estimation of state of charge for lithium-ion battery based on finite difference extended kalman filter.
- [242] J.; Nuli Y.; Wang-B.; Xu-J. Zhang, Z.; Yang. Copx synthesis and lithiation by ball-milling for anode materials of lithium ion cells. 176, 693697.
- [243] Chang-Ying Zhao, Wei Lu, and Yuan Tian. Heat transfer enhancement for thermal energy storage using metal foams embedded within phase change materials (pcms). *Solar Energy*, 84(8):1402–1412, 2010.
- [244] Chang-Ying Zhao and ZG Wu. Heat transfer enhancement of high temperature thermal energy storage using metal foams and expanded graphite. *Solar Energy Materials and Solar Cells*, 95(2):636–643, 2011.
- [245] Yu Zhao, Yu Ding, Yutao Li, Lele Peng, Hye Ryung Byon, John B. Goodenough, and Guihua Yu. A chemistry and material perspective on lithium redox flow batteries towards high-density electrical energy storage. *Chem. Soc. Rev.*, 44:7968–7996, 2015.
- [246] S.; Li L.; Wang-D.-W.; Wang-S.; Huang-K.; Yin L.-C.; Li F.; Cheng H.-M. Zhou, G.; Pei. A graphene-pure-sulfur sandwich structure for ultrafast, long-life lithium-sulfur batteries. *adv.* 26, 625631, 664.
- [247] Qi ZP. Zhou L. Modeling and control of a flywheel energy storage system for uninterruptible power supply. *Sustain Power Gener Supply*.



VRIJE
UNIVERSITEIT
BRUSSEL

